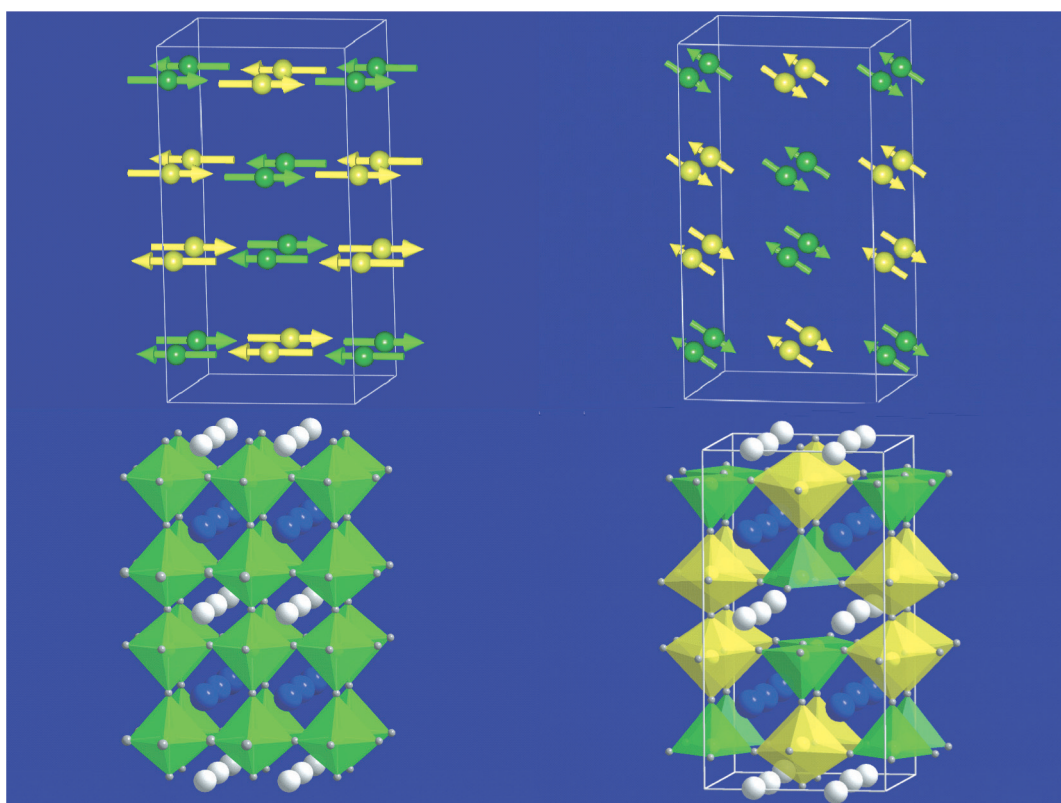


Scientific Report

2003-2004

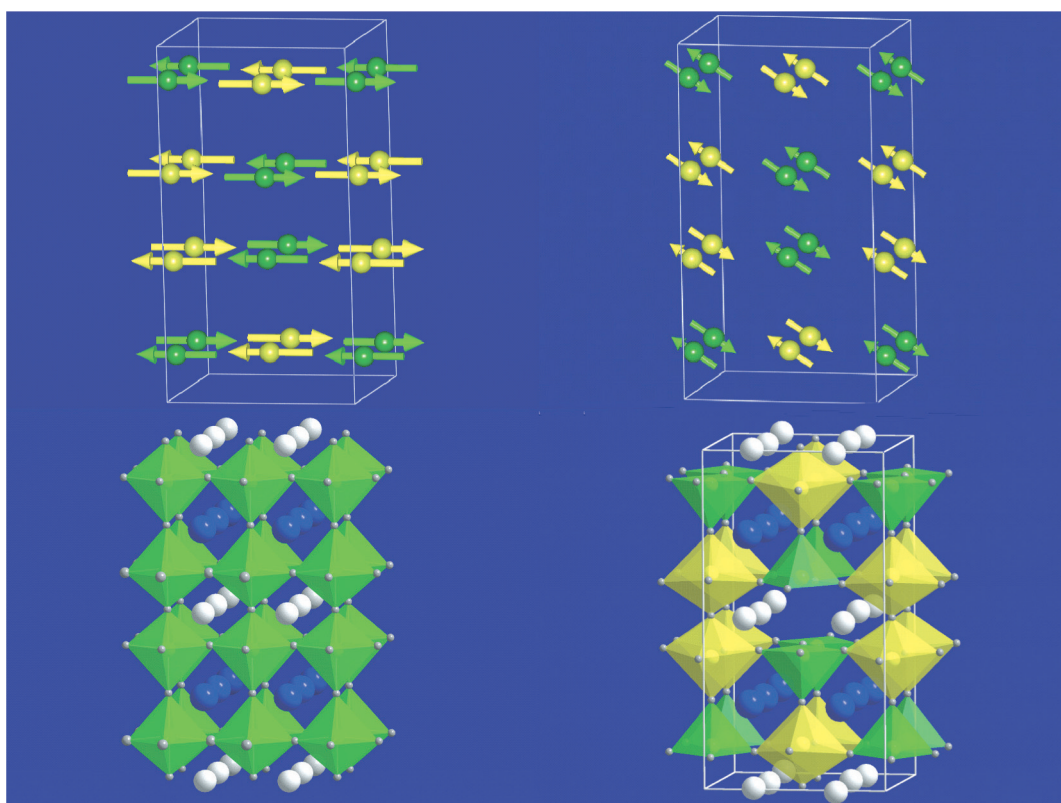


LABORATOIRE LÉON BRILLOUIN

Top: Magnetic structure of $\text{YBaMn}_2\text{O}_{5.5}$ at 1.5K (left) and 125K (right). A spin reorientation from nearly along the [001] direction to the [100] one takes place between $T_N \approx 150\text{K}$ and $T_R \approx 110\text{K}$.
Bottom: Perspective view of YBaMn_2O_6 ($\text{Mn}^{3+}/\text{Mn}^{4+}$ disordered phase, left) and $\text{YBaMn}_2\text{O}_{5.5}$ (pure Mn^{3+} , right) perovskites. The latter is obtained from the former in a reducing atmosphere.

Scientific Report

2003-2004



LABORATOIRE LÉON BRILLOUIN

LLB 2003-2004

Contents

Foreword	1
Scientific Highlights	
1. Structures and Phase Transitions	3
2. Magnetism and Superconductivity	35
3. Materials Science	63
4. Physical Chemistry and Soft Matter	87
5. Life Science	111
6. Modelling	131
7. Technical and Instrumental Developments	149
Experimental Programme and User Activities	167
Presentation of LLB	183
Publications	189

1 - STRUCTURES AND PHASE TRANSITIONS

1. Crystallographic Structures of austenitic and martensitic hydrides of $\text{Ti}_{0.64}\text{Zr}_{0.36}\text{Ni}$ intermetallic compound **14**
F. Cuevas, M. Latroche, A. Percheron-Guégan.
2. Giant H/D isotopic effect in $\text{YFe}_2(\text{H}_y\text{D}_{1-y})_{4.2}$ compounds **15**
V. Paul-Boncour, M. Guillot, G. André, F. Bourée, G. Wiesinger, A. Percheron-Guégan
3. Silicon doped hydroxyapatites **16**
D. Arcos, J. Rodríguez-Carvajal, M. Vallet-Regí
4. Simulated annealing on neutron and synchrotron powder diffraction DATA **18**
A. Carretero-Genevri, F. Damay, A. Cousson, W. Van Beek, J. Rodríguez-Carvajal
5. Magnetic structures of transition metal (Mn, Co, Ni, Cu) Hydroxysulfates **20**
S. Vilminot, G. André, M. Richard-Plouet, M. Kurmoo, F. Bourée-Vigner, M. Ben Salah
6. Crystal and magnetic structures of the Mn^{3+} orbital ordered manganite $\text{Y}_2\text{Ba}_2\text{Mn}_4\text{O}_{11}$ **22**
L. Pinsard-Gaudart, C. Perca, A. Daoud-Aladine, M. T. Fernández-Díaz, J. Rodríguez-Carvajal
7. Spin Speierls ground state in $(\text{TMTTF})_2\text{PF}_6$ **24**
P. Foury-Leylekian, D. Le Bolloc'h, B. Hennion, S. Ravy, A. Moradpour, J.-P. Pouget
8. Neutral-to-ionic phase transition under pressure: towards the quantum limit **26**
M.H. Lemée-Cailleau, M. Buron, E. Collet, H. Cailleau, T. Luty, B. Ouladdiaf, F. Moussa, T. Hasegawa
9. Interactions in self-Assembled molecular crystals **28**
L. Bourgeois, B. Toudic, C. Ecolivet, P. Bourges, T. Breczewski
10. Phonon anomalies in high T_c superconductors related to charge stripe order **30**
D. Reznik, L. Pintschovius, M. Sato, M. Itoh, S. Iikubo, S. Yamada
11. Magnetic order in high-pressure oxygen **32**
I. Goncharenko, O. Makarova, L. Ulivi

2 - MAGNETISM AND SUPERCONDUCTIVITY

1. Two-dimensional geometry of spin excitations in the high-transition-temperature superconductor $\text{YBa}_2\text{Cu}_3\text{O}_{6.85}$ **44**
V. Hinkov, S. Pailhès, P. Bourges, Y. Sidis, A. Ivanov, A. Kulakov, C. T. Lin, D. P. Chen, C. Bernhard, B. Keimer
2. Small Angle Neutron Scattering from the flux lines lattice: new developments **46**
A. Pautrat, Ch. Simon, G. Poullain, C. Goupil, J. Scola, P. Mathieu, A. Brûlet
3. Lattice distortions related to charge ordering in $\text{Sr}_{14}\text{Cu}_{24}\text{O}_{41}$ **48**
M. Braden, J. Etrillard, A. Gukasov, U. Ammerahl, A. Revcolevschi
4. $\text{La}_{-5}(\text{Sr,Ca})_9\text{Cu}_{24}\text{O}_{41}$: a 1D Toy model for hole doped cuprates **50**
R. Klingeler, A. Gukasov, T. Kroll, J. Geck, M. Hücker, U. Ammerahl, A. Revcolevschi, B. Büchner
5. Confined spin waves reveal an assembly of nanosize domains in $\text{La}_{1-x}\text{Ca}_x\text{MnO}_3$ ($x=0.17, 0.2$) **52**
M. Hennion, F. Moussa, P. Kober-Lehouelleur, F. Wang, A. Ivanov, L. P. Regnault, J. Kulda
6. Magnetic filaments in resistive manganites **54**
M. Viret, F. Ott, J.P. Renard, H. Glättli, L. Pinsard-Gaudart, A. Revcolevschi
7. Magnetic ground state in the frustrated $S=1/2$ square lattice of V^{4+} in $\text{Li}_2\text{VO}_2\text{SiO}_4$ **56**
A. Bombardi, J. Rodríguez-Carvajal, S. Di Matteo, F. de Bergevin, L. Paolasini, P. Carretta, P. Millet, R. Caciuffo
8. Temperature renormalization of the spin correlations in the dimer spin-Liquid TlCuCl_3 **58**
Ch. Rüegg, Ch. Niedermayer, A. Furrer, J. Mesot, M. Matsumoto, B. Normand, M. Sgrist, T.M. Rice, K.W. Krämer, H.-U. Güdel, H. Mutka, P. Bourges, Y. Sidis
9. Domain structures in $\text{Fe}/\text{Fe}_2\text{N}$ multilayers **60**
W. Szuszkiewicz, K. Fronc, B. Hennion, and M. Aleszkiewicz

3 - MATERIALS SCIENCE

1. Residual stress redistribution in a wheel/axle assembly due to cyclic loading **72**
A. Yameogo', A. Carrado, C. Prioul, A. Lodini
2. Residual stresses in welded aluminium joints for aerospace applications **74**
V. Stelmukh, S. Ganguly, L. Edwards and M. E. Fitzpatrick
3. Investigation of the α and β texture evolution of hot forged titanium alloy products **76**
J. Delfosse, C. Rey, M.H. Mathon
4. Impurities effects on the mechanisms of recrystallization of wire-drawn copper **78**
S. Jakani, T. Baudin, M. Benyoucef, Ph. Gerber, C.H. de Novion, M.H. Mathon
5. Nanocluster formation in electron irradiated lithium oxide **80**
G. Krexner, M. Prem, F. Beuneu, P. Vajda
6. Combined X-ray & neutron powder diffraction study of a dimorphic C_{60} solvate: $C_{60} \cdot CH_2Cl_2$ **82**
R.J. Papoular, R. Céolin, H. Allouchi, P. Espeau, A. Kurbakov', J.-LL. Tamarit
7. Local order around Nd^{3+} ions in an organic solution as determined by neutron scattering experiment **84**
B. Belhorma, M.-C. Bellissent-Funel, M.-C. Charbonnel, J.-P. Dognon

1. Bottle brush shape polymacromonomers : conformation and dynamics in solutions and melts **94**
S. Desvergne, F. Boué, A. Brûlet, V. Héroguez, Y. Gnanou
2. Aqueous supramolecular polymer formed by an amphiphilic perylene derivative **96**
Alix Arnaud, Joël Belleney, François Boué, Laurent Bouteiller, Géraldine Carrot, Véronique Wintgens
3. Swelling and collapse of a weak polyelectrolyte as a function of pH **98**
P. Topham, c. J. Crook, J. R. Howse, A. J. Ryan, A. J. Parnell, L. Ruiz-Pérez, R. A. L. Jones, M. Geoghegan, A. Menelle
4. Polymer-polymer adhesion of uncrosslinked elastomers studied by neutron reflectivity **100**
R. Schach, C. Creton, Y. Tran
5. Atom transfer radical polymerization from silica nanoparticles : following chemical synthesis using S.A.N.S. **102**
A. El Harrak, G. Carrot, J. Oberdisse, J. Jestin, F. Boué
6. Highly stretched polymer brushes with a low swelling capacity **104**
C. Devaux, F. Cousin, J-P. Chapel
7. New structural model for Nafion® membranes **106**
Laurent Rubatat, Olivier Diat, Gérard Gebel
8. Local dynamics of bulk and nanoparticle filled poly(vinyl acetate) observed by quasielastic neutron scattering **108**
Chuhong Zhang, Valeria Arrighi

1. Experimental evidence of a liquid-liquid transition at 0 K in interfacial water 118
J.-M. Zanotti, M.-C. Bellissent-Funel, S.-H. Chen
2. Hydration water dynamics of hydrophobic oligopeptide 120
D. Russo, P. Baglioni, E. Peroni, J. Teixeira
3. Hydration of ds-DNA and ss-DNA 122
M. Bastos, V. Castro, G. Mrevlishvili, J. Teixeira
4. Diffusion of water in halophilic archaea 124
K. Wood, S. Longeville, B. Franzetti, M.-C. Bellissent-Funel, D. Oesterhelt, G. Zaccai, B.-Z. Ginzburg
5. Structure of proteins-polyelectrolyte complexes 126
F. Cousin, J. Gummel, I. Schmidt, C. Huchon, F. Boué, M. Axelos

6 - MODELLING

1. The weakly coupled Rotor-Morse oscillator system: A toy model for selective chemical dissociation. **140**
S. Aubry and A. Memboeuf
2. Spin dynamics of the electron-doped high T_c superconducting cuprates **143**
F. Onufrieva and P. Pfeuty
3. Faults, a new program for refinement of powder diffraction patterns from layered structures **144**
M. Casas-Cabanas, J. Rodríguez-Carvajal, M.R. Palacín
4. Dynamics of lysozyme under pressure seen by molecular simulation and neutron scattering **146**
G.R. Kneller, K. Hinsén, V. Hamon, M.-C. Bellissent-Funel

7 - TECHNICAL AND INSTRUMENTAL DEVELOPMENTS

- 1 Papyrus : a dedicated tool to study surfaces at the nanoscale **155**
G. Chaboussant, F. Cousin, S. Gautrot, H. Glatli, J. Jestin, F. Ott, M. Viret
2. Very small angle neutron scattering spectrometer (TPA) **158**
J. Oberdisse, R. Kahn, V. Thévenot, A. Gabriel, P. Permingeat, D. Lairez, B. Hannighofer, S. Désert, A. Brûlet
3. Technical developmentS dedicated to “in situ” temperature analysis of crystallographic textures by neutron diffraction **160**
Ph. Gerber, J.P. Ambroise, M.H. Mathon
4. Neutron holographic study of palladium hydride **162**
L. Cser, G. Krexner, M. Prem, I. Sharkov, Gy. Török
5. Replacement of first elements of Guides 1 to 6 **164**
A. Menelle
6. Report on a first neutron test of a new D position-sensitive detector of thermal neutrons **165**
A. Kuklin, G.Eckold , V.Gordeliy, S.Kutuzov, A.Islamov, A.Smirnov, P.Utrobin, A.Bogdzal, N.Alekseev, V.Comparat, A.Pelissier, J. Ballon, J. Teixeira , G.Koskas, A.Gabriel

LLB Director's Foreword in 2003-2004

This scientific report describes an overview of the Laboratoire Léon Brillouin (LLB) activities during the 2003-2004 period, using the neutron beams provided by the ORPHEE research reactor in SACLAY, France. The LLB is a CNRS-CEA mixed research unit ("Unité Mixte de Recherche", UMR12) funded by the French research agencies, the "Centre National de la Recherche Scientifique" (CNRS) and the "Commissariat à l'Énergie Atomique" (CEA). Since more than twenty (20) years, LLB is one of the best *large-scale* facilities for *small* science, where many "small" teams of scientists spend a few days performing specific experiments in physics, chemistry, biology, material or earth sciences.

The LLB, the French Neutron Laboratory, is:

- a **Large-scale National Facility** dedicated to neutron scattering experiments proposed by external users, from French academic laboratories, and also industrial firms, performed in the best conditions,
- a **Research Laboratory** with its own scientific activity centered on the use of the LLB facilities with experiments performed by permanent or associated teams,
- a **Training centre** for young researchers, in particular thesis students preparing PhD diploma essentially based on neutron scattering techniques and instrumentation.

This triple character of the LLB mission, neutron facility, research laboratory and training centre, leads to an integrated scientific platform of excellence and the research performed at the LLB is acknowledged worldwide in many scientific fields. The LLB, as the French national neutron facility, benefits from the quality of the Orphée reactor, almost exclusively dedicated to research. Orphée is flawlessly run and maintained by the Direction of the Nuclear Energy (DEN) of the CEA.

Orphée-LLB and the European Community (EC):

Brussels has selected the LLB since 1993 in the access programs for large installations. After the fifth program (FP5) operated until May 2004, Orphée-LLB is part of the "Neutron and Muon Infrastructure Integrated Initiative" (NMI3) of the sixth EU framework programme for Research and Technological Development (FP6). In the framework of this program, the LLB will deliver 500 days of neutron beam time during 4.5 years, from 2004 to 2008, to the research teams of the EC and associated countries. Aside the access program, LLB participates actively to technical network projects ("JRA" for Joint Research Activities) on neutron optics, polarisation techniques and detectors.

Neutron beam time for French and foreign researchers:

In the normal operation mode (180 days of neutron delivery per year) about 3500 beam time days are delivered on 23 spectrometers: 64% for the French community, 25% for EC countries including PECO countries now full participants in the EC, 4% for Russia and 7% for "other" countries. On average, nearly five hundred (500) experiments are performed every year by more than eight hundred (800) scientists for all over the world.

Research done at LLB is following the main strategic schemes and topmost priorities of the French research agencies, namely the CNRS and the CEA.

Condensed matter physics

The LLB is a leading centre for studies on superconductivity and magnetism. Internationally acknowledged highlights are focussing on magnetic excitations in the high T_C superconducting state and spin-charge-lattice interactions in manganites. New progresses have been achieved in photo-induced molecular magnetism, as well as in geometrically frustrated magnetic systems (crystallisation of a spin liquid under pressure); and low dimensional magnetic systems. A new magnetic phase has also been discovered for oxygen in extreme pressure conditions, a field of excellence at LLB.

Nanosciences

Adhesion phenomena, solubilization, chemical reactivity and grafting on nanocomposites, protein interactions are important processes operating at interfaces that can be studied by standard neutron reflectivity whereas polarised neutron techniques probe the magnetic structures of layered devices for the future spin electronics. Off-specular scattering experiments are now developed and will bring very valuable information on structure and magnetism of laterally-patterned systems.

Technologies for energy

New projects are developed at the LLB concerning environmental problems, earth sciences, innovative materials for cleaner energies like membranes for fuel cells, lithium batteries, special steels for new reactors (e.g. aging behaviour of dedicated steels under irradiation).

Life sciences

The focus at the LLB is on protein unfolding and structure-function relationship in biological systems. Neutron diffusion allows also characterizing bio-polymers from plants and polyelectrolytes that are important for technological interest in the

food industry. Neutron spectroscopy is a powerful tool to resolve the protein motions in the time range from picoseconds to tens of nanoseconds, with the help of the large cross section of hydrogen/deuterium atoms.

Instrumental developments at Orphee-LLB

These projects are gathered under the item CAP2010. The neutron spectrometers must be continuously refurbished and upgraded to be kept attractive at an international level. The upgraded 3T2 high-resolution powder diffractometer will be in operation in the 2005 summer. The time-of flight reflectometer EROS is upgraded to face the growing studies on liquid interfaces in soft matter and complex systems. The new very small angle spectrometer TPA is now in its building phase (the monochromating sections and detector housings will be available in 2005 and a multibeam collimator is currently designed and tested on the G5B position). The last project concerns the high-resolution TOF (Time-of-Flight) and NRSE (Neutron Resonance Spin Echo) machines Mibemol and Muses: a new TOF spectrometer Fa# is under study and will be placed on the G3 end-guide position and a multidetector secondary spectrometer is studied for Muses. Aside these six major instrumental projects, there is a rising request of supermirror guides and two-dimensional detectors to be financed and built.

Orphee-LLB in the French Research turmoil in 2003-2004

In 2003, the LLB was in the middle of nowhere, “Il Casino Totale” in Italian. In March 2003, the French government decided to cancel 10% of the budget for research (out of salaries) and to freeze 30% of this budget. The consequence on Orphée-LLB in 2003 was the CNRS reduced financial contribution to 60 days of beam time, compared to the 180 days scheduled. Also, due to foreseeable budget difficulties in the following years, the CNRS was considering to discontinue its financial support to the installation. A great support from France and abroad users as well as from international organisations and Institutions yielded to a temporary CNRS-CEA agreement for 2004 and 2005 with a limited number of neutron days (6 cycles of 19 days, i.e. 114 days). In autumn 2003 and spring 2004, an international evaluation committee (chaired by Ph. Nozières) and many delegations from CNRS, CEA and French Ministry of Research have intensively scrutinized the strategic and scientific activities of Orphée-LLB. This procedure led to the decision of the extraordinary steering committee held on 4 October 2004 to have Orphée-LLB back to normal working conditions – namely, a minimum of 180 days per year- as soon as possible in 2006. This decision sticks to the Minister of Research instructions aimed at the Chief Executive Officer of the CEA and the Director-General of the CNRS. This conclusion put an end to the high anxiety about the Orphée-LLB fate after 2005. A new CNRS-CEA contract will be signed in the beginning of 2005; this new agreement will start on January 2006 for five (5) years and will be renewed for 5 year-periods by tacit approval. The LLB has now a clear future.

Orphee-LLB in the neutron European and International landscape

The Munich reactor FRMII started in 2004 and will complement the neutron work done at Jülich and Berlin. ISIS is investing 100M£ to build a second target station and the related instrumentation to be in operation in 2007, in phase with the new DIAMOND synchrotron. We are still in a stimulating phase when the main European countries, like Great Britain and Germany, develop their national neutron sources while reinforcing their association with the ILL, the European high-flux reactor.

The LLB collaborated closely with all these centres to promote the case of the European Spallation Source ESS in the last years. However, Europe has lost the neutron initiative and the ESS project was shut down in 2003. Following the move done in Europe towards the ESS project, the US is now *building* in Oakridge its next generation Spallation Neutron Source SNS. And the Japan Hadron Facility J-PARC includes a Megawatt spallation source much more powerful than ISIS, showing that Neutron Scattering is an essential technique in many research domains, like material science, superconductivity, nanosciences, chemical physics and life science. With a bright future, the LLB will be able, on the long term, to reinforce the European scientific community among the other European synchrotron sources, laser and RMN platforms and, of course, neutron centres.

The Saclay platform: Orphée-LLB Neutron Centre and SOLEIL Synchrotron

The two French facilities will start in 2005 regular workshops focusing on scientific or technical subjects of interest for the neutron and synchrotron community. The first workshop, “Magnétisme et Nanostructures”, is scheduled in May 2005. It is foreseen that, in a near future, the “Saclay Plateau” will become a meeting point for complementary techniques and we hope that this will be as successful on a French stand as in other countries (Germany, Switzerland and UK) or in Grenoble on a European level with the ILL and the ESRF.

Finally, early in February 2005, Philippe Mangin will take the position of Director of the LLB and will replace P. Monceau who will go back to Grenoble, to the “Centre de Recherches sur les Très Basses Températures” (CRTBT).

M. ALBA, P. MONCEAU
January 13, 2005

1 - STRUCTURES AND PHASE TRANSITIONS

1 - STRUCTURES AND PHASE TRANSITIONS

Studies on both crystallographic and magnetic structural phase transitions are an important part of Laboratoire Léon Brillouin's scientific activity. Neutron studies, either diffraction and/or inelastic scattering, are performed as a function of external parameters, namely temperature and pressure. Many different physical problems, either fundamental and/or applied, are in connection with structural phase transitions and the present summary intends to show the main results of the research in the field in 2003 and 2004.

HYDRIDES: STRUCTURAL STUDIES

Metallic hydrides absorb reversibly hydrogen near ambient pressure and room temperature. These remarkable properties lead to both fundamental research and application development in the frame of energy storage. To localize hydrogen atoms within the metallic matrix, to study magnetic structures of the resulting hydrides, neutron diffraction is a crucial technique. The first **Highlight** below is partly dedicated to the (Zr,Ti)Ni system, a potential compound for hydrogen storage, partly to the $\text{YFe}_2(\text{H}_y\text{D}_{1-y})_4$ system. By using different elaboration techniques, two different crystallographic forms of the same solid solution $\text{Ti}_{0.64}\text{Zr}_{0.36}\text{Ni}$ are available at room temperature, which exhibit different hydrogenation properties. An accurate description of the α (cubic), β and γ (orthorhombic) $\text{Ti}_{0.64}\text{Zr}_{0.36}\text{Ni}$ hydrides has been obtained through the determination of hydrogen Wyckoff positions in the crystal structure(s). In a more fundamental point of view, the magnetic properties of the Laves phases $\text{YFe}_2(\text{H}_y\text{D}_{1-y})_{4.2}$ have been carefully studied, as a function of temperature but also depending of the nature of the hydrogen atoms (H or D), showing unexpected isotopic effects on the magnetic behaviour.

[Collaborations: Laboratoire de Chimie Métallurgique des Terres Rares - CNRS, Thiais]

BIOMATERIALS: STRUCTURAL STUDIES

Synthetic hydroxyapatite (HA) is one of the most important bioceramics used in dentistry and orthopaedic surgery. In order to explain the higher bioactivity of the silicon-substituted hydroxyapatite (SiHA), synthetic HA and SiHA have been structurally studied by neutron scattering. The Rietveld refinements have shown that the final compounds are oxy-hydroxyapatites, when obtained by solid-state synthesis under air atmosphere. By using neutron diffraction, the substitution of P by Si into the apatite structure has been corroborated in these compounds. Moreover these studies also allowed to understand the better bioactive behaviour of SiHA in terms of higher thermal displacement parameters of the H located at the (4e) site (see **Highlight**).

FERROELECTRICS MATERIALS

Morphotropic phases in giant piezoelectric/dielectric lead-based compounds in bulk and thin films: correlation between chemical disorder and polar ordering

Insulating perovskite solid solutions are of tremendous technological importance due to their exceptional piezoelectric and dielectric properties. Up to date, the largest electromechanical and dielectric responses have been found in PbTiO_3 -based alloys -- PZT [$\text{Pb}(\text{Zr},\text{Ti})\text{O}_3$], PMN-PT [$\text{Pb}(\text{Mg},\text{Nb},\text{Ti})\text{O}_3$], PZN-PT [$\text{Pb}(\text{Zn},\text{Nb},\text{Ti})\text{O}_3$] -- in a large temperature range but in a narrow composition range, known as the morphotropic phase boundary (MPB). In this context PSN-PT [$\text{Pb}(\text{Sc},\text{Nb},\text{Ti})\text{O}_3$] is of peculiar importance due to the fact that this alloy exhibits the highest piezoelectric constant ever reported and chemical ordering of Sc / Nb / Ti cations via long time annealing is known to have strong consequences on the piezoelectric properties. When decreasing the Ti composition across the MPB, the overall sequence of crystal structures deduced from the analysis of both neutron and high resolution X-ray diffraction data on PSN-PT is: "Tetragonal - Monoclinic C - Monoclinic B - Rhombohedral". From theoretical calculations this rather unusual scheme (Monoclinic C and Monoclinic B phases observed, instead of Monoclinic A) has been shown to exist only if the samples "deviate" from the perfectly homogeneous and disordered situation, in the form of chemically-ordered regions.

In the case of films with MPB compositions the structural evolutions show a competition between bulk monoclinic symmetries and substrate-induced tetragonal distortion which can result, depending on the composition of the substrate (STO or MgO) and the thickness of the films (between 50nm and 500nm), in the disappearance of phases or large shifts for the critical temperature value, with strong consequences on the piezo/dielectric properties.

[Collaboration : SPMS - Ecole Centrale, Paris ; L. Bellaïche, Arkansas University, USA; Y. Uesu, Waseda University, Tokyo, Japan]

[R. Haumont et al, PRB 68 (2003) 014114; PRB (2005)]

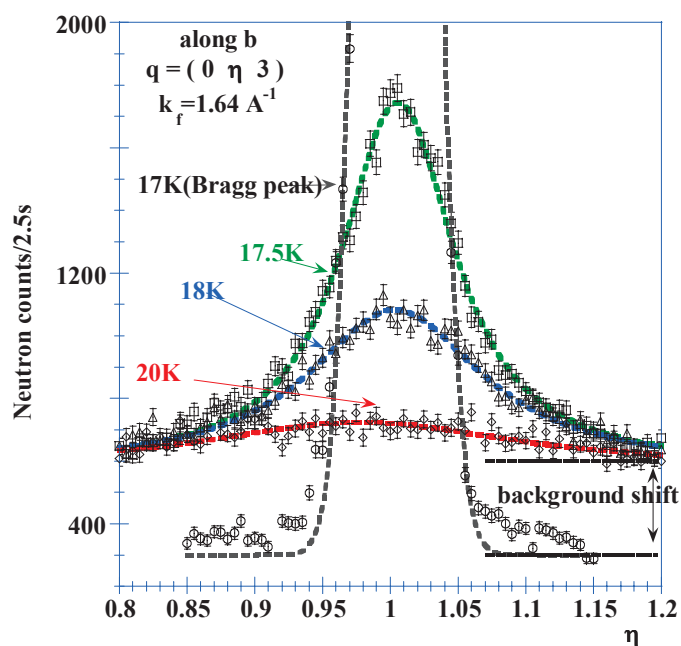
MOLECULAR CRYSTALS: CH₃ AND H DYNAMICS

Investigating the interplay of crystal structure and rotational dynamics of methyl groups is of crucial importance to understand the phase transitions that undergo methylated compounds in the solid state. Such a study is presented (see **Highlight**) in the case of the 4-methyl N-oxy pyridine, **C₅H₄NO[CH₃]**, which exhibits two structural phase transitions below room temperature (RT).

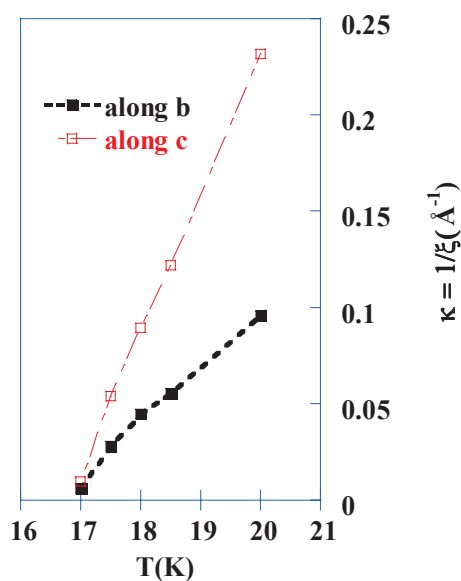
Lithium acetate (LiCH₃COO,2H₂O) is another prototype system to investigate this interplay. The roles of H and/or D on methyl rotation was evidenced in lithium acetate comparing the neutron diffraction data obtained with either fully hydrogenated, either fully deuterated, either "mixed" (CH_{3-x}D_x) systems. Whatever the temperature, the crystal structure of LiCH₃COO,2H₂O is orthorhombic, with *Cmmm* symmetry, and free rotation observed for methyl groups. Neutron diffraction applied to the partially deuterated analogues, LiCD₃COO,2D₂O has evidenced a crystal phase transition from *Cmmm* to *Pman*, with CD₃ groups ordered at low temperature. The *Cmmm* to *Pman* transition is observed at T_C= 17K (x = 3), T_C= 14K (x = 2) and T_C = 6K (x = 1). According to symmetry analysis the structural transition is predicted to occur at the Y *Cmmm* space group zone boundary point. This has been effectively observed in LiCD₃COO,2D₂O, with pre-transitional anisotropic diffuse neutron scattering measured above T_C, condensing into the (013) Bragg peak at T_C and (013) quasielastic scattering also measured above T_C, associated to a life-time of correlated domains (≈10⁻⁶s) which in turn diverges at T_C. Another feature observed at the transition, is a strong reduction of the incoherent elastic background. Finally, anomalies in the energy-scan of a phonon measured at the zone boundary and at T_C can be understood in the frame of an order-disorder-displacive mechanism.

[Collaboration: LADIR, Thiais, F. Fillaux; LLB: A Cousson, M. Quilichini, P. Teles, PhD]

[B. Nicolai, A. Cousson and F. Fillaux Chem. Phys. **290** (2003) 101-120].



Pre-transitional neutron diffuse scattering observed in fully deuterated lithium acetate, at the expected transition location in reciprocal space, for temperatures just above T_C = 17K, along the **b** direction.



Anisotropic thermal variation of the Half Width at Half Maximum (HWHM-κ), measured along the two high-symmetry directions (**b, c**)

Crystal structures and proton dynamics in potassium and cesium hydrogen bistrifluoroacetate salts with strong symmetric hydrogen bonds

The crystal structures of potassium and cesium bistrifluoroacetates, $MH(CF_3COO)_2$ with $M= K$ or Cs , were determined at room temperature and at 20K and 14K, respectively, with the single crystal neutron diffraction technique, utilising the four circle diffractometer 5C2 at LLB. There is no visible phase transition. For both crystals, the trifluoroacetate entities form dimers linked by very short hydrogen bonds lying across a centre of inversion (Figure 1). Any proton disorder or double minimum potential can be rejected. The inelastic neutron scattering spectral profiles in the OH stretching region between 500 and 1000 cm^{-1} previously published [F. Fillaux *et al*, Chem. Phys. 158(1991)113] were reanalyzed. The best fitting potential has the major characteristics already reported for potassium hydrogen maleate [F. Fillaux *et al*, Chem. Phys. 244(1999)387], composed of a narrow well containing the ground state and a shallow upper part corresponding to dissociation of the hydrogen bond upon excitation of the OH stretching mode. [Collaboration: F. Fillaux, LADIR, Thiais; A Cousson, LLB; J.F.R. Archilla, Sevilla, Spain; J. Tomkinson, RAL, UK]

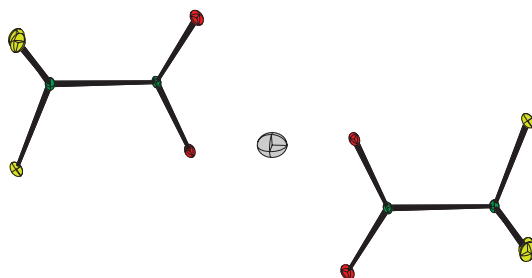


Figure 1. Schematic representation of the centrosymmetric dimers in the $KH(CF_3COO)_2$ crystal at 14K

MAGNETIC STRUCTURES IN INTERMETALLIC COMPOUNDS

$LaFe_{11.4}Si_{1.6}$

Crystallographic and magnetic structures of giant magnetocaloric intermetallic compound $LaFe_{11.4}Si_{1.6}$ have been studied by means of neutron powder diffraction. Rietveld analysis indicates that Si atoms substitute for Fe atoms randomly on the two different Fe sites of the cubic $NaZn_{13}$ -type structure. All spins in the unit cell are aligned ferromagnetically with the Fe^I (8b) moment smaller than the Fe^{II} (96i) one. The long-range FM (FM = FerroMagnetic) ordering induces a drastic expansion of the lattice and the coexistence of large and small volume phases near the Curie temperature T_C . Even in the FM state, the lattice expansion still correlates strongly with the spontaneous magnetic moment, marked by a large positive magneto-volume coupling constant [$1.14 \cdot 10^{-8} cm^6 emu^{-2}$]. From the temperature dependence of Fe-Fe bond lengths, it was suggested that the magnetic exchange interaction between the clusters (each formed by a central Fe^I atom and 12 surrounding Fe^{II} atoms) plays an important role in the magnetic properties of $La(Fe_{1-x}Al/Si_x)_{13}$.

F. Wang, G-J. Wang, F-X. Hu, A. Kurbakov, B-G. Shen, Z-H. Cheng - Strong interplay between structure and magnetism in the giant magnetocaloric intermetallic compound $LaFe_{11.4}Si_{1.6}$: a neutron diffraction study - *J.Phys.: Condens.Matter* 15 (2003) 5269-5278 .

$U(Pd_{1-x}M_x)_2Ge_2$

The crystal and magnetic structures of $U(Pd_{1-x}M_x)_2Ge_2$ compounds with $M = Fe, Co, Ru$ has been studied by neutron powder diffraction [G4.2 and G6.1 LLB-diffractometers] and μSR . The effects of M doping and external applied pressure on the crystal and magnetic structures were compared. It was found that even at small M-doping level the magnetic structure drastically changes, while the values of the lattice parameters and interatomic distances change only slightly. In contrast, high external pressure modifies the crystal structure more significantly, while the magnetic structure remains the same. The drastic changes of magnetic structure of $U(Pd_{1-x}M_x)_2Ge_2$ compounds with increased M doping could then result from modifications of the RKKY indirect exchange interactions due to variation of conduction-electron number per U atom, rather than from lattice contraction.

V.V. Sikolenko, E.V. Pomjakushina, V.Yu. Pomjakushin, A.V. Gribanov, U. Zimmermann, A.I. Kurbakov, D.P. Kozlenko, I.N. Goncharenko, A.M. Balagurov - Modulated spin-density waves in uranium intermetallic compounds with $ThCr_2Si_2$ structure - *Physica B: Condensed Matter* 350 (2004) 163-166.

HoFe₄Ge₂

The re-entrant magneto-elastic transition of the AFM (AFM = AntiFerroMagnetic) HoFe₄Ge₂ compound has been studied by neutron powder diffraction at D1B, D2B, G4.1 and G4.2 2-axis diffractometers as a function of temperature. The magnetic phase diagram is complex, including three wave vectors (\mathbf{q}_{10} ; \mathbf{q}_{20} ; \mathbf{q}_{1t}) and three magnetic transitions, two of them occurring simultaneously with a structural change at $T_C = T_N = 52\text{K}$ and $T_C = T_{ic1} = 15\text{K}$ respectively, the third being purely magnetic at $T_{ic2} = 40\text{K}$. From high [HT] to low [LT], via intermediate [IT] temperatures, the sequence of phases is: $P4_2/mnm$ (HT) $\setminus T_C = T_N = 52\text{K} \setminus Cmmm$ (IT) ; $\mathbf{q}_{10} = (0, \frac{1}{2}, 0) \setminus T_{ic2} = 40\text{K} \Rightarrow \mathbf{q}_{20} = (0, q_y, 0) \setminus T_C = T_{ic1} = 15\text{K} \setminus P4_2/mnm$ (LT); $\mathbf{q}_{1t} = (0, \frac{1}{2}, 0)$. The first transition is of second order while the latter two of first order. The magnetic structures described by the wave vectors (\mathbf{q}_{10} ; \mathbf{q}_{20} and \mathbf{q}_{1t}), where the components are referred to the reciprocal basis of the conventional Cmmm cell, correspond to canted multi-axial arrangements. Solving the magnetic structures of all the phases appearing in this complex situation, arising from competing ordering mechanisms and anisotropies of the underlying sublattices, has been only possible via high-resolution neutron powder diffraction data and simulated annealing data treatment.

P. Schobinger-Papamantellos, J. Rodríguez-Carvajal, G. André, C. Ritter and K. H. J. Buschow - Re-entrant magneto-elastic transition in HoFe₄Ge₂ a neutron diffraction study - *JMMM* 280 (2004) 119-142

MAGNETIC STRUCTURES IN IONIC COMPOUNDS

Among ionic compounds, transition metal oxides attract a lot of interest from the solid-state chemist community, due to “remarkable” properties of some of these materials, such as manganese perovskites and ferroelectrics. Magnetic properties of “other” oxides are also very interesting, showing for instance frustration effects (pyrochlore-type oxides with antiferromagnetic interactions...). Among them, the geometrically frustrated pyrochlore system, **Tb₂Ti₂O₇**, offers the very intriguing case of a spin liquid state for large classical spins, persisting down to very low temperatures ($\leq 70\text{mK}$), well below the energy scale of antiferromagnetic interactions given by the Curie-Weiss constant (-19K). In the liquid state, Tb³⁺ magnetic moments fluctuate down to $T \approx 0\text{K}$, being strongly correlated in a large T range [0-100K], yielding a liquid-type peak in the neutron diffraction patterns, the position of which corresponds to first neighbours distances. In bulk samples (powders), we previously observed the “crystallization” of the spin liquid under high pressure, namely the onset of long range antiferromagnetic order below $T_N = 2.1\text{K}$ (Nature 2002). We have now performed neutron diffraction experiments on oriented **Tb₂Ti₂O₇** single crystals (PRL 2004, in press), combining extreme conditions: high pressures (2.8GPa), anisotropic stress (0.3GPa), low temperature (0.1K) and magnetic field (7T). These new measurements allow to clarify the role of pressure. The isotropic pressure component enhances the exchange interactions between the fluctuating spins in the spin liquid state above T_N . Applying additional uniaxial stress induces magnetic order, and one can tune both T_N and the ordered terbium magnetic moment by varying the orientation of the stress relative to the crystal structure. The stress is then more efficient along the [110] direction, suggesting that it relieves the frustration by creating uncompensated bonds of near neighbour Tb³⁺ spins. Under magnetic field, the pressure induced AF structure transforms into a non collinear ferromagnetic structure at 0.6T and the non-collinearity persists up to 7T. We performed a quantitative structure analysis, showing that a small field reorients tetrahedra of strongly coupled Tb³⁺ spins, whereas much higher fields are needed to align spins in a tetrahedron. These measurements provide a key to understand and control the mechanisms which govern the stability of anomalous magnetic phases in highly frustrated magnets.

[Collaboration: I. Mirebeau, I. Goncharenko, A. Gukasov, A. Cousson, LLB; G. Dhalle, A. Revcolevschi, Orsay University]

Hydroxysulfates of 3d-elements have been carefully studied by mineralogists, where the principal interests were the identification of the crystal phases and the mechanism(s) of their formation with respect to their geographical location. Only the crystal structures of the most abundant forms have been characterized, and there are more phases that are not characterized due to the lack of single crystals in the natural sources of sufficient purity and quality. With the advances in hydrothermal synthesis, some of these missing links could be realized in the laboratory and on a shorter time scale. Furthermore, compounds prepared by hydrothermal method in the laboratory allow one to study the properties of pure samples, whereas samples from the mineral source are usually quite complex due to the presence of mixtures or traces of several cations and anions. In the case of transition metal hydroxysulfates, studies of their magnetic properties are sparse due to the low purity of samples from the mineral source. In the case of copper hydroxysulfates, hydrothermal synthesis gave two compounds that are isostructural with the corresponding minerals, **antlerite**

Cu₃(OH)₄SO₄ and **brochantite Cu₄(OH)₆SO₄**. No other phase was obtained under all the experimental conditions attempted. For **M = Mn, Co** and **Ni**, numerous new compounds have been obtained and the isostructural **M₃(OD)₂(SO₄)₂(D₂O)₂** family has been investigated by neutron powder diffraction. The magnetic structures of all these ionic compounds have been obtained (see **Highlight**). As magnetic structure determination in insulating compounds was recently renewed by ab-initio methods able to predict the fundamental states from the super-exchange (M-O-M') and/or super-super-exchange M-O-O-M' interactions, the next step in the present work will be to analyse the topology of magnetic exchange interactions and minimize the classical magnetic energy in each of the studied geometries [SIMBO and ENERMAG computing programs].

MANGANITES: CHARGE (CO), ORBITAL (OO) AND SPIN ORDERING

The perovskite manganites Ln_{1-x}A_xMnO₃ (Ln = La, Y or Rare Earth, A = alkaline earth) became subjects of considerable research effort because of their prospects as materials of colossal magnetoresistance (CMR) or metallic conductors with spin polarized carriers. These materials are interesting also from a fundamental viewpoint: in the manganites the charge, spin, and lattice degrees of freedom are strongly coupled together, leading to a delicate balance of interactions that gives rise to a rich variety of physical phenomena in condensed matter science. Recently, much interest was attracted to unusual phase separation processes: in mixed valent manganese-oxides, within specific electronic doping ranges, the ground state, is intrinsically inhomogeneous, usually composed of ferromagnetic metallic (FM-M) and charge ordered, orbital ordered (CO/OO) antiferromagnetic insulating (AFM-I) domains that co-exist and compete at a nano- and/or sub-micrometer scale.

For several years already, a strong collaboration does exist between CRISMAT [ENSICAEN] and LLB, with both macroscopic [magnetic and transport properties] and microscopic techniques [X-ray, neutron powder diffraction (NPD) and transmission electronic microscopy (TEM)] systematically used on the same samples. C. Autret's PhD [2002, Université de Caen] focused on the "half-doped" manganites, characterized by a Mn³⁺:Mn⁴⁺ = 1:1 ratio, with **Pr_{0.5}Sr_{0.5-x}Ba_xMnO₃** and **Pr_{0.5}Sr_{0.5-x}Ca_xMnO₃** systems carefully investigated (crystal and magnetic phase diagrams) and on **Pr_{2-x}Ca_xMnO₄** compounds (1.5 ≤ x ≤ 1.75), n = 1 member of the Ruddlesden-Popper family (K₂NiF₄-type structure), in order to study the effect of "dimensionality" on the physical properties (magnetism, charge order, CMR). A new common PhD work started in early 2004 [M. Giot], devoted to Bi_{1-x}A_xMnO₃ manganites (A = Ca, Sr) and charge ordering (CO) properties within.

No CO is present in the **Y₂Ba₂Mn₄O₁₁** manganite, a "CO/OO" system (only Mn³⁺ ions) for which crystal and magnetic structures have been investigated (see **Highlight**).
[Collaboration: LLB, LPCES, Orsay]

From neutron powder diffraction investigations and electrical resistivity measurements on **¹⁵²Sm_{0.55}Sr_{0.45}MnO₃** (SSM) and **(Nd_{0.545}Tb_{0.455})_{0.55}Sr_{0.45}MnO₃** (NTSM) manganites, replacement of the "rare-earth" cation while leaving <r_A> unchanged (Nd and Tb contents in the latter composition are such that the average radius of the A cation <r_A> in the two compounds is the same) was shown to have practically no effect; indeed, both compounds are metals at low temperatures, have the same crystal structure from liquid-helium to room temperature, and exhibit the same pattern of structural distortions at the onset of magnetic ordering. Magnetic moments of Mn ions in both compositions are ferromagnetically ordered at low temperatures, with T_C = 122 and 90 K for the SSM and NTSM, respectively. Below 80 K, the rare-earth cation moments in NTSM undergo additional ordering.

In contrast to compositions that are close in Sr concentration (x_{Sr} = 0.4, 0.5), which feature a phase-separated state with a mixture of the the FM-M [ferromagnetic metallic] and AFM-I [antiferromagnetic insulating] phases in **¹⁵²Sm_{1-x}Sr_xMnO₃** manganites, the ground state of both studied compositions with x_{Sr} = 0.45 is uniformly ferromagnetic and metallic. However, Oxygen isotope substitution, ¹⁶O → ¹⁸O, was shown to bring about a substantial change in the **¹⁵²Sm_{1-x}Sr_xMn¹⁶O₃** phase diagram in the intermediate region 0.4 < x < 0.6, inducing for instance a phase-separated state in the case of **¹⁵²Sm_{0.55}Sr_{0.45}Mn¹⁸O₃**.

[Collaboration: LLB, A. Kurbakov; Petersburg Nuclear Physics Institute, Moscow State University, Russia]. Interplay between crystal structure(s) and physical properties in transition metal oxide compounds with strong electronic correlations is also evident in **Ca_{2-x}Sr_xRuO₄**, **La_{1-x}Sr_xTiO_{3+δ}** and **La_{1-x}Sr_{1+x}MnO₄** systems, as studied by M. BRADEN's team at Cologne University.

The phase diagram of the $\text{Ca}_{2-x}\text{Sr}_x\text{RuO}_4$ exhibits an astonishing variety of physical phenomena in view of the fact that one changes only the radius of the earth-alkali ion. Through the smaller radius of Ca compared to Sr, structural distortions are induced, which consecutively reduce the electronic band widths. In this sense the electronic correlations get enhanced with increasing Ca content. The structural-electronic coupling in these layered ruthenates may be resumed as following:

1. a first rotational transition is related with a change of the Fermi-surface topology,
2. an additional tilting of the RuO_6 -octahedra reduces the tendency towards ferromagnetism at intermediate Ca content. Metamagnetism in such compounds is related with a change in orbital occupation as evidenced by changes in the RuO-bond lengths,
3. different tilt and rotation stacking schemes yield different magnetic ground states due to orbital ordering effects,
4. the metal insulator transition finally is associated with a pronounced flattening of the octahedron.

A direct relation between minor structural distortions and the magnetic as well as the electronic properties could also be established for $\text{La}_{1-x}\text{Sr}_x\text{TiO}_{3+\delta}$; in particular it has been shown that pure LaTiO_3 exhibits orbital ordering and is not a realisation of an orbital liquid model.

Layered manganates, $\text{La}_{1-x}\text{Sr}_{1+x}\text{MnO}_4$ were found to exhibit a strong structural variation both with temperature and with doping, which arise from a change in the orbital occupation. When going from the undoped antiferromagnet, LaSrMnO_4 , to the CE-type ordered material at half doping, $\text{La}_{0.5}\text{Sr}_{1.5}\text{MnO}_4$, the e_g orbitals appear to flip from the c-axis into the a,b-planes. Similar effects are studied in layered cobaltates.

PHASE TRANSITIONS WITH ELECTRON LOCALIZATION OR TRANSFER

In organic systems made of stacks of potentially donors and acceptors of electrons, the properties of the electrons, nearly always coupled with the lattice, are at the origin of very rich phase diagrams. Two cases of such transitions are presented in this report.

Spin-Peierls ground state in $(\text{TMTTF})_2\text{PF}_6$ (Highlight)

A first study of the Spin-Peierls (SP) transition in the $(\text{TMTTF})_2\text{PF}_6$ organic conductor by elastic neutron scattering has been achieved at LLB. Indeed, at 18K, a Spin-Peierls [SP] transition occurs: two electrons (one per dimer of TMTTF molecules) form a localized pair, leading to a $S = 0$ state through a tetramerization of the organic stacks. Because of such electron-lattice coupling, this non-magnetic state is detected by a superstructure Bragg peak ($\frac{1}{2} \frac{1}{2} \frac{1}{2}$). When compared with other similar organic systems where a SP transition occurs, the intensity of this satellite reflection appears very small, several explanations are proposed to account for the weakness of the 3D-SP amplitude of distortion in the $(\text{TMTTF})_2\text{PF}_6$ system.

[Collaboration: LPS Orsay; LLB]

Neutral-to-Ionic phase transition under pressure (Highlight)

The prototype compound TTF-CA exhibits a phase transition from a high temperature Neutral paraelectric phase (N) to a low temperature Ionic and ferroelectric phase (I) where an electron is transferred from a donor to an acceptor molecule. This charge transfer occurs together with a dimerization, so it can be detected by neutron scattering through a structural distortion inducing a change in the symmetry between the (N) and (I) phases. A Bragg peak, forbidden in the (N) phase, is lighted in the (I) phase. The "Pressure, Temperature" phase diagram has been compared to a Gas-Liquid-Solid phase diagram. Recently, a study under pressure on a similar compound, (BEDT-TTF)-(ClMeTCNQ), reveals that the (N)-(I) transition which does not exist at ambient pressure, is induced near $T = 0$ K, by a moderate pressure: 2Kbar. When compared to TTF-CA, the phase diagram of this new compound shows both similar and different properties, the most interesting feature is that this compound shows an example of transition near 0K, so it appears as a quantum limit case.

[Collaboration: GPMS, Université de Rennes ; LLB ; ILL]

COMPOSITE SYSTEMS

Phonon studies have always represented an important activity in the laboratory. They often display interesting dynamic signature(s) of the structural transitions. The phonons are also measured in more complex compounds. In the composites, they are the proof that this system has characteristic acoustic modes, and in the superconductors, they underline a strong electron-phonon coupling.

The properties of the incommensurate composites are fascinating. These systems are built from at least two interpenetrating subsystems with incommensurate periodicities in at least one crystallographic direction. The resulting Bragg peaks are then indexed in a super-space: some of them are characteristic of each subsystem, the others, the satellites, are characteristic of the inter-modulation. The lattice dynamics appears also very rich. Two such composites have been investigated at LLB: Alkane-Urea and MnSi_x .

Alkane-Urea (Highlight)

In that case, the host network (hexagonal symmetry) is made of honeycomb-like channels of helical ribbons of urea molecules in which linear guests, alkane molecules, are packed in a 1D arrangement. Under normal pressure, an hexagonal to orthorhombic transition occurs at $T=150\text{K}$ in the basal plane: a neutron diffraction signature is the (2 2 0) Bragg peak splitting and Brillouin scattering shows a splitting of the longitudinal phonons modes. At 5Kbar, the “same” transition occurs at 225 K, but even if the symmetry at low temperature is orthorhombic, the metric remains hexagonal: no splitting of the Bragg peak, nor of the sound velocity are observed. Alkane-Urea is the first example where ordering in self-organized materials occurs without any significant deformation of the host matrix.

[Collaboration: GPCM, Université de Rennes ;LLB ; Universidad del Pais Basco, Bilbao, Spain]

MnSi_x

The MnSi_x system has the advantage to present much less disorder than alkane-urea. So, neutron inelastic scattering has successfully allowed the determination of the different long-wavelength collective phonons originating from every kind of Bragg peaks: two low frequency optical phonon branches characteristic of both Mn and Si subsystems, and **one acoustic branch characteristic of the composite** (the same one visible by Brillouin scattering but on a much larger q-range). We must underline that it is the first time that an acoustic mode of a composite is measured by neutron scattering. The main argument at the origin of the attribution of the different branches is based on the q-dependence of the intensity of the modes. As q or the energy increases, the scattered neutron intensity is progressively transferred from the acoustic mode to the optic ones.

[Collaboration: L. Bourgeois (LLB), P. Bourges (LLB), R. Currat (ILL), J. Etrillard (Université de Rennes), S.B. Vakhrushev (St. Petersburg), S.V. Ordin (St. Petersburg)].

SUPERCONDUCTING MATERIALS

Phonon Anomalies in High T_C Superconductors related to Charge Stripe Order

The Karlsruhe group has continued its long-standing effort to explore the phonon properties of perovskite materials, i.e. primarily cuprates, but also manganites and nickelates. It has been established that the lattice dynamics of the undoped parent compounds is governed by strong Coulomb forces typical of ionic insulators. On doping, however, a particular kind of phonon modes, i.e. the metal-oxygen bond-stretching vibrations, shows strong deviations from the classical behaviour. It has been long conjectured that this anomalous behaviour is related to the various charge ordering phenomena occurring. Recent results on $\text{La}_{1.48}\text{Nd}_{0.4}\text{Sr}_{0.12}\text{CuO}_4$ (see **Highlight**) have provided strong support for this view. When doped with Sr or Ba, the La_2CuO_4 system becomes superconductor. But if the hole doping rate is close to 1/8, the holes tend to segregate into stripes that separate antiphase AF domains and the superconductivity is suppressed. Static stripe order has been found in $\text{La}_{1.48}\text{Nd}_{0.4}\text{Sr}_{0.12}\text{CuO}_4$ and $\text{La}_{1.875}\text{Ba}_{0.125}\text{CuO}_4$. The new idea was that a tendency to hole segregation into stripes may also exist in the superconductor phase, but instead of being static, these stripes should be dynamic. This was demonstrated in $\text{La}_{1.48}\text{Nd}_{0.4}\text{Sr}_{0.12}\text{CuO}_4$ where the damping of a peculiar bond-stretching phonon has been found to be maximum at the precise q-position of the static stripe. This is the signature of strong electron-phonon coupling. The thermal evolution of the same phonon mode (half bond-stretching) in YBCO seems to confirm a tendency to dynamic stripe order also in this compound.

[Collaboration: Forschungszentrum, Karlsruhe; LLB; Nagoya University, Japan; Tohoku University, JJapan]

Ab Initio Study of Carbon substitution in the superconductor $\text{Mg}(\text{B}_{1-x}\text{C}_x)_2$

The effects of C substitutions in MgB_2 are studied within the two-band model in the Eliashberg formulation. The B-B stretching mode frequency and the partial densities of states $N_N^\sigma(E_F)$ and $N_N^\pi(E_F)$, calculated at various x values from first-principles density functional methods, are used as input of this model. In particular, the predicted hardening of the stretching mode with increasing x, agrees pretty well with the Raman data. The prefactor in the Coulomb pseudopotential matrix, μ , and the interband scattering

parameter, Γ^{opt} , are taken as the only adjustable parameters. The C content dependence of T_C and of the gaps Δ_σ and Δ_π experimentally measured in single crystals, indicates an almost linear decrease of μ on increasing x , with an increase in interband scattering that makes the gaps merge at $x=0.132$. However, further ab-initio studies are required to improve the agreement with experimental data.
[Hamid Moudden, LLB]

PHASE TRANSITIONS: LATTICE DYNAMICS UNDER PRESSURE

Among the twelve crystalline phases known presently, **ordinary ice Ih** shows two distinct anomalies which have been extensively studied in the past. Ice Ih has a negative thermal expansion coefficient below 70 K, and under pressure applied at low temperatures (<130 K), ice Ih transforms to high density amorphous ice (HDA). The microscopic origin for these two phenomena has remained unclear, though it was suspected that the key for its understanding lies in a detailed study of the lattice dynamics of ice.

In a recent study (it is the first detailed investigation of the pressure dependence of the phonons in ice), we have investigated the phonon dispersion of ice Ih under purely hydrostatic pressure by coherent inelastic neutron scattering. The experiments were carried out at the 1T1 triple axis spectrometer using the LLB gas cell up to 0.5GPa and fluid nitrogen as pressure transmitting medium.

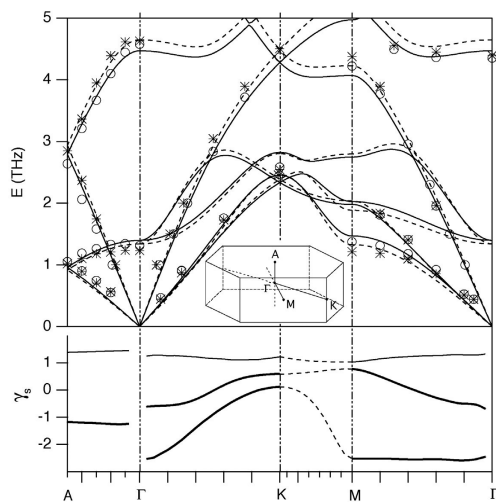


Figure 2a. Upper: Phonon dispersion of low-energy branches of ice Ih ($T=140$ K) at 0.05GPa (circles) and 0.5GPa (stars). The lines through the data are fits to a Born-von- Kármán model. Lower: mode Grüneisen parameters $\gamma_s(q)=-\partial \ln E_s(q)/\partial \ln V$ of transverse and longitudinal acoustic branches (thick and thin lines, respectively).

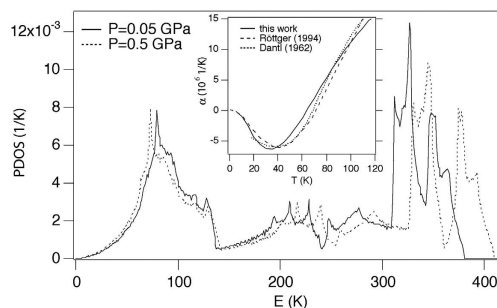


Figure 2b: Phonon density of states (PDOS) of ice ($T=140$ K) at 0.05GPa and 0.5GPa (main figure) and reconstructed thermal expansion coefficient compared to literature data (inset).

The measurements revealed a pronounced softening of various low-energy phonon branches, in particular the TA modes along [100] (Γ -M) with polarisation in the hexagonal plane (Figure 2a). The data were fitted to a Born-von-Kármán model, which allowed calculating the phonon density of states as well as the thermal expansion coefficient from the measured mode Grüneisen parameters (Figure 2b). The extrapolation of the model parameters to higher pressures indicates a violation of Born's stability criteria at a pressure of ~ 2 GPa which appears to be associated with the observed pressure-induced amorphisation (PIA). PIA seems therefore to be a consequence of a "mechanical melting" of ice under compression.

These investigations revealed hence that the negative thermal expansion coefficient and the PIA of ice Ih have their common origin in an instability of the lattice. Since PIA occurs in various other compounds (some of them of geophysical importance, such as SiO_2), our measurements contribute to a better understanding of this phenomenon in general.

[Collaboration : LLB ; Université P&M Curie, Paris; Université de Cologne, RFA]
[Th. Strässle, M. Saitta, S. Klotz & M. Braden, Phys. Rev. Lett. 93, 225901 (2004)]

PHASE TRANSITIONS: NEUTRON DIFFRACTION UNDER VERY HIGH PRESSURE

As for experimental conditions, non "ambient" temperatures and samples under controlled atmospheres are easily available with neutron scattering. A "new" parameter is also more and more used in neutron experiments: "high pressure". And, in the recent years, neutron diffraction experiments under very high

hydrostatic or quasi-hydrostatic pressures became available at the LLB, either with powder or single-crystal samples. At the present moment, the LLB disposes of higher pressures (up to 50GPa) than any other neutron source in the world. New “hybride” pressure cells allow us to carry out combined X-ray and neutron studies under pressure on the same sample.

The capabilities of the LLB pressure and neutron techniques have been demonstrated in the recent study of magnetic order in high-pressure **oxygen (Highlight)**.

1. Crystallographic Structures of austenitic and martensitic hydrides of $\text{Ti}_{0.64}\text{Zr}_{0.36}\text{Ni}$ intermetallic compound **14**
F. Cuevas, M. Latroche, A. Percheron-Guégan.
2. Giant H/D isotopic effect in $\text{YFe}_2(\text{H}_y\text{D}_{1-y})_{4.2}$ compounds **15**
V. Paul-Boncour, M. Guillot, G. André, F. Bourée, G. Wiesinger, A. Percheron-Guégan
3. Silicon doped hydroxyapatites **16**
D. Arcos, J. Rodríguez-Carvajal, M. Vallet-Regí
4. Simulated annealing on neutron and synchrotron powder diffraction DATA **18**
A. Carretero-Genevri, F. Damay, A. Cousson, W. Van Beek, J. Rodríguez-Carvajal
5. Magnetic structures of transition metal (Mn, Co, Ni, Cu) Hydroxysulfates **20**
S. Vilminot, G. André, M. Richard-Plouet, M. Kurmoo, F. Bourée-Vigneron, M. Ben Salah
6. Crystal and magnetic structures of the Mn^{3+} orbital ordered manganite $\text{Y}_2\text{Ba}_2\text{Mn}_4\text{O}_{11}$ **22**
L. Pinsard-Gaudart, C. Perca, A. Daoud-Aladine, M. T. Fernández-Díaz, J. Rodríguez-Carvajal
7. Spin Speierls ground state in $(\text{TMTTF})_2\text{PF}_6$ **24**
P. Foury-Leylekian, D. Le Bolloc'h, B. Hennion, S. Ravy, A. Moradpour, J.-P. Pouget
8. Neutral-to-ionic phase transition under pressure: towards the quantum limit **26**
M.H. Lemée-Cailleau, M. Buron, E. Collet, H. Cailleau, T. Luty, B. Ouladdiaf, F. Moussa, T. Hasegawa
9. Interactions in self-Assembled molecular crystals **28**
L. Bourgeois, B. Toudic, C. Ecolivet, P. Bourges, T. Breczewski
10. Phonon anomalies in high T_c superconductors related to charge stripe order **30**
D. Reznik, L. Pintschovius, M. Sato, M. Itoh, S. Iikubo, S. Yamada
11. Magnetic order in high-pressure oxygen **32**
I. Goncharenko, O. Makarova, L. Ulivi

CRISTALLOGRAPHIC STRUCTURES OF AUSTENITIC AND MARTENSITIC HYDRIDES OF $\text{Ti}_{0.64}\text{Zr}_{0.36}\text{Ni}$ INTERMETALLIC COMPOUND

F. Cuevas, M. Latroche, A. Percheron-Guégan.

LCMTR-UPR 209-ISCSA-CNRS, 2-8 rue Henri Dunant, F-94320, Thiais Cedex.

Collaborations : F. Bourée, LLB-CNRS, Saclay. P. Ochin, CECM-CNRS, Vitry sur Seine.

TiNi alloy is polymorphic. It exhibits a martensitic transition near room temperature between a cubic CsCl-type (austenite) and a monoclinic TiNi-type (martensite) structure. This transformation is at the origin of its shape memory effect. In addition, TiNi has good hydrogen storage properties under normal conditions of pressure and temperature. In austenitic form, TiNi absorbs 1.4 H/f.u. under atmospheric pressure. No plateau is observed in the pressure composition isotherm curve (PCI) showing that hydrogen is absorbed in solid solution [1]. Hydrogenation properties of the martensite form are unknown. By adjusting a partial substitution of Ti by Zr and by using different elaboration techniques (melt spinning and induction melting), we were able to stabilize the two different crystallographic forms at room temperature for the same composition: $\text{Ti}_{0.64}\text{Zr}_{0.36}\text{Ni}$. The austenitic phase exhibits hydrogenation properties close to those of cubic TiNi. The martensitic phase absorbs up to 2.8 H/f.u. and shows a pressure plateau ranging between 1 and 2.5 H/u.f. This plateau indicates the presence of two hydride phases in equilibrium. These results lead to the conclusion that hydrogenation properties of TiNi-type alloy are strongly influenced by the structural polymorphism [2] of the parent alloy.

Crystallographic structures of $\text{Ti}_{0.64}\text{Zr}_{0.36}\text{NiD}_{1.6}$, obtained from austenite and of $\text{Ti}_{0.64}\text{Zr}_{0.36}\text{NiD}_{1.3}$, $\text{Ti}_{0.64}\text{Zr}_{0.36}\text{NiD}_{1.8}$ and $\text{Ti}_{0.64}\text{Zr}_{0.36}\text{NiD}_{2.8}$, prepared from martensitic alloy have been studied by X-ray and neutron diffraction. Hydrogenation of the austenitic alloy $\text{Ti}_{0.64}\text{Zr}_{0.36}\text{Ni}$ does not change the CsCl-type structure of the metallic sublattice. The deuteride $\text{Ti}_{0.64}\text{Zr}_{0.36}\text{NiD}_{1.6}$ can be indexed with the space group $Pm\bar{3}m$ and deuterium atoms occupy 50% of the octahedral sites $3d$. Partial occupation of sites $3d$ seems related to a short distance (2.25 Å) between two neighboring sites $3d$. The cell volume increases of 10 % during hydride formation. In contrary to the binary compound TiNi that undergoes a tetragonal distortion after

absorption, Ti substitution by Zr seems to limit the appearance of such distortion.

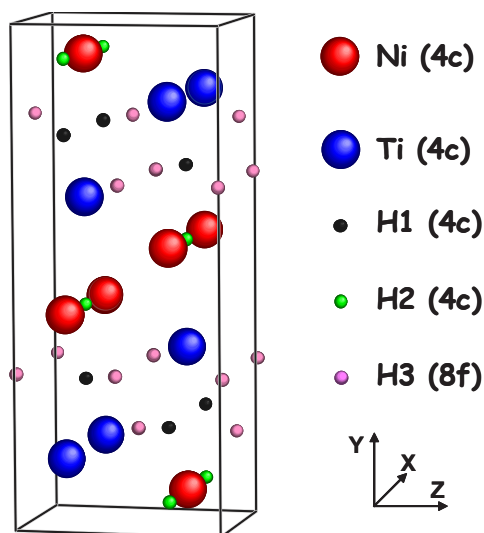


Figure 1. Structure of the martensitic-type hydrides $\beta\text{-Ti}_{0.64}\text{Zr}_{0.36}\text{NiD}$ and $\gamma\text{-Ti}_{0.64}\text{Zr}_{0.36}\text{NiD}_{2.5}$ (S.G. $Cmcm$). For the β phase, site H1 is fully occupied. In the γ phase, site H3 is fully occupied and site H2 is half filled (50%).

Hydrogenation of martensitic $\text{Ti}_{0.64}\text{Zr}_{0.36}\text{Ni}$ induces a symmetry change from a monoclinic TiNi-type to an orthorhombic CrB-type structure. Two hydride phases are clearly observed (S.G. $Cmcm$) with two different compositions $\text{Ti}_{0.64}\text{Zr}_{0.36}\text{NiD}$ and $\text{Ti}_{0.64}\text{Zr}_{0.36}\text{NiD}_{2.5}$. The first hydride (phase β) shows a cell volume increase of 5.4% and the second (phase γ) of 12.2%. For the β phase, hydrogen occupies all the tetrahedral sites $4c$ (H1 in Figure 1) whereas in the γ phase, hydrogen totally fills tetrahedral sites $8f$ (H3) and half fills pyramidal sites $4c$ (H2). This configuration is very similar to that observed for the compound ZrNi, that forms a stoichiometric γ hydride (ZrNiH_3) obtained by a complete filling of sites H2 and H3.

References

- [1] R. Burch, N. B. Mason, *J. Chem. Soc. Faraday Trans. I*, **75** (1979) 561.
 [2] F. Cuevas, M. Latroche et al., *J. Alloys Comp.*, **330-332** (2002) 250.

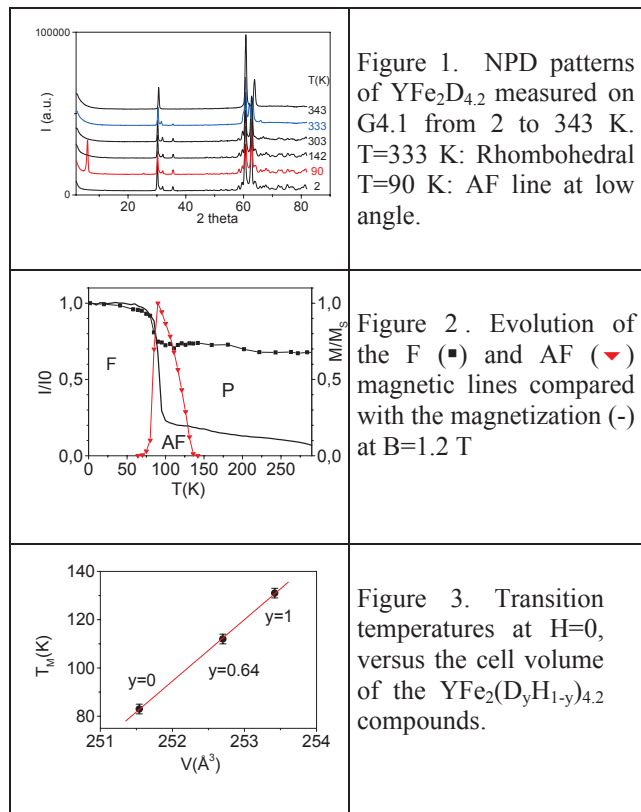
GIANT H/D ISOTOPIC EFFECT IN $\text{YFe}_2(\text{H}_y\text{D}_{1-y})_{4.2}$ COMPOUNDSV. Paul-Boncour¹, M. Guillot², G. André³, F. Bourée³, G. Wiesinger⁴, A. Percheron-Guégan¹¹ LCMTR, CNRS, 2 rue H. Dunant, 94320 Thiais Cedex, France² LCMI, CNRS-MPI, BP166, 38042 Grenoble Cedex 9, France³ LLB, CE-Saclay, 91191 Gif/ Yvette, France⁴ IFP, T.U. Wien, Wiedner Hauptstrasse 8-10, 1040 Vienne, Autriche

Hydrogen absorption in RM_2 ($R=\text{Y}$, Rare earth, $M=\text{Mn, Fe, Co}$) Laves phase compounds has been widely studied due to its strong effect on the electronic and magnetic properties of these compounds [1]. In YFe_2D_x deuterides, D absorption leads to a decrease of the Curie temperature and an increase of the mean Fe moment up to $x=3.5$ [2]. For $x=5$ a strong decrease of the Fe moments occurs, due to a predominant effect of the Fe-D bonding, which shift the Fe 3d band towards the valence band and leads to a strong decrease of the DOS at the Fermi level [3]. $\text{YFe}_2\text{D}_{4.2}$, which lies in the range of magnetic instability, displays a sharp first-order magnetic transition from a ferromagnetic state to low magnetic state at 83 K. Neutron powder diffraction (NPD) experiments were performed on 3T2 and G4.1 to determine both the nuclear and magnetic structures of $\text{YFe}_2\text{D}_{4.2}$. From 343 down to 303 K, a progressive lowering of the crystal symmetry from cubic (C15) to rhombohedral and then monoclinic structure is observed (Fig. 1). At 303 K $\text{YFe}_2\text{D}_{4.2}$ crystallizes in a primitive monoclinic space group P1c attributed to D order. This lowering of crystal symmetry leads to very different D neighbours distribution around each Fe site: 3.2 D for Fe1, 4.4 D for Fe2 and 5.2 D for Fe3. This nuclear structure remains down to 2 K, but a 0.55 % increase of the cell volume is observed around 90 K for the deuteride [4-5]. From 80 K to 132 K additional antiferromagnetic (AF) lines can be indexed with a doubling of the cell along b (Fig.1 and 2). Below 80 K, these AF lines disappear and a ferromagnetic (F) order is observed down to 2 K (Fig. 2). With the support of Mössbauer spectroscopy, the F-AF transition can be attributed to the collapse of the Fe3 moment which is close to the ferromagnetic instability. Above the F-AF transition, the magnetization curves show an

itinerant electron metamagnetic (IEM) behaviour as observed in RCO_2 compounds [6].

A partial or complete substitution of deuterium by hydrogen atom leads to a linear increase of the transition temperature from 83 up to 131 K (extrapolated at $H=0$) and to an increase of $0.4 \mu\text{B}$ of the saturation magnetization at 4.2 K.

$\text{YFe}_2(\text{D}_y\text{H}_{1-y})_{4.2}$ compounds have the same monoclinic structure than $\text{YFe}_2\text{D}_{4.2}$ ($y=1$) at 290 K, but the cell volume of the hydride is 0.75 % larger than for the deuteride due to strong zero point vibration effect. This cell volume expansion can explain the large isotopic effect (Fig. 3), since it has been observed for other IEM compounds that a volume increase stabilizes the ferromagnetism [7].



References

1. G. Wiesinger, G. Hilsher. Topics in Applied Physics. L. Schlapbach. Berlin, Springer-Verlag. **63** (1988) 285
2. V. Paul-Boncour, A. Percheron-Guégan, J. Alloys Comp., **293-295** (1999) 237
3. V. Paul-Boncour, S. Matar, Phys. Rev. B, (2004) in press
4. V. Paul-Boncour, G. André, F. Bourée, M. Guillot, G. Wiesinger, A. Percheron-Guégan, Physica B, **350**, 2004, e27
5. V. Paul-Boncour, M. Guillot, G. G. André, F. Bourée, G. Wiesinger, A. Percheron-Guégan, J. Alloys Comp. (2004) submitted
6. D. Gignoux and D. Schmitt, Handbook of the Physics and Chemistry of Rare Earths. J. Gschneidner, K. A. and J. a. L. Eyring Eds., Elsevier Science B.V. **20** (1995) 293
7. H. Wada, K. Yoshimura, G. Kido, M. Shiga, M. Mekata, Y. Nakamura, Solid State Comm., **65** (1988) 23

SILICON DOPED HYDROXYAPATITES

D. Arcos¹, J. Rodríguez-Carvajal¹, M. Vallet-Regí²¹ Laboratoire Léon Brillouin (CEA-CNRS), CEA- Saclay, 91191 Gif sur Yvette Cedex, France²Dpto. Química Inorgánica y Bioinorgánica, Ftd. Farmacia, UCM, 28040 Madrid, Spain

The use of implants for bone filling and replacement has acquired a great importance during the last three decades in the developed countries. Actually, the high development of our societies has led to an increase of the lifespan and, consequently, an increase of the osteoporosis incidence and other illness related with advanced ages. As an example, it is estimated that about 40% of asian and caucasian women older than 50 years will suffer an osteoporotic fracture. In this sense, the bioceramics for filling and restoring damaged bones and teeth are one of the most important topics in the field of orthopaedic and oral surgery.

Between the different bioceramics, the hydroxyapatite, $\text{Ca}_{10}(\text{PO}_4)_6(\text{OH})_2$, is the most important calcium phosphate used for bone replacement (1,2). From the point of view of the *biocompatibility*, the hydroxyapatite shows an excellent performance, due to its similarity with the mineral component of the bone. However its *bioactive behaviour*, that is, the ability to join to the living bone when they are implanted, is lower compared to other biomaterials such as bioactive glasses. One of the alternatives to improve the *bioactivity* of hydroxyapatite, is to incorporate silicon into the apatite structure (3). The experimental results have demonstrated the better bioactive behaviour of these *silicon doped* apatites, but the chemical and structural effects on the hydroxyapatite host matrix were not well known (4,5).

From these evidences, we have used powder neutron and X-ray diffraction techniques to carry out a deep structural characterization of these improved bioceramics. Structural analyses were carried out by combining X-ray and neutron diffraction (ND). The structure was refined by the Rietveld method.

Figure 1 shows a scheme of the HA structure. An important feature of neutron diffraction is that neutrons are highly scattered by H atoms. For this reason we can quantify, even if it is small quantity, the amount of H that takes part in the hydroxyl groups (OH^-) at the $4e$ position. Our results indicate that SiHA are more hydroxylated than non-substituted HA. That is, the $\text{OH}^-/\text{O}^{2-}$ ratio

characteristic of these compounds (6) when are treated at high temperature, is higher for SiHA.

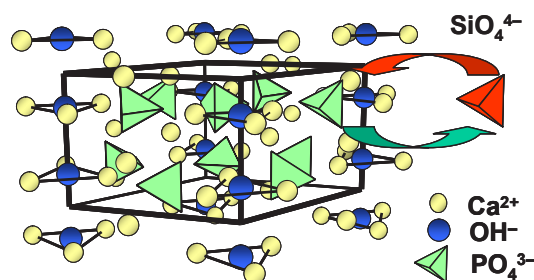


Figure 1. Structure of HA. The SiO_4^{4-} substitution for PO_4^{3-} in Si substituted hydroxyapatite is indicated.

These OH groups sited at the $4e$ Wyckoff position are one of the most important sites for the HA reactivity (7). Figure 2 shows the displacement ellipsoids for HA and SiHA calculated from the refined anisotropic displacement parameters. The thermal displacement of the H atom along the c -axis is more than twice for SiHA. The authors did not report on the static or dynamic disorder that yield this volume increase of the displacement ellipsoids. However, this disorder could contribute to the higher reactivity of SiHA (8).

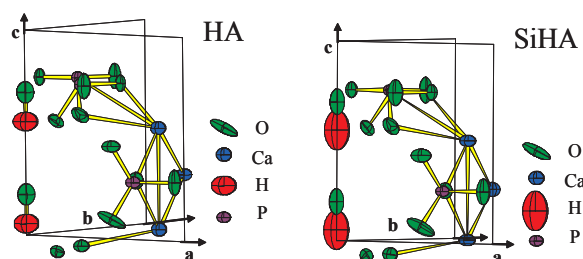


Figure 2. Thermal displacement ellipsoids for HA and SiHA

Under the synthesis conditions used in this work (high temperature and air atmosphere), the formation of HPO_4^{2-} from PO_4^{3-} is possible through the following mechanism



Although this is a widely accepted statement, there is no reference in the scientific literature providing atomic coordinates for the H atom of the HPO_4^{2-} group. Figure 3 shows the scattering density (SD) Fourier difference maps, calculated from the structural model proposed for HA and SiHA. In the case of SiHA sample, the projection over the mirror plane, parallel to (0 0 1) and sited at $\frac{1}{4}$ and $\frac{3}{4}$ of the c axis, clearly show negative SD positions close to the O2 atoms, sited on the mirror plane. These sites correspond to H atoms (they are the only ones that have negative Fermi lengths in this compound) and are sited at the $6h$ Wyckoff position. For SiHA, the H atoms seem to be clearly localized at 0.4746, 0.1666 and 0.25 for x, y and z respectively (next to O2 atoms), whereas in HA the negative density sites have lower intensity and appear scattered at the mirror plane at $z = 0.25$. The negative SD points out that our initial structural model is not complete and additional H atoms should be included. New refinements were carried out for SiHA including H atoms at the position described above, obtaining a better adjustment during the Rietveld refinement (9). Even if the fraction of the SD of the additional H atoms is quite small, we clearly see them in the Fourier maps. These results demonstrate the presence of HPO_4^{2-} in SiHA. The presence of SiO_4^{4-} in SiHA seems to fix higher amount of H atoms, next to the O2 sites. The stronger charge attraction of the SiO_4^{4-} respect to PO_4^{3-} would explain this difference, facilitating the H^+ incorporation to the PO_4 (or SiO_4) tetrahedrons following the mechanism:

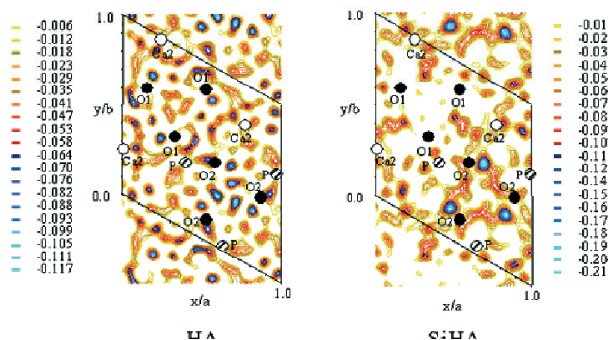
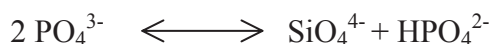


Figure 3. Difference Fourier maps for neutron SD in HA and SiHA. The negative SD (in blue) in SiHA correspond to H atoms (see text).

In this study we have provided a direct evidence of this kind of substitution mechanism, taking into account that HA obtained by ceramic method under air atmosphere are not pure hydroxyapatites but oxy-hydroxyapatites, $\text{Ca}_{10}(\text{PO}_4)_6(\text{OH})_x\text{O}_y$, or more exactly $\text{Ca}_{10}(\text{PO}_4)_{6-x}(\text{HPO}_4)_x(\text{OH})_y\text{O}_z$. For first time, we have calculated the hydroxylation degree in oxy-hydroxyapatites and provide crystallographic positions for the H atoms of the HPO_4^{2-} groups by means of a neutron diffraction study.

References

1. J.C. Elliott, Structure and Chemistry of the Apatites and Other Calcium Orthophosphates. Amsterdam: Elsevier; 1994.
2. M. Vallet-Regí, *J. Chem Soc Dalton Trans*, 2001, 2, 97.
3. I.R. Gibson, S.M. Best, W. Bonfield, *J. Biomed. Mater. Res.* 1999, 44, 422.
4. A.E. Porter, et al. *Biomaterials*, 2003, 24, 4609.
5. F. Balas, J. Pérez-Pariente; M. Vallet-Regí, *J. Biomed. Mater. Res.* 2003, 66A, 364.
6. J.C. Trombe, G. Montel, *J. Inorg. Nucl. Chem.*, 1978, 40, 15.
7. D. Arcos, J. Rodríguez-Carvajal, M. Vallet-Regí, *Physica B*, 2004, 350, e607.
8. M. I. Kay, R. A. Young, A. S. Posner, *Nature* 1964, 204, 1050.
9. D. Arcos, J. Rodríguez-Carvajal, M. Vallet-Regí, *Solid State Sciences*, 2004, 6, 987.

LOW TEMPERATURE STRUCTURE OF THE N-OXY γ -PICOLINE BY USING SIMULATED ANNEALING ON NEUTRON AND SYNCHROTRON POWDER DIFFRACTION DATA

A. Carretero-Genevri¹, F. Damay¹, A. Cousson¹, W. Van Beek², J. Rodríguez-Carvajal¹

¹ Laboratoire Léon Brillouin (CEA-CNRS), CEA- Saclay, 91191 Gif sur Yvette Cedex, France

² European Synchrotron Radiation Facility (ESRF), Avenue des Martyrs, 98000 Grenoble Cedex 09, France

The study of the rotation dynamics of methyl groups is of paramount importance to understand the phase transitions that undergo methylated compounds in the solid state. It is supposed that the non-linear excitations generated by the methyl dynamics (*breathers* and *rotobreathers*) [1,2] play a fundamental role in the biological functions of aminoacids and proteins. To tackle the study of the methyl dynamics it is necessary to know the crystal structure at different temperatures of the concerned model compounds. In this document we present the case of the 4-methyl N-oxy pyridine (N-oxy γ -picoline, $C_5H_4NO[CH_3]$, hereafter NOPic) that presents two structural phase transitions below room temperature (RT). These transitions generate modifications in the distribution density of the methyl groups in a way similar to that observed in 4-methyl pyridine [2]. The structure of NOPic at RT ($I4_1/amd$, $a=7.943(3)$, $c=19.621(5)$ Å) has $Z=8$ molecules in

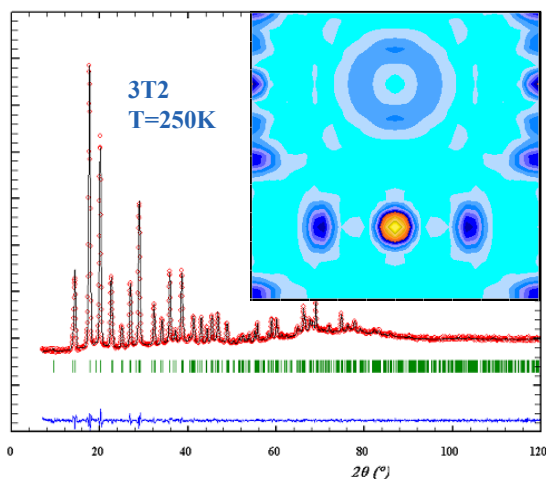


Figure 1. Refinement of the RT phase of NOPic and Fourier map of a section containing methyl groups. Notice the nearly circular proton density.

the unit cell and shows a complete disorder of the methyl groups. The CH_3 groups are rotating, around the axis of the molecule, giving rise to a quasi-circular distribution of proton density (Fig. 1) [2, 3]. Below $T_2=138$ K the structure becomes orthorhombic ($Fddd$, $a=12.140(1)$, $b=10.239(1)$, $c=19.573(1)$ Å, $Z=16$) and the planes of the molecules become tilted (rotation around the c -

axis) with respect to the RT phase. The methyl groups are still disordered and the proton density distribution is modified slightly (Fig. 2). A new

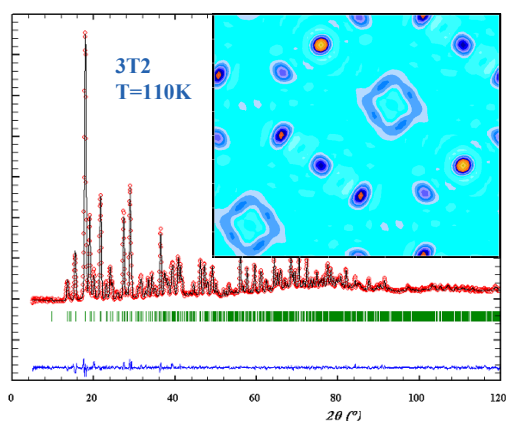


Figure 2. Refinement of the intermediate phase of NOPic and Fourier map of a section containing methyl groups.

phase transition is observed at $T_1=91$ K, as can be seen in the portions of neutron diffraction patterns presented in Figure 3 showing the three kinds of diffraction patterns observed for NOPic. The structure of the low temperature phase was not known before this work. The study using single crystals has been up to now hampered by the strong twinning observed in the $Fddd$ phase that, on the other hand, was refined using neutron powder diffraction. We have used the LLB high-resolution powder diffractometers G4.2 ($\lambda=2.38$ y 3.13 Å) and 3T2 ($\lambda=1.23$ Å), using a deuterated sample to eliminate the incoherent scattering of protons, to get the appropriate structural information. However, we were not able to succeed in indexing the Bragg peaks of the low temperature (LT) phase using neutrons. The unit cell of the LT phase was the unknown before performing the experiments in the Swiss-Norwegian Beam Line (SNBL, $\lambda=0.689$ Å) at the ESRF. Thanks to the very good resolution of the powder diffractometer in the SNBL and the use of indexing programs distributed within the *FullProf Suite* [5] we got the LT unit cell that turns out to

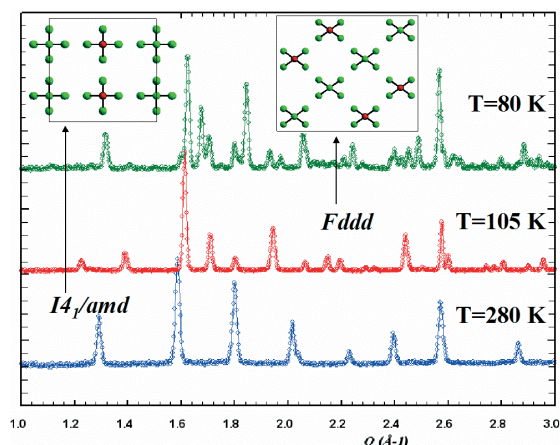


Figure 3. Limited portions of the neutron diffraction patterns of the N-oxy γ -picoline. Schematic structure of the two previously known structures as seen from [001]. Hydrogen atoms are not represented.

be tetragonal ($a=15.943(3)$, $c=19.621(5)$ Å, $Z=32$). So, there is a sequence of phase transitions on cooling where the tetragonal symmetry of the RT phase is partially recovered in the LT phase ($a_{LT} \approx 2 \times a_{RT}$, $c_{LT} \approx c_{RT}$). The possible space groups were studied starting with those of higher symmetry compatible with the molecular distribution in the RT phase. The resolution of the structure was performed by the Simulated Annealing option implemented in FullProf [5], using clusters of overlapped integrated intensities. The space group finally found is $P4_1$, in which there are $Z/4=8$ independent NOPic molecules. The success of the resolution critically depends on the use of rigid body modelling parameters, the number of free parameters (6 per rigid block) used in the resolution of the structure was $6 \times Z/4 = 48$, and a proper election of their variation limits. It is interesting to notice that the data from long wavelengths neutrons of G4.2 ($\lambda=3.13$ Å) are as

References

- 1 MacKay, R.S. and Aubry, S. *Nonlinearity* **7**, 1623 (1994)
- 2 Fillaux, F.; Nicolai, B.; Paulus, W.; Kaiser-Morris, E.; Cousson, A. *Phys. Rev. B* **68**, 224301 (2004).
- 3 Kaiser, E.; Paulus, W.; Cousson, A. *Z. für Kristallographie* **213**, 80 (1998)
- 4 Kaiser, E. *PhD Thesis*, Laboratoire Léon Brillouin (CEA-CNRS), (1997, unpublished).
- 5 Rodríguez-Carvajal, J; *Physica B* **192**, 55 (1993). See also CPD (IUCr), Newsletter **26**, 12 (2001), that can be obtained at <http://journals.iucr.org/iucr-top/comm/cpd/Newsletters/>.

good as those of synchrotron for solving the structure. The asymmetric unit has 120 atoms and preliminary refinements, with the Rietveld method, using the 3T2 data has confirmed that the phase transition takes place by shifting the centres of the molecules and making small tilts of the molecular planes that remain otherwise nearly parallel to the c -axis like at the other temperatures. The methyl groups seem to be well localized but with an unexpected configuration. It is interesting to realise that the LT phase has mixed characteristics of the two higher temperature phases (Fig.4).

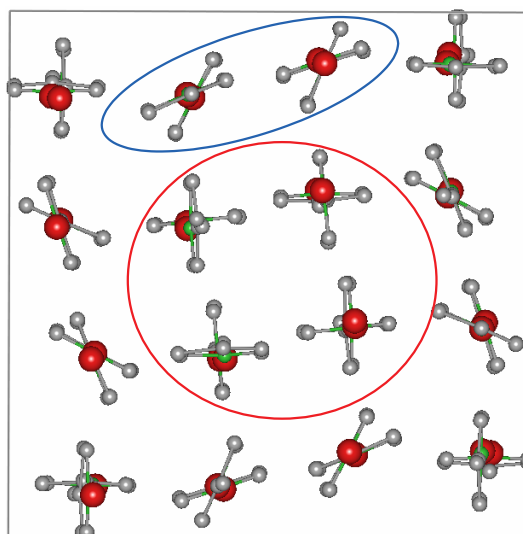


Figure 4. View along [001] of the NOPic structure in its LT phase as obtained from simulated annealing. There are parts of the structure roughly similar to the high temperature (red ellipse) and to the intermediate phase (blue ellipse). The hydrogen atoms are not shown.

MAGNETIC STRUCTURES OF TRANSITION METAL (Mn, Co, Ni, Cu) HYDROXYSULFATES

S. Vilminot¹, G. André², M. Richard-Plouet^{1,3}, M. Kurmoo⁴, F. Bourée-Vigneron², M. Ben Salah¹¹ Groupe des Matériaux Inorganiques, IPCMS, UMR CNRS-ULP 7504, BP 43, 67034 Strasbourg Cedex 02² Laboratoire Léon Brillouin (CEA-CNRS), CEA – Saclay, 91191 Gif-sur-Yvette Cedex³ Institut des Matériaux Jean Rouxel, UMR CNRS 6502, 2 rue de la Houssinière, BP 32229, 44322 Nantes Cedex 03⁴ Laboratoire de Chimie de Coordination Organique, UMR CNRS 7140, Tectonique du Solide, 4 rue B. Pascal, 67000 Strasbourg Cedex

Recently, there has been widespread interest in hydrothermal synthesis particularly in creating porous compounds. In our case, hydrothermal synthesis has been used for the elaboration of 3d transition metal hydroxysulfates. Such compounds have been carefully studied by mineralogists [1], where the principal interests were the identification of the crystal phases and the mechanism of their formation with respect to their geographic location. However, the magnetic characterizations of the minerals are sparse and this stimulated the study of the relations between structure and magnetic properties.

With $M = \text{Cu}$, two compounds are obtained, $\text{Cu}_3(\text{OH})_4\text{SO}_4$ and $\text{Cu}_4(\text{OH})_6\text{SO}_4$ corresponding to the minerals antlerite and brochantite [2-3], respectively. The structure of the former contains triple chains of edge-sharing copper octahedra, running in the b -axis direction and connected to each other by sulfate groups. Neutron powder data collected on 94% deuterated sample on G4.1 diffractometer allow the determination of the magnetic structure and its thermal evolution, the D atomic positions and the H/D ratio being refined from 3T2 data. Below $T_N = 5 \text{ K}$, the magnetic structure can be viewed as a copper triple chain consisting of ferromagnetic outer chains, with magnetic moments in the c -axis direction ($0.88(5) \mu_B$), antiparallel to each other (Figure 1). As regards the central chain, the best fit gives a zero magnetic moment on metal ions, explained by some misorientation of the magnetic moments (idle spin behaviour). The triple chains are then AF coupled to each other [4].

For $\text{Cu}_4(\text{OH})_6\text{SO}_4$, double chains of edge-shared copper octahedra are corner-shared to give rise to corrugated planes. The magnetic structure (below $T_N = 7 \text{ K}$) consists of neighbouring ferromagnetic chains antiparallel to each other. The moments are quite weak, $0.16(5)$ and $0.45(4) \mu_B$, in agreement with the low signal magnitude. Moreover, at low θ values, the evolution with temperature of the diffusion signal has been related to the presence of ferromagnetic clusters [5].

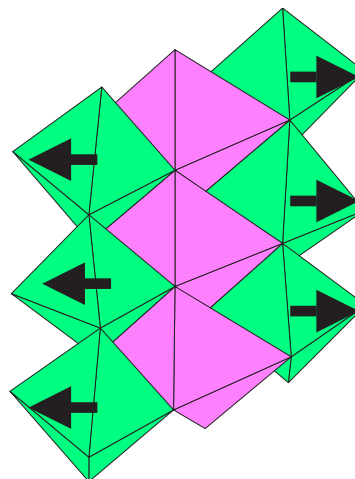


Figure 1. View of a triple chain in $\text{Cu}_3(\text{OD})_4\text{SO}_4$ with the magnetic moments as arrows pointing in the c -axis direction.

For $M = \text{Mn}$, Co and Ni , numerous new compounds have been obtained by hydrothermal synthesis and we will focus on the isostructural $\text{M}_3(\text{OD})_2(\text{SO}_4)_2(\text{D}_2\text{O})_2$ family. The structure contains zig-zag chains of edge-shared $\text{M}(1)$ octahedra running in the c -axis direction. $\text{M}(2)$ octahedra are corner-shared to the $\text{M}(1)$ chains building up corrugated planes. In the case of $M = \text{Ni}$ [6], all magnetic moments ($2.00(4)$ and $1.67(6) \mu_B$ for $\text{Ni}(1)$ and $\text{Ni}(2)$, respectively) are aligned along the b -axis direction and this magnetic structure is observed for any T below $T_N = 29 \text{ K}$. The magnetic model is slightly different in the case of $M = \text{Mn}$ and Co . For the former [7], the magnetic moments of $\text{Mn}(2)$ ions ($4.44(7) \mu_B$) are aligned along the c -axis direction, those of $\text{Mn}(1)$ ions ($4.34(7) \mu_B$) being located inside the bc -plane and making an angle around 20° with the c -axis direction. When the temperature raises up to $T_N = 26 \text{ K}$, the $\text{Mn}(1)$ moment moves towards a direction closer to the b -axis with a value of 74° with respect to the c -axis at 25 K . For $M = \text{Co}$, all moments are oriented along the c -axis direction with values of $2.99(6)$ and $3.31(7) \mu_B$ for $\text{Co}(1)$ and $\text{Co}(2)$, respectively. The magnetic structure is

observed up to $T_N = 42$ K. For $M = \text{Mn}$ and Co , another feature clearly appears on the neutron powder diffractograms. An increase in the background is evident and gives rise to a broad hump with a maximum around $2\theta = 30^\circ$ that is visually clearer for data recorded at T close to T_N , where its intensity reaches a maximum. Moreover, other less visible humps are also present. These broad humps are magnetic in origin and have been related to magnetic short-range ordering (SRO). Therefore, a second magnetic phase with the same structure and irreducible representation, but with a different coherence length, has been refined. Such an approach supposes that the volume distribution of both magnetic phases is homogeneous. Some differences appear between Mn and Co concerning the SRO phase. Whereas for Mn the broad hump is visible down to the lowest measurement temperature (1.4 K), it disappears below 34 K in the case of cobalt. For Co , the moments are oriented along the c -axis direction and are in the bc -plane for Mn , their direction turning towards the b -axis.

Other hydroxysulfates are under study to determine their magnetic structure. The substitution of the sulfate group by the seleniate one allows for

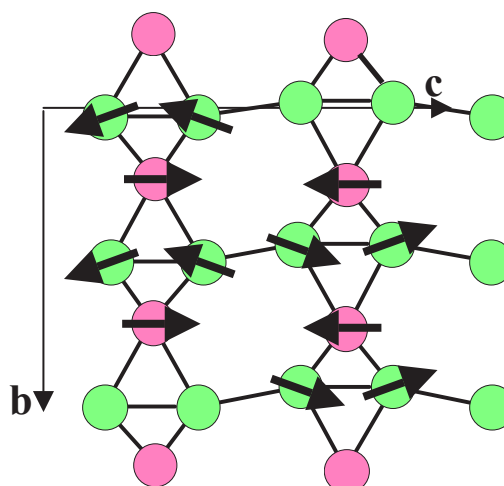


Figure 2. Projection on the bc -plane of the magnetic structure of $\text{Mn}_3(\text{OD})_2(\text{SO}_4)_2(\text{D}_2\text{O})_2$ with $\text{Mn}(1)$ in green and $\text{Mn}(2)$ in pink.

copper a structure similar to antlerite, $\text{Cu}_3(\text{OH})_4\text{SeO}_4$, to be obtained. Below $T_N = 8$ K, an incommensurate magnetic structure is evidenced.

References.

- [1] R. K. Eby and F. C. Hawthorne, *Acta Cryst.* B49 (1993) 28-56.
- [2] F. C. Hawthorne, L. A. Groat and R. K. Eby, *Can. Mineral.* 27 (1989) 205-209.
- [3] M. Helliwell and J. V. Smith, *Acta Cryst.* C53 (1997) 1369-1371.
- [4] S. Vilminot, M. Richard-Plouet, G. André, D. Swierczynski, M. Guillot, F. Bourée-Vignerón and M. Drillon, *J. Solid State Chem.* 170 (2003) 255-264.
- [5] S. Vilminot, M. Richard-Plouet, G. André, D. Swierczynski, F. Bourée-Vignerón, A. Derory and M. Kurmoo, *Eur. J. Inorg. Chem.* To be submitted
- [6] S. Vilminot, M. Richard-Plouet, G. André, D. Swierczynski, F. Bourée-Vignerón and M. Kurmoo, *Inorg. Chem.* 42 (2003) 6859-6867.
- [7] M. Ben Salah, S. Vilminot, G. André, M. Richard-Plouet, F. Bourée-Vignerón, T. Mhiri and M. Kurmoo, *Chem. Eur. J.* 10 (2004) 2048-2057.

CRYSTAL AND MAGNETIC STRUCTURES OF THE Mn^{3+} ORBITAL ORDERED MANGANITE $Y_2Ba_2Mn_4O_{11}$ L. Pinsard-Gaudart¹, C. Perca¹, A. Daoud-Aladine², M. T. Fernández-Díaz³
and J. Rodríguez-Carvajal⁴¹ Laboratoire de Physico-Chimie de l'Etat Solide, Université de Paris Sud, Bât. 414, 91405 Orsay Cedex, France² Laboratory for Neutron Scattering ETH/PSI, Paul Scherrer Institut, CH-5232 Villigen, Switzerland³ Institut Laue-Langevin, BP 156, 38042 Grenoble Cedex, France⁴ Laboratoire Léon Brillouin (CEA-CNRS), CEA/Saclay, 91191 Gif sur Yvette Cedex, France

The discovery of the colossal magnetoresistance in manganese oxide perovskites ($AMnO_3$) of general formula $R_{1-x}D_xMnO_3$ (R = trivalent rare earth cations, D = divalent cations like Ca, Sr, Ba, Pb...) [1] has recently attracted the focus of many research efforts, in order to understand and to improve their properties. By changing the D-cation and/or the doping level, one can tune their physical properties from ferromagnetic (F) conductors to antiferromagnetic (AF) insulators. For a large average radius of the A-site ($\langle r_A \rangle$) the conduction band is broad and the material has, in general, a metallic-like behaviour. This is usually explained by the double exchange mechanism [2]. If $\langle r_A \rangle$ is small enough the conduction band is narrow, leading to a localization of the charge carriers on specific atomic sites. In some cases the localization occurs in a spatially ordered way. This phenomenon is called charge ordering (CO) and it is accompanied by an increase of the resistivity. Goodenough [3], using super-exchange theory, and stressing the role of the Jahn-Teller effect on Mn^{3+} , was the first to propose a model explaining qualitatively the magnetic structure of $LaMnO_3$. Combining these concepts with a specific charge and orbital ordering he was able to provide an explanation for the low temperature observations in half-doped ($x=1/2$) manganites. Recently, Daoud-Aladine *et al.* [4] have proposed an alternative model in which the electrons localize in regions formed by Mn-O-Mn ferromagnetic pairs (Zener polarons), which are stabilized by a local double exchange mechanism and a structural distortion. In order to test different hypotheses about the nature of the CO/OO transitions new compounds have to be studied in both mixed and integer valence materials. To overcome the disorder in the A-site of the Mn perovskites we are exploring new compounds presenting well ordered structures.

The first example of A-cation ordered manganese perovskite was $YBaMn_2O_5$ (Fig. 1), in which Y^{3+} and Ba^{2+} cations are ordered in alternating layers perpendicular to [001] and the oxygen sites in the Y-layer are empty. Neutron diffraction studies showed that $YBaMn_2O_5$ has a tetragonal symmetry

[5] and a charge ordered arrangement of Mn^{2+} and Mn^{3+} ions. By low temperature oxygenation it is, in principle, possible to obtain mixed valence compounds of formula $YBaMn_2O_{5+\delta}$ so that it is expected to have Mn^{2+}/Mn^{3+} for $\delta < 0.5$ and Mn^{3+}/Mn^{4+} for $\delta > 0.5$. For $\delta = 0.5$, we obtained a stoichiometric compound that can be formulated as $Y_2Ba_2Mn_4O_{11}$ or $YBaMn_2O_{5.5}$ and which have only Mn^{3+} .

The compound $YBaMn_2O_{5.5}$, has been prepared by oxidizing/reducing $YBaMn_2O_5/YBaMn_2O_6$ in mild conditions. We used the combined data of three independent diffraction patterns at room temperature: one X-ray and two neutron powder patterns to refine the structure. The crystal structure of this manganite was solved in the space

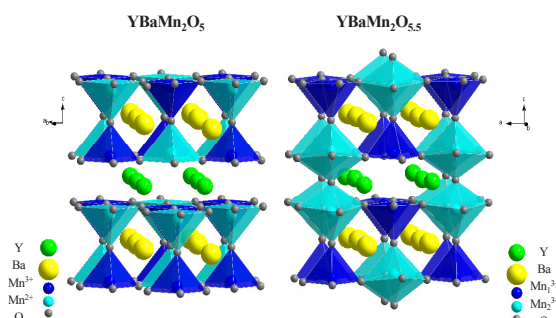


Figure 1. Perspective view of the $YBaMn_2O_5$ and $YBaMn_2O_{5.5}$ perovskites

group $Icma$ ($a \approx 8.161 \text{ \AA}$, $b \approx 7.546 \text{ \AA}$, $c \approx 15.279 \text{ \AA}$) [6]. We have shown that a doubling of the cell is present in this case, as compared to the La-based compound [7], due to a tilting ($a^0b^0c^-$) of the polyhedra around the [001] direction. Even though the formal oxidation degree of manganese ions is 3+, in the structure there are two different sites: one with a square pyramidal coordination (Mn1) and another one with octahedral coordination (Mn2). In the ab plane, the structure consists of rows of MnO_6 octahedra and MnO_5 pyramids parallel to the b direction. In the a direction the rows are formed of alternating octahedra and pyramids and in the c direction the rows consists of alternating pairs of octahedra and pyramids following the site sequence 1-1-2-2-1-1-2-2. The

result of this stacking is the presence of tunnels along the b direction (Fig. 1). The existence of two distinct types of Mn^{3+} cations, in square pyramidal and octahedral coordination, leads to the formation of a particular orbital ordering.

We have also investigated its magnetic and transport properties. The resistivity measurements have shown an insulator-like activated behaviour with a low activated energy, comparable to that of $LaMnO_3$. Magnetic susceptibility shows an antiferromagnetic transition at a Néel temperature of $T_N \approx 140$ K. The neutron powder diffraction patterns of $YBaMn_2O_{5.5}$ obtained below the Néel temperature show the presence of magnetic reflections that can be indexed by using the propagation vector $\mathbf{k}=(0,0,0)$. The refinement of the magnetic structure, at 1.7 K, gives the best result with the $G_x+G'_x$ mode (the first term refers to octahedral and the second -primed- to pyramidal Mn^{3+} ions). This leads to a picture of the magnetic structure, identical to that of $LaBaMn_2O_{5.5}$ [7], as a network of parallel ferromagnetic spin-ladders (Fig. 2a). Each F spin ladder lies along the a -axis, in the (010) plane, and it is AF-connected along the b and c axes to the neighbouring one. In the (010) plane, half of the manganese ions of every ladder are connected to adjacent ladders by the Mn2-O-Mn2 AF pathway. Along the [010] direction, all the Mn ions of a ladder are AF-connected to the upper and lower ladders. At 1.7K, the magnetic moment of the two kinds of Mn^{3+} ions are slightly different, $3.5(1)\mu_B$ for the pyramidal site and $3.7(1)\mu_B$ for the octahedral site. The reduction with respect to the expected moment is due to a combination of covalence and zero-point fluctuations of the AF structure.

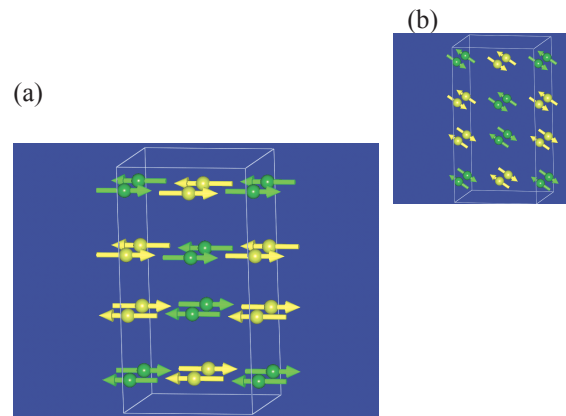


Figure 2. Magnetic structure of $YBaMn_2O_{5.5}$ at 1.5K (a) and 125K (b). Mn atoms in octahedral coordination are represented with black arrows. Mn atoms in pyramidal coordination are represented with grey arrows.

Moreover if we consider the magnetic interactions between the Mn^{3+} ions according to the orbital ordering deduced from the crystal structure we have shown that the analysis of the super-exchange paths, and the prediction of the signs of exchange interactions following the Goodenough-Kanamori-Anderson (GKA) rules is perfectly compatible with the observed magnetic structure.

Near the transition temperature ($T \sim 120$ K), a component along the c -axis must be taken into account in order to fit properly the neutron diffraction pattern (Fig. 2b). The presence of a single mode ($G_x+G'_x, 0, G_z+G'_z$) in both x and z directions implies a mixing of irreducible representations and this is a signature of the low magneto-crystalline anisotropy in this compound.

References

- [1] R. von Helmolt, J. Wecker, B. Holzapfel, L. Schultz, and K. Samwer, *Phys. Rev. Lett.* 71, 2331 (1993), M. McCormack, S. Jin, T. H. Tiefel, R. M. Fleming, Julia M. Phillips and R. Ramesh, *Appl. Phys. Lett.* 64, 3045 (1994). R. Mahesh, R. Mahendiran, A. K. Raychaudhuri and C. N. R. Rao, *J. Solid. State. Chem.* 114, 297 (1995).
- [2] C. Zener, *Phys. Rev.* 81, 440 (1951).
- [3] J. B. Goodenough, *Phys. Rev.* 100, 564 (1955).
- [4] A. Daoud-Aladine, J. Rodríguez-Carvajal, L. Pinsard-Gaudart, M. T. Fernández-Díaz, and A. Revcolevschi, *Phys. Rev. Lett.* 89, 097205 (2002).
- [5] J. P. Chapman, J. P. Attfield, M. Molgg, C. M. Friend and T. P. Beales, *Angew. Chem. Int. Ed. Engl.* 21, 108 (1996), F. Millange, E. Suard, V. Caignaert and B. Raveau, *Mat. Res. Bul.* 34, 1 (1999).
- [6] C. Perca, L. Pinsard-Gaudart, A. Daoud-Aladine, M.T. Fernández-Díaz and J. Rodríguez-Carvajal, submitted to *Chem. Mater.*
- [7] V. Caignaert, F. Millange, B. Domengès, B. Raveau and E. Suard, *Chem. Mater.* 11, 930 (1999).

SPIN PEIERLS GROUND STATE IN (TMTTF)₂PF₆P. Foury-Leylekian¹, D. Le Bolloc'h¹, B. Hennion², S. Ravy^{1,3}, A. Moradpour¹ and J.-P. Pouget¹¹ Laboratoire de Physique des Solides, CNRS UMR 8502, Bat. 510, Université Paris Sud, 91405 Orsay Cedex, France² Laboratoire Léon Brillouin, CEA-CNRS UMR 12, 91191 Gif-sur-Yvette Cedex, France³ Synchrotron Soleil, L'orme des Merisiers, Saint-Aubain, BP 48, 91192 Gif-sur-Yvette Cedex, France

The isostructural series of 2:1 cation radical salts based on monovalent anions X such as PF₆, AsF₆, ReO₄, NO₃, SCN and Br and deriving from TMTTF (tetramethyl-tetrathiofulvalene) and from TMTSF (tetramethyltetraselenofulvalene) show remarkable quasi one-dimensional (1D) electronic properties. These salts are made of slightly dimerized zig-zag stacks of TMTTF or TMTSF running along the *a* direction, which delimit cavities in which the monovalent anions X are located [1]. This gives rise to a large number of competing low-temperature ground states, ranging from antiferro-magnetism (AF) and spin-Peierls (SP) pairing in the localized limit, to spin density wave (SDW) in the metallic limit. At present, all the information concerning the AF or SDW modulation comes from NMR investigations, because the small value ($\approx 0.1 \mu_B$) of the magnetic moment and the small available sample size preclude neutron diffraction measurements.

Very little is known on the SP transition. A first signature of such a transition was found by the observation with X-ray scattering of very weak superlattice reflections in (TMTTF)₂PF₆ at T=10K [2]. These peaks originate from the tetramerization of the organic stacks, leading to the pairing of localized spins (one spin per dimer of TMTTF molecules) resulting into the formation of non-magnetic singlets, S=0. This is identified by a drop in the spin-susceptibility, observed by EPR [3-5] and NMR [5] below $T_{SP} \approx 19$ K in (TMTTF)₂PF₆. However, no accurate study of the structural origin of the SP transition could be performed because of the extreme sensitivity of the TMTTF molecule to X-ray irradiation damages. Up to now, the difficulty to get large samples and the fact that they are hydrogenated have prevented from getting significant results with neutron diffraction.

The synthesis of the organic salts of the TMTSF and TMTTF samples has been strongly improved. A 17mm³ crystalline sample of (TMTTF)₂PF₆ has been elaborated in Orsay, which offered the possibility of a structural study of the SP transition. The experiment has been carried out on the triple axis spectrometer 4F2 of the Orphée reactor at the Laboratoire Léon Brillouin.

The experimental conditions were: $k_i = 2.662 \text{ \AA}^{-1}$, 60' collimations on each side of the analyzer, and graphite filters on k_i and k_f . The (a^*, b^*, c^*) and the

($a^*, b^* + c^*$) scattering planes were explored. Such samples are always twinned, but the ratio of (2,0,0) reflections of the two twins indicated that the twinning ratio was 7:1. Upon cooling, due to the constraint of the fixing procedure, the main twin was found to split into three components (a small component and two large ones separated by about 1.4 degree). At T=11K, the intensity of the Bragg reflections of the component used for the measurements was of 7000 c/s for the (0,1,1), 2000 c/s for the (2,0,0), 1200 c/s for the (2,1,1) and 1100 c/s for the (4,0,0), leading to an average Bragg intensity of about 3000 c/s.

At this temperature, a survey of about 20 reciprocal positions expected for the q_{SP} superlattice reflections was performed with a counting time of 645s per step, in both (a^*, b^*, c^*) and ($a^*, b^* + c^*$) reciprocal planes. Because of a large background of 3 to 5 c/s, due to the incoherent scattering of the hydrogen atoms present in TMTTF molecules, only two very weak superlattice reflections were detected in the (a^*, b^*, c^*) reciprocal plane and none in the ($a^*, b^* + c^*$) plane. The observed reflections could be indexed as $(-4, 1, -2) + q_{SP}$ and $(-3, 1, -2) + q_{SP}$, where $q_{SP} = (1/2, 1/2, 1/2)$, and their intensities were about $1/10^{\text{th}}$ of the background.

Figure 1 shows a rocking-curve (ω -scan) and a longitudinal scan around the $(-7/2, 3/2, -3/2)$ reciprocal lattice position, which confirm that the observed scattering is a well defined Bragg reflection.

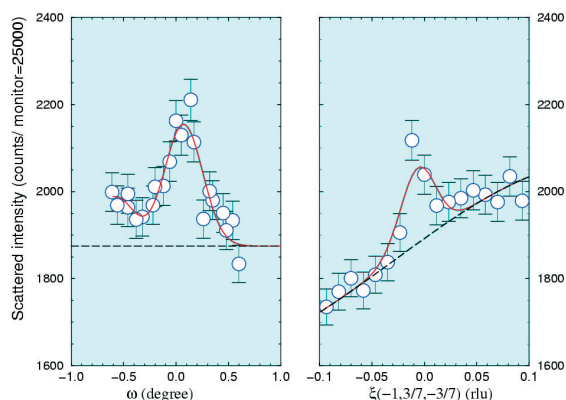


Figure 1. Transverse and longitudinal scans through the $(-7/2, 3/2, -3/2)$ superstructure reflection at T=11K. The dashed lines gives the background level.

The experimental width of the peak corresponds to the instrumental resolution, which implies a long range 3D SP order (i.e. $> 1000 \text{ \AA}$). The absence of second harmonic contamination has been checked. Finally the temperature dependence of the peak has been determined, as shown in the Figure 2, which unambiguously evidences the intensity drop at a temperature about 18-19 K. This ascertained the value of $q_{SP}=(1/2, 1/2, 1/2)$.

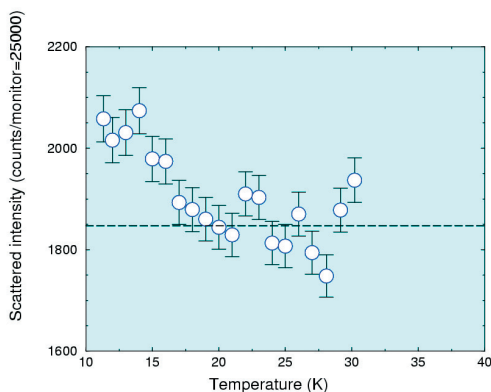


Figure 2. Temperature dependence of the $(-7/2, 3/2, -3/2)$ peak intensity. The dashed line gives the background level

The peak intensity I_S of the superlattice reflection is ~ 0.35 c/s. This is about 10^{-4} times the intensity I_B of an average Bragg reflection measured in the same experimental conditions. As the superlattice reflection intensity is proportional to the square of the long range atomic displacement, this means that the distortion undergone by the organic stack in $(\text{TMTTF})_2\text{PF}_6$ is quite small compared to similar compounds, e.g. one order of magnitude smaller than in $(\text{BCPTTF})_2\text{AsF}_6$. For comparison the ratio I_S/I_B in $\text{MEM}(\text{TCNQ})_2$ and CuGeO_3 is $\sim 10^{-3}$. The shift u_{3D} of the TMTTF molecules is thus estimated to $\sim 3 \cdot 10^{-3} \text{ \AA}$.

On the other hand, the amount of dimerization δ may be deduced from the spin gap value and the near neighbor exchange interaction J of the $S=1/2$ AF Heisenberg chain undergoing the Peierls instability. This gives another parameter u_{1D} corresponding to the intrachain displacement, with $\delta=2u_{1D}\ln(J)/du$. Numerical calculations [6] yield $\delta=4.5\%$ in $(\text{TMTTF})_2\text{PF}_6$, about two times smaller than $\delta=8\%$ found in $(\text{BCPTTF})_2\text{PF}_6$, while there is about one order of magnitude between their respective u_{3D} .

Why the δ value does not scale with the amplitude u_{3D} of the 3D-SP distortion in $(\text{TMTTF})_2\text{PF}_6$ opens new issues in the understanding of this organic conductor. Several assumptions may be done. This could for instance point out the stabilization of a different mode of displacement. For example, in $(\text{BCPTTF})_2\text{PF}_6$, the SP distortion could be directed along the long direction of the BCPTTF molecule, while in $(\text{TMTTF})_2\text{PF}_6$, along the short direction of the TMTTF molecule. On the other hand, the SP distortion of the organic sublattice should deform the cavities where the anion X are located. This could lead to different shifts of the anions.

A better understanding of this problem would require a structural refinement of the SP superstructure of $(\text{TMTTF})_2\text{PF}_6$. This could be achieved on large deuterated single crystals, with a strong reduction of the incoherent elastic scattering.

Finally, the present study demonstrates that deuterated samples of comparable volume that the hydrogenated used here, would make it possible to observe superlattice reflections of about 10^{-5} of an average Bragg reflections. This opens interesting perspective for the study of AF and SDW modulations in the $(\text{TMTTF})_2\text{X}$ and $(\text{TMTSF})_2\text{X}$ salts, respectively.

References

- [1] J.P. Pouget and S. Ravy, *J. Phys.* I **6**, 1501 (1996).
- [2] J.P. Pouget, R. Moret, R. Comès, K. Bechgaard, J.M. Fabre and L. Giral. *Mol. Cryst. Liq. Cryst.* **79**, 129 (1982).
- [3] C. Coulon, P. Delhaes, S. Flandrois, R. Lagnier, E. Bonjour, and J.M. Fabre, *J. Phys. Lett. (France)*, **43**, 1059 (1982).
- [4] M. Dumm, A. Loidl, B.W. Fravel, K.P. Stanley, L.K. Montgomery and M. Dressel, *Phys. Rev. B* **61**, 511 (2000).
- [5] F. Creuset, C. Bourbonnais, L.G. Caron, D. Jérôme and K. Bechgaard, *Synth. Met.* **19**, 289 (1987).
- [6] Yokoyama and Saiga, *J. Phys. Soc. Japan* **66**, 3617 (1997).

NEUTRAL-TO-IONIC PHASE TRANSITION UNDER PRESSURE:
TOWARDS THE QUANTUM LIMIT

M.H. Lemée-Cailleau ¹, M. Buron ², E. Collet ², H. Cailleau ², T. Luty ³,
B. Ouladdiaf ¹, F. Moussa ⁴, T. Hasegawa ⁵

¹ Institut Laue Langevin, BP 156, 38042 Grenoble Cedex, France

² Groupe Matière Condensée et Matériaux, UMR 6626 CNRS - Université de Rennes 1, Campus de Beaulieu, 35042 Rennes Cedex, France

³ Institut of Physical and Theoretical Chemistry, Polytechnique University of Wrocław, 50370 Wrocław Poland

⁴ Laboratoire Léon Brillouin (CEA-CNRS), CEA- Saclay, 91191 Gif sur Yvette Cedex

⁵ Research Institut of Electronic Sciences, Hokkaido University, Sapporo, and Correlated Electron Research Center, National Institute of Advanced Industrial Science and Technology, Tsukuba, Ibaraki, 305-8562 Japan

One of the most fascinating features of molecular materials, is the possibility to tune in a co-operative way the state (valence, spin...) of the molecules under the effect of pressure, temperature or with light. The transfer of electron is fundamental to many chemical and biological processes in nature, but in solids, it may be highly efficient because of the intrinsic co-operativity of the organized condensed matter. Beside many insulating solids where an excited electron induces a local structural distortion, in some unconventional materials the relaxation of excited states results in drastic structural changes involving a large number of atoms and electrons [1]. TTF-CA is a prototype for such co-operative phenomena, as it exhibits the so-called neutral-ionic (N-I) transition where the electronic and structural aspects are strongly coupled [2]. This transition occurs in some quasi-one-dimensional charge transfer (CT) organic crystals with a mixed stack architecture (alternation of electron donor (D) and electron acceptor (A) molecules along chains). The electron transfer is intermolecular, mostly along the chain, and gives rise to a change of molecular ionicity, i.e. the degree of CT, associated with a dimerization process leading to the formation of (D⁺A⁻) pairs along the stack in the I phase. With regards to the regular N chains, the dimerization distortion for the I chains is associated with the inversion centre loss with two possible degenerated ferroelectric states (Fig 1). At finite temperature, localized CT exciton-strings, made of hundreds of adjacent (D⁺A⁻) excited pairs along the stack [3] may be thermally induced:



Specific to low-dimensional systems where electron-phonon couplings are important, these

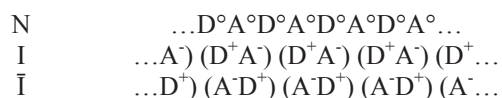


Figure 1. N and I (degenerated) states of a stack.

non-linear excitations can be discussed in term of self-trapped excitons which can self-multiply, and governed numbers of intriguing physical properties: photo-induced transformation [4,5], giant dielectric response ... In these insulators, the co-operative effects may expand to extreme, on contrary to classical insulator like NaCl where excitonic processes remain local. For the prototype complex TTF-CA, the thermodynamics of the N-I transition can be described in terms of three dimensional condensation of these non-linear CT excitations and there simultaneous or successive ordering, with a profound analogy with the solid-liquid-gas phase diagram [6]. Three phases are identified in the (P,T) phase diagram: the N_{para} paraelectric phase, dominantly N with a low concentration in I fluctuating CT strings, the I_{para} one, with a high concentration in I fluctuating CT strings, while the third I_{ferro} phase is characterized by a ferroelectric ordering between I strings.

Since its discovery, most of the efforts to understand the mechanism of the transition were focussed on the finite temperature transition and plenty of its unusual physical changes are now well understood in terms of thermal activation mechanisms [5,7]. However fundamental questions such as the universality of the solid-liquid-gas phase diagram for the N-I transition or the crossover from thermal to quantum mechanism responsible of the N-I transition when it goes to take place in the ground state, remain and the (BEDT-TTF)-(ClMeTCNQ) [8] complex appears as a good guinea pig among the family of mixed-stack CT compounds. In that compound electrical resistivity and spectroscopy measurements have evidence a N-I transition, similar to that of TTF-CA, which should go down to zero Kelvin under pressure [8]. Therefore we have taken advantage of the new high pressure facilities developed at LLB (Helium pressure cell up to 650 MPa), combined with ILL ones (either with the classical He pressure cell or the new TiZr liquid one) to

investigate the structural aspects related to this phase transition, going down to zero Kelvin. Helium presents the priceless advantage to remain fluid over a very wide range of pressure and temperature, assuring a perfectly hydrostatic and controlled pressure on the samples, a control of external conditions which is essential for molecular crystals. From the symmetry point of view, the neutron analysis combined with a new X-ray measurement, has revealed that, on contrary to the literature which gives a $P2_1/n$ space group alike TTF-CA, the diffraction pattern is characteristic of a $P2_1$ space group, with a clear $(0k0)$: $k=2n+1$ systematic absence, related to the twofold screw axis. (reflexions with indices $(h0l)$: $h+l=2n+1$ are clearly present in the diffraction pattern and their width is always characteristic of long range order). It is the first time that a neutral phase corresponds to a $P2_1$ non-centrosymmetric space group. It means that the dimerization already exists between D and A molecules in the neutral state, where the ionicity of molecules is weak ($\rho \sim 0.3$). In order to understand this unexpected phenomena of dimerization in the neutral state, a complete analysis of the structure is presently in progress, taking into account the combination of the effects

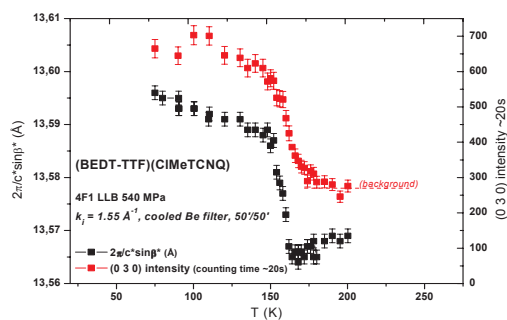


Figure 2. (BEDT-TTF)-(ClMeTCNQ) c cell parameter and intensity of (030) Bragg peak versus temperature at different pressures.

due to Madelung interactions and to the electrical field due to the non-centrosymmetry of the ClMeTCNQ molecule. Under pressure at low temperature, we have evidenced, thanks to neutron diffraction experiments (4F1 at LLB and D10 at ILL), that the transition is related to the appearance of $(0k0)$: $k=2n+1$ Bragg peaks, characteristic of the symmetry breaking, and to clear unit-cell parameter anomalies (Fig. 2). The transition is therefore associated to a $P2_1 \rightarrow P1$ change of symmetry and it goes down to absolute zero under a moderate pressure of ~ 200 MPa. On contrary to TTF-CA, only the symmetry breaking transition is observed, becoming more and more first order as pressure increases, with phase coexistence phenomena (as testify by the enhancement of Bragg peak width when crossing the transition), and with a very strong sample dependence of the low temperature limit of metastability. (BEDT-TTF)-(ClMeTCNQ) appears as a rather more complex case of N-I transition than TTF-CA but gives also the opportunity to investigate the related phenomena in a more rich case up to the quantum regime and including localized field effects.

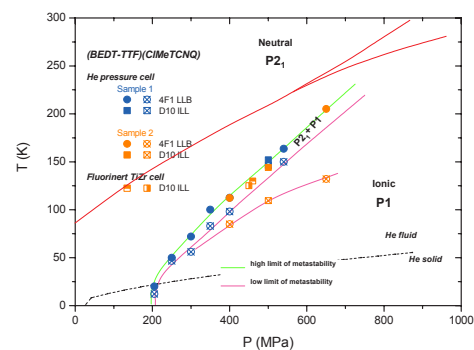


Figure 3. (P,T) phase diagram of (BEDT-TTF)(ClMeTCNQ). One can clearly see the difference of low temperature metastability limit according to sample, while the high temperature limit is weakly affected. The red lines give the TTF-CA diagram.

References

- [1] Relaxations of excited states and photo-induced structural phase transitions, Springer Serie, Solid. State Sciences **124** (1997).
- [2] TTF-CA: tetrathiafulvalene - *para*-chloranile; Le Cointe M., M.H. Lemée-Cailleau, H. Cailleau et al, Phys. Rev. B **51**, 3374 (1995) and references therein.
- [3] Collet E., M.H. Lemée-Cailleau, M. Buron, H. Cailleau, et al, Europhys. Lett. **57**(1) 67 (2002).
- [4] Collet E., M.H. Lemée-Cailleau, M. Buron-Le Cointe, H. Cailleau, S. Techert, M. Wulff, T. Luty, S. Koshihara et al, Science **300**, 612 (2003)
- [5] Luty T., H. Cailleau, S. Koshihara, E. Collet et al, Europhys. Lett. **59**(4) 619 (2002)
- [6] Lemée-Cailleau M.H., M. Le Cointe, H. Cailleau, T. Luty et al., Phys. Rev. Lett. **79**, 1690 (1997).
- [7] Cailleau H., T. Luty, M.H. Lemée-Cailleau, E. Collet, M. Buron-Le Cointe, E. Zienkiewicz, F. Moussa, NATO Science Series II **48**, 167 (2002)
- [8] (BEDT-TTF)(ClMeTCNQ): bisethylenedithiotetra-thiafulvalene - 2-Cl-5-methyltetracyanoquinodimethane; Hasegawa T., T. Mochida, R. Kondo, S. Kagoshima et al, Phys. Rev. B **62**, 10059 (2000) & Hasegawa T. et al Phys. Rev. B **64**, 085106 (2001)

INTERACTIONS IN SELF-ASSEMBLED MOLECULAR CRYSTALS

L. Bourgeois^{1,2}, B. Toudic¹, C. Ecolivet¹, P. Bourges², T. Breczewski³¹ Groupe Matière Condensée et Matériaux, UMR CNRS 6626, Université de Rennes 1, 35042 Rennes, France² Laboratoire Léon Brillouin, CEA-CNRS, CEA Saclay, 91191 Gif-sur-Yvette, France³ Facultad de Ciencias, Universidad del País Vasco, Apdo 644, Bilbao, Spain

Self-assembly is ubiquitous in nature. The key elements are chemical complementarities and structural compatibility through non-covalent bonds [1]. A fundamental question in organic supramolecular and biological materials is the knowledge of the actually involved interactions. Peptides are short molecules yielding to numerous examples of molecular self-organized systems. Urea, which is the smallest molecules containing the peptide linkage and urea inclusion compounds constitute a prototype family of intergrowth nanoporous crystals [2]. In these crystals, the host network is made of honeycomb-like channels formed by helical ribbons of urea molecules. Each infinite and parallel channel exhibits an available diameter of ca. 5.25 Å in which linear guest molecules are densely packed in a one-dimensional arrangement. Aperiodicity in these materials generate quite new properties, such as a specific diffraction pattern [3], a matter transport through molecularly selective capillaries [4] or a selective compressibility [5].

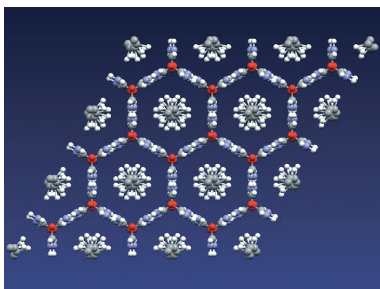


Figure 1. A projection in the basal hexagonal plane of the urea-alkane molecules within the disordered high symmetry phase.

Inside the urea hexagonal channel, alkane molecules occupy at room temperature a six-fold symmetry site which requires an orientational disorder about the long molecular axis, as illustrated in the figure 1. The urea sublattice has been characterized by the space group $P6_122$ with cell parameters in the commensurate plane: $a = b = 8.22$ Å at 295 K. At atmospheric pressure, this structure transforms into an orthorhombic phase, which has been described for urea by $P2_12_12_1$. The transition temperature, T_c , is 150 K for fully deuterated nonadecane-urea. It

increases versus pressure with a rather linear slope of 10K/kbar up to 6kbar.

Diffraction techniques at best identify symmetry breakings. Neutron scattering experiments were performed at the Laboratoire Léon Brillouin (Orphée reactor, Saclay, France). The data were collected on a triple axis spectrometer installed on a cold neutron source (4F). The incident wave vector was $k_i = 1.55$ Å⁻¹ with a refrigerated beryllium filter removing higher order contaminations.

At atmospheric pressure, the symmetry lowering, by the loss of threefold symmetry, generates three families of ferroelastic orthorhombic domains. They are related to the deformation of three orthohexagonal sublattices of metrics $b_0 = \sqrt{3} a_0$ and shifted by 120°. This ferroelastic phase transition generates then six equivalent twinned domains which impose the splitting of the Bragg reflections into six peaks, two of which being superimposed along the crystallographic axes. In the figure 2, is shown this already known splitting [6], characteristic of the low temperature ordered phase at atmospheric pressure.

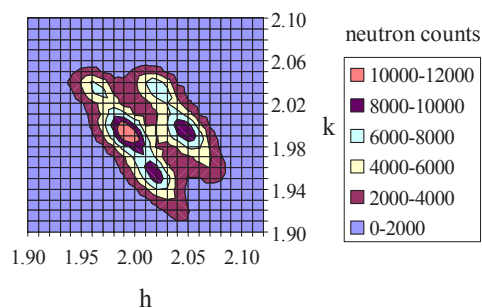


Figure 2. A neutron diffraction map of the (2 2 0) Bragg peak measured at in the orthorhombic ordered phase at atmospheric pressure at $T=120$ K.

Such Bragg peaks of the structure have been measured versus temperature and pressure going through the transition line which is evidenced by the appearance of superstructure Bragg peaks. The same map performed at 5.3kbar and 120 K, then far below the transition temperature T_c' (≈ 200 K), is shown in the figure 3. This measurement does not show any

splitting of the Bragg reflections in the ordered phase on the contrary to the atmospheric pressure case. In this high-pressure low symmetry phase, hexagonal metrics is kept within the limit of the spatial resolution, meaning that no significant shearing occurs in the structure.

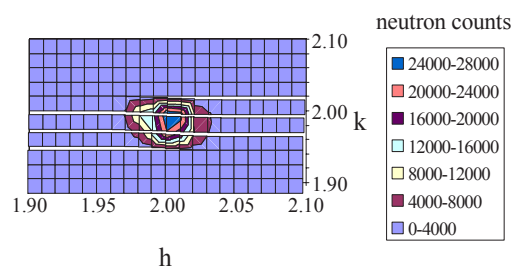


Figure 3. same as figure 2 but in the high pressure ordered phase ($P=5.3\text{kbar}$, $T=120\text{K}$): no splitting of the Bragg proves no apparent shearing of the structure.

This structural analysis of the mechanism triggering the phase transitions in self-organized supramolecular crystals is of fundamental importance for a deeper understanding of the actual interactions between the different networks. A first theoretical approach of this atmospheric pressure phase transition, based on a basal plane picture, considers it as resulting from a translation-rotation coupling between the rotational ordering of the chains and the shearing of the host sublattice [7]. This model describes the regime of this transition as both order-disorder and displacive. It was expected to be quite general, since to our best knowledge, in similar systems, the architecture of all the ordered structures at atmospheric pressure exhibits a large shearing of a few degrees. Clearly, the diffraction results reported here rule out this interpretation, at least under pressure.

Elastic properties are, of course, also very sensitive to structural modifications and provide for interactions changes through temperature or pressure anomalies. Sound velocity anomalies are related to the order parameter and conveniently studied by Brillouin scattering. Ferroelastic phase transitions are

usually characterized by a splitting of Brillouin lines resulting from the appearance of domains at low temperature which induce scattering along non equivalent crystallographic directions.

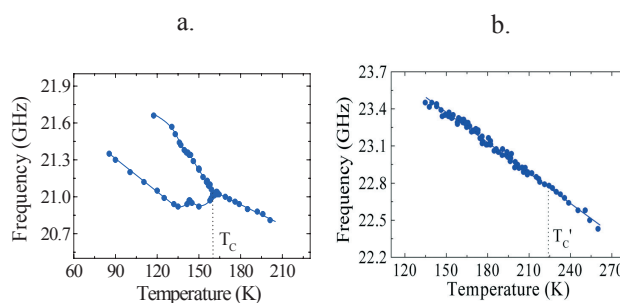


Figure 4. Brillouin longitudinal shift versus temperature a) at atmospheric pressure, b) at 5kbar.

Experimental results are here presented at atmospheric pressure and 5kbar. At atmospheric pressure, the figure 4a shows a splitting below 160 K, where each curve is due to different ferroelastic domains. The frequency change is typical of a static biquadratic coupling between the elastic strains and the square of the order parameter, independently of its fluctuation dynamics. At 5kbar, no elastic anomaly and therefore no splitting is observed (figure 4b), indicating no measurable coupling between the order parameter of this transition and the elastic strains of the composite structure. As the elastic properties mainly correspond to the rigid hydrogen-bonded urea network, it indicates that, in average, no significant urea reorientation occurs which could modify the elastic interactions at the scale of the phonon wavelength.

In conclusion, for the first time, we show that the ordering in self-organized materials may occur without any significant deformation of the host matrix. It invalidates at high pressure models which would consider the large shearing of the host sublattice as a driving force of the phase transition. This fundamental observation reported here could be of essential importance when considering the interactions in more complex architectures involving mutually interpenetrating supramolecular or tubular biological networks.

References

- [1] J. M. Lehn, *Science*, **295**, 2400 (2002).
- [2] M. D. Hollingsworth and K. D. M. Harris, *Comprehensive Supramolecular Chemistry* (Vol. 6; Solid State Supramolecular Chemistry: Crystal Engineering), pp. 177-237 (1996).
- [3] R. Lefort, J. Etrillard, B. Toudic, F. Guillaume, T. Breczewski, P. Bourges, *Phys. Rev. Lett.*, **77**, 4027 (1996).
- [4] A.A. Khan, S.T. Bramwell, K.D.M. Harris, B.M. Kariuki, M.R. Truter, *Chem. Phys. Lett.*, **307**, 320 (1999).
- [5] L. Bourgeois, C. Ecolivet, B. Toudic, P. Bourges, T. Breczewski, *Phys. Rev. Lett.*, **91**, 025504 (2003).
- [6] R. Forst, H. Jagodzinski, H. Boysen and F. Frey, *Acta Crystallogr. B* **43**, 187 (1987).
- [7] R.M. Lynden-Bell, *Mol. Phys.*, **79**(2), 313 (1993).
- [8] L. Bourgeois, B. Toudic, C. Ecolivet, J.C. Ameline, P. Bourges, F. Guillaume, T. Breczewski, *Phys. Rev. Lett.*, **93**, 026101(2004).

PHONON ANOMALIES IN HIGH T_c SUPERCONDUCTORS RELATED TO CHARGE STRIPE ORDERD. Reznik^{1,2}, L. Pintschovius¹, M. Sato³, M. Itoh³, S. Iikubo³, S. Yamada⁴¹Forschungszentrum Karlsruhe, IFP, POB 3640, D-76021 Karlsruhe, Germany²Laboratoire Léon Brillouin, CE Saclay, F-91191 Gif-sur-Yvette Cedex, France³Department of Physics, Division of Materials Science, Nagoya University, Nagoya 464-8602, Japan⁴Institute for Materials Research, Tohoku University, Katahira, Sendai 980-8577, Japan

It is a widespread belief that the holes doped into the CuO_2 planes of the cuprate superconductors tend to segregate into stripes that separate antiphase antiferromagnetic domains. However, solid evidence for such stripe order was obtained so far only for the particular compound $\text{La}_{1.48}\text{Nd}_{0.4}\text{Sr}_{0.12}\text{CuO}_4$ (LNSCO) and the closely related one $\text{La}_{1.875}\text{Ba}_{0.125}\text{CuO}_4$. In these two compounds, nuclear and magnetic superlattice peaks were observed indicative of static stripe order [1]. These compounds are special in that their doping level is about 1/8 and in that their low temperature structure provides a pinning potential for the charge stripes. We note that static stripe order seems to suppress superconductivity and therefore, stripe order is assumed to be dynamic in the superconducting cuprates.

Inelastic neutron scattering may be used to look for signatures of dynamic stripe both in the charge and in the spin channel. Here, we focus on the charge channel. Although neutrons cannot observe directly an inhomogeneous charge distribution, they may do so indirectly by looking at the atomic displacements induced by the inhomogeneous charge. More precisely, they can probe atomic vibrations and those vibrations having a displacement pattern closely related to charge stripe order should manifest themselves by an anomalous behaviour. Since an inhomogeneous charge distribution will modulate the Cu-O bond length, stripe-related phonon anomalies are expected to be strongest in Cu-O bond-stretching vibrations. Several neutron scattering investigations carried out at LLB on a number of doped and undoped high T_c compounds have indeed shown that doping induces pronounced anomalies in just those phonon branches associated with plane-polarized Cu-O bond-stretching vibrations whereas nearly all other modes show little change upon doping [2]. More precisely, doping induces a pronounced frequency renormalization of zone boundary modes in the (100) direction (Fig. 1) and, to a smaller extent, also in the (110) direction.

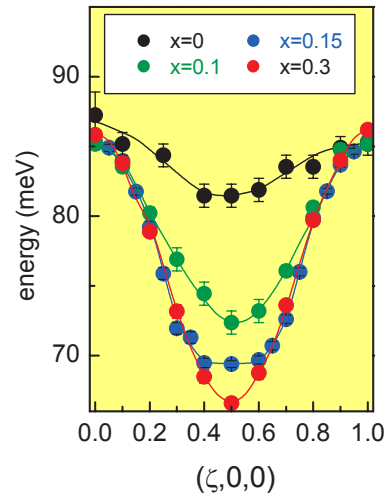


Figure 1. Dispersion of longitudinal Cu-O bond-stretching vibrations along the (100)-direction determined by inelastic neutron scattering at $T = 10$ K on $\text{La}_{2-x}\text{Sr}_x\text{CuO}_4$ for insulating ($x = 0$), underdoped ($x = 0.1$), optimally doped ($x = 0.15$) and overdoped ($x = 0.3$) samples.

The doping induced frequency renormalization can certainly be seen as evidence of a strong electron-phonon coupling of these modes but on the other hand, it is by no means obvious that this coupling is related to charge-density formation. Experiments carried out recently on the above mentioned stripe-ordered compound LNSCO have allowed us for the first time to establish a clear relationship between a certain phonon anomaly and charge stripe formation: the evidence comes not so much from the phonon dispersion which is intermediate between the curves for $x = 0.1$ and $x = 0.15$ shown in Fig. 1 but from the phonon linewidth: the linewidth, which is the most direct measure of the electron-phonon coupling strength, shows a very pronounced peak just at the ordering wave vector $q_{\text{CD}} = (0.24, 0, 0)$ of the charge-density wave [3] (Fig. 2). Moreover, the linewidth shrinks considerably on raising the temperature indicating that it is linked to an electronic instability. Last not

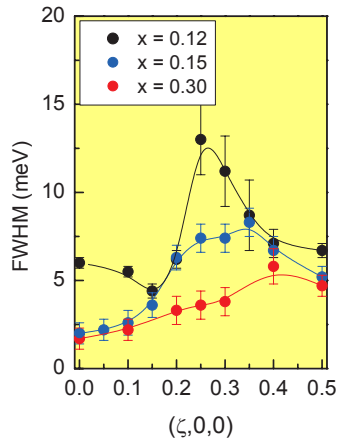


Figure 2. Resolution-corrected linewidths of Cu-O bond-stretching phonons along the (100)-direction observed on an optimally doped ($x = 0.15$) as well on an overdoped ($x = 0.30$) sample of LSCO at $T = 10$ K. The data for $x = 0.12$ were taken on LNSCO showing static stripe order with a wave vector $q = (0.24, 0, 0)$.

least, the displacement pattern of the anomalous mode is such that it favors dynamic charge accumulation on every fourth row of atoms as is observed in the static stripe pattern (Fig. 3). We note that a careful investigation of the next lower phonon branch with bond-bending character did not reveal any anomaly, in line with the fact that the displacement pattern of these phonons is unrelated to charge-density wave formation. We emphasize that the anomaly under discussion occurs in a high frequency branch at about 60 meV whereas practically all phonon anomalies observed previously in other compounds were found in low frequency branches. A notable exception is the extremely large linewidth observed recently for a high frequency mode (about 60 meV) in the 40 K classical superconductor MgB_2 . The strength of the phonon anomaly in LNSCO is somewhat surprising in view of the fact that the charge order related superlattice peaks are extremely weak and hence, only a small fraction of an elementary charge seems to be pinned to the static stripes. We presume that much larger charges are involved in strong fluctuations which persist below the charge ordering temperature.

References

- [1] J. M. Tranquada et al., Nature 375,561 (1995).
- [2] For a review, see L. Pintschovius and W. Reichardt, in "Neutron Scattering in Layered Copper-Oxide Superconductors", A. Furrer Ed., Phys. and Chem. of Materials with Low Dimensional Structures, Vol. 20, Kluwer Academic, Dordrecht 1998, p.165
- [3] L. Pintschovius, D. Reznik, M. Itoh, S. Iikubo and M. Sato, manuscript in preparation.
- [4] L. Pintschovius, D. Reznik, K. Yamada, manuscript in preparation.
- [5] L. Pintschovius, D. Reznik, et al., Phys. Rev. B 69, 214506 (2004).
- [6] L. Pintschovius, D. Reznik, et al., cond-mat/0308357

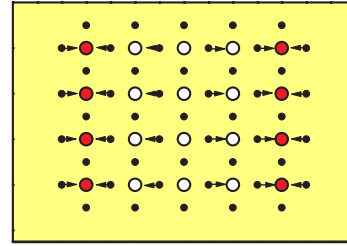


Figure 3. Displacement pattern of the anomalous bond-stretching phonon with wave vector $q = (0.25, 0, 0)$. Only the displacements in the CuO_2 plane are shown which are the dominant ones. The atoms highlighted in red are those where dynamic charge accumulation is favored by the displacements of the oxygen atoms

The results obtained on LNSCO allow us to look for precursor effects of charge stripe formation in compounds which do not develop any static order. Inspection of Figs. 2 shows that the behavior in $\text{La}_{1.85}\text{Sr}_{0.15}\text{CuO}_4$ is indeed reminiscent of that observed in LNSCO indicating that optimally doped LSCO is still close to a charge stripe instability. On the other hand, no such precursor effects are observed in overdoped LSCO [4] in line with the general belief that overdoped cuprates behave essentially like ordinary metals.

The question remains whether or not the tendency towards stripe order is restricted to LSCO. Extensive investigations of the magnetic excitations in the prototypical high T_c compound $\text{YBa}_2\text{Cu}_3\text{O}_{7-x}$ have not led to a generally accepted conclusion. We note that we recently embarked on a detailed study of the phonons in optimally doped $\text{YBa}_2\text{Cu}_3\text{O}_{6.95}$ [5] and that we did find pronounced precursor effects of charge stripe order [6]. In this case, the evidence came primarily from the anomalous temperature dependence of certain phonon modes whereas the line broadenings are difficult to measure because of strong hybridization of bond-stretching phonons with other phonon modes. Nevertheless, it is safe to say that the effects observed in optimally doped YBCO resemble those found in the static stripe compound LNSCO. This indicates that the tendency towards stripe order is not a peculiarity of the LSCO system.

MAGNETIC ORDER IN HIGH-PRESSURE OXYGEN

I. Goncharenko¹, O. Makarova^{1,2}, L. Ulivi³¹ Laboratoire Léon Brillouin (CEA-CNRS), CEA- Saclay, 91191 Gif sur Yvette Cedex² Russian Research Center "Kurchatov Institute", Moscow 123182, Russia³ Istituto di Fisica applicata "N. Carrara", Via della Madonna del piano, I-50019 Sesto Fiorentino, Italy.

While being one of the most casual elements in our planet, elementary oxygen shows many unusual features. O₂ is the only elementary molecule which carries a magnetic moment ($S=1$). At ambient pressure, solid oxygen is an antiferromagnetic insulator. Magnetic interactions between O₂ molecules are comparable with weak intermolecular forces, therefore magnetism plays an important role in stabilization of a particular crystal structure. In this respect, oxygen is different from any other solid. Magnetic interactions were claimed to be responsible for a structural transition from the rhombohedral β -phase to a monoclinic α -phase at $T=24$ K and ambient pressure. Under high pressures, solid oxygen transform successively into an orthorhombic δ -phase ($P=6$ GPa), then into a monoclinic ε -phase ($P=8$ GPa) and finally to a metallic and superconducting ξ -phase ($P=96$ GPa, $T_c=0.6$ K [1]).

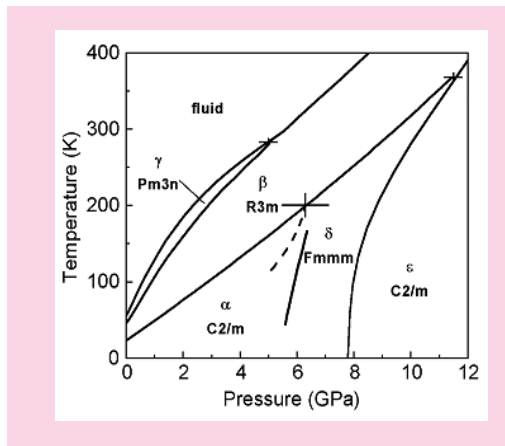


Figure 1. Pressure-temperature phase diagram of solid oxygen at $P < 12$ GPa [2].

Undoubtedly, magnetism should play an important role in these transformations. Pressure could change a balance between the intermolecular and magnetic interactions. Under very high pressures, hybridisation between molecular orbitals could lead to a partial suppression of the localized magnetic moments. Finally, before the transition to the superconductive state one might expect a complete magnetic collapse. Even more intriguing,

magnetic properties of dense oxygen are directly related to the fundamental properties of the diatomic molecules under pressure. Do they transform directly from a diatomic state to a metallic monoatomic state? Are there any intermediate “polymerised” states? Magnetic properties give a possibility for monitoring of the molecular state. Formation of a “molecular polymer” or multi-atomic molecules X_n ($n > 2$) are expected to break the magnetic order.

Until now there was no any direct information on magnetic order in high-pressure oxygen. Measuring of vibron modes by optical spectroscopy suggested that solid oxygen remain antiferromagnetic up to 7 GPa [3]. No evidence for new magnetic structures was found by the indirect probes and theoretical simulations.

Only neutron diffraction could answer the question about magnetic orderings in high-pressure oxygen. Due to high penetration, relatively low intensity of magnetic peaks and problems of preferable orientation, neutron studies of high-pressure oxygen is a difficult task. At the LLB, we carried out a first neutron diffraction study of magnetic order in solid oxygen under pressures up to 7 GPa [4]. We used the original pressure and neutron setups developed at the LLB and allowing to study magnetic orders under pressures as high as 50 GPa and temperatures as low as 0.1 K. Liquid O₂ was loaded in the pressure cell with anvils made from superhard boron nitride. Neutron diffraction spectra in the temperature range 4-300 K were measured on the specialized high-pressure diffractometer G6.1 “MICRO”.

In the region of stability of the α -phase ($P < 6.2$ GPa) we found a remarkable enhancement of magnetic interactions between O₂ molecules. Temperature of transition towards to long-range ordered antiferromagnetic state increases by order of magnitude, from 24 K at $P=0$ up to 200 K at $P=6.2$ GPa (T_{LRO}). The disappearance of the magnetic signal exactly coincides with the α - β structural transition. Our results provide a direct confirmation of the magneto-structural origin of the α - β transition in a wide range of interatomic distances.

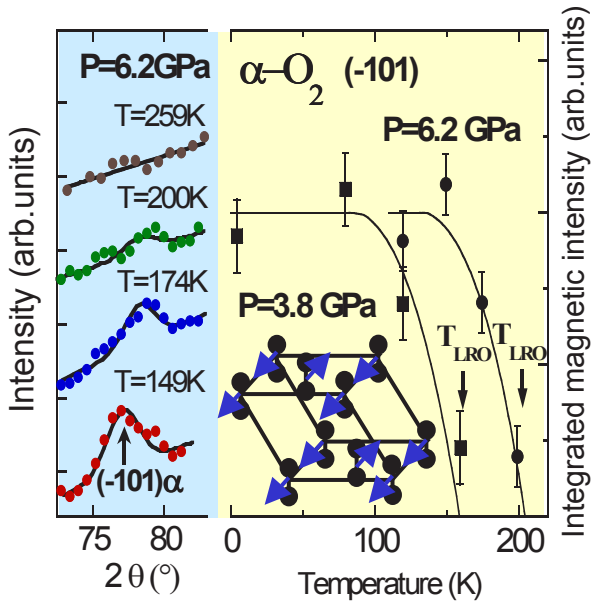


Figure 2 Left: temperature evolution of the magnetic peak (10-1) measured in α -O₂ at P=6.2 GPa. Right: integrated magnetic intensity of the (10-1) peak versus temperature at pressures of 3.8 GPa (squares) and 6.2 GPa (circles). In inset: magnetic structure of α -O₂.

At P=6.2 GPa we crossed the transition line between the α - and δ - phases. At this pressure and low temperature (<100 K) we observed new diffraction peaks which were not found in previous X-ray measurements and should be attributed to a magnetic order in the δ phase. Surprisingly, the magnetic peaks from α - and δ phases are located at completely different scattering angles. The crystal structures of α - and δ -O₂ are very similar and can be described in the same monoclinic unit cell with only slightly different lattice parameters. One can naturally expect that the magnetic scattering in δ -O₂ will be essentially the same as in α -O₂ except a tiny shift in the peak position due to the change in lattice parameters. Contrary to these expectations, neutron diffraction results show that the magnetic structures in α -O₂ and δ -O₂ are completely different (Fig. 3). In Fig. 3 we show calculated scattering profiles assuming the same type of order as in the α -phase and new type of order with ferromagnetic stacking of the O₂ plane. The first model completely disagrees with our experiment whereas the later model fits perfectly our data.

References

- [1] K. Shimizu et al., Nature (London) 393 (1998), 767.
- [2] F. A. Gorelli et al., Phys. Rev. B 65 (2002), 172106.
- [3] F. A. Gorelli, et al., Phys. Rev. B 62 (2000), R3604.
- [4] I.N. Goncharenko, O.L. Makarova, L. Ulivi, Phys. Rev. Lett. 93 (2004), 055502

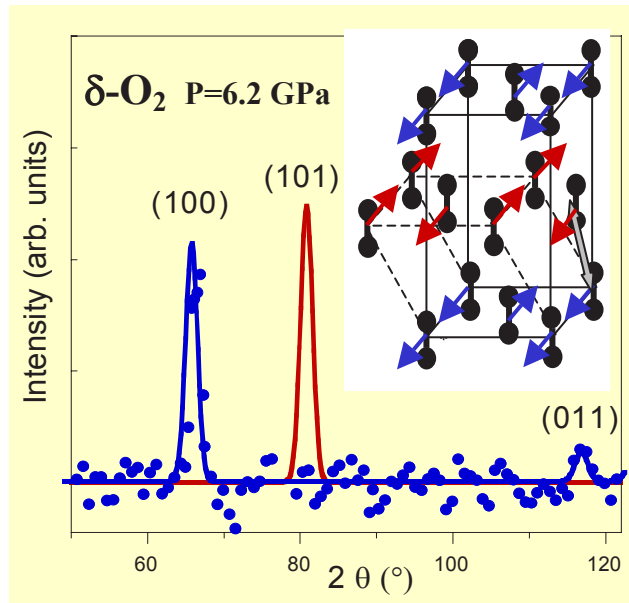


Figure 3. Dots: experimental data on magnetic scattering in δ -O₂ at P=6.2 GPa and T=4 K. Lines: calculated profiles assuming the same type of magnetic structure as in α -O₂ (in red) and new type of magnetic structure shown in inset (in blue).

The magnetic structure of δ -O₂ is very intriguing. It was not suggested by indirect measurements and it was not found in ab-initio calculations. Especially ferromagnetic coupling between the nearest off-plane neighbours (Fig. 3) is very surprising. Simple quantum considerations suggest negative sign of exchange constant favouring antiparallel spin arrangements. One can think that the interplanar magnetic stackings in the δ -phase is driven by long-range magnetic interactions with second and third off-plane neighbours, which are negligible at P=0. The growing importance of the long-range magnetic interactions should be attributed to a growing delocalisation of the O₂ orbitals under pressure and could be a first sign of a magnetic collapse expected at higher pressures. In conclusion, we show that practically all phase transitions in solid O₂ at pressures P<7 GPa have magneto-structural character. Neutron diffraction study of magnetic order in ϵ -O₂, now in progress, should clarify how this “spin controlled” molecular crystal transforms into a metallic superconductor

2 - MAGNETISM AND SUPERCONDUCTIVITY

2 - MAGNETISM AND SUPERCONDUCTIVITY

Magnetism is a virtually unlimited field of activity for neutron scattering studies. Applications range from well-established topics like high-temperature superconductors, « colossal magnetoresistance » manganites, or heavy-fermion compounds, to more emerging problems : photomagnetism, magnetic structures and excitations in epitaxial films, incommensurabilities in composite systems, etc. In many cases, neutrons are unchallenged in their ability to reveal details of the time and space dependencies of relevant interactions at a microscopic level. A number of examples can be found in the following sections, which present an overview of the most significant results obtained over the last two years.

STRONGLY CORRELATED ELECTRON SYSTEMS

Spin dynamics in hole-doped high-temperature superconducting cuprates

Ph. Bourges, S. Pailhès [Ph. D. thesis], Y. Sidis (LLB) - B. Keimer, V. Hinkov (MPI Stuttgart) [Ph. D. thesis] - D. Reznik, L. Pinschovius (KFK Karlsruhe) - M. Braden (Univ. Cologne) - M. Tranquada (Brookhaven National Lab.) - Y. Endoh (IMR, Tohoku Univ. Sendai)

In order to understand electron pairing in high-temperature superconducting (SC) copper oxides, one needs first to shed light on the intrinsic nature of the CuO_2 planes on a microscopic scale. There are, for the time being, two main schools of thought. For the first one, the CuO_2 planes are characterized by a uniform 2D liquid of itinerant charge carriers in strong interaction. The second one rather assumes that a spin-charge segregation takes place in the CuO_2 planes, resulting in hole-rich nonmagnetic lines playing the role of anti-phase boundaries between hole-poor antiferromagnetic domains. The study of the spin excitation spectrum by inelastic neutron scattering (INS) can provide valuable information to discriminate between a 2D itinerant picture or a 1D “stripes” scenario. To this aim, we have developed a strategy based on : *i*) comparison with canonical stripe-ordered systems, *ii*) search for uniaxial anisotropy in orthorhombic systems, *iii*) search for hallmarks of the physics of CuO_2 planes in the dispersion of magnetic collective modes *iv*) study of the effect of inter-plane interactions on the spin dynamics in bilayer systems. Results obtained along these lines are summarized hereafter.

i) In several cuprates such as $\text{YBa}_2\text{Cu}_3\text{O}_{6+x}$, the spin excitation spectrum is characterized by the appearance, in the SC state, of an antiferromagnetic (AF) excitation whose energy scales with the critical temperature: the so-called “magnetic resonance peak”. This excitation exhibits a downward dispersion and was first interpreted in terms of triplet exciton which can develop in a *d*-wave superconductor according to itinerant models. Alternatively, it has been proposed that this $S = 1$ collective mode might be reminiscent of magnons in a disordered stripe system. To test this suggestion, INS experiments were performed in the diagonal-stripe-ordered system $\text{La}_{1.69}\text{Sr}_{0.31}\text{NiO}_4$. The spin waves are actually found to merge at the AF wave vector as predicted, while their overall evolution as a function of temperature or wave vector does not match that reported for the magnetic resonance peak in cuprates, pointing to marked differences between the spin dynamics of stripe-ordered-nickelates and superconducting cuprates.

ii) The INS measurements carried out at the LLB and the ILL on almost fully detwinned $\text{YBa}_2\text{Cu}_3\text{O}_{6+x}$ single crystals revealed 2D spin fluctuations in the SC state, with an incipient 1D anisotropy at an energy well below that of the magnetic resonance peak. This result, valid from optimal doping ($x = 0.9$) to the underdoped regime ($x = 0.66$), implies that the orientation of stripes (if any) has to fluctuate. In contrast, in an itinerant picture, the anisotropy of the magnetic response should reflect the effects of orthorhombicity and a possible Pomeranchuk instability on Fermi surface (see *Highlights*: Hinkov et al.).

iii) Close examination of the upper part of the spin excitation spectrum in optimally doped $\text{YBa}_2\text{Cu}_3\text{O}_{6.95}$ has revealed an unsuspected upward dispersive resonant magnetic mode, starting near or at the magnetic resonance peak. In slightly underdoped $\text{YBa}_2\text{Cu}_3\text{O}_{6.85}$, the upward branch was found to become evanescent when approaching particular wave vectors. This phenomenon could reflect the electron-hole decay of collective spin fluctuations within the magnetic continuum in the SC state, as predicted in itinerant models. Surprisingly, the X-shape dispersion around the AF wave-vector can also be found in many stripe models.

iv) $\text{YBa}_2\text{Cu}_3\text{O}_{6+x}$ is a bilayer system (containing two CuO_2 planes per unit cell), and intra-bilayer interactions should thus lift the degeneracy of purely planar spin fluctuations. In addition to the magnetic resonance peak of odd symmetry with respect to the exchange of spin within the bilayer, a second resonant excitation of

much weaker intensity and of even symmetry has recently been observed at higher energies. The asymmetric intensity of both odd and even resonant modes has been used to pinpoint the threshold of the SC spin-flip continuum at the AF wave vector, which scales with the maximum of the SC gap, as expected in the itinerant picture. On the other hand, the odd or even symmetry of the spin fluctuation implies that charge stripes should be stacked on top of each other within the bilayer: a rather unfavorable arrangement in terms of Coulomb energy.

Long- and short-range magnetic order, charge transfer and superconductivity in $\text{YBa}_2\text{Cu}_{3-x}\text{Co}_x\text{O}_7$

F. Maury (DRECAM/LSI CEA Saclay) - I. Mirebeau, Ph. Bourges, Y. Sidis (LLB) - J. A. Hodges, A. Forget (DRECAM/SPEC CEA Saclay)

In the $\text{YBa}_2\text{Cu}_{3-x}\text{Co}_x\text{O}_7$ system, Co substitution suppresses superconductivity at $x_c = 0.42$ and antiferromagnetic long-range order emerges above this concentrations. Previous measurements performed at the LLB on a single crystal (Hodges et al. Phys. Rev. B 2002, *LLB report* 2001-2002), had shown that AF order might exist in some superconducting fully oxidized crystals at low Co content ($x \sim 0.04$). The phase diagram derived from systematic powder experiments in a wide concentration range ($0.03 \leq x \leq 0.72$) did not evidence such coexistence but revealed a number of new interesting features. The Co ions substitute almost only on the charge reservoirs, the Cu1 sites, and that their charge varies from 4+ to 3+ with increasing Co content. The antiferromagnetic order survives at much higher hole doping than in related systems ($p = 0.14$ hole/Cu2 plane instead of ~ 0.04 in YBCO_y and Ca-YBCO_6). This suggests that Co substitution does not only change the hole concentration in the Cu2 planes but also reduces the hole mobility. This interpretation is supported by the fact that the metal-insulating transition coincides with the onset of AF long-range order at x_c . The AF order shows notable differences compared to that found in $\text{YBa}_2\text{Cu}_3\text{O}_6$. In particular the unit cell is doubled along the c axis, with a non-zero moment on the Cu1 sites. The Co moments remain mostly disordered, forming random AF next-nearest-neighbor pairs. For $x > x_c$, these pairs compete with the ordered AF structure, which can explain the surprisingly low value of the ordered moments at the Cu1 sites.

Spin dynamics of the electron-doped high-Tc cuprate $\text{Nd}_{2-x}\text{Ce}_x\text{CuO}_4$

D. Petitgrand (LLB) - K. Yamada, T. Uefuji (Kyoto University) - M. Greven, E. Motoyama (Stanford University)

i) Electron-doped versus hole-doped superconductors

The electron-doped superconductors $\text{Nd}_{2-x}\text{Ce}_x\text{CuO}_4$ share some common features with their p -type counterparts (typically the CuO_2 planes sandwiched by donor/acceptor rare-earth blocks). However significant differences have also been found, which may help elucidate the common mechanism for superconductivity involved in the two families. Among interesting results obtained at the LLB is the detailed characterization of the magnetic excitation spectrum as a function of energy and temperature.

ii) Low temperature magnetic excitations

Magnetic excitations are found to be confined to the magnetic 2D rod $\mathbf{Q} = (1/2, 1/2, \zeta)$, and do not show any incommensurate feature. At low temperature the magnetic excitation spectrum shows a well-defined spin gap of 2.9 meV. Above the gap there exists a continuum of excitations, in contrast to the magnetic resonance peak observed in p -type HTSC.

iii) Temperature dependence of the spin gap

An in-depth study of the temperature dependence of the spectrum has been done by performing constant-energy \mathbf{Q} scans through the rod. The dynamical susceptibility below an energy of 2 meV decreases with decreasing temperature, as the sample enters the superconducting state, vanishing completely at $T = 1.6$ K. This clearly demonstrates the suppression of electronic states below 2 meV in the superconducting state. The distortion of the excitation spectrum can be described as a decrease of the spin gap when temperature is increased up to T_c . Additional measurements at lower energies, measured with $k_f = 1.97$ and 1.64 \AA^{-1} , give evidence that the normal state spectrum is gapless down to very low energies. The spectrum at $T = 1.6$ K, when compared with that at $T = 26$ K, reveals a broad range of energies above the gap, between 2 and 4 meV, where the density of excitations is only partially reduced. The latter feature may be associated with the anisotropic d -wave gap order parameter.

Vortex lattice studies

A. Pautrat, Ch. Simon, G. Poullain, C. Goupil, J. Scola [Ph. D. Thesis] (CRISMAT Caen) - P. Mathieu, A. Brûlet (LLB)

Vortex lattice studies are important to understand critical currents in superconductors. Small angle neutron scattering measurements on YBaCuO samples with different densities of twin boundaries have revealed that these twin boundaries produce both a meandering of the flux lines and, as their density increases, a change in the apparent symmetry of the flux line lattice from hexagonal to square (see *Highlight*: Pautrat et al.).

Spin-ladder compounds

M. Braden (Univ. Cologne) - R. Klingeler, T. Kroll, J. Geck, B. Büchner (Leibnitz Institute IFW Dresden) - J. Etrillard (Univ. Rennes) - A. Gukasov (LLB) - M. Hücker, U. Ammerahl, A. Revcolevschi (Univ. Paris Sud)

The compound $\text{Sr}_{14}\text{Cu}_{24}\text{O}_{41}$ exhibits an incommensurate structural modulation resulting from a misfit between the c lattice parameters of the two planar components (CuO_2 chains, and $\text{Sr}_2\text{Cu}_2\text{O}_3$ ladders) of its composite structure. High- Q -resolution experiments on the triple-axis spectrometer 4F2 have shed light on the controversial charge-ordering transition occurring near 250 K. The results suggest that charge ordering is indeed responsible from the superstructure reflections observed below the transition, but that its modulation locks onto that of the composite structure (see *Highlights*: Braden et al.).

Hole-doping of these materials by La substitution causes pronounced effects on their magnetic properties, which may be taken as a paradigm for understanding those found in cuprates. Neutron diffraction experiments on $\text{La}_5\text{Ca}_9\text{Cu}_{24}\text{O}_{41}$ have shown correlations with a very weak value of the induced ferromagnetic component. This behavior is interpreted as a coupled spin-charge effect in which a motion of the holes along the chains is accompanied by a motion of the magnetic domain walls (see *Highlights*: Klingeler et al.).

Manganites

P. Kober-Lehouelleur [Ph. D. thesis], M. Hennion, F. Moussa, F. Wang, A. Gukasov, F. Ott (LLB) - M. Viret, H. Glättli (DRECAM CEA Saclay) - J.-P. Renard (IEP, Univ. Paris-Sud) -R. Suryanarayanan, M. Apostu, L. Pinsard-Gaudart, A. Revcolevschi (Univ. Paris-Sud) - A. Ivanov, J. Kulda (ILL) - L.-P. Regnault (DRFMC CEA Grenoble)

Among the numerous challenges faced in understanding colossal magnetoresistance (CMR) manganites $\text{La}_{1-x}\text{Ca}_x\text{MnO}_3$, the possible existence of mixed phases has been pointed out by numerical studies. In recent inelastic neutron scattering experiments for the compositions $x = 0.17$ and 0.22 , remarkable anomalies have been observed in the dispersion of magnetic excitations, which could be interpreted in terms of spin waves confined within finite-size, hole-poor, orbital-ordered regions (see *Highlights* : M. Hennion et al.).

Other aspects of phase coexistence have been investigated in the Pr compound $\text{Pr}_{0.67}\text{Ca}_{0.33}\text{MnO}_3$. At low temperature, this compound is insulating and residual conductivity takes place only through a « variable-range-hopping » process. It is proposed that, in this situation, a new channel of magnetic exchange interaction termed «hopping exchange » exists, leading to the segregation of a filamentary phase in which Mn spins are parallel, with (AF-coupled) spins outside the filaments playing the role of a magnetic shield. This view is supported by the observation of a fractal law with exponent $5/3$, reminiscent of polymer physics, in polarized small-angle neutron scattering measurements as well as in Monte Carlo simulations (see *Highlights* : Viret et al.).

New studies have been undertaken on the bilayer manganite $(\text{La}_{0.4}\text{Pr}_{0.6})_{1.2}\text{Sr}_{1.8}\text{Mn}_2\text{O}_7$. $\text{La}_{1.2}\text{Sr}_{1.8}\text{Mn}_2\text{O}_7$, exhibits a phase transition from a paramagnetic insulating (PI) to a ferromagnetic metallic (FM) state with a CMR effect. Upon 60% Pr substitution, magnetic order and PI to FM transition are suppressed. Application of a moderate magnetic field restores a FM state with a CMR effect. Neutron scattering by a single crystal of, under a magnetic field of 5 T, has revealed a long-range and homogeneous ferromagnetic order. In the PI phase, under zero field, correlated lattice polarons have been detected. At 28 K, under 5 T, the spin wave dispersion curve determines an in-plane isotropic spin wave stiffness constant of $146 \text{ meV } \text{Å}^2$. So the magnetic field not only generates a homogeneous ferromagnetic ground state, but also restores a magnetic coupling characteristic of FM CMR manganites. Unpolarized and polarized neutron diffraction measurements have also been carried out on this compound. Magnetization density reconstruction by the maximum-entropy method, together with multipole refinement on flipping ratios, evidence the existence of two distinct field-induced ferromagnetic (FIFM) states. For $H \parallel c$, the FIFM(c) state is characterized by the presence of a magnetic moment of $0.48(2) \mu_B$ on the Sr site, due to Pr substitution, and by a high population of the $3z^2-r^2$ orbitals of Mn^{3+} . For $H \parallel a, b$ no magnetization density was found at the Sr site and the x^2-y^2 orbital is slightly more populated than the $3z^2-r^2$ orbital.

Anomalous rare-earth magnetism

i) Spin dynamics in mixed-valence systems and Kondo insulators

J.-M. Mignot (LLB) - P. A. Alekseev, K. Nemkovski, E. Nefeodova (RRC “Kurchatov Institute” Moscow) - N. Yu. Shitsevalova, Yu. B. Paderno (IPMS Kiev) - F. Iga, T. Takabatake (ADSM Hiroshima)

Previous studies of the low-temperature spin-gap state in YbB_{12} (*LLB report* 2001-2002) had revealed a pronounced Q dependence of the sharp magnetic mode denoted $M1$ near 15 meV, with a minimum in the dispersion and a maximum in the intensity at the AF point $(\frac{1}{2}, \frac{1}{2}, \frac{1}{2})$. This behavior has been fully confirmed by new polarized-neutron experiments on IN20 (ILL), as well as the magnetic character of the second mode $M2$ (20 meV), whose Q and T behaviors differ markedly from those of $M1$. It is suggested that $M1$ may correspond to the spin-exciton *in-gap* mode predicted by Riseborough, i.e. a bound state of an electron-hole pair produced by strong AF correlations. Time-of-flight measurements on $\text{Yb}_{0.25}\text{Lu}_{0.75}\text{B}_{12}$ (HET ISIS) have confirmed that the spin-gap response persists far into the diluted regime, where the electronic state is unambiguously metallic, supporting the view that the spin-gap formation is based, at least partly, on a local mechanism and does not directly depend on the existence of the hybridization gap.

Previous work on Sm mixed-valence (MV) systems has been extended to another compound, EuCu_2Si_2 , in which Eu fluctuates between the 3+ state (same electronic configuration as Sm^{2+}) and the pure-spin state Eu^{2+} ($J = S = 7/2$). The spin-orbit $J = 0 \rightarrow J = 1$ transition has been observed on isotopic (^{154}Eu) powder at ISIS (HET), with the interesting result that the excitation is sharp but split into a doublet and shifted with respect to the value expected for the free ion. A crystal-field splitting of the $J = 1$ state would be compatible with the site symmetry but quite unexpected in view of the strong degree of valence mixing. Other interpretations (exciton state, coupling to phonons, ...) are currently under consideration.

ii) Magnetic polarons, p-f mixing

K. Iwasa (Tohoku Univ.) - M. Kohgi (Tokyo Metropolitan Univ.) - M. Braden (Univ. Cologne) - J.-M. Mignot (LLB) - H. Kitazawa (National Institute for Materials Science, Japan) - T. Suzuki (Tsukuba Institute of Science and Technology)

CeX ($X = \text{P, As, Sb and Bi}$) compounds are known to exhibit magnetic structures with two different Ce magnetic moments originated from the different crystal-field states Γ_7 and Γ_8 . This feature is explained by the magnetic-polaron effect produced by the localization of the low-density carriers and the strong *p-f* mixing between the Ce-ion Γ_8 state and the *p*-hole state of neighboring *X* ions. Inelastic neutron scattering experiments on CeSb and CeBi have revealed a new phonon existing only in the magnetically ordered phases due to the *p-f* mixing effect. The observed new phonon is a stretching mode of the Ce-*X* bond forming the *p-f* mixing orbital. This fact indicates a novel coupling between electronic states by the *p-f* mixing and the crystal lattice.

iii) Multipolar interactions in Ce-based hexaborides

J.-M. Mignot, G. André (LLB) - F. Iga, M. Sera (ADSM Hiroshima)

Light rare-earth hexaborides RB_6 ($R = \text{Ce, Pr, Nd}$) are unique examples of the interplay between different types of multipole couplings as, for instance, in the so-called “phase II” of pure CeB_6 whose description requires consideration of dipole, quadrupole, and octupole interactions. The evolution of (H, T) magnetic phase diagrams in the $(\text{Ce,Nd})\text{B}_6$ and $(\text{Ce,Pr})\text{B}_6$ solid solutions has been studied by both powder and single-crystal neutron diffraction. A number of new phases have been observed and characterized including, for $x_{\text{Pr}} = 0.3$, a novel regime tentatively ascribed to an incommensurate order of quadrupole moments.

Quantum magnetism, spin liquids

i) Magnetic structure of a frustrated $S = \frac{1}{2}$ square lattice (Highlights : Bombardi et al.)

The controversial issue of the exact magnetic structure of $\text{Li}_2\text{VOSiO}_4$ has been settled by combining results of powder neutron and x-ray diffraction. It consists of a FM stacking, along the *c* axis, of collinear AF *a-b* layers. The ordered magnetic moment is larger than previously reported and compatible with the large next-nearest-neighbor exchange ($J_2/J_1 \gg 1$) predicted by local density calculations.

ii) Spin correlations in a dimer spin liquid (Highlights : Rüegg et al.)

Elementary singlet-triplet excitations in the spin-liquid dimer ground state of TlCuCl_3 have been determined as a function of temperature up to $k_B T \approx J_{\text{intra}}$, the dominant AF exchange interaction. Tracing the renormalization of spin correlations at high enough temperatures provides an insight into the correct statistical description of this quantum many-body system. Excellent agreement is found with the Troyer-Tsunetsugu-Würtz mean-field theory.

MAGNETIC FILMS AND MULTILAYERS

Diffraction on thin layers and multilayers using three-axis spectrometers

B. Hennion (LLB)

Significant results have been obtained recently in diffraction measurements on thin layers or multilayers performed on 4F1 and 4F2. The main advantages of using cold-beam three-axis spectrometers for such studies are: *i)* the high flux of cold neutrons, *ii)* the good resolution, *iii)* the background reduction provided by the analyzer, *iv)* the availability of a full polarization analysis of the scattering process. Up to now, most studies have been devoted to the determination of magnetic structures.

The recent search for materials suitable for applications in the field of so-called “spintronics”, where control of the carrier spin state is required, has stimulated new demand for magnetic characterization of thin layers. Indeed a variety of new systems are now produced by such methods as beam epitaxy, sputtering, vapor deposit, etc. These systems often consist of a stacking of layers with different physical properties. For instance, ferro-magnetic layers can be sandwiched with a nonmagnetic spacer. For thin enough layers, a magnetic interlayer coupling often takes place, the mechanism of which is not yet fully understood. The existence of AF coupling between ferromagnetic layers offers the possibility to trigger the system by means of an external parameter (e.g. magnetic field or illumination). In other systems, the characteristics of an AF layer can be influenced by the magnetization of a ferromagnetic coating layer. In this case domain structuration seems to be the relevant parameter.

Neutron diffraction measurements provide valuable information on such systems because, on the one hand, they give direct evidence for the existence of AF correlations or long-range order, and on the other hand they can determine the size of magnetic domains when distances of less than about 100 nm are involved. Recent measurements on various systems (Si/Fe, Fe/Fe₂N multilayers [see *Highlights*: Szuszkiewicz et al.], NiO, MnPt, FeF₂ thin layers) have demonstrated the feasibility of such measurements on samples with an area of typically 1 cm² and a thickness as low as 5 nm. Improvements of sample environments are underway to extend the possibilities of such measurements.

Magnetic behavior of Eu epitaxial thin films

S. Soriano [Ph. D. thesis], K. Dumesnil, C. Dufour, Ph. Mangin (LPM Nancy) - M. Hennion (LLB)

Bulk Eu is known to undergo a magnetic phase transition to a helical order phase at $T = 90$ K. The helical axis is aligned along one of the equivalent cubic $\langle 100 \rangle$ directions, leading to the formation of 3 magnetic domains. Elastic neutron scattering experiments on Eu MBE thin films performed by the Nancy group, both at the LLB and NIST (USA) have shown that external stress modifies the magnetic behavior of Eu by making the domain inequivalent (destabilization of the domain with in-plane helical wave vector; rotation of the out-of-plane wave vectors initially aligned along cubic axes). Domain population can be further modified by applying a magnetic field, giving rise to magnetic irreversibility. Basing on symmetry considerations and on correlations between deformation amplitudes and magnetic effects, two types of models have been considered, involving either exchange magnetoelasticity or magnetostriction.

Magnetic exchange interactions in hexagonal MnTe

B. Hennion (LLB) - W. Szuszkiewicz, B. Witkowska, E. Łusakowska, A. Mycielsky (Polish Academy of Science, Warsaw)

The Mn element is involved in many magnetic systems, either as a constituent or as a dopant. The resulting magnetic properties depend on the details of exchange interactions, which are very sensitive to the crystal structure of the compound. This property is actually used on a phenomenological basis to modify the properties of semiconducting materials, with a significant renewal due to the possibility of growing novel systems by such methods as, e.g., beam epitaxy or sputtering. In pure systems one can achieve an accurate

determination of magnetic exchange interactions and anisotropies through the analysis of the spin-wave dispersion. Single-crystal inelastic neutron scattering is the only technique providing direct access to the spin-wave spectrum, from which an insight can be gained into the microscopic mechanisms responsible for the magnetic exchange.

Such an analysis has already been performed for cubic (zinc-blende structure) MnTe obtained by beam epitaxy. MnTe naturally crystallizes in the NiAs hexagonal structure, and is magnetically ordered (type-I AF) up to ~ 310 K. Cubic MnTe, on the other hand, orders in a type-III antiferromagnetic structure below T_N

67 K. This difference gives us an opportunity to determine a new set of exchange interactions complementing those previously determined for the cubic phase.

A single crystal of volume ~ 30 mm³ was grown at the Institute of Physics in Warsaw. Spin-wave measurements were performed on the thermal-beam three-axis spectrometer 2T, and a complete set of dispersion curves has been determined at $T = 15$ K, along the [100], [001], and [101] directions of the reciprocal lattice. The determination of exchange integrals and anisotropies is in progress and will involve exchanges at least up to third nearest neighbors.

Neutrons surface scattering techniques applied to the study of magnetic thin films

F. Ott, G. Chaboussant, S. Gautrot (LLB)

In the last two years, a number of scattering techniques have been applied to the study of thin films. Besides the classical specular reflectivity technique (PRISM), Grazing Incidence Small Angle Neutron Scattering (GISANS) has been implemented on the new spectrometer PAPHYRUS (see chapter on Technical and Instrumental Developments). Direct diffraction has been applied to characterize the atomic structure of magnetic films as thin as 10 nm. Using this panel of techniques, one can now probe the structure of thin films in an extremely wide range of Q vectors spanning over 5 orders of magnitude:

Off-specular reflectivity (OSR)	$6 \times 10^{-5} < Q < 6 \times 10^{-3} \text{ nm}^{-1}$
Specular reflectivity (SR) and GISANS	$6 \times 10^{-2} < Q$ and $Q_{\parallel} < 1 \text{ nm}^{-1}$
Diffraction	$1 < Q < 20 \text{ nm}^{-1}$

This makes it possible to cover a broad range of topics ranging from magnetic order in epitaxial thin films (FeF₂, Fe₂O₃, NiO, MnPt) or magnetism at interfaces (Fe/FeN, Fe/Si, GaAs/GaMnAs, Gd/Cr, Gd/V, Fe₃O₄/Fe₂O₃, FeF₂/Fe...), to thin-film magnetic nanostructures (Fe nanodots, magnetic aggregates) and magnetic domains (Fe/FeF₂, FePd).

These type of measurements are illustrated by measurements on FePd thin films mixing different types of magnetic anisotropies and domain structures.

Besides the above developments of surface scattering techniques, significant effort is now devoted to improving sample environments for magnetic studies (high fields, wide temperature range).

MOLECULAR MAGNETISM, PHOTOMAGNETISM

A. Goujon, B. Gillon, G. André, A. Cousson, A. Goukassov (LLB) - C. Sangregorio et al. (University of Florence) – G. McIntyre (ILL Grenoble)

High-spin molecular clusters are of particular interest because they behave as “single-molecule magnets”. The magnetic ground state ($S = 10$) of the high-spin cluster [(tacn)₆Fe₈O₂(OH)₁₂] has been characterized by polarized neutron diffraction, in collaboration with D. Gatteschi’s group. The relative strengths of competing intramolecular magnetic interactions are clearly established from the experimental spin distribution.

In the field of photomagnetism significant progress has been made in the study of structural changes induced by the switching from the low-spin state to the photo-excited high-spin state. The nuclear structures in the ground and the photo-induced states of the spin-transition complex [Fe^{II}(ptz)₆](BF₄)₂ have recently been investigated on the Laue neutron diffractometer VIVALDI at the ILL. An in-situ photo-excitation setup was installed especially for that experiment, in collaboration with G. McIntyre. Photo-induced structural changes were clearly evidenced in this complex, for which the magnetization density in the photo-excited state was determined by polarized neutron diffraction. Structure determinations are underway.

Promising results have also been obtained in powder neutron diffraction under light illumination. Partial photo-excitation of a powder sample of a Fe^{II} spin-transition complex has been obtained with the help of a new setup installed on the G4.1 diffractometer. This should prove quite useful for studies of photo-induced magnetic ordering.

1. Two-dimensional geometry of spin excitations in the high-transition-temperature superconductor $\text{YBa}_2\text{Cu}_3\text{O}_{6.85}$
V. Hinkov, S. Pailhès, P. Bourges, Y. Sidis, A. Ivanov, A. Kulakov, C. T. Lin, D. P. Chen, C. Bernhard, B. Keimer

44
2. Small Angle Neutron Scattering from the flux lines lattice: new developments
A. Pautrat, Ch. Simon, G. Poullain, C. Goupil, J. Scola, P. Mathieu, A. Brûlet

46
3. Lattice distortions related to charge ordering in $\text{Sr}_{14}\text{Cu}_{24}\text{O}_{41}$
M. Braden, J. Etrillard, A. Gukasov, U. Ammerahl, A. Revcolevschi

48
4. $\text{La}_{-5}(\text{Sr},\text{Ca})_9\text{Cu}_{24}\text{O}_{41}$: a 1D Toy model for hole doped cuprates
R. Klingeler, A. Gukasov, T. Kroll, J. Geck, M. Hücker, U. Ammerahl, A. Revcolevschi, B. Büchner

50
5. Confined spin waves reveal an assembly of nanosize domains in $\text{La}_{1-x}\text{Ca}_x\text{MnO}_3$ ($x=0.17, 0.2$)
M. Hennion, F. Moussa, P. Kober-Lehouelleur, F. Wang, A. Ivanov, L. P. Regnault, J. Kulda

52
6. Magnetic filaments in resistive manganites
M. Viret, F. Ott, J.P. Renard, H. Glättli, L. Pinsard-Gaudart, A. Revcolevschi

54
7. Magnetic ground state in the frustrated $S=1/2$ square lattice of V^{4+} in $\text{Li}_2\text{VO}_2\text{SiO}_4$
A. Bombardi, J. Rodríguez-Carvajal, S. Di Matteo, F. de Bergevin, L. Paolasini, P. Carretta, P. Millet, R. Caciuffo

56
8. Temperature renormalization of the spin correlations in the dimer spin-Liquid TlCuCl_3
Ch. Rüegg, Ch. Niedermayer, A. Furrer, J. Mesot, M. Matsumoto, B. Normand, M. Sgrist, T.M. Rice, K.W. Krämer, H.-U. Güdel, H. Mutka, P. Bourges, Y. Sidis

58
9. Domain structures in $\text{Fe}/\text{Fe}_2\text{N}$ multilayers
W. Szuszkiewicz, K. Fronc, B. Hennion, and M. Aleszkiewicz

60

TWO-DIMENSIONAL GEOMETRY OF SPIN EXCITATIONS IN THE HIGH-TRANSITION-TEMPERATURE SUPERCONDUCTOR $\text{YBa}_2\text{Cu}_3\text{O}_{6.85}$

V. Hinkov¹, S. Pailhès², P. Bourges², Y. Sidis², A. Ivanov³, A. Kulakov¹, C. T. Lin¹, D. P. Chen¹, C. Bernhard¹ and B. Keimer¹

¹Max-Planck-Institut für Festkörperforschung, 70569 Stuttgart, Germany

²Laboratoire Léon Brillouin, CEA-CNRS, CEA-Saclay, 91191 Gif-sur-Yvette, France

³Institut Laue-Langevin, 156X, 38042 Grenoble cedex 9, France

The fundamental building block of the copper oxide superconductors is a Cu_4O_4 square plaquette. In most of these materials, the plaquettes are slightly distorted and form a rectangular lattice. An influential theory of high temperature superconductivity predicts that this two-dimensional lattice is intrinsically unstable towards a “striped” state with *one-dimensional* spin and charge order [1,2]. Static stripe order has indeed been reported in specific layered copper oxides in which superconductivity is suppressed, but the theory also predicts phases in which robust superconductivity coexists microscopically with liquid-crystal-like stripe order. The liquid-crystal order parameter is expected to align itself preferentially along one of the axes of the rectangular lattice, generating a quasi-one-dimensional pattern in scattering experiments [3]. Testing this prediction requires “untwinned” specimens in which the orientation of the rectangular lattice is maintained throughout the entire volume. However, almost all neutron experiments thus far reported have been carried out on fully ‘twinned’ crystals with equal proportions of micrometre-scale twin domains in which the rectangular Cu_4O_4 plaquettes are rotated by 90° with respect to one another. Because the scattering pattern from such crystals consists of equal contributions from both twin domains, even perfectly one-dimensional spin fluctuations generate a fourfold symmetric pattern, so that they cannot be discriminated from microscopically two-dimensional fluctuations. The results of previous neutron scattering experiments on partially detwinned $\text{YBa}_2\text{Cu}_3\text{O}_{6+x}$ crystals have been interpreted as evidence of a one-dimensional character of the magnetic fluctuations [4]. However, owing to significant contributions from the minority domain, the full geometry of the excitation spectrum has remained unclear. Using neutron scattering from a mosaic of fully untwinned, nearly optimally doped $\text{YBa}_2\text{Cu}_3\text{O}_{6.85}$ crystals [4], we have resolved this issue. Scans through the (200) and (020) Bragg reflections of the $\text{YBa}_2\text{Cu}_3\text{O}_{6.85}$ array reveal a bulk population ratio between majority and minority twin domains of about 95:5 (Fig. 1b) [5]. This is one order of

magnitude larger than in previous experiments[4]. The contribution of the minority domain to the magnetic scattering pattern is thus negligible in our experiments.

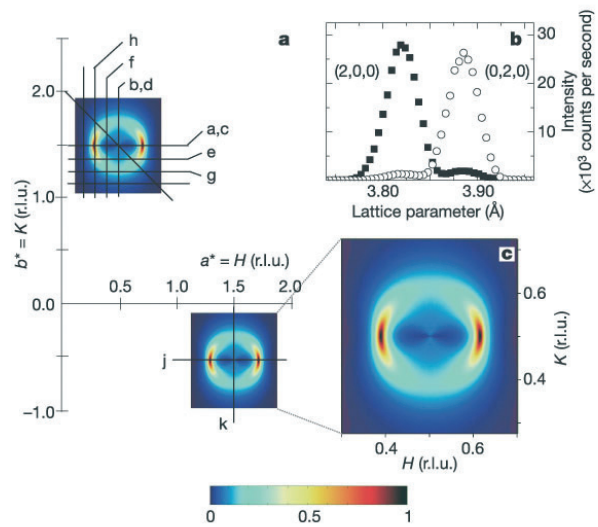


Figure 1. Layout of the reciprocal lattice and magnetic spectral weight of $\text{YBa}_2\text{Cu}_3\text{O}_{6.85}$. a) In-plane projection of the $\text{YBa}_2\text{Cu}_3\text{O}_{6.85}$ reciprocal lattice indicating the trajectories of the constant-energy scans shown in Fig. 2. b) Longitudinal elastic scans through the (2, 0, 0) and (0, 2, 0) crystallographic Bragg reflections, demonstrating a twin domain population ratio of (95:5). c) Intrinsic magnetic spectral weight at 35 meV (see text).

Figure 2 shows magnetic neutron scattering data from this crystal array. The overall features of the neutron cross-section are in good agreement with prior work on twinned crystals. The observed magnetic excitations are incommensurate (Fig 2) around the in-plane wave vector $\mathbf{Q}_{AF} = (0.5, 1.5)$. The incommensurate excitation branches disperse towards \mathbf{Q}_{AF} with increasing excitation energy (Fig. 2), and they merge at 41 meV, giving rise to the ‘resonance peak’.

The new aspect of this work is the determination of the in-plane geometry of the spin excitations. Figure 2c–j shows representative scans from a

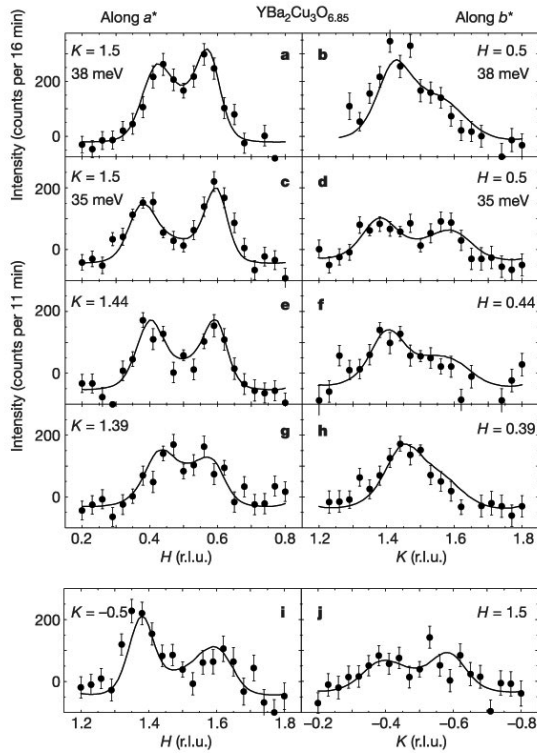


Figure 2. Constant-energy scans along the trajectories indicated in Fig. 1a. The excitation energies are $\hbar\omega = 38$ meV (a, b) and 35 meV (c–j). The wave vector $Q = (H, K, 1.7)$ is given in reciprocal lattice units, r.l.u.. We show subtractions of the intensities at $T = 10$ K ($\ll T_c$) and $T = 100$ K ($> T_c$). The data in panels c, d and i, j were taken in two different Brillouin zones with exchanged resolution conditions. The observed anisotropy between a^* and b^* is thus not due to resolution effects.

comprehensive map of the spin fluctuation spectral weight at $\hbar\omega = 35$ meV. More limited data sets were also taken at $\hbar\omega = 33$ and 37 (not shown), and 38 meV (Fig. 2a,b). The most important observation is that well-defined incommensurate peaks are present in scans along both a^* and b^* (Fig. 2a-d). This demonstrates the intrinsic two-dimensional

nature of the spin excitations. To extract the magnetic spectral weight from the experimentally determined scattering profiles, we have numerically convoluted an anisotropic damped harmonic oscillator cross-section with the spectrometer resolution function. The computed profiles, shown as solid lines in Fig. 2, provide excellent descriptions of the experimental data. We find that the locus of maximum spin fluctuation spectral weight approximately forms a circle in momentum space, in agreement with its two-dimensional geometry. However, the damping and amplitude along the circle are modulated in a one-dimensional fashion. The intrinsic magnetic spectral weight at 35meV extracted from this analysis is depicted in Fig. 1c. The strength of this modulation also depends strongly on the excitation energy.

Which models can describe the observed one-dimensional amplitude and width anisotropy? i) Theories based on a one-dimensional, rigid array of stripes predict a 100% intensity anisotropy and cannot account for the two-dimensional scattering pattern. The map of the magnetic intensity at 35meV does, however, bear a resemblance to the scattering pattern generated by a nematic liquid crystal close to a nematic-to-smectic critical point [3]. In this scenario, the structural anisotropy between the a and b axes may act as an aligning field for the nematic director.

ii) Prior Fermi-liquid-based theoretical scenarios for the spin dynamics of $\text{YBa}_2\text{Cu}_3\text{O}_{6+x}$ had only considered independent CuO_2 layers, ignoring a possible influence of the b -axis-oriented CuO chains [6]. Their impact (via an orthorhombic anisotropy) on the spin dynamics has to be assessed in quantitative calculations. Other factors, such as proximity to a ‘Pomeranchuk’ instability of the Fermi surface [7], may also contribute to the anisotropy of the spin dynamics.

References

- [1] Zaanen, J. & Gunnarson, O. Charged magnetic domain lines and the magnetism of high- T_c oxides. *Phys. Rev. B* **40**, 7391-7394 (1989).
- [2] Emery, V. J. & Kivelson, S. A. Frustrated electronic phase separation and high-temperature superconductors *Physica C* **209**, 597-621 (1993)
- [3] Kivelson, S. A. et al. How to detect fluctuating stripes in the high-temperature superconductors. *Rev. Mod. Phys.* **75**, 1201-1241 (2003).
- [4] Mook, H. A., Dai, P., Dogan, F. & Hunt, R. D. One-dimensional nature of the magnetic fluctuations in $\text{YBa}_2\text{Cu}_3\text{O}_{6.6}$. *Nature* **404**, 729-731 (2000).
- [5] Hinkov, V. et al. One Two-dimensional geometry of spin excitations in the high-transition-temperature superconductor $\text{YBa}_2\text{Cu}_3\text{O}_{6+x}$. *Nature* **430**, 650-653 (2004).
- [6] Onufrieva, F. & Pfeuty, P. Spin dynamics of a two-dimensional metal in a superconducting state: Application to the high- T_c cuprates. *Phys. Rev. B* **65**, 054515 (2002).
- [7] Halboth, C. J. & Metzner, W. d -wave superconductivity and Pomeranchuk instability in the two dimensional Hubbard model. *Phys. Rev. Lett.* **85**, 5162–5165 (2000).

SMALL ANGLE NEUTRON SCATTERING FROM THE FLUX LINES LATTICE: NEW DEVELOPMENTS

A. Pautrat¹, Ch. Simon¹, G. Poullain¹, C. Goupil¹, J. Scola^{1*}, P. Mathieu², A. Brûlet³¹CRISMAT/EnsiCaen, UMR6507 CNRS, Caen. (*.Ph.D Thesis)²Laboratoire Pierre Aigrain de l'ENS, UMR 8551, Paris.³Laboratoire Léon Brillouin, CEA/SACLAY, 91191 Gif-sur-Yvette cedex

In the mixed state of type II superconductors, the magnetic field B penetrates as flux lines (vortices). The critical current is directly related to the vortex pinning by defects and the knowledge of the vortex structure is of primary importance. Among existing experimental techniques, small angle neutron scattering (SANS) remains one of the best ways to investigate the bulk of the vortex lattice, by applying magnetic fields of 0.02 to 20 T which correspond to inter-vortex distances of 1 to 10 μm . In classical SANS measurements, the vortex is aligned with the applied field and diffraction intensity only exists in the plane perpendicular to the magnetic field. Recent developments of this technique are related to the existence of diffracted intensity out of this plane. This is the case if the vortices meander to adjust their position to extended bulk defects such as columnar defects or twin boundaries. This is also the case of surface pinning where the vortices are curved to accommodate the presence of transport current J ($\text{curl } B = \mu_0 J$).

In the presence of twin boundaries, the critical current is strongly modified by the interaction with these extended defects, with a peak of critical current when B is aligned onto the defects. In order to understand this feature, we have studied the influence of twin boundaries (TB) on the vortex lattice structure in a high T_c cuprate **YBaCuO**. We have studied samples possessing different TB densities and performed diffraction measurements on two diffraction planes. We find that the effect of TB's is double: the flux lines are not straight in the direction of the field but are meandering along to choose the TB direction. Depending on the ratio of the flux line density to the twin boundary density, a deformation of the Flux Lines Lattice (FLL) unit cell is also observed. This is likely due to the fact that the screening currents are no longer cylindrical, in agreement with an image-like effect [1]. In twinned YBaCuO, the FLL apparent symmetry is square whereas Abrikosov lattice observed in untwinned crystals is usually hexagonal (Fig 1).

Concerning the nature of the vortex pinning, we have investigated the **role of surface pinning**. Most of the time, FLL properties are analyzed with

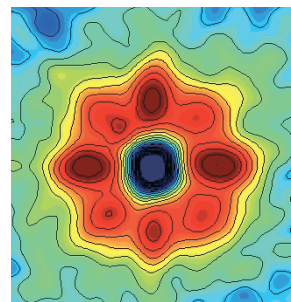


Figure 1. Diffraction pattern from the FLL in a twinned YBaCuO sample ($T=4\text{K}$, $B//c\text{-axis}=0.1\text{T}$). The apparent square symmetry is due to the twin boundaries.

the help of electronic transport measurements. The pinning of the FLL explains the existence of a critical current below which the current flow is non-resistive. For overcritical current, the FLL flows in the bulk of the sample in a resistive manner. There is a long-standing debate concerning the real nature of pinning (bulk versus surface) since pertinent probes are really rare. Nevertheless, these two models differ by the fact that below the critical current, bulk pinning predicts bulk penetration of the applied current, whereas surface pinning predicts surface current only. As a consequence of Maxwell equations, bulk current leads to a bending of the flux lines, which broadens the Bragg peaks in a particular direction (Fig. 2). Using this property, we have

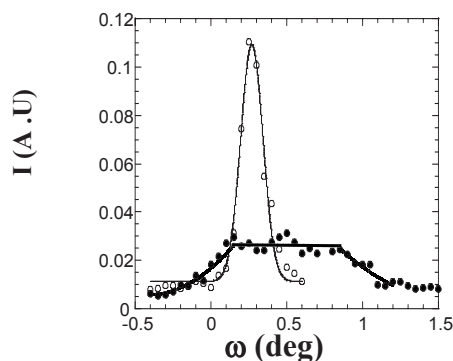


Figure 2. Bragg peak of the FLL in PbIn for straight lines (thin peak, $I_{\text{bulk}}=0$) and lines curved by the current induced self field component (broad peak, $I_{\text{bulk}}=18\text{A}$) ($T=2\text{K}$, $B=0.1\text{T}$).

shown that the pinning by the surface strongly dominates in a conventional low T_c superconductor (**PbIn**)[2]. Furthermore, it is proved that inhomogeneous surface state at large scale leads to an inhomogeneous current distribution.

A very peculiar case of flux lines pinning appears in the “peak effect” observed in **NbSe₂**, i.e. a sudden increase of the critical current I_c close to the superconducting-normal transition. It is an open question: does this correspond to a bulk disordering transition in the FLL? As shown in the fig. 3, we were able by field cooling (FC) or zero field cooling the sample (ZFC) to get this high I_c state as well as the low I_c state in a **NbSe₂** crystal. In both cases, there is a nice FLL. The main

difference lays in the rocking curves, which suggest that both states are due to surface pinning, and that the double peak reflects a tilting of the FLL by the pinning currents surrounding the sample in the FC process. The anomalous transport properties observed after FC are in this picture linked to the annealing of these metastable surface currents by the transport current and to the disappearance of this double peak structure [3].

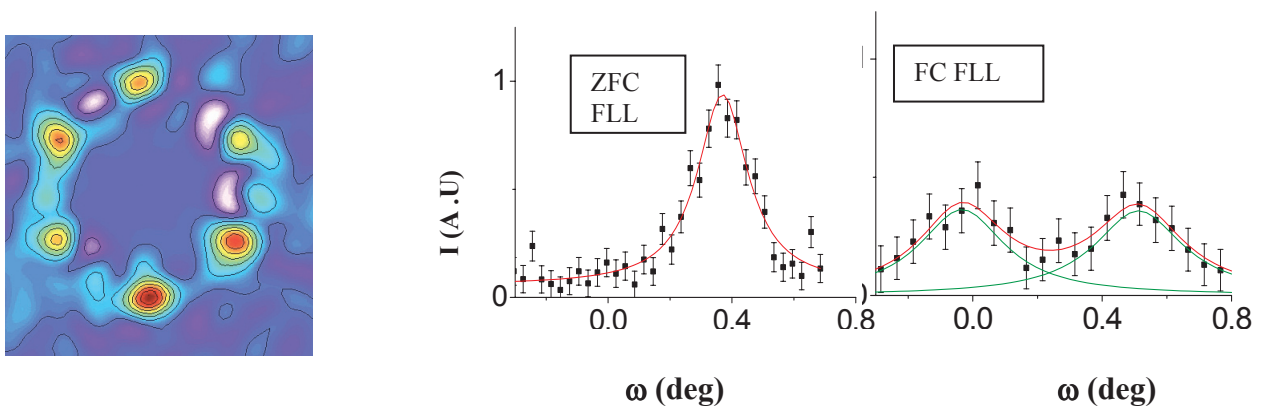


Figure 3. Left: Diffraction pattern from the FLL in **NbSe₂** ($T=2K$, $B=0.4T$). Right: Rocking curve around the framed peak after zero field cooling (ZFC) and after field cooling (FC). Note the double peak after the FC.

References

- [1] Ch. Simon, A. Pautrat, G. Poullain, C. Goupil, C. Leblond-Harnois, X. Chaud and A. Brûlet, *Phys. Rev. B* **70**, 024502 (2004).
- [2] A. Pautrat, C. Goupil, Ch. Simon, D. Charalambous, E. M. Forgan, G. Lazard, P. Mathieu, and A. Brûlet, *Phys. Rev. Lett.* **90**, 087002 (2003).
- [3] A. Pautrat, J. Scola, Ch. Simon, P. Mathieu, C. Goupil, M. J. Higgins, S. Bhattacharya and A. Brûlet, submitted to *Phys Rev B*.

LATTICE DISTORTIONS RELATED TO CHARGE ORDERING IN $\text{Sr}_{14}\text{Cu}_{24}\text{O}_{41}$ M. Braden¹, J. Etrillard², A. Gukasov³, U. Ammerahl⁴, A. Revcolevschi⁴¹II. Physikalisches Institut, Universität zu Köln, Zùlpicher Str. 77, D-50937 Köln, Germany²Groupe Matière Condensée et Matériaux, UMR au CNRS 6626, Université de Rennes I, 35042 Rennes Cedex, France³Laboratoire Léon Brillouin (CEA-CNRS), CEA- Saclay, 91191 Gif sur Yvette Cedex⁴Laboratoire de Physico-Chimie de l'Etat Solide, Université Paris Sud, 91405 Orsay Cedex, France

The spin-ladders compounds with formula $\text{Sr}_{14}\text{Cu}_{24}\text{O}_{41}$ or related exhibit a rather complex crystallographic structure due to their composite character. The materials consist of an alternating stacking of two distinct types of layers. One is formed by $\text{Sr}_2\text{Cu}_2\text{O}_3$ with a ladder-like structure and the other contains CuO_2 chains. The incommensurate modulation results from the misfit between the c-lattice-parameters of these planar elements. Whereas the a-parameter, $a \sim 11.47 \text{ \AA}$, is the same in both sub-lattices due to the free arrangement of the two CuO_2 -chains, the c-parameters reflect the different Cu-O-Cu bonding, 180 and 90° in ladders and chains respectively. The b-parameter corresponding to the stacking is the same for both elements. We have studied the crystal structure of this composite material by neutron diffraction focusing on the charge ordering transition occurring near 250K [1,2].

We have first analysed the temperature dependence of the mean crystal structure in $\text{Sr}_{14}\text{Cu}_{24}\text{O}_{41}$ by collecting large sets of Bragg reflection intensities on a four circle diffractometer; a large number of low order satellite reflections arising from the composite structure were included [1]. The crystal structure remains essentially unchanged between room and low temperature; in particular, the strongest satellite reflections show only little temperature dependence indicating that the main modulation of the composite is not changing with temperature. However the Debye-Waller factors and some weak fundamental reflections depend sensitively on temperature. The former may be attributed to a low lying phonon branch associated with the sliding of the chains against the ladders.

There has been a controversy in the literature about the onset of charge ordering in $\text{Sr}_{14}\text{Cu}_{24}\text{O}_{41}$, Cox et al. [3] reported a quadrupling of the chain lattice at low temperature, whereas Fukuda et al. [4] found superstructure reflection which are indexed by a modulation vector of (0.2,0,0) within the chain sublattice. However, van Smaalen argued that these reflections do not indicate charge ordering but should be interpreted as high order satellite reflections of the composite structure [5].

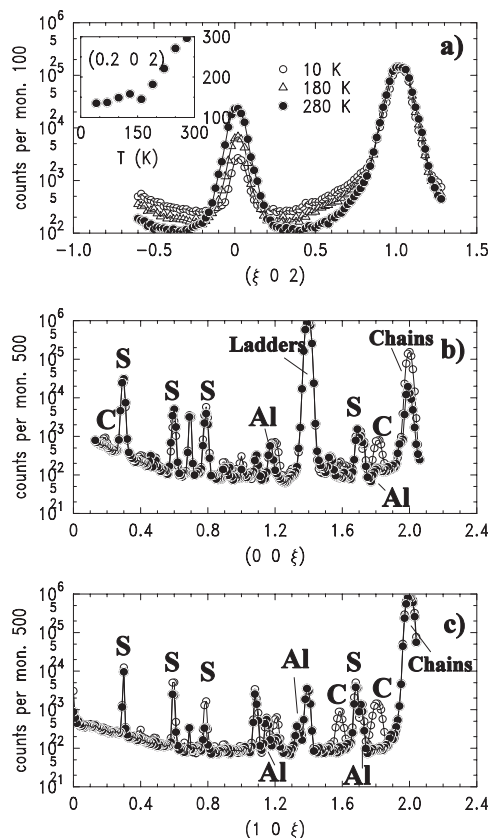


Figure 1. a) Scans along the a^* -direction across the chain lattice Bragg peaks $(1\ 0\ 2\ 0)$ and $(0\ 0\ 2\ 0)$, note that the latter is weaker and strongly temperature dependent. The inset shows the height of the diffuse scattering at $(0.2\ 0\ 2)$ as function of temperature. b) Scans along the c^* -direction across the ladder reflection $(0\ 0\ 0\ 2) = (0\ 0\ 1.395)$ and the chain reflection $(0\ 0\ 2\ 0) = (0\ 0\ 2)$. c) Scans along the c -direction across $(1\ 0\ 2\ 0) = (1\ 0\ 2)$. S denotes pure satellite reflections, AI a contamination by the Aluminum sample holder and C a low temperature superstructure peak; $\lambda/2$ denotes a weak contamination through neutrons of half wavelength [2].

We have studied the occurrence of additional reflections on the 4F triple axis spectrometer, which offers a high dynamical range and Q-resolution. The main results are shown in the figures 1 and 2.

Whereas the low order satellites change little in intensity upon cooling, we find additional reflections at low temperature, which are typically an order of magnitude smaller than the strongest satellites. In contrast to the results by Fukuda et al. [4] these reflections completely disappear at high temperature. Also the position does not perfectly match with the previous study. We may index most of the additional reflections by a modulation $(0,0,0.190(4))$ in respect with the chain lattice. However, we find that not only the chain-system but also the ladders are modulated with this modulation. Some weaker additional peaks are observed near but not precisely at the positions where second order reflections are expected. Due to the high resolution of the 4F-spectrometer the observed differences are clearly significant.

The new reflections appear close to the temperature where the transport properties exhibit strong anomalies. One should connect them hence with the onset of charge ordering. However, the totality of the data cannot be explained by a single modulation on the chain subsystem.

We propose an interpretation intermediate between references [4] and [5]. We argue that the reflections, we find to appear at low-temperature, are originating from the charge ordering. But charge ordering does not seem to induce its proper modulation instead the charge order induced modulation seems to fall into the composite modulations existing anyway. All the reflections, we observe, can be indexed as high order satellites of the composite lattice. But in an ordinary modulated system one may not understand why we find so many superstructure reflections corresponding to the special value of $q=(0,0,0.19)$. The modulation of the charge ordering seems to lock into the modulation of the composite

structure, somehow similar to the typical lock-in transitions of structural phase transitions on commensurate values.

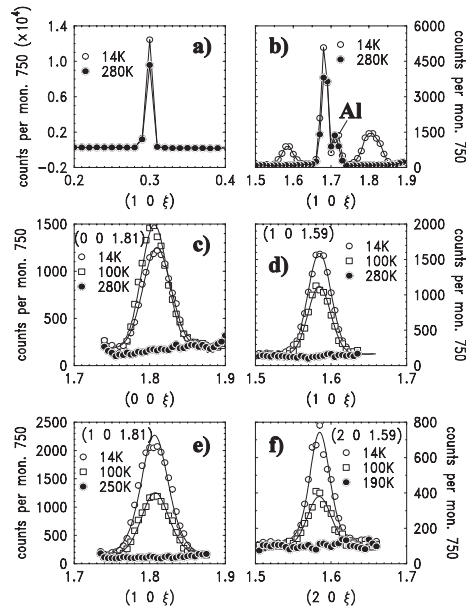


Figure 2. Scans across satellite and the additional peaks demonstrating their different temperature dependencies and peak widths. a) Scan across the satellite $(1\ 0\ 0.3)=(1\ 0\ 1\ -1)$ at 14 and 280K. b) Scan across the satellite $(1\ 0\ 1.69)=(0\ 0\ 1\ 1)$ at 14 and 280 K; near $(1\ 0\ 1.59)$ and $(1\ 0\ 1.81)$ new superstructure peaks appear at low temperature which exhibit significant broadening, **Al** indicates an Al-contamination. c)-d) Scans across the low temperature reflections $(0\ 0\ 1.81)$, $(1\ 0\ 1.59)$, $(1\ 0\ 1.81)$ and $(2\ 0\ 1.59)$ at low and high temperatures. Lines denote fits with a Lorentzian peak profile convoluted with the resolution of the triple axis spectrometer.

References

- [1] J. Etrillard, M. Braden, A. Gukasov, U. Ammerahl, and A. Revcolevschi; *Physica C* **403**, 290-296 (2004).
- [2] M. Braden, J. Etrillard, A. Gukasov, U. Ammerahl, and A. Revcolevschi, *Phys. Rev.* **B69**, 214426 (2004).
- [3] D.E. Cox, T. Iglesias, K. Hirota, G. Shirane, M. Matsuda, N. Motoyama, H. Eisaki, and S. Uchida, *Phys. Rev.* **B57**, 10750 (1998).
- [4] T. Fukuda, J. Mizuki, and M. Matsuda, *Phys. Rev.* **B66**, 012104 (2002).
- [5] S. van Smaalen, *Phys. Rev. B* **67**, 026101 (2003).

$\text{La}_{\geq 5}(\text{Sr,Ca})_{\leq 9}\text{Cu}_{24}\text{O}_{41}$: A 1D TOY MODEL FOR HOLE DOPED CUPRATES

R. Klingeler¹, A. Gukasov², T. Kroll¹, J. Geck¹, M. Hücker^{3,4},
U. Ammerahl⁴, A. Revcolevschi⁴, B. Büchner¹

¹ Leibniz-Institute for Solid State and Materials Research IFW Dresden, 01171 Dresden, Germany

² Laboratoire Léon Brillouin, CEA-Saclay, 91191 Gif sur Yvette, France

³ Physics Department, Brookhaven National Laboratory, Upton, New York 11973

⁴ Laboratoire de Physico-Chimie des Solides, Université Paris-Sud, 91405 Orsay Cedex, France

The interplay between low-dimensional antiferromagnetism and the mobility of holes in layered cuprates is studied intensively nowadays. A different approach to investigate this interplay considers quasi-one-dimensional (1D) systems. For 1D systems, theory is much more predictive and experiments yield more pronounced results. In our 1D model system $(\text{Sr,Ca,La})_{14}\text{Cu}_{24}\text{O}_{41}$ for doped cuprates, a small number of charge carriers significantly affects the magnetic properties. In particular, the mobility of holes can be tuned by a magnetic field and thus a long range AFM spin order, which is present if the holes are static, is destroyed by the motion of the depinned holes.

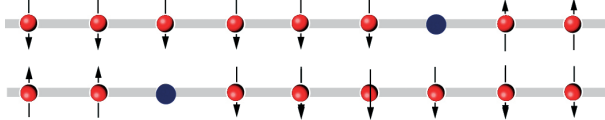


Figure 1. Sketch of adjacent doped spin chains.

In $(\text{Sr,Ca,La})_{14}\text{Cu}_{24}\text{O}_{41}$, two quasi-1D magnetic substructures are realized, i.e. Cu_2O_3 spin ladders and CuO_2 spin chains. In the ladders, applying a hydrostatic pressure in $\text{Sr}_{14-x}\text{Ca}_x\text{Cu}_{24}\text{O}_{41}$ ($x \geq 11$) results in a superconducting state. However, the ladders do not contribute significantly to the low temperature magnetic response, since they exhibit a large spin gap of $\Delta \sim 400\text{K}$. The chains consist of edge-sharing CuO_4 -plaquettes containing Cu^{2+} -ions with $S = \frac{1}{2}$ in the undoped case. The Cu-O-Cu bonding angle amounts to $\sim 93^\circ$, which results in a ferromagnetic (FM) superexchange between adjacent (NN) spins and in an uniaxial anisotropy. Hole doping introduces non-magnetic Zhang-Rice singlets. The magnetic coupling of next nearest neighbor (NNN) Cu-spins via a hole is AFM, similar to the stripes in layered cuprates. For the low doped $(\text{Sr,Ca,La})_{14}\text{Cu}_{24}\text{O}_{41}$ with $x \sim 5$, i.e. $\sim 10\%$ holes, the Cu-spins in the chains form FM chain fragments which are coupled antiferromagnetically via the few non-magnetic holes (cf. Fig. 1). Due to a finite interchain coupling $J_\perp \sim 10\text{K}$ a long range (LR) AFM spin order evolves below $T_N \sim 10\text{K}$ [1].

Experiments and results

We performed a detailed investigation of the low temperature spin correlations in the chains of

$\text{La}_x(\text{Sr,Ca})_{14-x}\text{Cu}_{24}\text{O}_{41}$ ($x \geq 5$). The experiments were carried out on the 6T2 diffractometer with the 7.5T cryomagnet using unpolarized neutrons of wavelength $\lambda_n = 0.90\text{\AA}$. Polarized neutron flipping ratios were measured on the lifting-counter diffractometer 5C1 using neutrons with $\lambda_n = 0.84\text{\AA}$ obtained with a Heusler alloy monochromator. We used single crystals of approximately 0.2cm^3 grown by the floating zone technique which were oriented with the b -axis either vertical or parallel to the magnetic field direction.

$\text{La}_5\text{Sr}_9\text{Cu}_{24}\text{O}_{41}$ was characterized at 300K using the 6T2 diffractometer in the four-circle mode. A refinement on neutron scattering structure amplitudes has been done using the superspace formalism and the crystallographic program JANA2000. In contrast to recent findings for $\text{Sr}_{14}\text{Cu}_{24}\text{O}_{41}$ [2], our refinement for $\text{La}_5\text{Sr}_9\text{Cu}_{24}\text{O}_{41}$ at room temperature yields the shift along the c -axis of adjacent chains in the ac -plane $\delta = 0.01(1)$, which corresponds to an *in line* arrangement of adjacent chains along the a axis.

LR spin order due to a finite J_\perp is a generic feature of quasi-1D magnets. Unusually for cuprates, for $\text{La}_x(\text{Sr,Ca})_{14-x}\text{Cu}_{24}\text{O}_{41}$ ($x \geq 5$) there is a strong anisotropy of the magnetic phase diagram. As demonstrated in Fig. 2, the intensity of the AFM (1,1,0) reflection strongly decreases if a magnetic $B \parallel b$ is applied. In particular, the intensity of the (1,1,0) reflection almost disappears for $B \parallel b \geq 4\text{T}$. The suppression of the LR spin order is confirmed by

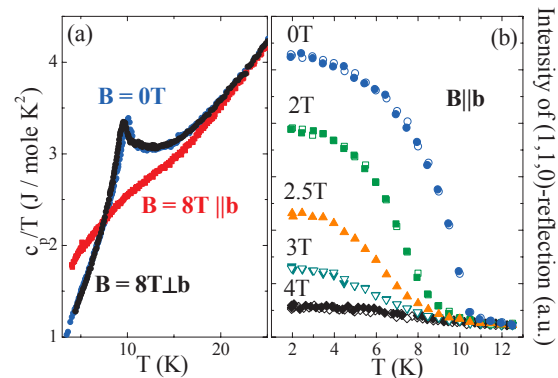


Figure 2: (a) Specific heat c_p/T of $\text{La}_{5.2}\text{Ca}_{8.8}\text{Cu}_{24}\text{O}_{41}$ for $B = 0$, $B = 8\text{T} \parallel b$, and $B = 8\text{T} \perp b$. (b) Maximum intensity of the AFM (1,1,0) reflection for different B at cooling.

the specific heat data. For $B\parallel b=8\text{T}$, there is no signature of LR spin order at $T \geq 3\text{K}$. Whereas, the specific heat shows that the LR spin ordered phase is hardly influenced by $B\perp b = 8\text{T}$. The anisotropic phase diagram is also confirmed by neutron diffraction, magnetization and specific heat for $\text{La}_x(\text{Sr,Ca})_{14-x}\text{Cu}_{24}\text{O}_{41}$ with $x = 5, 5.2, 5.6$ [3].

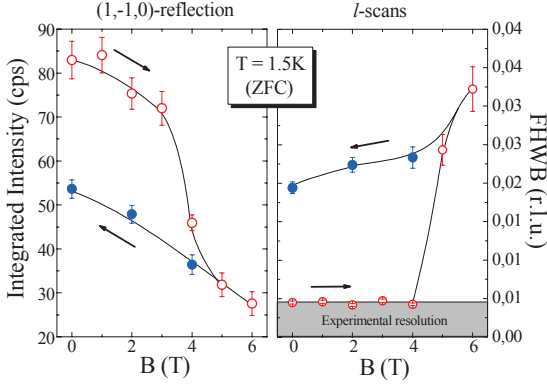


Figure 3. (a) Integrated intensity (from l -scans) and (b) FWHM of the AFM (1,-1,0)-reflection in $\text{La}_5\text{Sr}_9\text{Cu}_{24}\text{O}_{41}$ at $T=1.5\text{K}$. Lines are guides to the eyes. Arrows denote the course of the measurements, starting from ZFC.

In Fig. 3, the magnetic field dependencies of the integrated intensity of the AFM (1,-1,0)-reflection of $\text{La}_5\text{Sr}_9\text{Cu}_{24}\text{O}_{41}$ and of its width (FWHM) are displayed. The data show that small magnetic fields cause a moderate suppression of the AFM order parameter (OP), while any effect on the FWHM, respectively on the correlation length ξ , is beyond the resolution of the experiment. At $B = B_C \sim 4\text{T}$, a sharp decrease of the intensity of the (1,1,0)-reflection is observed, but the integrated intensity remains finite for $B > B_C$, where LR spin order is absent. In the mean time, the width of the (1,1,0)-reflection sharply increases at B_C but remains finite in higher fields. Both facts evidence short range (SR) AFM correlations for $B\parallel b > B_C$. Note, that at B_C no spin reorientation occurs since the anisotropy field amounts to $B \sim 7.5\text{T} \gg B_C$ [3]. The data in Fig. 3 exhibit a pronounced hysteresis, i.e. switching off the magnetic field does not restore the AFM order completely. This is most evident if the effect of switching off the field is considered in the field cooled (FC) state at $T = 2\text{K}$, i.e. after cooling in $B\parallel b = 4\text{T}$ (Fig. 4). The AFM OP in the FC state is considerably reduced compared to the zero field cooled (ZFC) value. Thus, additional thermal energy is needed to restore the ZFC properties. This also holds for cooling in $B = 2.5\text{T} < B_C$. The presence of the hysteresis implies a glassy

nature of the SR spin ordered phase at $B\parallel b > B_C$.

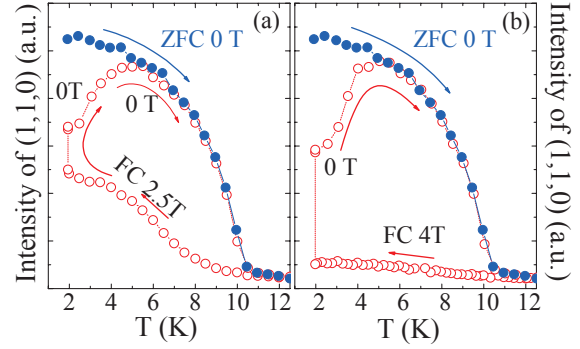


Figure 4. AFM peak intensity of the (1,1,0) reflection in $\text{La}_5\text{Ca}_9\text{Cu}_{24}\text{O}_{41}$ for different B vs. temperature. ZFC (FC) data are shown by full (open) circles.

Our data rule out pure spin models to explain the anomalous melting of the LR spin order. In particular, the magnetic excitations induced by the field are no spin flips. This fact follows not only from the specific heat data but also from a very small value of the magnetization at $B > B_C$. Our polarized neutron study also yields $\mu_{\text{FM}} \sim 0.07\mu_{\text{B}}/\text{Cu}$ at $B = 6\text{T}$, which is much smaller than the AFM sublattice magnetization ($0.63\mu_{\text{B}}$ at 2K) of the Cu-ions. Hence, the data imply that $B\parallel b$ induces excitations, which are not purely magnetic but also include other degrees of freedom.

To explain our data, both the positions of the holes and the type of magnetic excitations must be considered. (1) If the holes are distributed randomly, the interchain coupling is frustrated and the LR spin order should not evolve (cf. Fig. 1). Thus, the observation of a LR AFM spin order implies a particular arrangement of the holes in adjacent chains. E.g., LR spin order is possible if the holes are arranged in stripes along the a axis. (2) Regarding the excitations, for an Ising-like spin chain a large magnetic field is necessary to induce a spin flop or a spin flip. However, even for small fields, a domain wall motion, i.e. a hole motion, along the chains results in a gain of Zeeman energy, since FM chain fragments parallel to B are enlarged. Therefore, we suggest that coupled spin-charge excitations, i.e. the motion of holes along the chains, occur when $B\parallel b$ is applied. This destroys the arrangement of holes, being present for $B = 0$, and yields a melting of the LR spin order. In contrast, applying $B\perp b$ induces a conventional spin canting with no domain wall motion involved. Hysteresis effects are easily explained in this model, since hole motion is thermally activated.

References

- [1] U. Ammerahl, B. Büchner, C. Kerpen, R. Gross, A. Revcolevschi, Phys. Rev. B **62**, 3592 (2000)
- [2] J. Etrillard, M. Braden, A. Gukasov, U. Ammerahl, A. Revcolevschi, Physica C **403**, 290 (2004)
- [3] T. Kroll, R. Klingeler, J. Geck, B. Büchner, W. Selke, M. Hücker, A. Gukasov, J. Magn. Magn. Mat., in print.

CONFINED SPIN WAVES REVEAL AN ASSEMBLY OF NANOSIZE DOMAINS IN $\text{La}_{1-x}\text{Ca}_x\text{MnO}_3$ ($x=0.17, 0.2$)

M. Hennion¹, F. Moussa¹, P. Kober-Lehouelleur¹, F. Wang^{1,*}, A. Ivanov², L. P. Regnault³, J. Kulda²

¹ Laboratoire Léon Brillouin, CEA-CNRS, CEA Saclay, 91191 Gif-sur-Yvette, France

*Present address: Institute of Physics Chinese Academy of Sciences, 100080 Beijing

² Institut Laue-Langevin, 156X, 38042 Grenoble Cedex 9, France

³ CENG Centres d'Etudes Nucléaires (38041) Grenoble Cedex, France

This study concerns the physics of metal-insulator transition in manganites with colossal magnetoresistance (CMR). This topic still provides a challenge for theories. The possibility of mixed-phases to explain the CMR properties in $\text{La}_{1-x}\text{Ca}_x\text{MnO}_3$ at hole doping $x \sim 0.3$, has been pointed out by numerical studies [1]. However, in this doping range, the experiments are not conclusive. We have investigated two compounds at $x=0.17$ and $x=0.2$, close to $x=0.22$ where the ferromagnetic metallic (FM) phase with CMR properties occurs [2]. The compounds, which are ferromagnetic (F), exhibit a “quasi-metallic” behaviour below T_C ($T_C=175\text{K}$ and 180K for $x=0.17$ and 0.2 resp.) as expected from double-exchange coupling. At lower temperature, however, they become insulating, which reveals additional processes not accounted by double-exchange. Inelastic neutron scattering performed in the quasi-metallic state, reveals that the spin-wave spectrum is strongly anomalous. Instead of a continuous cosine law as for a F spin wave dispersion (cf the dashed line in Fig. 1), nearly dispersionless levels are observed at large q values. They can be quantitatively described by spin waves confined inside finite-size clusters [3,4]. This analysis allows us to determine (i) the shape (evolving from two-dimensional for $x=0.17$ to three-dimensional for $x=0.2$), (ii) the size (decreasing from 4 to 2 lattice spacings with increasing x) and (iii) the super-exchange (SE) coupling constants inside the clusters. The use of SE coupling constants, in an Heisenberg model, indicates that the clusters are “hole-poor” or orbital-ordered, implying hole-rich and orbital-disordered boundaries. These observations could be crucial for clarifying CMR. Moreover, confined spin waves inside ultra-fine domains are observed for the first time.

Let us first focus on the $x=0.2$ compound, the results on $x=0.17$ being summarized below. Fig 1 displays the spin-wave spectrum in the quasi-metallic state ($T=150\text{K}$, left panel) and in the insulating state (right panel) along the $[100]$, $[010]$, $[001]$ axis, superimposed because of twinning, in cubic indexation. At 150K , at small q up to $q \sim 0.25$, the spectrum consists of a dispersed curve. Beyond, the intensity is divided into three levels moderately

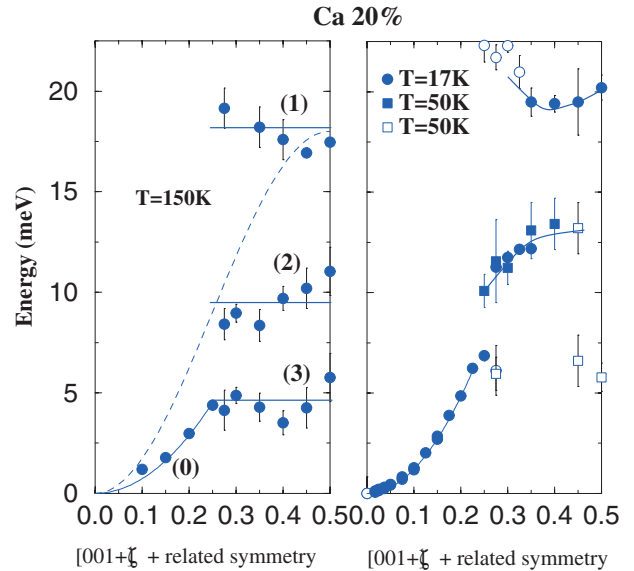


Figure 1. Spin wave dispersion along $[001]+[010]+[001]$ in a zero-field experiment (after applying a magnetic field) at 150K (left panel) and 50K and 17K (right panel).

dispersed, numbered from (1) to (3). At low temperature, in the insulating state, the dispersion of the levels increases and the low-energy level (3) disappears. The same type of dispersionless modes are observed along all symmetry directions. The spin-wave spectrum along the $[110]$, $[011]$, $[101]$ directions (diagonal of the cubic face) and along $[111]$ (main diagonal of the cube for which all domains are equivalent) are reported in Fig. 2 at $T=150\text{K}$. Beyond a dispersed curve at small q values, only two levels are observed along $[111]$ whereas several can be determined along $[110]$. From the expression for the energy of a propagating spin wave in a Heisenberg model, one gets relations between the zone boundary energies E_B , along each symmetry direction, and the superexchange (SE) magnetic coupling constants, $J_{a,b}$ along the \mathbf{a} or \mathbf{b} axis (equivalent) and J_c along the \mathbf{c} axis of the perovskite cube. These relations are also valid for finite-size clusters, where E_B is the largest energy level. According to predictions [3], the lowest energy confined wave corresponds to a half-wave and its energy should be a sub-multiple of E_B . The cluster size ξ is deduced from

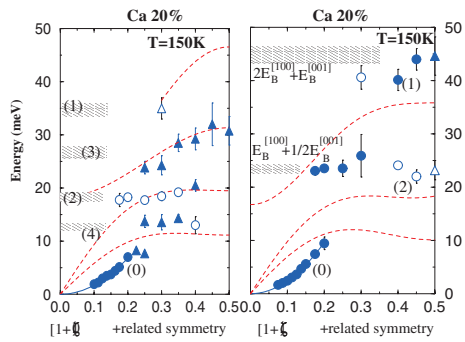


Figure 2. Magnetic excitations for q along $[110]$, $[101]$, $[011]$ (left panel) and $[111]$ (right panel) at $T=150\text{K}$, measured with unpolarised neutrons (circles) and polarized neutrons (triangles). Full (empty) symbols refer to modes with main (weak) intensity. The black hatched area correspond to calculated levels (see text) and the red dashed lines represent the phonon branches.

the ratio between this lowest energy level and E_B . In Figure 1, the largest energy level at $E_B=18\text{ meV}$ and the level at 9 meV , are attributed to a full-wave and half-wave along $[100]$ or $[010]$, whereas the same level at 9 meV (accidental coincidence) and that at 4.5 meV are attributed to the full and half waves along $[001]$ (see drawing in Fig 4). This assignment defines $J_{a,b}$ and J_c (reported in Fig 3) and the values of all energy levels along the other three symmetry directions (indicated by hatched areas, instead of lines, due to the experimental uncertainty), labeled (1) and (2) for $[110]$, (3) and (4) for $[011]+[101]$, in Fig 2-left panel, and (1) and (2) for $[111]$ in Fig 2-right panel. The good agreement with experiment supports this attribution. A cluster size ξ of 2 lattice spacings is obtained. The small- q dispersed curve implies that the small domains are ferromagnetically coupled together.

A similar study for $x=0.17$ where the flat levels exist only in the (a, b) plane and not along the c direction, leads to the $J_{a,b}$ value reported in Fig 3 and determines a cluster size of 4 lattice spacings within the (a, b) plane. The general evolution of $J_{a,b}$ and J_c deduced from the dispersionless levels for $x>0.125$ (for $x=0.17$, J_c is obtained from E_B^{110}

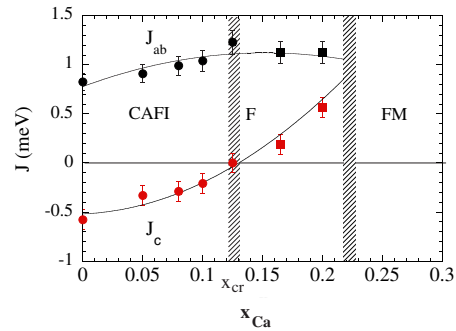


Figure 3. Variation of the magnetic coupling constants $J_{a,b}$ and J_c with doping. Vertical hatched lines indicate the CAFI/F and the F/FM transitions

and E_B^{111}) and from the “normal” spin wave branch for $x<0.125$ (in the canted antiferromagnetic insulating state or CAFI) are reported in Fig 3. It shows a monotonic effect of the hole-doping on the SE coupling constants, starting from undoped LaMnO_3 . These constants characterize an orbital-ordered or “hole-poor” spin system. A general evolution of the charge segregation with hole doping is displayed in Fig 4. The hole-rich domains, strongly anisotropic, embedded in an orbital-ordered matrix observed for $x<0.125$ [5], percolate at $x=0.125$ ($J_c=0$), whereas small orbital-ordered domains with 2D ($x=0.17$) and 3D ($x=0.2$) character are formed as x increases beyond 0.125 .

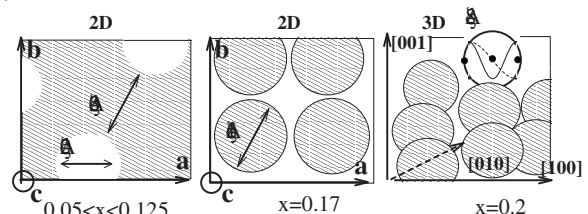


Figure 4. Schematic drawing showing the evolution of the charge segregation with doping x into 3 steps: from hole-rich (empty) clusters to hole-poor (hatched) domains with a 2D character and then to 3D isotropic clusters. A half and full standing waves are shown inside a cluster for $x=0.2$.

References

- [1] A. Moreo, Seiji Yunoki, Elbio Dagotto, Science Vol. 283 pp 2034 (1999).
- [2] P. Kober, Thesis Université Paris-Sud, defended on the 10th of December (2004)
- [3] M. Hennion, F. Moussa, F. Wang, P. Lehouelleur, A. Ivanov, Y. M. Mukovskii and D. Shulyatev, Phys. Rev. Lett. (2005)
- [4] P. V. Hendriksen, S. Linderoth and P. A. Lindgård Phys. Rev. B 48 pp 11600 (2000)
- [5] G. Biotteau, M. Hennion, F. Moussa, J. Rodríguez-Carvajal, Pinsard and A. Revcolevschi, Y. M. Mukovskii and D. Shulyatev Phys. Rev. B 64 pp 104421 (2001)

MAGNETIC FILAMENTS IN RESISTIVE MANGANITES

M. Viret¹, F. Ott², J.P. Renard³, H. Glättli¹, L. Pinsard-Gaudart⁴ and A. Revcolevschi⁴

1. Service de Physique de l'Etat Condensé, *DRECAM-CNRS URA2464*, CEA-Saclay, 91191 Gif-sur-Yvette cedex, France.
2. Laboratoire Léon Brillouin CEA/CNRS UMR12, CEA-Saclay, 91191 Gif-sur-Yvette CEDEX, France.
3. Institut d'Electronique Fondamentale, UMR CNRS 8622, Université Paris-Sud, 91405 Orsay cedex, France.
4. Laboratoire de Physico-Chimie de l'Etat Condensé, UMR 8648 CNRS, Université Paris-Sud, 91405 Orsay cedex, France

In oxides where magnetic cations are separated by oxygen anions, exchange interactions are mediated through the oxygen p orbitals. The resulting "super-exchange" (SE) is found to be usually antiferromagnetic. When electrons can delocalize on at least two magnetic ions, a ferromagnetic interaction called "double exchange" (DE) can take place. The manganites exhibit a rich physical behaviour where structural, transport and magnetic properties are intricately related¹. It has also been suggested that the competition between SE and DE interactions lead to a magnetic phase separation². The $\text{Pr}_{0.67}\text{Ca}_{0.33}\text{MnO}_3$ compound has a ferromagnetic transition below which the application of a magnetic field produces a first order transition from an insulating to a conducting state³. In this induced metallic-like state, the magnetization relaxes with time, leading to impressive resistive transitions⁴. This can be understood in a percolation picture where ferromagnetic regions are thermally activated into an antiferromagnetic insulating state. When the last percolation path breaks, the resistivity suddenly jumps to immeasurably large values. In order to finely characterize the phase separation in $\text{Pr}_{0.67}\text{Ca}_{0.33}\text{MnO}_3$ we have carried out Polarised Small Angle Neutron Scattering (PSANS) under applied fields along with electrical transport and magnetization measurements. The results presented here were obtained on a $1 \times 1 \times 3 \text{ mm}^3$ single crystal. The PSANS measurements were carried out at the ORPHEE reactor in Saclay on the spectrometer PAPOL. The SANS intensity angular dependence gives the Fourier transform of chemical and magnetic heterogeneities with sizes ranging from 1 nm to 100 nm. As shown on the typical spectrum in the inset of Fig.1, the SANS signal is characteristic of magnetic scattering with a contribution in $\sin^2\alpha$ from the direction of the applied field. The intensities recorded at 4.2K under applied fields $>1.5\text{T}$, follow a q^{-n} law with $1.6 < n < 1.7$. These exponents, close to $5/3$, are reminiscent of fractal dimensions as found for dilute polymers in good solvent. The parallel with polymer physics is instructive here because it suggests that the phase separation is of a filamentary type. We show below that the exchange interactions in these compounds can indeed lead to such a phase separation.

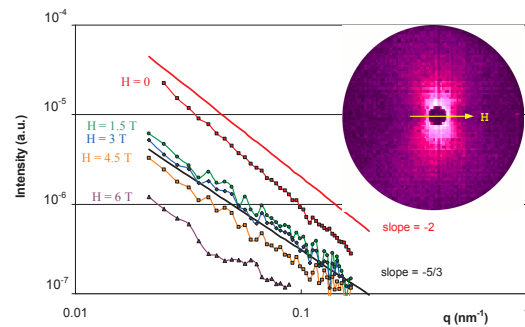


Figure 1. Magnetic SANS intensity from a $\text{Pr}_{0.67}\text{Ca}_{0.33}\text{MnO}_3$ single crystal, for a set of increasing fields from 0 to 6 T after Zero Field Cooling to 4.2K. The two straight lines are power laws with exponents -2 and $-5/3$. Inset: Typical PSANS spectrum showing the $\sin^2\alpha$ contribution of magnetic scattering.

In the $\text{Pr}_{0.67}\text{Ca}_{0.33}\text{MnO}_3$ compound, charge carriers are localized by a random magnetic potential. Thermal activation makes electrons hop in a random walk fashion to sites beyond their nearest neighbours. This is called "Variable Range Hopping" (VRH). The localizing potential has been attributed to random spin disorder which generates potential barriers coming from the Hund coupling energy between e_g and t_{2g} electrons on each Mn atom (of the order of 1eV). In insulating manganites, the electrons are localized on individual Mn ions. In that case, DE is not possible. Instead, we propose a picture in which, after every electronic hop, the electron gets localized in the e_g level of its new site and their spins become aligned. In the process, the total angular momentum of the electron and the Mn ion is preserved. Spatially, the interaction both follows and influences the random walk paths of hopping electrons through changes in the local magnetic potential. Because hopping happens preferentially between ions of similar spin direction, the exchange becomes stronger as spins are more closely aligned, which naturally results in a tendency to phase segregate. Indeed, once one Mn has in its vicinity another Mn with parallel spin, the hopping probability between this pair is overwhelmingly large and the ferromagnetic interaction will occur exclusively between these two ions. The remaining surrounding Mn ions interact only via SE. In order to demonstrate that this model leads to a filamentary phase segregation, we have carried out Monte Carlo

simulations treating transport and magnetism in a self-consistent manner (more details can be found in ref. 5. When hopping is turned on, magnetic filaments containing many parallel spin carriers with an enhanced mobility appear, as shown in Fig. 2.

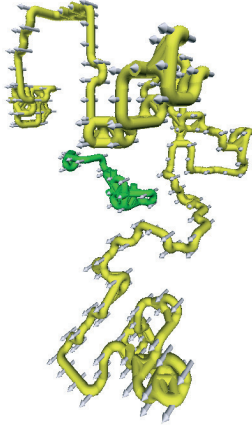


Figure 2. Magnetic filaments as obtained by Monte-Carlo simulations. The long yellow filament has a spin aligned with the external field whereas the small green one has its spin at 25° (the spins are all parallel within the filaments).

In the zero field-cooled (ZFC) state at $H=0$, the PSANS intensity can be well fitted with an exponent close to -2 (Fig. 1), i.e. a Debye function. This is consistent with previously published SANS data recorded at zero field and interpreted as an average coherence⁶ or a "red cabbage structure"⁷. Debye functions being reminiscent of polymer melts, this indicates, in our picture, that the magnetic filaments are entangled and do not self-avoid. Here, "SE-screening" does not work since electrons tunnel over distances longer than the screening length. Hence, gaussian, entangled, randomly magnetized filaments are generated by a ZFC procedure as shown in Fig.3a. When a field is applied, those filaments with their magnetization parallel to the field grow while others shrink. Within the filaments, mobility is large and carriers proceed by nearest-neighbour-hops, mediating ferromagnetic "hopping exchange". Super-exchange interactions screen the filaments to make them self-avoiding (see Fig.3b) and the measured power laws are $-5/3$. This exponent remains unchanged ; only the global SANS intensity decreases with field (fig.1). The variation in intensity results from a combination of a reduction

in magnetic contrast as the background is forced to become more ferromagnetic and an increase in density due to the growth of the filaments.

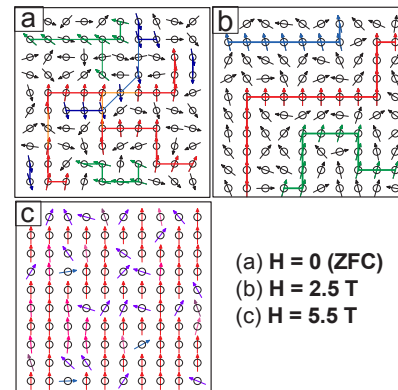


Figure 3. Schematics of the evolution of the filamentary phase with the applied field. From a disordered assembly of small filaments after the ZFC procedure, the applied field makes filaments with spins parallel to H grow, and shrinks the other ones. As the field continues to increase, the filaments percolate at 3.9T and then fade into the background when the difference in magnetization is too low to keep the carriers inside the filaments.

Complementary magnetization measurements allow us to conclude that the volume fraction of the filamentary phase increases monotonically as the field is raised. This naturally leads to a picture of magnetic filaments existing across the entire range of fields and becoming fainter as the background magnetization increases. At higher fields, the carriers leak out of the filaments into the entire volume (fig. 3c) which is almost fully magnetized, and produces a homogeneous ferromagnetic phase. The percolation at 3.9 T has no signature since nothing dramatic happens for the magnetic configuration.

In conclusion, we propose here that a ferromagnetic interaction due to electron hopping is responsible for the phase separation in resistive manganites. The random walk motion of the charge carriers leads to the appearance of magnetic filaments which were evidenced by neutron scattering in $\text{Pr}_{0.66}\text{Ca}_{0.33}\text{MnO}_3$ single crystals and supported by Monte-Carlo simulations.

References

- [1] J.M. D. Coey et al., Adv. Phys. **48**, 167 (1999).
- [2] E. Dagotto, *Nanoscale phase separation and colossal magnetoresistance: the physics of manganites and related compounds* (Springer-Verlag, Berlin, 2003).
- [3] Y. Tomioka, et al., J. Phys. Soc. Jpn. **64**, 3626 (1995).
- [4] A. Anane et al., Phys. Rev. B **59**, 7 (1999).
- [5] M. Viret, F. Ott, J. P. Renard, H. Glättli, L. Pinsard-Gaudart and A. Revcolevschi, Phys. Rev. Lett. **93** (2004) 217402.
- [6] P.G. Radaelli et al., Phys. Rev. B **63**, 172419 (2001).
- [7] Ch Simon, S. Mercone, N. Guiblin, C. Martin, A. Brulet and G. Andre, Phys. Rev. Lett. **89**, 2072021 (2002).

MAGNETIC GROUND STATE IN THE FRUSTRATED $S = 1/2$ SQUARE LATTICE OF V^{4+} IN $\text{Li}_2\text{VOSiO}_4$

A. Bombardi¹, J. Rodríguez-Carvajal², S. Di Matteo^{3,4}, F. de Bergevin¹, L. Paolasini¹, P. Carretta⁵, P. Millet⁶, and R. Caciuffo⁷

¹ European Synchrotron Radiation Facility (ESRF), Avenue des Martyrs, 98000 Grenoble Cedex 09, France

² Laboratoire Léon Brillouin (CEA-CNRS), CEA- Saclay, 91191 Gif sur Yvette Cedex, France

³ Laboratori Nazionali di Frascati-INFN, via E. Fermi 40, I-00044 Frascati (Roma), Italy

⁴ Dipartimento di Fisica E. Amaldi, Università di Roma III, via della Vasca Navale 84, I-00146 Roma, Italy

⁵ Istituto Nazionale per la Fisica della Materia, Università di Pavia, Via Bassi 6, I-27100 Pavia, Italy

⁶ Centre d'Elaboration des Matériaux et d'Etudes Structurales, CNRS, 31055 Toulouse Cedex, France.

⁷ Istituto Nazionale per la Fisica della Materia and Dipartimento di Fisica e d'Ingegneria dei Materiali, Università Politecnica delle Marche, Via Brecce Bianche, I-60131 Ancona, Italy

The phase diagram of two-dimensional (2D) frustrated Heisenberg quantum systems on a square lattice has been the subject of a number of theoretical studies [1]. Thanks to the synthesis of new model compounds theoretical predictions can be explored experimentally. This opportunity has renewed the interest toward the so-called J_1 - J_2 model, where J_1 and J_2 are the nearest- and the next-nearest-neighbour antiferromagnetic (AF) exchange integrals. In this model different situations can occur. For $0.35 \leq |J_2/J_1| \leq 0.65$ a spin liquid or dimer ground state is predicted. For $|J_2/J_1| \leq 0.35$ an AF order should develop, whereas for $|J_2/J_1| \geq 0.65$ the ordering by the disorder mechanism [1, 2] is expected to stabilize a twofold degenerate collinear order. Some theoretical studies suggested the possibility that such a twofold residual degeneracy leads to a finite-temperature Ising-like phase transition, with the chosen ground state being collinear or anti-collinear [1]. However, coupling to the lattice may induce, as in the Jahn-Teller effect, a lattice distortion and remove the twofold degeneracy [3].

We have explored such a scenario by making low temperature neutron powder diffraction (using G4.2 and G4.1 at LLB) and single crystal magnetic resonant x-ray scattering (RXS) experiments (ID20, ESRF) on $\text{Li}_2\text{VOSiO}_4$, a system that has been proposed as a prototype of frustrated 2D quantum ($S = 1/2$) Heisenberg AF, and one of the most studied among the new J_1 - J_2 systems [3–5]. $\text{Li}_2\text{VOSiO}_4$ crystallizes in the tetragonal $P4/nmm$ space group, with room temperature lattice parameters $a \approx 6.37 \text{ \AA}$ and $c \approx 4.45 \text{ \AA}$. The magnetic sublattices of $S = 1/2$ V^{4+} ions are built up by layers of VO_5 square pyramids sharing corners with SiO_4 tetrahedra. This structure suggests significant super-super-exchange coupling both along the sides (J_1) and the diagonals (J_2) of the distorted V^{4+} square lattice (the ions have different z-coordinates, see Fig. 1). NMR, magnetization,

specific heat, and muon spin rotation measurements on $\text{Li}_2\text{VOSiO}_4$ [4] indicate that a collinear AF structure is established below $T_N = 2.8$ K, with magnetic moments lying in the a - b plane. The analysis of these experiments leads to a strongly reduced value for the ordered magnetic moment, $m(T \rightarrow 0) \approx 0.24 \mu_B$, which is considerably smaller than that expected [6] on a 2D lattice ($0.65 \mu_B$).

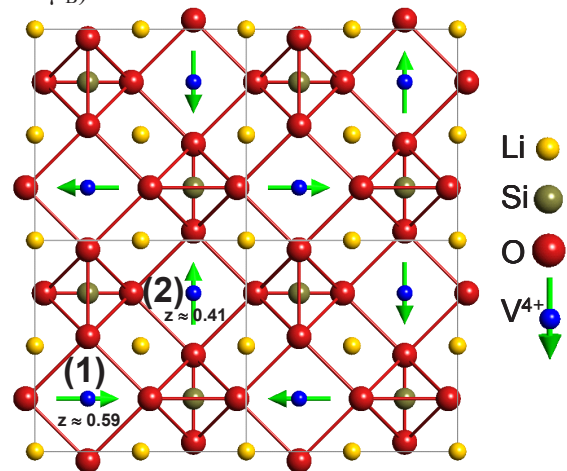


Figure 1. View along [001] of the crystal structure of $\text{Li}_2\text{VOSiO}_4$. The apical oxygen atoms of the VO_5 pyramids have not been represented in order to visualize properly the magnetic moments on V^{4+} of one of the non-collinear ground states that are compatible with powder neutron diffraction data.

More recently some doubts were raised [5] concerning the actual value of the ratio J_2/J_1 , which was found ≈ 12 from local density calculations. This result indicates that the system has a large J_2 , rather than being close to the border between the collinear and the dimer state. Moreover, it also immediately leads to discrepancy with the reported value of $\approx 0.24 \mu_B$, too low for a large J_2 state.

Our study [7] has allowed us to establish the low temperature magnetic structure. The propagation vector is $\mathbf{k} = (1/2, 1/2, 0)$ so that the little group is $G_{\mathbf{k}} = P4/nmm$. There are four two dimensional

irreducible representations of which only the Γ_4 , giving rise to Fourier components of the form $S_{\mathbf{k}}(1) = (u, v, 0)$ and $S_{\mathbf{k}}(2) = (v, u, 0)$ (see Fig.1), is compatible with the observations. Neutron powder diffraction data are degenerate with respect to the relative values of u and v , however RXS, exploiting the fact that the two V^{4+} ions have $z(1) \neq z(2)$, is able to confirm that $u=v$. For instance, in the case of the $(\pm 1/2, \pm 1/2, 3)$ reflection the π - σ magnetic scattering is strong, whereas the π - π signal is very weak, whatever the value of ϕ ($\tan^{-1}(v/u)$). On the other hand, for the $(\pm 1/2, \pm 1/2, 2)$ reflection, a negligible π - π magnetic scattering is expected only for $\phi=45^\circ$ or $\phi=225^\circ$. As the experiment shows significant π - σ magnetic scattering for both reflections, with no detectable π - π intensity, we can conclude that the structure is collinear.

The magnetic structure consists then of collinear a - b AF layers stacked F along the c axis (see Fig.2). The refined ordered magnetic moment $m=0.63(3)\mu_B$ is larger than previously reported, and consistent with $|J_2/J_1| \geq 1$, in good agreement with theoretical predictions [5].

High resolution powder neutron (G4.2, LLB) and X-ray diffraction (BM16 at 40 KeV) have also shown the absence of structural phase transition accompanying the magnetic ordering. This work is another example of the complementary use of neutron and synchrotron radiation in the study of magnetism.

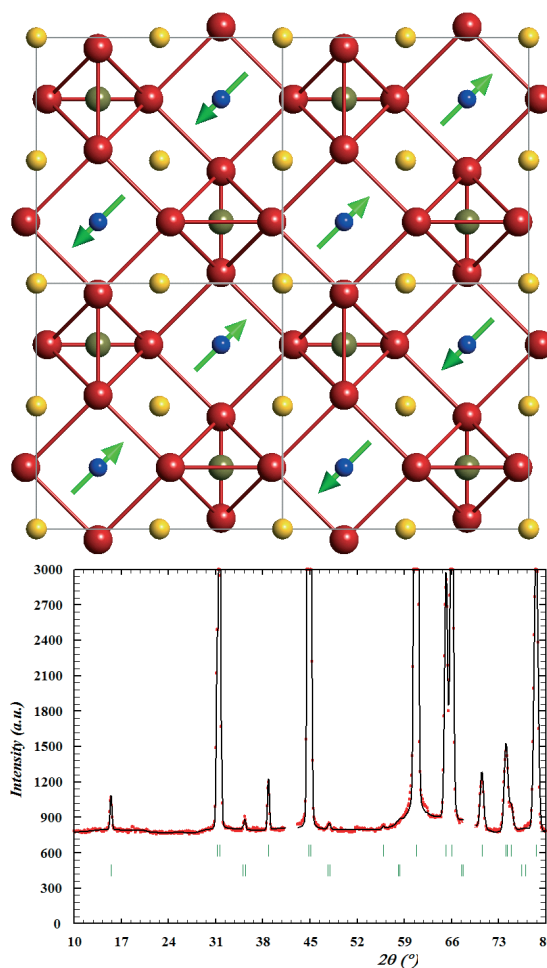


Figure 2. Refinement of the magnetic structure of $\text{Li}_2\text{VOSiO}_4$ and picture of its collinear structure. This is compatible with both neutron powder diffraction and resonant X-ray magnetic scattering on a single crystal.

References

- [1] C. L. Henley, Phys. Rev. Lett. **62**, 2056 (1989) ; P. Chandra *et al.*, Phys. Rev. Lett. **64**, 88 (1990) ; L. Capriotti *et al.*, Int. J. Mod. Phys. B **14**, 3386 (2000) and references therein.
- [2] E. F. Shender, Sov. Phys. JETP **56**, 178 (1982) ; J. Villain *et al.*, J. Phys. (Paris) **41**, 1263 (1980).
- [3] F. Becca and F. Mila, Phys. Rev. Lett. **89**, 037204 (2002).
- [4] R. Melzi *et al.*, Phys. Rev. Lett. **85**, 1318 (2000), R. Melzi *et al.*, Phys. Rev. B **64**, 024409 (2001).
- [5] H. Rosner *et al.*, Phys. Rev. Lett. **88**, 186405 (2002), H. Rosner *et al.*, Phys. Rev. B **67**, 014416 (2003).
- [6] H. J. Schulz *et al.*, J. Phys. I (France) **6**, 675 (1996).
- [7] A. Bombardi, J. Rodríguez-Carvajal, S. Di Matteo, F. de Bergevin, L. Paolasini, P. Carretta, P. Millet, and R. Caciuffo, Phys. Rev. Lett. **93**, 027202 (2004)

TEMPERATURE RENORMALIZATION OF THE SPIN CORRELATIONS IN THE DIMER SPIN-LIQUID TlCuCl_3 Ch. Rüegg¹, Ch. Niedermayer¹, A. Furrer¹, J. Mesot¹, M. Matsumoto², B. Normand³, M. Sigrist⁴, T.M. Rice⁴, K.W. Krämer⁵, H.-U. Güdel⁵, H. Mutka⁶, P. Bourges⁷, Y. Sidis⁷¹Laboratory for Neutron Scattering, ETH Zürich & Paul Scherrer Institut, 5232 Villigen PSI, Switzerland²Department of Physics, Faculty of Science, Shizuoka University, Shizuoka 422-8529, Japan³Département de Physique, Université de Fribourg, 1700 Fribourg, Switzerland⁴Institute for Theoretical Physics, ETH Zürich, 8093 Zürich, Switzerland⁵Department for Chemistry and Biochemistry, Universität Bern, 3000 Bern 9, Switzerland⁶Institut Laue-Langevin, 38042 Grenoble Cedex 9, France⁷Laboratoire Léon Brillouin (CEA-CNRS), CEA- Saclay, 91191 Gif sur Yvette Cedex, France

Spin-liquids are currently attracting a considerable interest because of the numerous novel phenomena related to quantum phase transitions [1]. The compound TlCuCl_3 is a nearly optimal model system showing field-, pressure- and doping-induced transitions to antiferromagnetic (AF) phases, which can be investigated by several experimental techniques and reveal unconventional ground states characterized by condensates of magnetic quasi-particles [2,3].

The two $S=1/2$ magnetic moments in a pair of Cu^{2+} ions are coupled in TlCuCl_3 by a dominant AF exchange interaction J_{intra} leading to an effective singlet ground state. The elementary excitations are then triplet states, which can hop to neighbouring dimer sites by residual interdimer interactions J_{inter} . These interdimer interactions are weak in the related compound KCuCl_3 but strong in TlCuCl_3 , which therefore has a singlet-triplet spin energy gap Δ of modest 0.7 meV or 8.1 K, see Fig 1. The softening of this gap in an external magnetic field or by pressure application is the basic mechanism causing the quantum phase transitions mentioned above.

However, even the zero-field and zero-pressure spin-liquid state provides an interesting testing ground for many-body quantum theories and needs to be characterized for future studies of the finite temperature properties in the different AF phases. The temperature dependence of the spin energy gap Δ is hereby of particular interest, see Fig. 1. Inelastic neutron scattering (INS) experiments have been performed on the thermal triple-axis spectrometer 2T (LLB, Saclay) to investigate the spin correlations in TlCuCl_3 up to $T \approx J_{\text{intra}}$. The results can now be compared with the related compound KCuCl_3 [4] and extent previous high-resolution but low-temperature studies carried out on the cold triple-axis spectrometers TASP (SINQ, Villigen) and IN14 (ILL, Grenoble).

Contour plots resulting from 14 constant Q -scans along the $Q=(qh\ 0\ 0)$ [r.l.u.] reciprocal direction are presented in Figure 2 for three representative

temperatures. A reduction of the triplet bandwidth is observed, which is even more pronounced along directions including the minimal spin energy gap Δ . We further report a considerable damping of the excitations, caused by a finite lifetime of the quasi-particles, and a reduction of the inelastic intensity by thermal depopulation of the singlet ground state. The renormalization of the excitation energies is in agreement with predictions from both Troyer-Tsunetsugu-Würtz (TTW-MF) [5] and Bose (Bose-MF) mean field theory at moderate temperatures. At $T \approx J_{\text{intra}}$ however, a better description of the new INS data results from TTW-MF, see Fig. 2, which is discussed below.

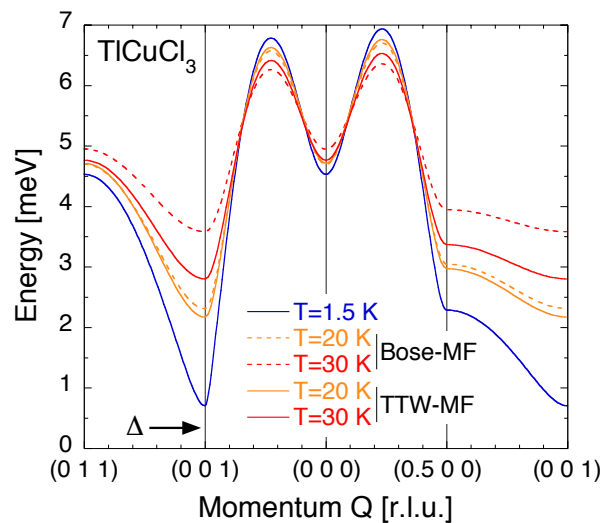


Figure 1. Theoretical predictions for the temperature renormalization of the elementary triplet excitations in the dimer spin-liquid TlCuCl_3 . TTW-MF and Bose-MF bond-operator theory as explained in the text. TTW-MF calculations show a considerably weaker renormalization at high temperatures.

Quantum fluctuations lead to a marginal admixture of triplet components to the singlet ground state even at the lowest temperatures $T=0$ K. But finite temperatures additionally cause a considerable thermal population of the triplet states,

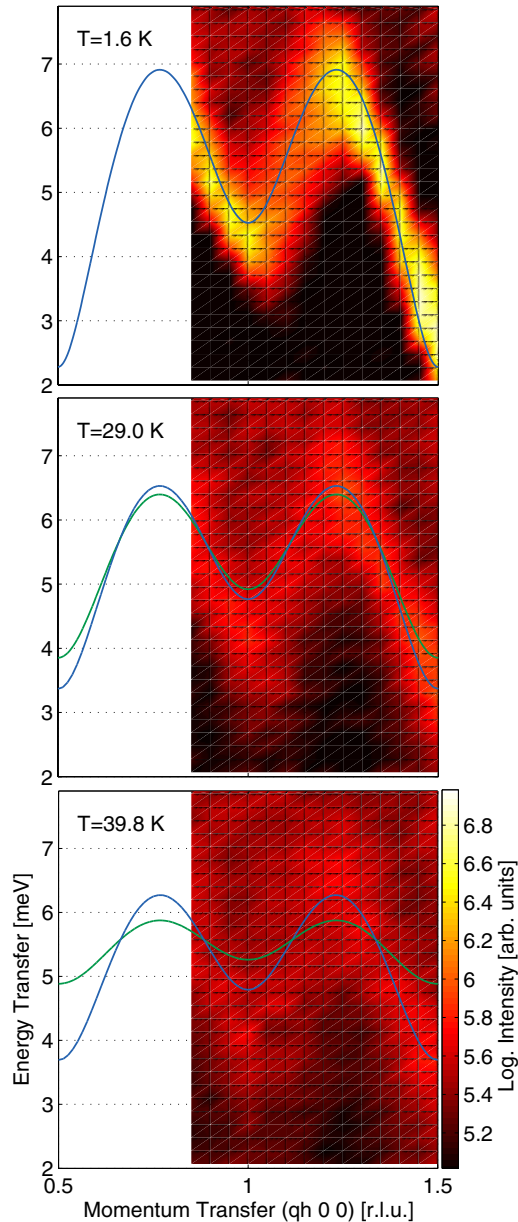


Figure 2. Contour plots of the INS intensity measured along $Q=(qh\ 0\ 0)$, reciprocal lattice units [r.l.u.], in TlCuCl_3 on 2T (LLB, Saclay). Solid lines correspond to TTW-MF (blue) and Bose-MF (green) theory as described in the text and presented for the whole dispersion curve in Fig. 1.

References

- [1] S. Sachdev, *Science* 288 (2000) 475.
- [2] M. Matsumoto, B. Normand, T.M. Rice, M. Sigrist, *Phys. Rev. Lett.* 84 (2002) 077203; *Phys. Rev. B* 69 (2004) 054423.
- [3] Ch. Rüegg et al., *Nature* 423 (2003) 62.
- [4] N. Cavadini, Ch. Rüegg, W. Henggeler, A. Furrer, H.-U. Güdel, K. Krämer, H. Mutka, *Eur. Phys. J. B* 18 (2000) 565.
- [5] M. Troyer, H. Tsunetsugu, D. Würtz, *Phys. Rev. B* 50 (1994) 13515.
- [6] Ch. Rüegg et al., in preparation.

especially at $T > \Delta$. However, it is a non-trivial problem to describe the resulting interaction among these quasi-particles correctly. Of particular interest is further the implementation of the hard-core constraint, which means that only one of the four possible states, the singlet or one of the three triplet states, can reside on each dimer site. In the dilute limit up to $T \approx \Delta$, where the triplet quasi-particle density is low, Bose-MF theory [2], which corresponds to TTW-MF in this regime, correctly reproduces the observed renormalization of the excitation energies. TTW-MF theory has been proposed to interpolate between the known low- and high-temperature limits. We report almost perfect agreement with the corresponding theoretical predictions. The complete analysis will be presented elsewhere [6].

To conclude, we have investigated the renormalization of the spin correlations in a quantum spin-liquid up to temperatures close to the dominant energy scale, the dimer exchange interaction, of the magnetic system. The results most probably answer the fundamental question about the correct statistical description of a quantum many-body system, where the particles are on the one hand fermions, the $S=1/2$ moments of each Cu^{2+} ion, but on the other hand hard-core bosons, as a consequence of the dominant correlation within the dimer. The present study at finite temperatures is therefore of general interest for the description of related systems with a spin energy gap as well as for the interpretation of their macroscopic bulk properties.

DOMAIN STRUCTURES IN Fe/Fe₂N MULTILAYERSW. Szuszkiewicz¹, K. Fronc¹, B. Hennion², and M. Aleszkiewicz¹¹ Institute of Physics, Polish Academy of Sciences, Al. Lotników 32/46, 02-668 Warsaw, Poland² Laboratoire Léon Brillouin, CEA-CNRS UMR 12, 91191 Gif-sur-Yvette Cedex, France

Many studies nowadays are concerned with the magnetic properties of thin magnetic layers or multilayers. The common goal is to find appropriate materials for so-called spintronics applications which require the control of the spin state of the carriers. Structures made of the stacking of ferromagnetic layers separated by non-magnetic layers attract a lot of attention because of possible interlayer exchange coupling in such systems. An antiferromagnetic coupling between ferromagnetic layers is of special interest as it makes it possible to control the behavior of the multilayer through an external factor like, e.g., a magnetic field or a light illumination. In spite of extensive experimental and theoretical studies the mechanism of the interlayer coupling is still not well understood.

The Fe/Fe₂N multilayers have been selected in order to study the interlayer coupling and to obtain a better understanding of magnetic phenomena (including the magnetization and demagnetization processes) in Fe-based system.

The Fe-N system presents a variety of phases, the crystal structure and the magnetic properties evolving with nitrogen concentrations (see [1,2] for details). In particular, orthorhombic Fe₂N does not show ferromagnetism at room temperature, and the Curie temperature lies between 4 and 60 K for this phase. Thus, when Fe₂N is used as a non-magnetic spacer between magnetic layers in a multilayered structure, one can expect an interesting temperature dependence of the magnetic properties of the system.

Fe/Fe₂N multilayers have been grown at the Institute of Physics of the Polish Academy of Sciences in Warsaw. Several multilayers Fe(4 nm)/Fe₂N(0.8-1.5 nm) were deposited on (001)-oriented GaAs substrate at room temperature by a sputtering technique. In order to avoid oxidation, a 10 nm thick Si cap layer was deposited on the top. X-ray diffraction and Kerr effect were used to characterize the samples at room temperature. The non-magnetic character of this phase was confirmed by the Kerr rotation measurements performed on a 31 nm thick amorphous layer, with a composition close to Fe₂N, as used for our multilayers.

Neutron diffraction measurements have been performed on a triple-axis spectrometer in order to achieve a good resolution. The 4F1 spectrometer,

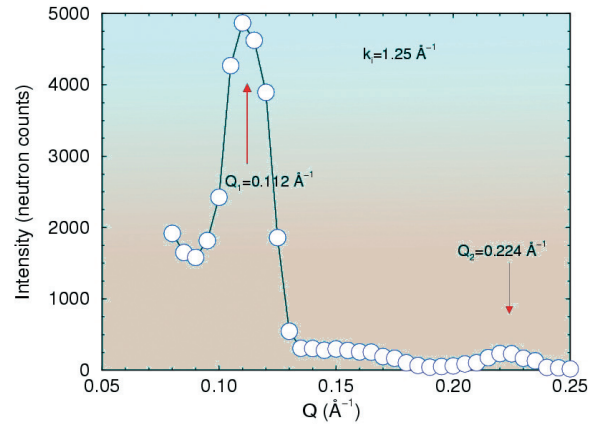


Figure 1. Magnetic peaks observed at room temperature at small angles on a multilayer Fe(4 nm)/Fe₂N(1.5 nm) deposited on a (001) GaAs substrate.

installed on a cold source of the Orphée reactor at the LLB, was used. The incident neutrons had a wave-vector $k_i = 1.55 \text{ \AA}^{-1}$ or 1.25 \AA^{-1} , the beam being filtered by a cooled Beryllium to avoid harmonic contamination, 40° Soller slits collimations were set on each side of the analyser.

Because of the layered structure, diffraction peaks are expected at positions $Q_n = 2n\pi/D$, where D is the period of the structure, sum of the thicknesses of a Fe layer and of a Fe₂N layer in the present case. The intensities of these peaks are given by $|F_{BL}(Q)|^2 \sin^2(n_m DQ/2) / \sin^2(DQ/2)$, where n_m is the number of bilayers and $F_{BL}(Q)$ the form factor of the elementary bilayer, which may consist of a nuclear and a magnetic contribution, and depends on the contrast between the two layers. In the present case the contrast between Fe and Fe₂N is nearly zero for the nuclear contribution, and a magnetic contribution will exist only if there is a magnetic coupling between adjacent bilayers. An antiferromagnetic coupling would be revealed by a signal corresponding to a 2D distance. The measurements were performed at small angles in order to keep the magnetic form factor near its maximum value. Fig. 1 displays the result of a typical measurement on a sample whose nominal composition was Fe(4 nm)/Fe₂N(1.5 nm), with 22 bilayers (~120 nm thick). Two peaks are observed, corresponding to $2n\pi/D$, with $n=1$ and 2, and $D=5.61$ nm. The small bump at about $n=3/2$ is not a signature of antiferromagnetic coupling as we

checked that no peak existed at $n=1/2$. It could be due to the Si coating of the sample. This means that the bilayers are ferromagnetically coupled.

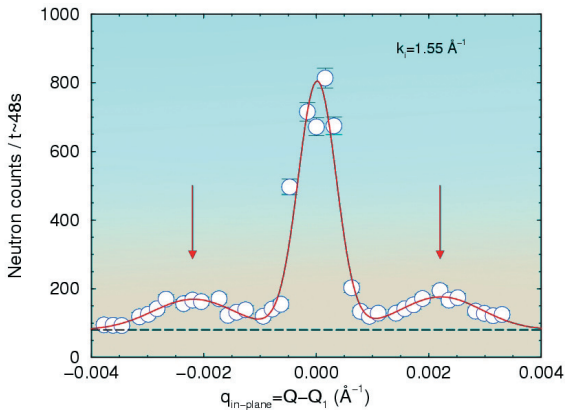


Figure 2. In-plane scan centered on the $Q_1=(0,0,0.112)$, position of the bilayer peak, evidencing a characteristic distance of ~ 285 nm.

In order to check the quality of the structure, an in-plane scan was performed, perpendicular to the peak at Q_1 . To our surprise, satellite peaks were found at $Q_1 \pm q_{\text{in-plane}}$, as reported on Fig. 2. These peaks are the signature of a characteristic in-plane distance $\Delta = 2\pi/q_{\text{in-plane}}$, with a long-range coherency along the stacking axis of the bilayers. This distance is then equal to 285 nm, and *a priori* points out a peculiar magnetic behavior of the multilayered structure.

MFM measurements have then been performed at the Institute of Physics of Warsaw, on several Fe/Fe₂N multilayers. They evidenced stripe-like magnetic domains on the surface of these samples, with a period varying with the Fe₂N layer thickness, typically between 180 and 240 nm. These numbers are somewhat smaller than that found by the neutron scattering, but it is likely that

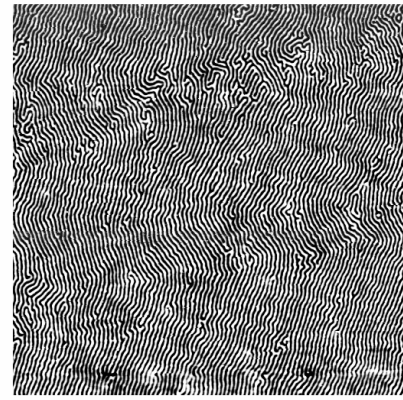


Figure 3. Stripe domains evidenced at the surface of the sample by MFM measurements (the period ~ 217 nm).

the two observations have a common origin, the neutron measurements revealing the coherent aspect of this domain structuration. The neutron measurement has been performed in the $[110]$ direction of the Fe layer, the $[-110]$ direction being perpendicular to the scattering plane. That means that the $[100]$ and $[010]$ axes were at ± 45 degrees with respect to this direction. If, in accordance with the symmetry of the system, the stripe domains were along these axes with a period P , the Δ value would represent $P/\cos(\pi/4)$, yielding $P=201.5$ nm. This would reconcile both results, if we suppose that effects due to the sample geometry could affect the domain structuration on the very surface, where zig-zag behavior, although visible, does not ascertain the 45 degrees assumption. Complementary neutron measurements, including reflectometry, as a function of temperature and magnetic field, should help us to get a deeper insight into this multilayer system, one of the only few for which stripe domains have been observed [3,4].

Note added in proof:

A last minute test confirmed that, in the $[100]$ - $[001]$ scattering plane, the satellite peaks are observed at $q_{\text{in-plane}}[100]=\sqrt{2}$ at $q_{\text{in-plane}}[110]$, which confirms that the domain structuration is along the $[100]$ and $[010]$ axis.

References

- [1] H. Naganuma, R. Nakatani, Y. Endo, Y. Kawamura, and M. Yamamoto, Jpn. J. Appl. Phys. **43**, 4166 (2004).
- [2] J.F. Bobo, H. Chatbi, M. Vergnat, L. Hennet, O. Lenoble, Ph. Bauer, and M. Piecuch, J. Appl. Phys. **77**, 5309 (1995).
- [3] S. Langridge, J. Schmalian, C.H. Marrows, D.T. Dekadjevi, and B.J. Hickey Phys. Rev. Lett. **85**, 4964 (2000).
- [4] W.S. Lew, S.P. li, L. Lopez-Diaz, D.C. Hatton, and J.A.C. Bland, Phys. Rev. Lett. **90**, 217201 (2003).

3 - MATERIALS SCIENCE

3 - MATERIALS SCIENCE

Materials science is a scientific field at the crossroads of physics, chemistry and engineering sciences, which aims at understanding how parameters such as chemical composition, atomic structure and microstructure determine the macroscopic properties of complex solid systems (alloys, polymers, geological materials...). The scientific productions and conclusions of this broad field of research have short-term consequences on the day-to-day applications and often concern plain industrial research.

The research in materials science covers two main domains :

- 1) Research on ill-condensed matter including liquids, glasses and disordered systems and
- 2) Metallurgy for which, the main research topics are focussed on the analysis of the residual stresses and the determination of crystallographic textures.

The LLB approach of materials science includes a particular attention to industrial needs and problems, but also a fundamental character in particular through the analysis of the mechanical behaviour of micro-heterogeneous materials, the study of crystallographic textures, the analysis of structural heterogeneities and the phenomena of precipitation as well as ageing in metal alloys.

The last part of this material section presents the structural studies of Polymorphs and Solvates of Fullerenes and research on molecular compounds.

Metallurgy

Residual stresses

(M. Ceretti, R. Levy, A. Menelle, LLB ; A. Lodini, University of Reims Champagne-Ardenne)

Internal and residual stresses in materials have a considerable effect on material properties, including fatigue resistance, fracture toughness and strength. Neutron diffraction provides a powerful non-destructive tool for stress analysis deep within a crystalline material. The principle of the technique, called Neutron Strain Scanning, is to use the crystal lattice as an atomic strain gauge to measure strain distributions with a sub-millimetre spatial resolution. The stresses are thus calculated from the measured strains using the well-known elasticity laws. The G5.2 diffractometer dedicated to the strain characterization has been improved in the past years, in particular with a new sample stage based on three coupled elevators (with a 300 mm extension range) controlled by three potentiometers. Mercury switches are installed under the upper table to insure the horizontality of the table during measurement. The precision in the position is of the order of 10 μ m. The new device (table +columns) is also equipped with a XY- table, each translation with a total course range of 150 mm. This device can handle very big samples, up to 500 kg in weight, with a good positioning precision and consequently presents a real interest for industrial applications.

Engineering activity at the LLB has significantly developed in the last two years. A large number of real industrial problems have been studied in collaboration with academic and industrial partners.

Among the principal industrial contracts, the work carried out in collaboration with DASSAULT Aviation can be mentioned. In the frame of a large research programme aimed to control the conception and the structural behaviour of fighter plane units, neutron diffraction has been used to characterize the residual stress fields in a representative wing of a MIRAGE 2000.

In the field of materials used in the aeronautics sector, neutron diffraction found a new application in the analysis of the residual stresses after a welding carried out by a very promising new process in rapid development : the Friction-Stir Welding (FSW) technique ("Highlight" of Stelmukh et al.).

Furthermore, the collaboration with SNCF concerning the evaluation of the residual stresses at the interface between the wheel and its axis has been continued and completed by finite element calculations. This work represents a large part of the thesis of A. Yameogo ("Highlight").

The diffraction technique gives elastic strain values averaged on the diffracting volume, but the materials can present heterogeneous strains between grains (different phases or crystallographic orientations) or in the grains (fluctuations). The experimental data analysis is therefore based on averaging techniques and scaling methods such as the well-known homogenisation method. The comparison between experimental and theoretical results allows to validate a model and to determine the effective properties of micro-heterogeneous materials. These approaches constitute a field of research presently under very active development because of the expected applications. In particular, the study of the inter and intragranular

elastic strain distributions in a Dual-Phase Steel was continued in collaboration with LMS (J. Crépin, D. Caldemaison, Ecole Polytechnique, Palaiseau, France) and LPMTM (O. Castelnau, N. Letouze, University of Villetaneuse). This material presents a very anisotropic local behaviour, for which every elastic loads induce a heterogeneous strain field. "In situ" neutron diffraction measurements, in the elastic range, have been realized adapting the loading machine of LMS. The measurements of in-situ peak broadening at different elastic loads allowed characterising the increase of strain heterogeneities, which are comparable with theoretical homogenisation predictions.

Crystallographic textures

(M.H. Mathon, P. Gerber, S. Jakani, C.H. de Novion, LLB; T. Baudin, A.L. Etter LPCES, Orsay University)

Crystallographic texture (preferential orientation of the grains) is one of the parameters describing the microstructure of a polycrystalline material, which controls partly its mechanical properties. In metal alloys, texture appears during solidification, then changes during stages of working (rolling, wiredrawing) and finally during the recrystallization.

Neutron diffraction is the best technique to determine the crystallographic texture of massive polycrystalline specimens (Volume $\sim 1 \text{ cm}^3$), in the form of a crystalline orientation distribution function. Its use is in particular necessary in the case of large grains materials (few mm^3) frequently met after primary or secondary recrystallization, for which the diffraction of conventional X-rays is not applicable.

The LLB has a 4-circles diffractometer dedicated to texture measurements, "6T1" on which, a furnace has been recently adapted on the Euler's cradle (see "Highlight") allowed to performed "in situ" measurements at high temperature (up to 1000°C). The possibility of carrying out an "in situ" texture analysis as a function of temperature, allows on the one hand to quantify the kinetics of formation or disappearance of the components, and on the other hand to understand the evolution of the preferential orientations during phase transformations.

Such a procedure represents a major asset for the textures study at high temperature in zirconium alloys within the framework of the development of a predictive model for the cladding tubes and guide tubes behaviour in accidental situation in Pressurized Water Reactors (PWR). For the first time, measurements were performed at room temperature and at 900°C to determine respectively the hexagonal α phase components and the cantered cubic β phase texture (see figure 1). They have shown that the main texture components follow the burger's law ($(110)_\beta // (00.2)_\alpha$ & $[-11-1]_\beta // [2-1.0]_\alpha$) in agreement with models. This study has been performed in collaboration with J.L. Béchade (CEA/DEN/SRMA). This protocol has been also applied to titanium alloys in collaboration with J. Delfosse (MSSMat, École Centrale Paris).

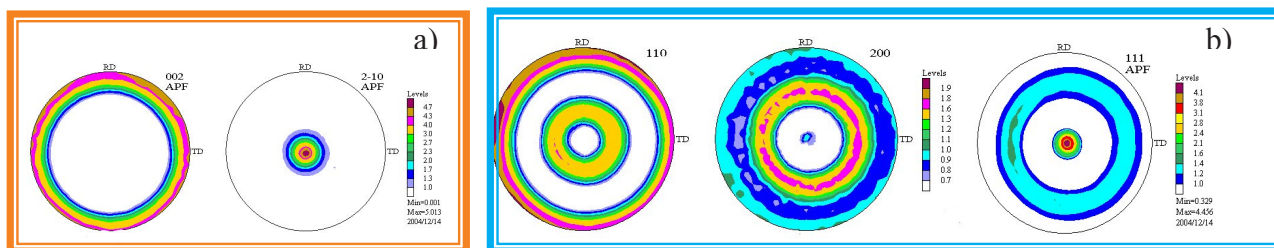


Figure 1 : Pole figures measured on the α hexagonal phase at room temperature (a) and on the β cubic cantered phase at 900°C (b). Some of them (2-10 for α and 111 for β) have been calculated from the Orientation Distribution Function to exhibit the burger's law.

A large part of the crystallographic texture activity is always dedicated to the recrystallization phenomena study in various materials (FeNi, two-phase alloys, etc.). More precisely, several works have for main goal to understand in face cantered cubic alloys, the development, during the recrystallization, of a strong "cube" component $\{100\}\langle 001\rangle$ beyond a critical deformation rate. The determination, from the diffraction peaks broadening, of the stored energy by the grains during the deformation, had highlighted that the grains of cubic orientation stored an energy lower than the grains belonging to the other preferential orientations (see the preceding activity report). The "in situ" follow-up of the preferential orientations during the recrystallization annealing brings additional information on the kinetics. For that, the diffracted intensity variation is followed versus time at various temperatures, for particular poles corresponding to deformation components that will disappear or on the contrary, to recrystallization components which will develop. From

the increase of the scattered intensity at the centre of the {100} pole figure, the activation energy of the recrystallization phenomena has been determined in cold rolled copper. It has been done for two rolling deformation rate (70 and 90 % reduction). Energy values respectively close to 34 and 24 k/mol have been found. These results can be correlated with the stored energy values determined previously in this material. Indeed the higher is the stored energy and consequently the driving force of recrystallization, the lower is the activation energy. These experimental activation energy determinations bring fundamental data to be introduced in statistically recrystallization models actually developed in the laboratory.

This parametric study has been realized in wire-drawn copper in the context of the "OPEFiC" research project partly subsidized by the French Research Ministry, including 3 laboratories (LLB, LPCES, LPMTM of Villetaneuse University) and 2 French producing copper wire rod companies (SCCC, SLC). The main objective of this project is to study the residual impurities (S, Pb) effect on the deformation and recrystallization mechanisms in order to understand the wire ductility decrease observed after thermomechanical (wiredrawing followed by heating) treatments. The "OPEFiC" research project has been the framework of S. Jakani thesis (see "Highlight"). This study has shown that the presence of the impurities in very low contents modifies the substructure of deformation (dislocations cell) and the total stored energy. The mechanisms of recrystallization are not modified but the kinetics is slow down because of a delay in the recovery phase as well as the decrease of the grain boundaries mobility in the presence of impurities.

Study of heterogeneities, Precipitation

(M.H. Mathon, C.H. de Novion, LLB; Y. de Carlan, A. Alamo, J.L. Béchade CEA/SRMA)

The studies of heterogeneities and of precipitation phenomena are integrated in various themes and are primarily based on Small Angle Neutron Scattering (SANS) experiments. These studies cover a large number of subjects and are the matter of collaborations in particular with the Laboratoire de Chimie du Solide Minéral (University of Nancy) concerning the ageing of Pb-Ca-Sn alloys used in the Pb accumulators and with the Ecole des Mines (Albi). This last collaboration with D. Delagnes et al. focus on the study of tool steels whose mechanical resistance is controlled by the dislocation distribution induced in the material during the quench treatment and by the carbide secondary precipitation produced during the tempering. TEM observations and SANS experiments were performed in order to analyse the carbides population evolution after a double tempering and a fatigue test in two steels containing respectively 1 wt-% and 0.35 wt-% of silicon. A considerable effect of silicon on the secondary carbides precipitation has been shown throughout a higher volume fraction of small secondary carbides (mainly vanadium carbides) in the low-silicon steel. The precipitation sequence is in fact modified and as a consequence, the secondary hardening peak of the low silicon grade is shifted towards higher temperatures.

These last years, many experiments were devoted to the study of ageing and of microstructural evolutions under neutron irradiation or thermal ageing in materials of nuclear interest.

In particular, the studies concerning the 7-12% Cr martensitic steels - candidates for the internal structure of future generation reactors or spallation sources – were continued. It was shown that when the Cr content of the b.c.c. ferritic matrix was larger than a critical threshold value (~ 7.2 at.% at 325°C), the ferrite separated under neutron irradiation into two isomorphous phases, Fe-rich (α) and Cr-rich (α'). The quantity of precipitated α' phase increases with the Cr content and the irradiation dose. The Cr solubility limit in iron at the irradiation temperature, was deduced from this study and we can conclude that the only effect of neutron irradiation is to speed up the precipitation.

A new study in collaboration with CEA/SRMA (J.L. Béchade, S. Doriot) concerns the microstructural evolution under neutron irradiation of Zr alloys used for cladding tubes. More precisely, SANS experiments were performed to provide quantitative and statistical information on the radiation-enhanced precipitation of β -Nb needles and possible other defect or solute clusters in two different industrial alloys (Zy4 used in REP and Zr-2.5%Nb). These experiments have pointed out a significant increase of the radiation-enhanced precipitation with the radiation dose (between 1.5 and 3 PWR cycles) as well as a notable modification of the precipitates shape that changes from a quasi spherical form to an elliptic one. Moreover, the formation of defects clusters of small size (coherent with dislocations loops) was observed.

Finally, a significant share of the activity in SANS domain was devoted to the study of oxides dispersion strengthened materials (ODS) worked out by mechanical alloying. The data treatment is under way.

Ill-Condensed Matter and New Technologies for Clean Energy

Neutron scattering is an essential technique for the study of disordered systems in general and, more specifically for the investigation of structural and dynamic properties of molecular liquids and glasses. This is essentially due to the possibilities of isotopic substitution and of incoherent scattering. Among the many studies undertaken in these fields of research, we will quote examples of experiments performed at LLB on the diffuse scattering diffractometer 7C2 and on the time-of-flight inelastic spectrometer MIBEMOL.

Parallel to the experimental works, molecular modelling is developed at the LLB and applied to the diffraction and scattering data interpretation in the research field of molecular compounds.

Study of liquids and glasses

(B. Beuneu, M.C. Bellissent-Funel, LLB ; B. Belhorma, CNESTEN Maroc)

There is a growing interest in structural studies of multi-component oxide glasses by means of neutron scattering, which are now a large part of the “disordered systems” studies. *First*, because, due to their complexity, the structural role of the various oxides is not yet clear, and in glasses of industrial use, it is of great importance to understand how each added oxide modifies the properties of the material. *Second*, because the recent simulation techniques (reverse Monte Carlo and molecular dynamics) open new fields to the analysis of the diffraction data of these complex materials with a well-defined short-range order. The other experimental techniques (NMR, Raman, Mossbauer, ...) give good information about the first coordination shell, but Neutron techniques can go much further in the reciprocal space and gather some information on medium range order, which can be extracted throughout these simulations.

With a group of the University of Rennes 1 (Deriano, Rouxel et al.), we had first studied the effect of nitrogen on the structural properties of high mechanical performance silicate glasses. Neutron diffraction combined with NMR has shown how nitrogen was increasing the benefit of adding magnesium for the mechanical properties: nitrogen helps magnesium to enter the network as a precursor in tetrahedral sites, which increases the bond strength of Mg-O. This collaboration is continuing (including now F. Lofaj from the Institute of Materials Research of SAS, Slovakia), through the study of silicate glasses which simulate the grain boundary phases of high temperature ceramics: the rheological properties of these ceramics are driven by this vitreous intergranular phase.

The structure of oxide glasses and liquids is also of great interest for the earth science, since they enter as a large part in the composition of the earth mantle. A group of the Laboratoire de Minéralogie-Cristallographie (L. Cormier, O. Majerus, G. Calas, et al., Université Paris 6) has undertaken a systematic study of the structural changes with temperature in some oxide glasses, by means of neutron diffraction studies which strongly imply the LLB, combined with X-ray diffraction, NMR, Mossbauer, or EXAFS measurements. Model cases of two-oxide glasses have been studied (alkali diborate glasses, which can be also a model for nuclear waste containment glasses, and alkali disilicate glasses). Diffraction data were taken on 7C2 at different temperatures from 300K to 1350K ($T_g \approx 700-850K$). The environment of Li was investigated using isotopic substitution. The pronounced change with temperature of the alkali environment is the main common features of the two studies. And although the atomic order decreases with temperature, a marked medium range order remains in the liquid phase. A detailed analysis of the K disilicate glass results by means of Reverse Monte Carlo and Molecular Dynamics simulations has shown that the FSDP (first sharp diffraction peak), that increases at high temperature, can be explained by correlations between well polymerised network domains surrounding K rich domains.

In addition, the interaction of trivalent neodymium ions with nitrate ions and neutral organic molecules is investigated in concentrated solution of $Nd(NO_3)_3$ dissolved in C_2D_5OD . Neutron scattering experiment combined with the first-order isotopic-difference method was applied to Nd^{3+} to determine the local order around Nd^{3+} ions. The results show that the trivalent neodymium ions have a coordination number between 8 and 9. The first salvation shell is composed of ethanol molecules and nitrate ions at distances of 2.26 Å and 2.45Å respectively (“Highlight”).

New Energies : the fuel cell systems and batteries

The fuel cells make possible a direct conversion of chemical energy into electric power. They are different according to the nature of their electrolyte and by the level of their operating temperature, their architecture and the applicability in which each type can be used. Cell systems, whose electrolyte is an membrane promoting the exchange of protons, concentrate a significant share of the world effort of research and

development on New Technologies of Energy (NTE). Converting today's oil based, inefficient and polluting transport technology into a more sustainable equivalent is a tough challenge. Proton Exchange Membrane Fuel Cells (PEMFC) will very likely play an important role by offering silent and emission-free electrical power for our future vehicles.

In this context, a study using the quasi-elastic neutron scattering was carried out at the LLB by J.C. Perrin, S. Lyonnard, O. Diat and G. Gébel (LPCI, CEA Grenoble) to study ionomer membranes. The ionomer membranes, such as the Nafion, are complex materials exhibiting a hierarchical structure, organised from the angstrom to the millimeter. They are characterized by a nanophase separation between hydrophobic and hydrophilic domains; their properties, notably the protonic conductivity, strongly depend on the water content. The study of the protonic diffusion mechanisms, and more generally the water management in these membranes, requires the use of many experimental techniques that cover a wide range of relaxation times, from the picosecond to the second. In addition to NMR spectroscopy and macroscopic characterisations, the quasi-elastic neutron scattering technique allows to investigate the proton dynamics at the molecular level. Two series of experiments performed on the spectrometer Mibemol allowed to study the elementary processes of diffusion in the Nafion as a function of the Relative Humidity (RH). Two types of motion have been identified : the first one corresponds to a fast local diffusion in a confined volume, the size of which increases (from 5 to 10 Å) when increasing the water amount, up to an 80% RH value. The second type of motion is a long-range diffusion, which has been surprisingly observed already in the very early phases of hydration. The Nafion do not behave as a typical "porous" material : it percolates immediately, and, beyond 80% RH, the structure swells very significantly without any modification of the underlying elementary dynamical processes. The neutrons are particularly well suited to study these perfluorinated polymers, the contrast with water being excellent. Two experiments on complementary spectrometers (spin-echo and backscattering) are programmed to reach longer relaxation times.

In the same field of "clean" energy, the influence of confinement on polymer-electrolyte relaxational dynamics was studied by J.-M. Zanotti (LLB and IPNS, Argonne) et al. In terms of stored energy and safety, solid-state devices using polymer electrolytes are highly desirable. One of the most studied systems is PEO (polyethylene oxide) complexed by Li salts. Polymer segmental motions and ionic conductivity are closely related. Bulk PEO is actually a biphasic system where an amorphous and a crystalline state ($T_g \approx 213$ K, $T_m \approx 335$ K) coexist. To improve ionic conduction in those systems requires a significant increase of the amorphous phase fraction where lithium conduction is known to mainly take place. Confinement strongly affects properties of condensed matter and in particular the collective phenomena inducing crystallization (*International Workshop on dynamics in confinement, edited by B. Frick, R. Zorn and H. Buttner, Journal de Physique, 10, PR7 (2000)*). Confinement of the polymer matrix is therefore a possible alternative route to the impractical use of high temperature.

Results of a quasi-elastic incoherent neutron scattering study of the influence of confinement on polyethylene oxide (PEO) and $(\text{PEO})_8\text{Li}^+[(\text{CF}_3\text{SO}_2)_2\text{N}]^-$ (or $(\text{PEO})_8\text{LiTFSI}$) dynamics are presented. The nano-confining media is Vycor, a silica based hydrophilic porous glass (characteristic size of the 3D pore network ≈ 50 Å). As expected, the presence of Li salt slows down the bulk polymer dynamics. The confinement also affects dramatically the apparent mean-square displacement of the polymer. Local relaxational PEO dynamics is described by the Kolhrausch-Williams-Watts (KWW) model. We also present an alternate model and show how the detailed polymer dynamics (correlation times and local geometry of the motions) can be described without the use of such stretched exponentials so as to access a rheology-related meaningful physical quantity: the monomeric friction coefficient (*Zanotti et al., Macromolecule, submitted*). Such a quantity could be an effective way to accurately estimate the viscosity of confined or interfacial polymer and/or polymer electrolytes.

Li_2O , a superionic conductor of interest in the context of solid state batteries, has been studied after electron irradiation by elastic diffuse neutron Huang scattering. The team of Krexner et al., (see the corresponding "Highlight") showed the formation under irradiation of Li precipitates which were characterised regarding their size, concentration, shape and defect strength.

Structural Studies of Polymorphs and Solvates of Fullerenes and other Molecular Compounds of Industrial or Pharmaceutical Interest

Initiated two years ago at LLB by Papoular, and carried out in collaboration with Prof. R. Céolin [Faculté de Pharmacie, Univ. Paris 5] and Prof. V. Agafonov [Faculté de Pharmacie, Univ. Tours], this new line of research involves molecular modeling and mostly X-Ray diffraction techniques. Molecular Modeling (using the commercial Hyperchem and Spartan softwares) is essential to obtain chemically sound structural restraints to be used in the GSAS-based Rietveld refinements of the powder diffraction data.

Polymorphs and solvates of fullerenes

(R.J. Papoular, LLB ; R. Céolin, P. Espeau, Paris 5 ; H. Allouchi, Tours ; J.-Ll. Tamarit, Barcelone)

A variety of hexagonal C₆₀ polymorphs and hexagonal/cubic C₆₀ solvates [with various solvents like CH₄, CH₃CCL₃, CH₂Cl₂ and C₉H₂₀] has been investigated by high-resolution X-ray powder/single-crystal diffraction as well as by thermodynamic measurements, namely thermogravimetric and differential scanning calorimetric studies, both at room and low temperatures. Modeling plays a key role in the obtention of ab initio structure solutions derived from the powder diffraction spectra. Results are currently being published [*Chem. Phys. Lett.*, 2004, *Carbon*, 2005].

The C₆₀.CH₂Cl₂ solvate has been measured using both X-Ray and Neutrons [*J.Phys.IV*, 2005]. It is described briefly as one of the “highlights” that follow this introduction.

Preferential adsorption of n-alkanes on Graphite

(P.Espeau, Paris 5 ; R.J. Papoular, LLB)

Monolayers of mixtures of n-alkanes [C₁₅H₃₂-C₁₇H₃₆, C₁₆H₃₄-C₁₇H₃₆, C₁₅H₃₂-C₁₆H₃₄] adsorbed on graphite [papyex] have been studied by very Small Angle X-ray Scattering (SAXS). The preferential adsorption of the longer chain [C₁₇ vs C₁₅, C₁₇ vs C₁₆] has been evidenced, and a simple theoretical formalism developed to account for it. These results are now published [*Applied Surface Science*, 2005]. Further work involves the detailed analysis of the 2D diffraction peak, which is characteristic of adsorbed monolayers. Albeit being strongly asymmetric, the observed experimental lineshape does not follow the widely-accepted Warren form [1941] that has been modified to account for the X-ray diffraction measurements.

Polymorphism of gamma- Butyrolactone [BL]

(R.J. Papoular, LLB ; H. Allouchi, V. Agafonov, D. Lemordant, Tours; A. Dzyabchenko, Moscow)

Both an important industrial compound for Li batteries but also a pharmacological agent, gamma-Butyrolactone is a liquid at room temperature that crystallizes into one of two polymorphs [BL1, stable ; BL2, metastable] at low temperature. The BL1 polymorph has been solved and refined at 180 K in the monoclinic system, whereas the BL2 polymorph crystallizes in the triclinic system (XRPD studies). Preliminary results are now published [*Acta Crystallogr. B*, 2005].

Extensions of this work currently in progress involve :

- i) understanding the connection between the liquid and the solid phases and
- ii) refining the triclinic BL2 phase (8 independent molecules), which may require synchrotron data.

3 - MATERIALS SCIENCE

1. Residual stress redistribution in a wheel/axle assembly due to cyclic loading **72**
A. Yameogo', A. Carrado, C. Prioul, A. Lodini
2. Residual stresses in welded aluminium joints for aerospace applications **74**
V. Stelmukh, S. Ganguly, L. Edwards and M. E. Fitzpatrick
3. Investigation of the α and β texture evolution of hot forged titanium alloy products **76**
J. Delfosse, C. Rey, M.H. Mathon
4. Impurities effects on the mechanisms of recrystallization of wire-drawn copper **78**
S. Jakani, T. Baudin, M. Benyoucef, Ph. Gerber, C.H. de Novion, M.H. Mathon
5. Nanocluster formation in electron irradiated lithium oxide **80**
G. Krexner, M. Prem, F. Beuneu, P. Vajda
6. Combined X-ray & neutron powder diffraction study of a dimorphic C_{60} solvate: $C_{60} \cdot CH_2Cl_2$ **82**
R.J. Papoular, R. Céolin, H. Allouchi, P. Espeau, A. Kurbakov', J.-LL. Tamarit
7. Local order around Nd^{3+} ions in an organic solution as determined by neutron scattering experiment **84**
B. Belhorma, M.-C. Bellissent-Funel, M.-C. Charbonnel, J.-P. Dognon

RESIDUAL STRESS REDISTRIBUTION IN A WHEEL/AXLE ASSEMBLY DUE TO CYCLIC LOADING

A. Yameogo^{1,2}, A. Carrado², C. Prioul¹, A. Lodini²

¹ LMSSMAT Ecole Centrale Paris, 92295 Chatenay-Malabry

² Laboratoire Léon Brillouin (CEA-CNRS), CEA- Saclay, 91191 Gif sur Yvette Cedex

Introduction

With increasing speed of the trains, fail safe design of the wheelset assembly has become of key interest. In some cases micro-cracks can be initiated close to the ends of the wheelset overhang. Fretting fatigue is usually associated with this crack initiation process. The present study is a contribution to a larger program devoted to safety assessment of the wheelset assembly. The aim of this work is to have a better knowledge of the in service evolution of the residual stresses in the structure.

Because of the very low penetration power of the X-rays, neutron diffraction experiments were conducted to characterise the stress state evolution at the interface between axle and wheel. Two reduced scale assemblies (1:3) have been tested before and after low cycle fatigue (1000 cycles) in rotary three point bending. In order to limit the neutron path, drilling holes access was performed according to the criteria established by a previous study (E. LABBE et al., Neutron diffraction residual stresses evaluation in railway wheels, Journal of Neutron Research (2001), vol 9, pp. 393-397).

Experiments

A three-dimensional modelling of the assembly has been performed to simulate the press fitting process and the cyclic loading. Numerical results are compared with experimental ones.

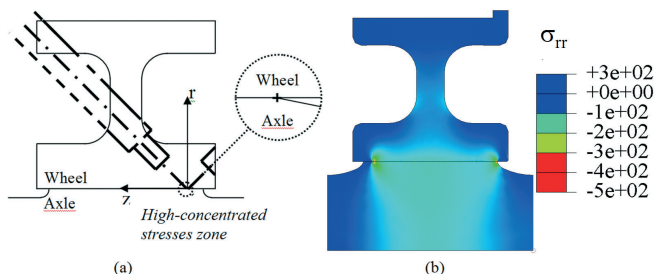


Figure 1. (a) Drilling orientation: radial strain measurement. (b) 2D axisymmetric press fitting simulation : high stress level zone.

These results have already been presented (Labbé et al.). The grid spacing is 1 mm. The shortest path for the neutrons gives the maximum of intensity, this maximum is around 3 mm above the interface (the dash pots line on the maps, figure 2) :

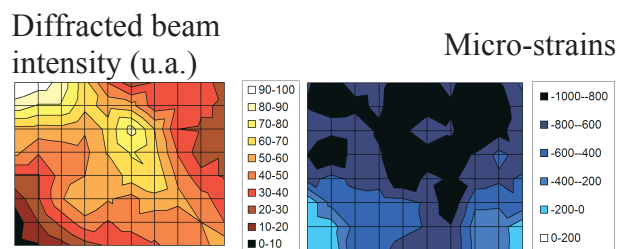


Figure 2. Radial strain measurement in a press fitted assembly after press fitting.

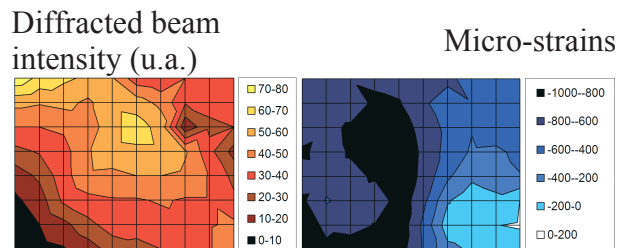


Figure 3. : Strain measurement in a press fitted assembly after press fitting and fatigue test.

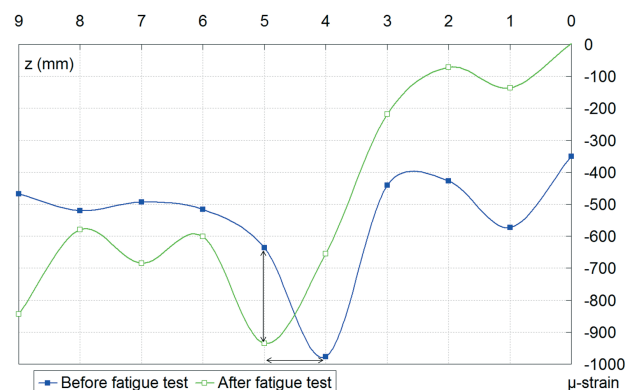


Figure 4: Experimental radial micro-strains along interface after press fitting and fatigue test.

The loss of clamp can be seen through the decrease of the micro-strain, $\Delta \approx 300$ micro-strains. The peak shift is equal to 1 mm. During the fatigue test cycles, the wheelset extremities (and of course the

geometrical singularity) were first deformed plastically and rapidly the contact between the wheel and the axle in this zone is lost.

Submodelling and loading :

To run a submodel is first to perform the complete analysis on the global structure, and then, from the result (displacement of the nodes), to “drive” in displacement the boundary of a substructure (zone of interest). The submodelling is very useful, because of the large dimensions of the assembly. In our case the substructure is the part of the assembly close to the interface.

Results

The submodelling gives the following results (figure 7) :

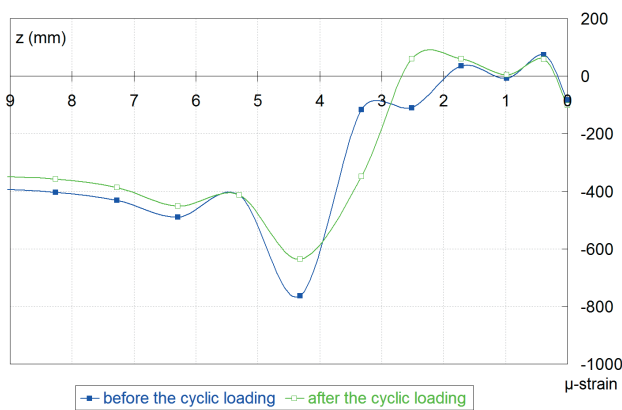


Figure 5 : Numerical radial micro-strains along interface after press fitting and cyclic loading.

A decrease of the compressive is observed, but no shift : 5 cycles is enough to initiate the plastic deformation of the geometrical singularity, but this loading can't produce a loss of contact at the extremity of the wheelseat.

The decrease is important and surely surestimated, this can be due to parameters of the model ($\sigma_0=199$ MPa).

Conclusion

Due to a penetration power, higher than the X-rays one, neutrons permit strain measurements inner an industrial assembly. The technique was very useful for the calibration of the numerical parameter for the simulation of fatigue process.

Neutron diffraction technique gives a precise description of the residual radial stress field induced by press fitting process in an industrial assembly. We have a very good agreement with the numerical modelling for the initial mechanical state.

In more, in a fatigue tested assembly, neutron measurements highlighted the loss of clamp between the two pieces. This decrease directly affects the mechanical integrity of the railway assembly. A local loss of clamp and the subsequent local loss of contact could lead to fretting fatigue crack to occur.

Presently, the numerical model doesn't show the peak shift, increase the cycle number in the model must improve results. Nevertheless, with only 5 cycles, the model is able to reproduce the decrease of the peak, provided a precise description of the constitutive equation of the material.

Ce travail a donné lieu à une publication dans Neutron Research, dont les références sont :

Residual Stress Redistribution due to Cyclic Loading in a Railway Wheel/Axle Assembly
 A.Yameogo, A. Carrado, A.M. Marechal, S. Pommier, C. Prioul, A. Lodini,
 Journal of Neutron Research, January-September 2004, vol.12 (1-3), pp. 63-68

RESIDUAL STRESSES IN WELDED ALUMINIUM JOINTS FOR AEROSPACE APPLICATIONS

V. Stelmukh, S. Ganguly, L. Edwards and M. E. Fitzpatrick

Department of Materials Engineering, The Open University, Walton Hall, Milton Keynes MK7 6AA, UK

The drive for lighter, more fuel-efficient and environmentally-friendly passenger aircraft is having a major impact on many of the design philosophies that underpin the construction of modern wide-bodied passenger jets. New designs such as the Airbus A380 and the Boeing 7e7 use a greater proportion of composite materials in their construction, and manufacturing methods are being developed to replace some mechanical joints by welded structures.

Traditionally, aircraft joining has relied heavily on rivets for fixing of the fuselage and wing skins. Welding offers the advantage of significant weight saving in joint design, as well as the possibility of fabricating internal structural members that would be difficult to manufacture by conventional routes. The change to welding means that different design philosophies have to be implemented, as welding leads to:

- An integral structure with single load path construction, removing the crack-arresting features such as panel edges where sections are riveted and so leading to an overall loss in damage-tolerance for the structure.
- Creation of a microstructure near the fusion- and heat-affected zones of the weld with a changed grain size and reduced strength.
- Formation of new sources for defect initiation not present in the wrought alloy.
- Creation of a local and global residual stress field.

All these factors, in particular the creation of a variable residual stress field across the weld, have profound influence on the fatigue life of the welded metallic members and components. The civil aircraft design specification demands damage-tolerance characteristics in safety-critical parts. Therefore, before implementation of such a process change it is necessary to understand and be able to predict the fatigue crack growth behaviour under the influence of the residual stress field. The relationship between the fatigue crack growth in the welded microstructure and the distribution of residual stress field is the most essential input for the damage-tolerant, fail-safe design of safety-critical components.

We have been undertaking a programme of work to analyse and quantify the residual stress distribution around welded joints in aerospace

aluminium alloys. We have looked at three candidate welding processes: metal-inert-gas (MIG) welding; variable-polarity plasma-arc (VPPA) welding; and friction-stir welding (FSW). Neutron diffraction has become a key technique in the determination of residual stresses in welded components and structures. Because neutrons can penetrate several centimetres into most metallic materials, they act as an effective probe of the strains within a sample. Measurement of the three principal strains allows the residual stress to be calculated, and by measuring at many locations a 'map' of the stress field around a weld can be constructed.

We have used the G5.2 spectrometer at LLB to measure the strains in Al2024 and Al7050 welded plates. These alloys are the principal damage-tolerant aluminium alloys used in upper and lower wing-skins. By careful positioning of the plates, a series of measurements can be made to measure strains at many locations, which can subsequently be converted to stress. Information on the diffraction peak intensity can also be obtained, which gives insight into variations in the preferred crystallographic orientations (texture) within the plate and the weld.

Figure 1 shows a macrograph of the cross-section of a MIG-welded Al2024 alloy plate.



Figure 1. Macrograph of weld cross-section showing the double-V shape of the weld. The weld was fabricated in two passes, on either side of the plate.

Example plots of the strain distribution near the centre of the MIG weld are shown in Fig. 2. The pattern of the residual strain field variation is tensile along the longitudinal direction, while the transverse and normal directions are compressive. These values, obtained at a series of lines through the plate thickness, can be combined to produce a map of the residual stress as shown in Fig. 3.

Obtaining strain/stress maps of this detail allows additional information to be obtained. For example, figure 4 shows the matrix of data points

that were measured from an Al7050 friction-stir weld:

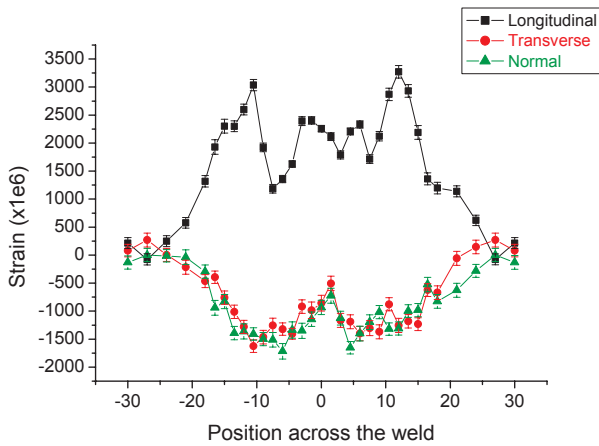


Figure 2. Strain distribution across the weld in the three principal directions near the central through-thickness line of the weld.

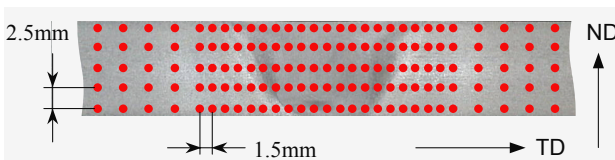


Figure 3. Macrograph of a friction stir weld, showing the matrix of points measured.

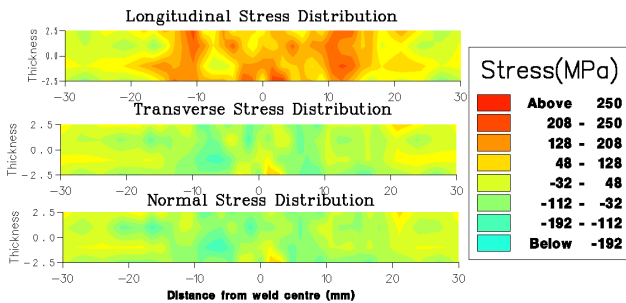


Figure 4. Stress distribution in MIG welded 2024-T351Al alloy.

We have demonstrated that residual strain distributions in specimens of this kind can be obtained by measurements of specific advantageous (hkl) peaks from the same family of preferentially-orientated grains present in both the parent material and the heat affected zones, and from a randomly-oriented fine grain structure within the weld's centre. The resultant strain distributions were converted into the longitudinal stress distribution, which is shown in Fig. 5b. Fig. 5a also shows the peak intensities obtained from measurements of the Al 111 planes at one of the orientations used (LD-19.5°). The changes in the crystallographic texture in the specimen can be seen clearly, with the texture changing across the weld zone.

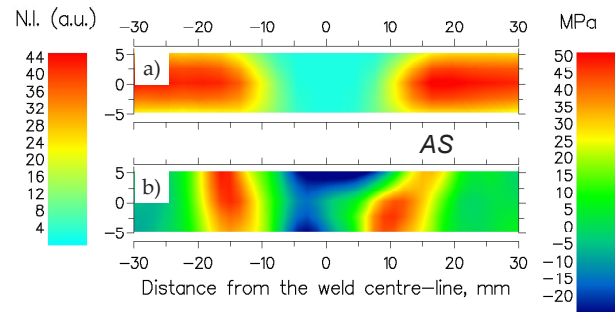


Figure 5a. Maps of normalized intensity (N.I.) of the (111) peak measured in the LD-19.5° direction; and (b) the resultant longitudinal stress. The position of the mapped area relative to the specimen's surfaces can be easily seen, as the distance between horizontal axes of each map is set to to the plate's thickness.

These measurements have been correlated with macroscopic fatigue crack growth data and strength measurement to give insight into the mechanisms of damage within the weld, and to develop models of the damage tolerant behaviour of components based on these welding technologies.

References

S. Ganguly, V. Stelmukh, M. E. Fitzpatrick, and L. Edwards, *J. Neutron Res.*, 2004:1-3:225-231

INVESTIGATION OF THE A AND B TEXTURE EVOLUTION OF HOT FORGED TITANIUM ALLOY PRODUCTS

J. Delfosse¹, C. Rey¹, M.H. Mathon²

¹Laboratoire MSSMat, CNRS UMR 8579, Ecole Centrale Paris, 92295 Châtenay-Malabry

²Laboratoire Léon Brillouin (CEA-CNRS), CEA-Saclay, 91191 Gif sur Yvette Cedex, France

Forged Ti17 titanium alloy is used in the aircraft industry for its superior mechanical properties. In order to understand fatigue life discrepancy in titanium alloy, previous studies were performed. They have emphasised the role of a crystallographic macro-structure, constituted by clusters of millimetre and centimetre sizes, on micro-cracks initiation on TA6V [1]. The macro-structure of the alloys was assumed to be correlated with the ex-β grains. Moreover, according to other authors, specific texture of the β phase improves fatigue toughness on Ti17 [2].

In order to understand the role of the as-received material initial microstructure and texture and the effects of the forging process in β phase ($T > T_\beta$) on macro-zones formation, a numerical simulation of the process has been undertaken, allowing us to follow the evolution of the crystallographic texture and morphology for different deformation rates. The evolution of β texture and grains morphology during the forging treatment is predicted by a crystalline approach implemented in the finite element code Abaqus.

Material and Thermomechanical process

At room temperature, Ti17 is a quasi β titanium alloy presenting 70% of α phase (hcp) and 30% of β phase (bcc). Above the transus temperature ($T_\beta = 890^\circ\text{C}$), a 100% bcc structure is obtained. In pure titanium, the hcp α phase generally transforms into the bcc β phase according to the Burgers relation (with sometimes orientation variant selections): $(110)_\beta // (00.2)_\alpha$ & $[-11-1]_\beta // [2-1.0]_\alpha$

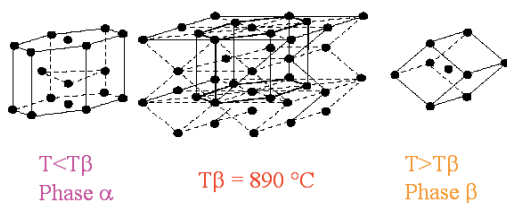


Figure 1. Burgers relation

The thermomechanical process used for Ti17 is given on figure 2: OA represents the heating stage where $\alpha \rightarrow \beta$ phase transformation occurs, AB corresponds to the deformation and BB'/BB'' to the cooling where transformation of 70% of β phase into α phase occurs.

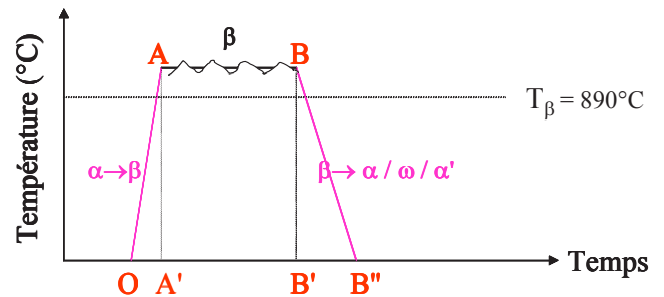


Figure 2. Thermomechanical treatment

The characterization of the texture of the β phase before forging was performed assuming that the texture and grain size in A is similar to the characteristics of A' (there is no effect of the $\beta \rightarrow \alpha$ transformation on the β texture [3]). The same process is used to obtain the final texture corresponding to B.

The as-received material, supplied by TIMET Savoie, presents a morphology constituted by ellipsoidal β grains up to 5mm with nodular α phase of about 1μm as pointed out by OIM analyses and tensile tests.

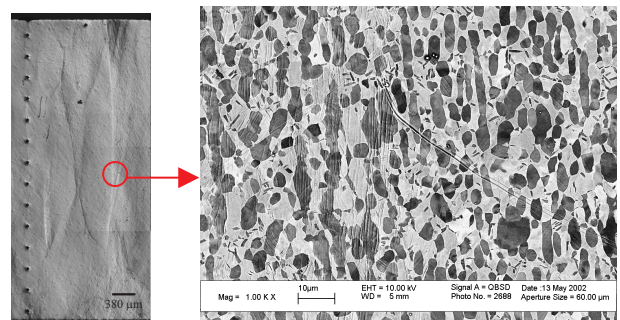


Figure 3. macro/micro-structure of the as received material

The **A' material** (solution treated for 20 min at $T > T_\beta$ then water quenched) presents well-defined grains (the average size is about 300μm) scattered by clusters of about one millimetre composed of grains slightly misoriented (Fig. 4). The **B' material** (solution treated for 20 min at $T > T_\beta$ before applying a specific plastic deformation ($\epsilon = 0.7$) and then water quenched) presents large grains up to 800μm (Fig. 4).

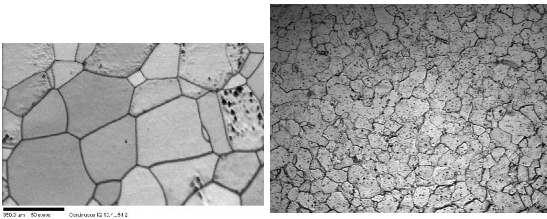


Figure 4. microstructure of A' and B' materials

Consequently, neutrons diffraction technique was necessary to obtain a quantitative description of the texture. Crystallographic textures at points O, A', B' were characterized at Léon Brillouin Laboratory (CEA-Saclay) on the 6T1 diffractometer.

The experimental poles figures are presented on figure 5, the normal direction corresponding to the forging axe.

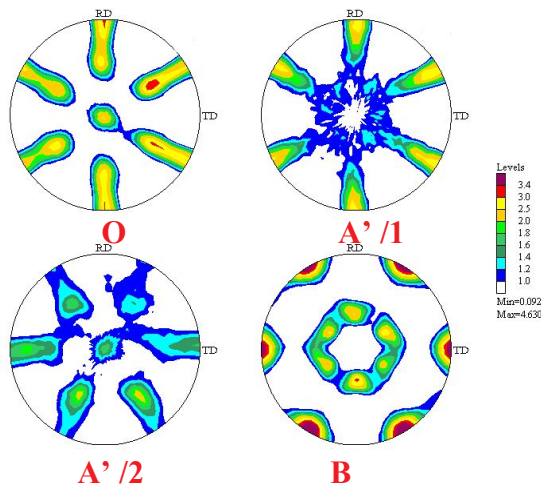


Figure 5: Experimental $(110)_\beta$ poles figures obtained by neutron diffraction.

Texture analysis of $(\alpha+\beta)$ materials in O and B' were relevant with some qualitative results of EBSD and DRX. The β phase texture of the as-received sample (O) is dominated by a $(110)\langle 112 \rangle$ orientation. After forging (B), we observe a very strong $(111)\langle -1-12 \rangle$ component, also than the orientations $(001)\langle 100 \rangle$ and $(001)\langle 110 \rangle$ which are pronounced.

Concerning A' material, several analyses were conducted. In all the cases, the (110) orientation disappeared whereas a weak (111) orientation

appeared, compared to the texture of the supplied material. But in the A' materials, the components are not precisely identical (see figure 5) and these differences seem to come from a non homogeneity of the heat treatment.

EBSD analyses (Figure 6) have clearly shown that the microstructure in the A'/2 sample was heterogeneous with different grain size compared with the results from the A'/1 which presented a well defined microstructure. The heat treatment applied to the A'/2 is not considered as valid.

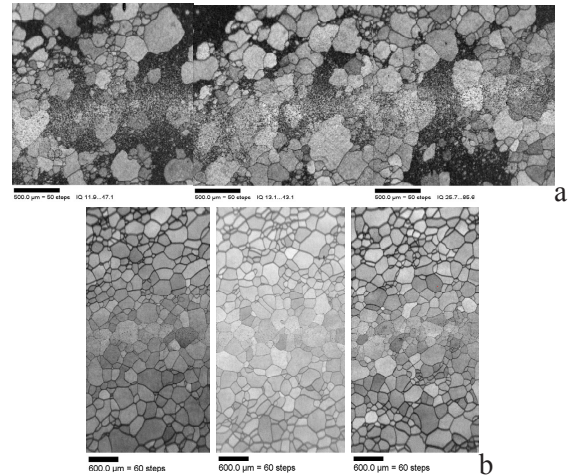


Figure 6. EBSD characterization of a) A'/2 and b) A'/1 samples.

The result of the forged materials was used to validate a plasticity modelling, presented elsewhere [4], developed in our laboratory to simulate the deformation of the β phase at high temperature. The numerical and experimental results are in good agreement and allow to go further in prediction of formation of large crystallographic entities after forging.

The study of the texture evolution during phase transformation in forged material, would gain with being carried out in-situ because only one axe is known. The in situ measurements are in progress, a furnace has been adapted to the diffractometer. They will contribute to understand the texture evolution during the phase transformation respecting the Burgers relation or from the pre-existing β nuclei in the matrix [5].

The authors wish to acknowledge Snecma Moteurs for providing the Ti-17 material used in this study.

References

1. K. Le Biavant, étude de l'amorçage de fissures de fatigue dans le TA6V, PhD, ECP, 2000.
2. O. Gourbesville, Caractérisation par DRX de la microstructure d'alliages à base de nickel et de titane forgés et traités, PhD, ENSAM, 2000.
3. Quesne *et al.* Proceedings of Titanium 99, 1711-1717
4. J. Delfosse *et al.* Proceedings of Titanium 03, 1315-1322
5. Wenk *et al.* Acta Mat. 52 (2004), 1899-1907

IMPURITIES EFFECTS ON THE MECHANISMS OF RECRYSTALLIZATION OF WIRE-DRAWN COPPER

S. Jakani¹, T. Baudin², M. Benyoucef³, Ph. Gerber¹, C.H. de Novion¹, M.H. Mathon¹

¹Laboratoire Léon Brillouin (CEA-CNRS), CEA-Saclay, 91191 Gif sur Yvette Cedex, France

²Laboratoire de Physico-Chimie de l'Etat Solide – CNRS-UMR 8648, Université Paris-Sud, 91405 Orsay, France

³Laboratoire des Sciences et Génie des Matériaux, Faculté des Sciences et Techniques, Marrakech, Maroc

Within the framework of project OPEFIC partly subsidized by the French ministry of research, the mechanisms of recrystallization in cold wire-drawn copper were finely studied in order to understand how the presence of very low content of impurities (sulphur in particular) can delay the recrystallization. After plastic deformation, the quantity of stored energy, mainly in dislocations form, is a parameter determining because it is the driving force of the static recrystallization process [1-4]. This stored energy is related to many parameters such as the material type, the deformation mode, temperature and level, the crystallographic orientation, the previous deformation crystallographic texture, etc.

However, very few direct investigations have been done to clarify the influence of impurities content on the stored energy in copper [5,6]. These works allowed to get some quantitative values of stored elastic energy in global scale through differential scanning calorimetry measurements. In order to obtain a relationship between crystallographic orientation and stored energy, neutron diffraction measurements have been done on the four-circles diffractometer 6T1. The global crystallographic texture has been characterized from experimental $\{111\}$, $\{200\}$, $\{220\}$ and $\{311\}$ pole figures; the Orientation Distribution Functions (ODF) were calculated by the discrete ADC method [11]. The stored energy values were deduced from the line broadening measurement achieved on different poles corresponding to the main preferential orientations.

Two kinds of commercial (including 99.99 mass %) copper, having different noticeable mechanical properties and chemical compositions were studied. The first selected copper, named A material, is very pure and consequently was regarded as reference (S amount about 3.2 ppm). The second one, copper B, has a higher S amount (about 8.2 ppm). Both of them have approximately the same oxygen content (about 170 ppm). The materials resulting from continuous casting, has undergone a hot-rolling to obtain a diameter of 8

mm. This treatment was followed by a cold wire-drawing to 6.3 mm (reduction of area $\Delta=38\%$).

After cold wire-drawing, the ODFs (figure 1) of materials A and B clearly show major $\langle 111 \rangle // \text{DN}$ and minor $\langle 001 \rangle // \text{DN}$ fiber textures at this level of reduction (38% reduction area). These two components are less pronounced in the material A than in the material B. The volume fractions of texture components including the reinforcements (determined by the Helming decomposition method [7]) are about $V_f=14\%$ and $V_f=43\%$ for the material A, and about $V_f=22\%$ and $V_f=52\%$ for the material B, respectively for the $\langle 001 \rangle // \text{DN}$ and $\langle 111 \rangle // \text{DN}$ fibers. Furthermore, it was noted that for both materials A and B the volume fraction of the fiber $\langle 111 \rangle // \text{DN}$ is almost twice larger than the $\langle 001 \rangle // \text{DN}$, taking into account that the dispersion around the fiber components is equal to about 15° .

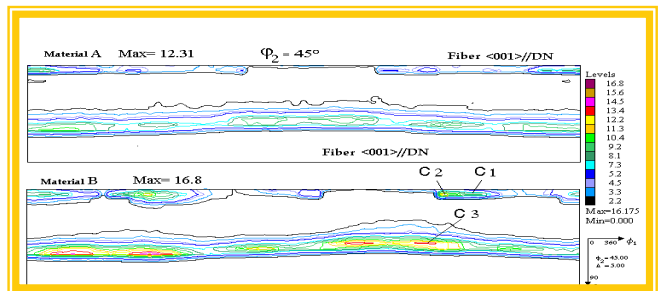


Figure 1: ϕ_2 sections (45°) of the ODFs after wire-drawing process for A material a) and B material b). The main reinforcements noted on the figure, are C1: $\{001\}\langle 110 \rangle$; C2: $\{001\}\langle 120 \rangle$ and C3: $\{111\}\langle 112 \rangle$.

Concerning the stored energy values, some line broadening measurements were carried out for the A and B materials. The figure 2 shows an example for a given point of the pole figure $\{200\}$ of a set of analysed diffracted peaks corresponding to the A material after a hot-rolling and a cold wire-drawing. The full width at half maximum (FWHM) is greater after wire-drawing of about 15% for copper A and by about 23% for copper B than after hot-rolling. This broadening contains two contributions, which have been separated, i.e. the contribution due to the size (D) of diffracting

domain and the contribution due to the microstrains related to plastic deformation, from which the stored elastic energy (SE) is estimated.

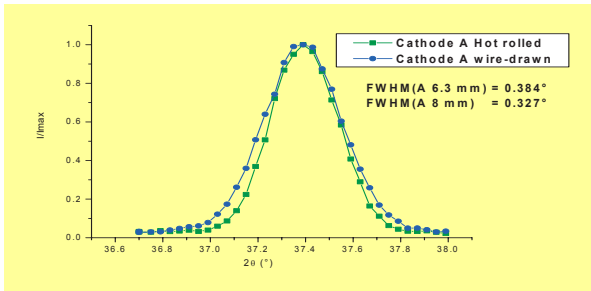


Figure 2 : θ - 2θ scan of $\{200\}$ Bragg peak corresponding to A material after hot-rolling and wire-drawing.

The measurements of the broadening peaks in the cold drawn copper have shown that :the stored elastic energy values are lying in a range between 1.8 - 4.6 J/mol (Table 1) and the stored elastic energy increases with the rate of residual impurities. On the other hand, the stored elastic energy ratio $\langle 111 \rangle / \langle 001 \rangle$ decreases when the rate of residual impurities increases.

	$\langle 111 \rangle$ fiber	$\langle 001 \rangle$ fiber	$E^{\langle 111 \rangle} / E^{\langle 001 \rangle}$
A material	3,6	1,8	2,0
B material	4,6	3,8	1,2

Table 1 : Stored energy values in the grains belonging to the two fiber components [8].

The deformation substructure has been studied by Transmission Electron Microscopy. The observations are in agreement with the measurements of the stored elastic energy. Indeed the grains associated to $\langle 111 \rangle // \text{DN}$ fiber are more

deformed than the grains associated to $\langle 001 \rangle // \text{DN}$ fiber. Moreover, the dislocation cells associated to the grains belonging to the fiber $\langle 001 \rangle // \text{DN}$ are less defined and present a weaker mean size in the presence of impurities (Figure 3).

During recrystallization annealing, the grains related to the $\langle 001 \rangle // \text{DN}$ fiber nucleate first by cell coalescence near in the highly deformed and misoriented regions taking into account the presence or not of the impurities.

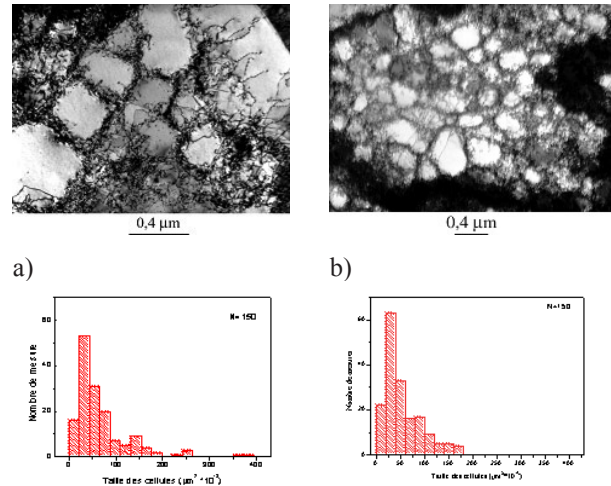


Figure 3. TEM observations and distribution of the cell size (on 150 measurements) on Material A a), and Material B b).

The stored elastic energy ratio would be a driving force during nucleation and explain why the pure copper recrystallizes first during annealing. These impurities seem to delay the process of recovery necessary to the formation of the nucleus as well as the mobility of the grain boundaries during the recrystallization by the means of an inter-granular segregation.

References

[1] R. D. Doherty, D. A. Hugues, and al., Mater. Sci. Eng., Vol. A238, pp. 219-274 (1997).
 [2] G. Mohamed, B. Bacroix., Acta Mat. Vol.48, pp. 3295-3302 (2000).
 [3] B. Bacroix, O. Castelnau, A. Miroux, H. Réglé, Proceedings of the 21st Risø Inter. Symp. on Materials Science, Eds N. Hansen et al, pp. 1-14 (2000).
 [4] B. Bacroix, Ph. Gerber, O. Castelnau, Recrystallization and Grain Growth- Proceedings of the First Joint International Conference, Eds G. Gottstein and D. A. Molodov, Springer Verlag, Vol.2, pp. 623-633 (2001).
 [5] J.M Guilemany, J.Fernández, F. Pergrin, O. Guixà, Materials Science Forum., Vols. 113-115, pp. 655-660 (1993).
 [6] J. Schamp, B. Verlinden, J. Van Humbeeck, Scripta. Mat., Vol. 34, pp. 1667-1672 (1996).
 [7] K. Helming, Materials Science Forum Vol. 363, pp. 157 (1994).
 [8] S. Jakani, M.H. Mathon, M. Benyoucef, Ph. Gerber, T. Baudin, C-H. de Novion, Journal of neutron research, Vol. 12, n°1-3, p. 249 (2004), Meca-Sens.

NANOCLUSTER FORMATION IN ELECTRON-IRRADIATED LITHIUM OXIDE

G. Krexner¹, M. Prem², F. Beuneu³, P. Vajda³¹ Institute of Experimental Physics, University of Vienna, Boltzmanngasse 5, A-1090 Vienna, Austria² Laboratoire Léon Brillouin (CEA-CNRS), CEA- Saclay, 91191 Gif sur Yvette Cedex³ Laboratoire des Solides Irradiés, Ecole Polytechnique (CEA-CNRS), F-91128 Palaiseau, France

Lithium oxide (Li_2O) is a material of considerable interest both to applied and fundamental research: Being a superionic conductor it acts as a model substance for solid state batteries [1], due to its potential as a tritium breeder it is in discussion as a first-wall material in future fusion reactors [2], and its character as a highly ionic solid without d electrons renders it attractive for first principle calculations of electronic structures [3], among others.

Electron irradiation of Li_2O near ambient temperature induces the formation of metallic lithium precipitates (usually termed 'colloids') which were detected by conduction electron spin resonance, ^7Li -nuclear magnetic resonance and differential scanning calorimetry [4-6]. Two types of lithium colloids were identified: Large precipitates with a typical size exceeding $10\mu\text{m}$ (volume fraction $\sim 2 \times 10^{-3}$) associated with molecular oxygen bubbles [7] and small lithium nanoclusters with a typical size of less than 10nm and a volume fraction of about 2×10^{-5} . Attempts to characterize the structure and the arrangements of the lithium colloids with X-ray and electron scattering failed due to the low atomic number of lithium and its strongly ionic character. Therefore, a neutron scattering study was performed.

Li_2O has a cubic antiferroite structure (space group $\text{Fm}\bar{3}\text{m}$) with a lattice parameter of 0.461nm . The sample used was a $4 \times 7 \times 0.7\text{mm}$ platelet (weight $\sim 40\text{mg}$) obtained from a float-zone grown single crystal. An unirradiated sample of similar dimensions served as a reference crystal. The sample was irradiated uniformly with 1MeV electrons from a Van de Graaff accelerator at 300K with a current of $\sim 40\mu\text{A}/\text{cm}^2$ up to a dose of $15\text{C}/\text{cm}^2$. The neutron scattering experiments were performed on the triple-axis spectrometer G4.3 VALSE located at a cold neutron guide at the LLB. The wavelength used was 0.292nm . A pyrolytic graphite analyser was set in the second order position leading to an improved resolution $< 0.01\text{\AA}^{-1}$ for radial scans. In addition, the discrimination of inelastic scattering contributions resulted in a favourably low background level.

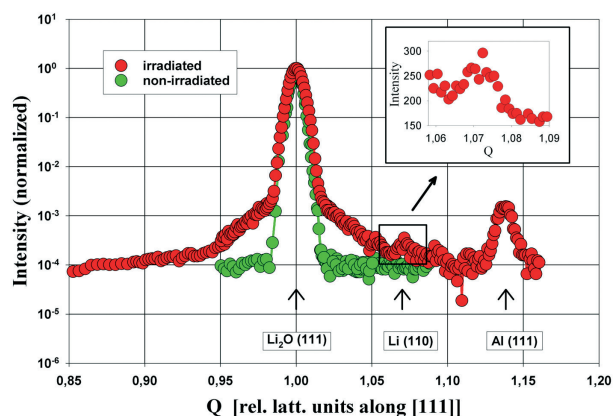


Figure 1. High-resolution radial scan through the (111) Bragg peak of the Li_2O matrix. The intensity is plotted on a logarithmic scale. The small peak at $Q \sim 1.07$ (see inset) corresponds to the Li (110) reflection of the large lithium colloids. The intensity at $Q \sim 1.14$ belongs to the aluminium (111) Debye-Scherrer line due to the sample wrapping. Distortion scattering around the (111) Bragg position of the matrix is clearly recognizable.

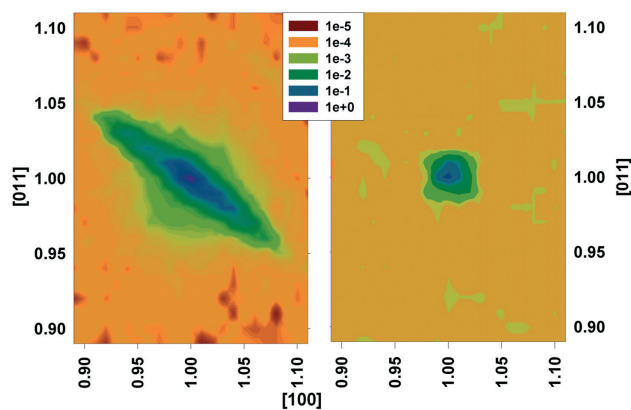


Figure 2. Diffuse scattering observed around the (111) Bragg peak of the Li_2O matrix in an irradiated (left) and an unirradiated (right) crystal. Results for the (200) and (220) peaks are similar.

Elastic diffuse scattering around the (111), (200) and (220) Bragg peaks was studied in a (110) scattering plane (Figs.1,2). In Fig. 3 the distortion scattering observed radially close to the (200) and (111) Bragg peaks is displayed, after background correction, in a doubly-logarithmic plot. The regions of Huang and asymptotic (Stokes-Wilson) scattering can be easily identified. The details of the intensity decrease that are observed beyond the

Huang region depend strongly on the type of defect giving rise to the scattering and may be different for the two sides of the Bragg peak as observed for the (111) peak in this study.

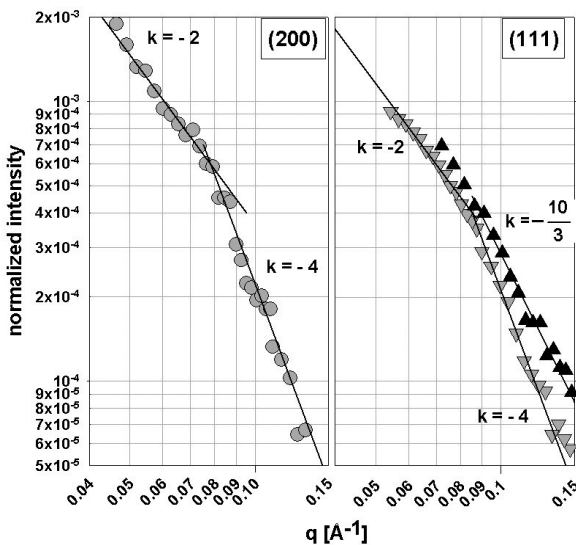


Figure 3. Distortion scattering close to the (200) and (111) Bragg peaks displayed on a doubly-logarithmic scale. For the (200) peak the symmetrized scattering distribution is shown. For the (111) peak the scattering at the low- Q and the high- Q side are plotted separately. The scattering first decreases as q^{-2} ('Huang scattering') followed by a q^{-4} or $q^{-10/3}$ dependence ('Stokes-Wilson scattering'). The crossover permits to determine the approximate size of the defect (i.e. the small colloids in the present case) along a particular direction.

Combining the data from several peaks and the observed lattice parameter shift due to irradiation provides information on the concentration of the small colloids and the associated distortion field. Careful evaluation [8,9] yields typical diameters of the defect clusters of $8 \times 8 \times 4$ nm along the crystallographic directions [011], [0-11] and [100], respectively. These values are in good accordance with small-angle scattering data of the same sample (not shown here) yielding an averaged Guinier radius of ~ 2.5 nm corresponding to a mean geometrical diameter of about 6.5 nm and about 10 000 Li atoms in one cluster.

References

- [1] N. Roux, C. Johnson, and K. Noda, *J. Nucl. Mater.* **191/194**, 15 (1992).
- [2] Y. Oishi *et al.*, *J. Nucl. Mater.* **87**, 341 (1979).
- [3] S. Albrecht, G. Onida, and L. Reining, *Phys. Rev. B* **55**, 10 278 (1997).
- [4] F. Beuneu, P. Vajda, *Phys. Rev. Lett.* **76**, 4544 (1996).
- [5] P. Vajda, F. Beuneu, *Phys. Rev. B* **53**, 5335 (1996).
- [6] F. Beuneu, P. Vajda, G. Jaskierowicz, M. Lafleurille *Phys. Rev. B* **55**, 11263 (1997).
- [7] F. Beuneu, P. Vajda, O. J. Zogal, *Phys. Rev. Lett.* **83**, 761 (1999).
- [8] P. Vajda, F. Beuneu, G. Krexner, M. Prem, O. Blaschko, and C. Maier, *Nucl. Instr. Meth. B* **166-167**, 275 (2000).
- [9] G. Krexner, M. Prem, F. Beuneu, and P. Vajda, *Phys. Rev. Lett.* **91**, 135502 (2003).
- [10] M. Prem, G. Krexner, F. Beuneu, and P. Vajda, *Physica B: Cond. Matter* **350**, Suppl. 1, p. E999 (2004).

The distortion scattering due to the small colloids was also investigated as a function of temperature and was found to remain unchanged on cooling from ambient temperature down to 30 K [10]. This means that, contrary to the large colloids [7], the small Li precipitates cannot be associated with oxygen bubbles. The volume change of oxygen upon freezing (about three orders of magnitude) would lead to a significant relaxation of the lattice strain around the defect clusters. This change, in turn, would lead to a concomitant decrease of the intensity of the observed distortion scattering which, however, was not found in the experiment.

For the large colloids, measurements of several well defined Bragg peaks – cf. the (110) peak in Fig.1 – confirm their composition to be elemental *bcc* lithium. Their orientation relations with respect to the Li_2O matrix is shown in Fig.4. It is defined by $[110]_{\text{Li}} \parallel [211]_{\text{Li}_2\text{O}} \pm 4.4^\circ$ (two variants), and $[001]_{\text{Li}} \parallel [011]_{\text{Li}_2\text{O}} \pm 4.4^\circ$ (two variants). The deviation of slightly more than 4° is due to the lattice misfit between matrix and precipitates. Perpendicularly to the plane shown in Fig. 4 the orientation relation is $[110]_{\text{Li}} \parallel [111]_{\text{Li}_2\text{O}}$.

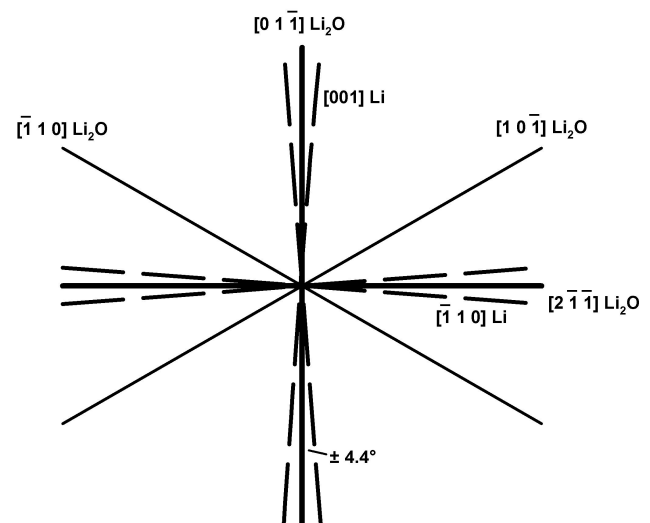


Figure 4. Orientation relation between the Li_2O matrix and the large lithium colloids.

COMBINED X-RAY & NEUTRON POWDER DIFFRACTION STUDY OF A DIMORPHIC C₆₀ SOLVATE: C₆₀ · 1.5 CH₂Cl₂

R.J. Papoular¹, R. Céolin^{2,5}, H. Allouchi³, P. Espeau², A. Kurbakov^{1,4}, J.-LL. Tamarit⁵

¹ Laboratoire Léon Brillouin (CEA-CNRS), CEA- Saclay, 91191 Gif sur Yvette Cedex, France.

² Laboratoire de Chimie Physique, Faculté de Pharmacie, Université Paris 5, 75006 Paris Cedex, France.

³ Laboratoire de Chimie Physique, Faculté de Pharmacie, Université de Tours, 37200 Tours Cedex, France.

⁴ Petersburg Nuclear Physics Institute, Russian Academy of Sciences, 188300 Gatchina, Russia.

⁵ Departament de Física i Enginyeria Nuclear, ETSEIB, Universitat Politècnica de Catalunya, 08028 Barcelona, Spain.

Fullerenes and derivative compounds have been around for 20 years and still remain an open field with unsolved mysteries. Among those, the characterization of C₆₀ solvates and the possible polymorphism of the latter still attract unrelenting attention [1,2]. Our primary focus rests with the structural determination of such compounds using laboratory X-rays and neutrons complemented

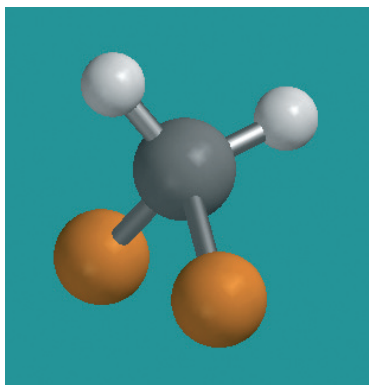


Figure 1a. The solvent molecule CH₂Cl₂ is optimized using Molecular Modeling in order to provide suitable bond lengths and angles to be used as restraints in GSAS.

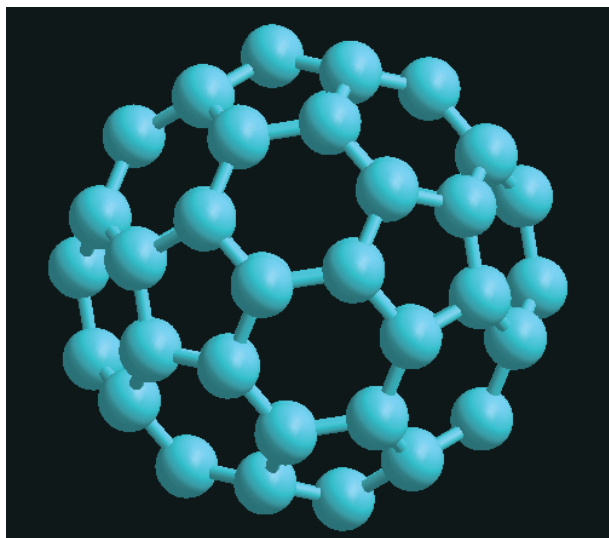


Figure 1b. The C₆₀ molecule is geometrically modeled using 6 independent atoms to allow Rigid Body refinement within any site symmetry using GSAS.

with macroscopic thermodynamic measurements. Structure determinations of C₆₀ solvates from

powder diffraction remain extremely rare and are usually borne from synchrotron measurements [3]. The stoichiometry and symmetry of the title compound have remained a puzzle until now [4,5], although the latter was first synthesized about 10 years ago. The present work resolves this dilemma.

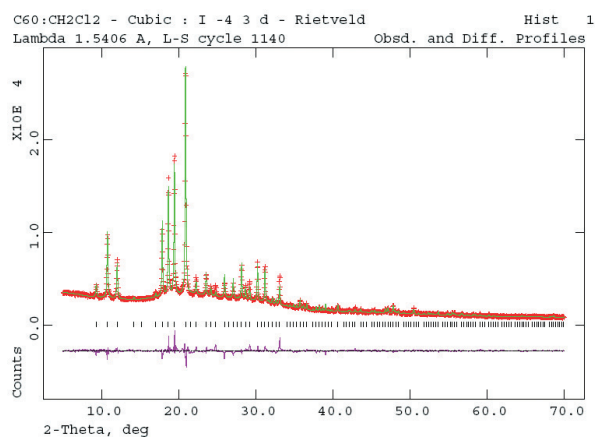


Figure 2a. A lab monochromatic X-ray experiment is carried out using an INEL CPS120 multidetector. It provides an acceptable space group I-4 3 d and the right stoichiometry [1.5 CH₂Cl₂ molecule per C₆₀]. The latter was subsequently confirmed via a most careful TGA (ThermoGravimetricAnalysis) experiment.

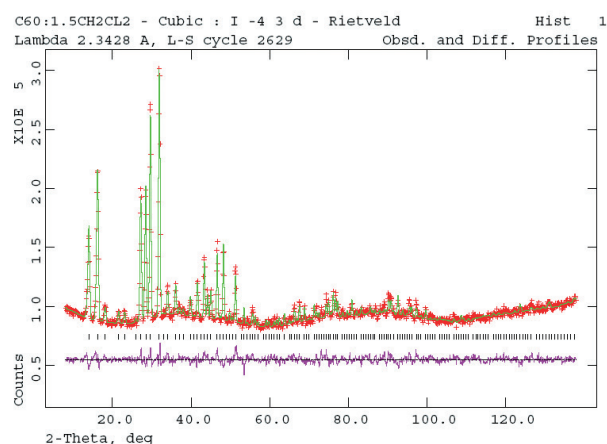


Figure 2b. A monochromatic neutron experiment is carried at the Orphée reactor on the G4.2 spectrometer using an hydrogenated sample. Protons are found and shown to belong to an ordered solvent molecule at T=250 K.

The limited number of experimentally available diffraction peaks makes it mandatory to use available chemical information as much as possible: eg, number of C_{60} buckyballs per unit cell, approximate geometry of solvent and C_{60} molecules. A reasonable geometry of the former is readily obtained using the widespread Molecular Modeling software Spartan'04 [6] (Fig.1a). Whereas the latter (Fig. 1b) is usually documented for specific cases only [7], we have worked out a general description valid for any site symmetry. We have eventually solved our compound structure from our lab X-ray data [Université de Tours] using an acentric space group (I-43d), and a cubic unit cell with a ca. 23 Å (Fig. 2b) . Stoichiometry

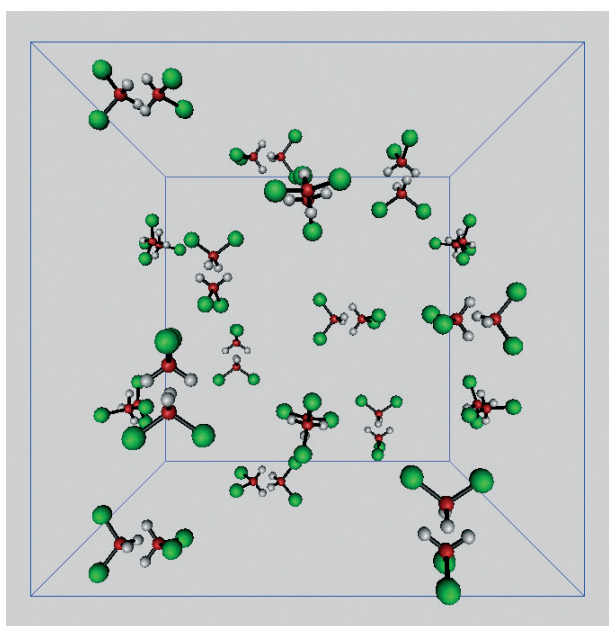


Figure 3. Detailed arrangement of the CH_2Cl_2 solvent molecules in the crystal unit cell, as refined from the neutron data at $T = 250K$. The C_{60} molecules, not shown for clarity, occupy off-centered x,x,x and related sites.

is found to be 1.5 CH_2Cl_2 per C_{60} , i.e. half-way between previously published results [4,5], and as

confirmed by recent most careful TGA experiments carried out by us at Université Paris 5. Neutrons provide the last but not least piece to the puzzle (Fig.2b), namely the detailed **ordered** arrangement of the solvent molecule within the unit-cell (Fig.3). In spite of incoherent scattering an hydrogenated sample does the trick due to an increased contrast between C, Cl and H atoms, due to the negative scattering length of Hydrogen, a unique feature of the neutron. A spherically disordered solvent molecule yields a much poorer fit, and must thus be discarded.

Finally, the low-temperature cryostat available on G4.2 was used to obtain data down to 1.5 K, evidencing at least one phase transition above $T=100$ K and possibly a second one between 100 K and 1.5 K (Fig. 4). The resulting structural modifications are currently being investigated.

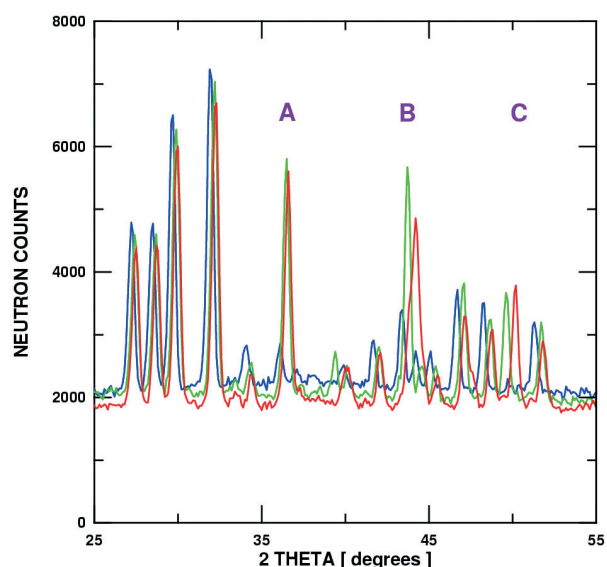


Figure 4. Zoomed part of the neutron data at $T = 250$ K (blue), 100 K (green) and 1.5 K (red), indicating a likely phase transition between 250 K and 100 K (peaks A & C). Distorted lineshapes (eg, peak B, red) may suggest a second phase transition between $T = 100$ K and $T = 1.5$ K.

References

- [1] R. Céolin, J.Ll. Tamarit, M. Barrio, D.O. Lopez, P. Espeau, H. Allouchi, R.J. Papoular, Carbon 43 (2005) 417-424
- [2] R. Céolin, D.O. Lopez, M. Barrio, J. Ll. Tamarit, P. Espeau, B. Nicolai, H. Allouchi, R.J. Papoular, Chem. Phys. Lett. 399 (2004) 401-405
- [3] R.E. Dinnebier, O. Gunnarsson, H. Brumm, E. Koch, P.W. Stephens, A. Huq, M. Jansen, Science 296 (2002) 109-113
- [4] M. Jansen & G. Waidmann, Z. Anorg. Allg. Chem. 621 (1995) 14-18
- [5] R. Céolin, J.Ll. Tamarit, M. Barrio, D.O. Lopez, S. Toscani, H. Allouchi, V. Agafonov, H. Szwarc, Chem. Mater. 13 (2001) 1349-1355
- [6] Spartan'04, Wavefunction, Inc. Irvine, CA, USA (2003)
- [7] R.E. Dinnebier, Powder. Diffr. 14 (1999) 84-92
- [8] GSAS, A.C. Larson & R. Von Dreele, LANSCE, Los Alamos National Laboratory, Report LAUR-86-748 (2001)

LOCAL ORDER AROUND Nd³⁺ IONS IN AN ORGANIC SOLUTION AS DETERMINED BY NEUTRON SCATTERING EXPERIMENT

B. Belhorma¹, M.-C. Bellissent-Funel², M.-C. Charbonnel³, J.-P. Dognon⁴

¹Département d'Analyse, CNESTEN, BP 1382 Rabat Principal, Maroc

²Laboratoire Léon Brillouin (CEA-CNRS), CEA- Saclay, 91191 Gif sur Yvette Cedex, France

³DEN/VRH/DRCP/SCPS/LCAM,

⁴DSM/SAC/DRECAM/SPAM/LCT, CEA- Saclay, 91191 Gif sur Yvette Cedex, France

The local structure of trivalent lanthanide ions in liquid media has a great interest in the lanthanide-actinide separation process. Numerous studies performed on lanthanide salts with different counter-ions and ligand molecules have shown a great dependence between the solvation number of the cations and the composition of the solution (nature of counter-ions, solvents and concentration). For lanthanide nitrates, earlier studies have shown that the coordination number ranges between 8 and 11, and the coordination distance Ln-O(NO₃) is about 2.5Å, where nitrate ions can have a mono- or bidentate structure.

In the present work, we investigate the structure of trivalent neodymium nitrate solvated in ethanol. The first-order isotopic-difference study of the Nd³⁺ based on isotopes of ^{nat}Nd and ¹⁴⁵Nd is applied to get direct information regarding the Nd³⁺ solvation. The concentration of the solutions is 1.56mol/l.

Experimental procedure

The samples were synthesised by dissolving the oxide Nd₂O₃ (91.58 % ¹⁴⁵Nd enrichment, from Oak Ridge National Laboratory) in DNO₃ (3M) following the chemical reaction:



The D₂O was completely evaporated after a magnetic mixing at 60°C. The obtained Nd(NO₃)₃ in solid state was then dissolved in deuterated ethanol. This procedure was performed in parallel for the two isotopic solutions containing ¹⁴⁵Nd and ^{nat}Nd. A first characterisation of the samples has been done with ICP (Induced Coupled Plasma) and IR (Infra-Red) techniques in order to check that the concentration of Nd was the same for both isotopic solutions and that no light water was present.

The neutron diffraction experiments were carried out on the spectrometer 7C2 situated at the hot source of the Orphée reactor at the Laboratoire Léon Brillouin, Saclay, with neutron beam of λ=0.963Å. The solution was contained in a cylindrical vanadium cell 0.1mm thick with an inner diameter of 6mm. Scattering data were

gathered on the two isotopic samples at room temperature and at -25°C. Scattering spectra were also measured for empty container, and the background (empty cryostat). Normalisation of all data was done by using a vanadium rod of 6mm diameter. Attenuation and multiple scattering corrections were applied to the normalised data sets¹.

Theoretical background

The first-difference method was applied to get directly interactions involving neodymium ions. The first-order difference function can be expressed as²:

$$\Delta_{Nd}(q) = c_{Nd}^2 (b_{Nd^{145}}^2 - b_{Nd^{nat}}^2) (S_{NdNd}(q) - 1) + \sum_{\alpha \neq Nd} 2c_{\alpha} c_{Nd} b_{\alpha} (b_{Nd^{145}} - b_{Nd^{nat}}) (S_{Nd-\alpha}(q) - 1)$$

where S_{Nd-α} is the structure factor of the interaction between Nd and the atoms of type α of atomic concentration c_α and a scattering length b_α. Information in the real space are obtained from the radial distribution function G_{Nd}(r) which is given by Fourier transformation of Δ_{Nd}(q).

The coordination number of atoms of type α in a spherical shell between the radii r₁ and r₂ around Nd³⁺ is given by:

$$N_{\alpha} = \frac{4\pi\rho c_{\alpha}}{2c_{\alpha} c_{Nd} b_{\alpha} \Delta b_{Nd}} \int_{r_1}^{r_2} (G_{Nd}(r) - \sum_{\alpha \neq Nd} 2c_{\alpha} c_{Nd} b_{\alpha} \Delta b_{Nd}) r^2 dr$$

Results and discussion

Figures 1 and 2 show the first order difference function Δ_{Nd}(q) and the radial distribution function G_{Nd}(r), respectively. The fitting of the experimental curve is obtained by RMC code³. Following earlier studies performed on lanthanide ions in different solvents⁴, The peak at c.a. 2.3Å corresponds to oxygen atoms of nitrate ions and/or ethanol molecules.

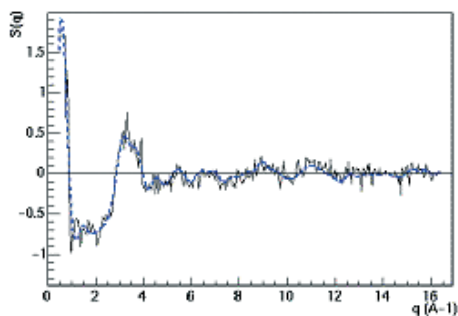


Figure 1. First order difference function $\Delta_{Nd}(q)$ for solution of 1.56 M neodymium nitrate in ethanol at -25°C . The dashed is the fitting of the experimental curve (continuous line).

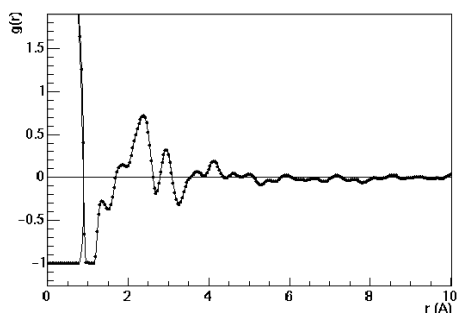


Figure 2 : The Nd^{3+} radial distribution function $G_{Nd}(r)$ for solution of 1.56 M neodymium nitrate in ethanol at -25°C .

Assuming that the ethanol molecules are disposed symmetrically with respect to the Nd-O bond axis, and following the geometry of the ethanol molecule⁵ the well resolved peak at 2.93\AA is attributed to D atoms of the alcohol group. This corresponds to a coordination number $N_{Nd}^D = 4.1 \pm 0.2$.

The number of O (N_{Nd}^O) atoms obtained by integrating over the peak at 2.31\AA , when fitted with a Gaussian function, is larger than N_{Nd}^D . This means that this first peak does not include only the O atoms of ethanol, but also O atoms of nitrate ions. Indeed, the region between 2.01\AA and 2.68\AA can be decomposed into two distinct

peaks as shown in figure 3. These are situated at 2.26\AA and 2.45\AA and correspond to $N_{Nd}^{O(OD)} = 4.2 \pm 0.2$ and $N_{Nd}^{O(NO_3)} = 4.4 \pm 0.2$ respectively. Conductivity measurements performed on solutions of $\text{Nd}(\text{NO}_3)_3$ dissolved in $\text{C}_2\text{H}_5\text{OH}$, of different concentrations (from 0.1M to 1.58M), have shown that no nitrate dissociation occurs in the solution which means that the three anions remain coordinated to Nd^{3+} . Hence, the coordination number $N_{Nd}^{O(NO_3)}$ comprised between 4 and 5 is consistent with one mono- and two bidentate, or two mono- and one bidentate nitrate.

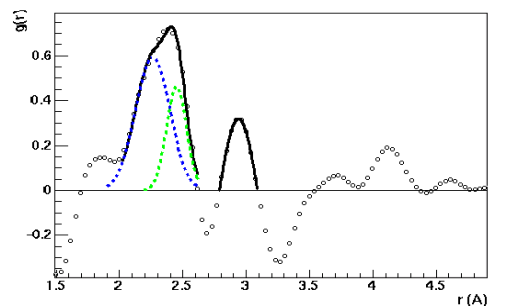


Figure 3 : Total radial distribution function $\Delta G_{Nd}(r)$ for our solution at -25°C . Continuous lines are the fit of the total $\Delta G_{Nd}(r)$; dashed lines represent the partials corresponding to $g_{Nd-O(OD)}(r)$ and $g_{Nd-O(NO_3)}(r)$

Thus we can deduce that the first solvation shell of the neodymium is composed of 4 ethanol molecules and 3 nitrate ions.

The first-order isotopic-difference technique have been applied to describe the local order around Nd^{3+} ions in presence of nitrate anions in ethanol. The obtained results indicate that both the nitrate anions and the ethanol molecules compete for the coordination sites to form $(\text{Nd}(\text{NO}_3)_3, 4\text{C}_2\text{D}_5\text{OD})$ species, with the coordination distances $\text{Nd}-\text{O}(\text{OD}) = 2.26\text{\AA}$ and $\text{Nd}-\text{O}(\text{NO}_3) = 2.45\text{\AA}$. Comparison between spectra measured at $+25^{\circ}\text{C}$ and -25°C does not show any evolution of the structure in this range of temperature.

References

- 1 G. Plaszek, Phys. Rev. 1952, 86 (3), 377; - H. H. Paalman, and C.J. Pings, J. of App. Phys., 1962, 33(8), 2635
J. L. Yarnell, M. J. Katz and R. G. Wenzel, S. H. Koenig, Phy. Rev. A, 1973, 7(6), 2130
- 2 The Physics and Chemistry of Aqueous Ionic Solutions, NATO ASI SERIES, Series C: Mathematical and Physical Sciences Vol. 205, 129-145
- 3 McGreavy R. L. and Pusztai L., Mol. Sim. 1, 359 (1988)
- 4 Interaction of trivalent lanthanide cations with nitrate anions: a quantum chemical investigation of monodentate/bidentate binding modes, New J. Chem., **25**, 1458-1465 (2001)
- 5 Structural Studies of liquid alcohols by neutron diffraction - II Deuterated ethyl alcohol. $\text{C}_2\text{D}_5\text{OD}$ Mol. Phys. Vol. 47, 6, 1405-1416 (1982) ; - The structure of liquid ethanol: a neutron diffraction study and molecular dynamics studies, J. Chem. Phys. Vol. 112,13, 5877-5883 (2000)

4 - PHYSICAL CHEMISTRY AND SOFT MATTER

Scientific activity in soft matter at LLB has two main features: research about new materials, either from chemical synthesis or by combining existing species in composite systems, and a call for a thorough understanding of some specific model systems. In both approaches, LLB is devoted to academic research that bears primers of applications planned aftermath.

Conformation of new macromolecular architectures: from synthesis to structure

SANS was developed at LLB in conjunction with the problems of polymer chain arrangement and conformation. Though the most important aspects are solved, the problem is interesting for new species recently synthesized from the large numbers of novel routes for model architectures of polymers. One aim of LLB is to offer chemists our knowledge for rapid and precise structural investigations.

Synthesized since a few months, polymers which are **both conjugated and polyelectrolytes** (J.M. Cathala, M. Rawiso, thesis of P. Vallat, I. Ch. Sadron) offer a new toolbox: precise identification of form and structure factors shows how to tune the balance between van der Waals attraction due to high polarisability and electrostatic repulsion due to high polyion charge.

Well defined **bottlebrushlike polymacromonomers** can be precisely modeled in terms of shape change as a function of polymerisation degree (from star to rod-like), compactness and interpenetration, in relation with their rheology and mechanical properties (thesis of S. Desvergne in collaboration with LPO, Bordeaux, see highlight).

Not implying synthesis, and classical - but not solved, is the question about the role and localization of metallic counterions and co-ions in **polyelectrolyte** solutions. Here the interesting approach is to use X rays, which “see” the metallic ions, in complement with neutrons which “see” the organic polyion part owing to labelling (M. Rawiso, J. Combet, F. Boué).

New tricks in self-assembling systems: copolymers and others

Self-assembly involves a composite structure of the object, the different parts of which can be “switched on or off” by varying their scattering length, a privilege of neutron scattering.

For example organic long **molecular threads** formed **spontaneously** in solution looks impressively well ordered, as seen on a Electronic microscopy picture below. SANS is used to measure their axial diameter which is one key of their association: this is measured using deuteration of the side-parts (M. Mesini, ICS Strasbourg, see Figure).

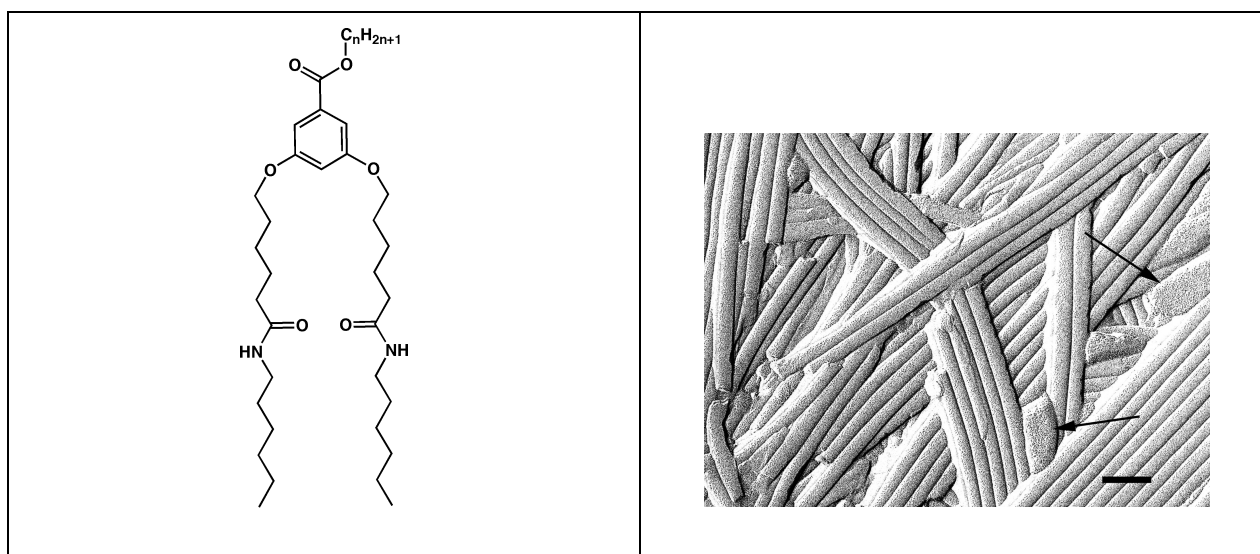


Figure. Organic long molecular threads formed **spontaneously** (from the molecules pictured on the left hand side) in solution as seen here by electronic microscopy are also studied by SANS in order to understand the effect on the axial diameter of a given part of the molecules, which is labelled.

Such **supramolecular association** (as named by J.M. Lehn) can also extend to **macromolecules**. The ability to self-assemble **in water** for elementary bricks including a polymer part has been directly monitored in terms of length and mass of the rods (see Highlight by L. Bouteiller et al), owing to the high contrast with D2O solvent.

Hydrophobic interactions are also source of association: copolymers, for example can be nicely combined with specific associations of the other block: a Bordeaux team has synthesized a polypeptide block which brings a (relatively unusual) rod-like feature, and lead to “**polymerosomes**” structures (Lecommandoux et al., LPO Bordeaux, see Figure below). The vesicle-like shape could be resolved only using SANS.

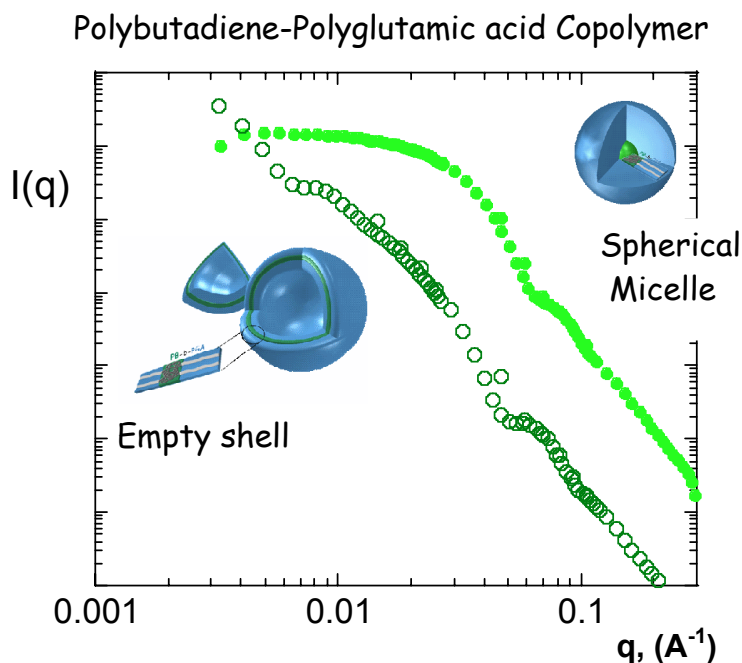


Figure. Scattering from polymerosomes.

Another example of mixed self-assembled systems is **surfactant phases containing copolymers** with hydrophobic blocks. Copolymers can modify the physical properties of various surfactant phases; this is a wide investigation field of the Rhodia Cranbury unit. Using labelled surfactants allows distinguishing them from the polymer. The effect of the chain confinement is also important here, and a balance between the two effects must be studied, which includes the case of homopolymers with surfactants (C. Ligoure, L. Ramos, Montpellier).

Other composite polymers with hydrophobic moieties attached in another way (e.g. pending), have associative properties also often studied. These moieties are labelable. The novelty is that they can be made **thermo-sensitive**, as for PNIPAM, leading to environment adaptative gels (Hourdet, ESPCI): microscopic regions of collapsed chains are immediately visible.

PH sensitive moieties are another route to adaptative response. Corresponding materials are often gels, and SANS gives the solvent (e.g. water) localization inside the gel, hence its kinetics, and its mechanical properties.

Reflectivity can also be useful, in relation with “adaptative adhesion”. One measures the penetration profile of a polymer brush into a pH sensitive gel layer (Geoghegan et al., highlight). Adhesion can also be studied by reflectivity through interpenetration of two different polymers layers (Schach et al., highlight).

Nanocomposites: particles plus polymers.

The dispersion of nanoparticles in a bulk polymer matrix has also many applications, permitting the best use of nanoparticles, or improvement of polymer properties, such as mechanical reinforcement. In all cases the use of contrast matching via partial deuteration of the solvent allows to see either the mineral part, or the organic part.

Nanoparticles can be made compatible with polymer by grafting: in LLB, contrast matching has been thoroughly used to follow the growth kinetics of polymer chains from the surface of silica nanoparticles (the

so-called “**grafting from**” method - G. Carrot, thesis of A. El Harrak, with J. Oberdisse and J. Jestin, LLB, see highlight). The polymer grafted silica nanoparticles are subsequently dispersed inside a polymer matrix, as can be followed by SANS.

Stabilization of silica **particles** is also done using copolymers, like in water for cosmetics (ESPCI, UMR Lafuma, contract with **Dior**), or using small molecules, like for fumed silica modification dispersed in an Epoxy resin (J.F. Gérard, INSA Lyon, E. Bugnicourt, thesis grant by **Wacker**).

A third way is to immobilize the nanoparticles inside a gel: in particular ferrofluids nanoparticles (8nm, stable in water) have been introduced inside natural alginate hydrogels (R. Perzynski, V. Cabuil, A. Bée, S. Roger). In such **ferrogels** the coupling can lead to modification of the magnetic suspension and its dynamics, as well as to macroscopic properties of the gel under magnetic field. Ferrofluid particles have also been introduced in the polymersomes described above (O. Sandre, S. Lecommandoux).

In nanoparticle synthesis routes, the “mixed” nature of the system can be inherent to the chemical route, like in the use of copolymers for the growth of mineral particles (C. Gérardin Montpellier) or at first stages of the **growth of metallic particles** where some organic ligands wrap the metallic initiator (M. Kahn, K. Phillipot, C. Amiens, A. Maisonat, B. Chaudret, Lab. Chimie de Coordination, Toulouse). In both cases we use contrast to follow the particle initial growth together with the organic medium organisation.

To close this section, let us recall **GI-SANS** measurements (see instrumentation section): in such case, instead of bulk dispersion, nanoparticles are dispatched on a surface.

Biotechnology

Biotechnological systems, for food, medicine can display simple situations in our field of competence: for example, the “ball + chain” association is present in the case of water soluble **polymers associated with proteins**. We are studying at LLB the case of synthetic polyelectrolytes (Sodium polystyrene sulfonate, PSSNa) mixed with lysozyme (F. Cousin, thesis of J. Gummel). This internal work is linked with similar studies of external users: C. Tribet, at ESPCI, uses hydrophobic moieties grafted on the chains, which can interact with the protein hydrophobic sequences; M. Axelos and I. Schmidt, at INRA (see highlight), use a pectin as the polyelectrolyte, and the protein is a napine, found in wheat. We then reach the field of **food research**; we unravel very similar structures for the two LLB and INRA systems, whereas the possibility of deuterating PSSNa makes a deeper analysis possible and useful in both cases. Deuteration has also been developed now by C. Tribet. All this work is also included in the CNRS-INRA GDR *Autoassemblages des molécules végétales* (biophysical aspect of plant growth, see below). The cases of polyelectrolyte plus surfactant complexes (D. Langevin, Orsay), as well as arabic gum (acacia; C. Sanchez, D. Renard) give also very close structures.

In **biomedical** aspects, physico -chemistry can also be important:

- association between **polycations and DNA** bears many resemblances with the case just evoked; this work is developed at Evry by L. Auvray, associate researcher of the lab.
- gels studies for **capillary electrophoresis** of DNA thermosensitive copolymers have been made by J. L. Viovy et al., at Institut Curie, Paris. They have a polyacrylamide backbone with grafted small chains of poly(N-isopropylacrylamide) or poly(N,N-dimethylacrylamide), which make them undergo a transition between a high and a low viscosity state. DNPA studies (thesis of V. Barbier, 2002, thesis price GFP 2003) show that the high viscosity state at high temperature retains some micellar aggregates which damage the separation properties, due to hydrophobic interactions with DNA.
- specific silicone gels for **artificial eye crystalline** display systematic solvent localisation heterogeneity in relation with the high softness required for the ophthalmologic application in cataract disease (with J. Hilborn et al., E.F.P.L. Lausanne, now at Uppsala).

Finally, let us quote the case of **biochips**. Here it is possible to use reflectivity to characterize the polymer layer used to bear the detecting macromolecule (oligonucleotide for example). Special copolymers have been developed by Biomérieux and characterized at the laboratory (F. Cousin, LLB, coll. with B. Cabane).

Films, foams, emulsions.

The polymer concentration profile of **polymers grafted** on an inorganic substrate is studied by **reflectivity**, as highlighted in the contribution of C. Devaux, J.P. Chapel, and F. Cousin, and of Geoghegan et al. Another surface grafting by L. Billon et al., Pau, is studied by reflectivity (wafer grafting of wafers). In the latter case, a SANS study is planned, on chain grafted on silica particles. There can be a link between reflectivity and SANS studies at this level.

Such relation between SANS and reflectivity is also present in the study of a special state of matter, the foams. This has been initiated at the lab in collaboration with M. Axelos, INRA. Two other groups are now working on it, R. Delanay, A. Renaud, and J. Etrillard (UMR A. Renaud Rennes; see Figure below) and C. Dame (th. CEA) with S. Faure (Cadarache - Marcoule, CEA) for **nuclear decontaminating foams**: interestingly, the SANS spectra scattered by a dry foam are very much like the reflectivity spectra by a thin film. This allows studying the films inside the foam, which can be different from an individual one.

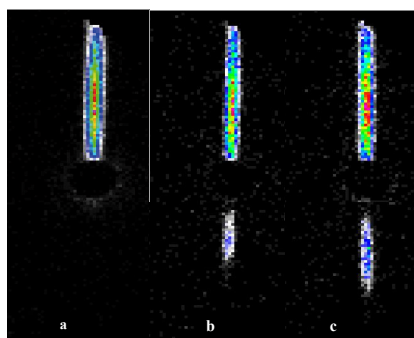


Figure. Neutron scattering by a single foam film (Rennes-INRA-LLB team)

A medium similar to foam is emulsion: studying **asphaltene water in oil emulsions** has been undergone by D. Langevin (L.P.S. Orsay) and L. Barré, C. Argyllier, T. Palermo, of Institut Français du Pétrole. This is the basis of a IFP-LLB contract (2004 post-doc grant of J. Jestin, now hired at LLB).

Soft matter under Constraint.

SANS shows a large versatility to various sample environment more complex than simple liquid or solid samples in a simple cell. A first widely developed at LLB field is the study under deformation.

In-situ shear ("Rheo -SANS") has been developed via the use of several shear cells, with various original geometries (Couette cell, cone-plate shear cell, (velocity, velocity gradient) cell), which can be made transparent to neutrons.

The main current field of shear investigation at LLB is the rheological response of different melts including **liquid crystal polymers** (LCPs), by L. Noirez and Hakima Mendil (thesis student; former studies were done by C. Pujolle-Robic (PhD) and S. Lerouge, post-doctoral position). LCP'S are interesting since they display in addition to the flow instabilities encountered for melts (extrusion defects, slip effects and other yet unsolved problems), some properties related to the long range ordering of liquid crystals. One of the most spectacular features of these non-linear LCPs' properties is the appearance within the isotropic phase, of a non-equilibrium phase induced above a critical shear rate. Strikingly, the characteristic times deduced from Small Angle Neutron Scattering under flow, from viscoelasticity and from rheo-birefringence disagree with conventional rheological models for linear amorphous polymers (Rouse, reptation). This suggests novel correlation scales at a supramolecular level, which should be generalized in a generic analysis of non-linear behaviours in non-newtonian fluids, underlining in particular the analogy between melts and lyotropic systems.

Some external groups such as the Pau group (J. Peyrelasse et al.) in collaboration with A. Lapp also study shear effects, looking at the induced modification of structure formed by **associative polymers**.

Stretching of complex polymer films is also under study in several cases:

- monitoring **particles displacement** under stretching - in order to understand mechanical **reinforcement**, in nanocomposites films obtained by mixing our polymer grafted silica nanoparticles

described above with the same polymer (thesis of A. El Harrak; this has been made formerly by J. Oberdisse for nanocomposites films obtained by mixing silica nanoparticles and latex nanoparticles).

- relaxation after a **step deformation** of melt made of **bottlebrush** polymacromonomers mixed with linear chains (S. Desvergne et al., highlight), allowing to understand the corresponding dynamics and their rheological properties.

- **glass transition** of polymers **under stretching**, by C. Alba - Simoniesco, Orsay, in coll. with F. Lequeux, ESPCI (SANS and inelastic neutron scattering, time of flight , MIBEMOL)

- **latex polymer films** (Y. Rharbi, Lab. de Rhéologie Grenoble) are actually biaxially stretched (in other words crashed along the third direction). This is linked with the study of interpenetration of polymer latex particles during filmification or coalescence, and their possible properties modification (like glass transition). From the point of view of polymer interpenetration, such bulk study meets the surface study made by neutron reflectivity quoted above.

- **ion conducting nafion membranes** have been studied by L. Rutabat (SFN thesis price 2004) thoroughly at rest but also in stretched state, which give additionnal information of the cylinders and fibres hierarchy of structure (see highlight), in particular owing to contrast matching.

National and European programs and Industrial collaborations

Another aim of LLB is to build **direct contracting** with different industries: we quoted above the cases of Rhodia Complex fluids Lab of Cranbury, US, as well as the Rhodia research unit of Aubervilliers (grafting polymer from silica particles), Institut Français du Pétrole, Biomérieux, CEA (foams for decontamination, special surfactant (F. Testard et al., thesis of J. Prevost, SCM, Saclay -Marcoule), dispersion of uranium by specific ligands (thesis of J. Causse Montpellier). It is important to understand that **at the same time, many other industrial applications are developed via the work of external users.**

LLB is implied in several programs. The national network “Groupe de Recherche” («**GDR**») «**ABV**», Autoassembly of Biomolécules Végétales” (BULEON Alain, INRA Nantes) is now launched (in parallel, a European NoE proposal Biopan will be re-submitted for a second round). This «GDR» establishes a bridge between CNRS and INRA teams working on plant growth, at the level of Plant walls, Polyphénols, and Albumen (wheat, starch, protein corpuscles), and interfacial properties. The national «GDR» «**PolyFUM** » (Dr Gunther Reiter), merged with the European RTN **Polyfilm**, studies thin films: our contribution has been to show that the conformation of polymers in film thinner than the chain equilibrium size is still a random walk at semi-local scale. We now observe the slowing down of the dynamics of polymers chain grafted at the surface of a silica particle. A European NOE on networks has been submitted but must be resubmitted (Gert Heinrich, M. Geoghegan, U. Sommer). A Marie Curie project on reinforcement is under curent proposition by J. Oberdisse. The GDR project on **foams** (MOUSSE, Michèle ADLER LPMDI, Université de Marne la Vallée) will be a good opportunity to make useful our in situ studies of the film thickness in foams.

1. Bottle brush shape polymacromonomers : conformation and dynamics in solutions and melts **94**
S. Desvergne, F. Boué, A. Brûlet, V. Héroguez, Y. Gnanou
2. Aqueous supramolecular polymer formed by an amphiphilic perylene derivative **96**
Alix Arnaud, Joël Belleney, François Boué, Laurent Bouteiller, Géraldine Carrot, Véronique Wintgens
3. Swelling and collapse of a weak polyelectrolyte as a function of pH **98**
P. Topham, c. J. Crook, J. R. Howse, A. J. Ryan, A. J. Parnell, L. Ruiz-Pérez, R. A. L. Jones, M. Geoghegan, A. Menelle
4. Polymer-polymer adhesion of uncrosslinked elastomers studied by neutron reflectivity **100**
R. Schach, C. Creton, Y. Tran
5. Atom transfer radical polymerization from silica nanoparticles : following chemical synthesis using S.A.N.S. **102**
A. El Harrak, G. Carrot, J. Oberdisse, J. Jestin, F. Boué
6. Highly stretched polymer brushes with a low swelling capacity **104**
C. Devaux, F. Cousin, J-P. Chapel
7. New structural model for Nafion® membranes **106**
Laurent Rubatat, Olivier Diat, Gérard Gebel
8. Local dynamics of bulk and nanoparticle filled poly(vinyl acetate) observed by quasielastic neutron scattering **108**
Chuhong Zhang, Valeria Arrighi

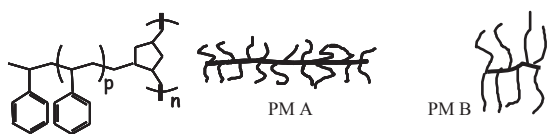
BOTTLE-BRUSH SHAPE POLYMACROMONOMERS: CONFORMATION AND DYNAMICS IN SOLUTIONS AND MELTS

 S. Desvergne^{*+}, F. Boué^{*}, A. Brûlet^{*}, V. Héroguez⁺, Y. Gnanou⁺
^{*}LLB, CEA/CNRS, Bâtiment 563, CEA Saclay - 91991 Gif-sur-Yvette Cedex - France

⁺LCPO - ENSCPB-CNRS, 16, avenue Pey-Berland - 33607 Pessac Cedex – France

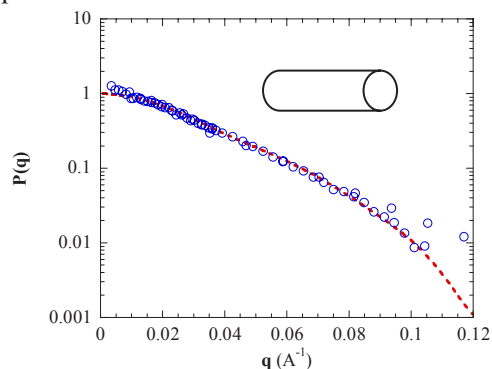
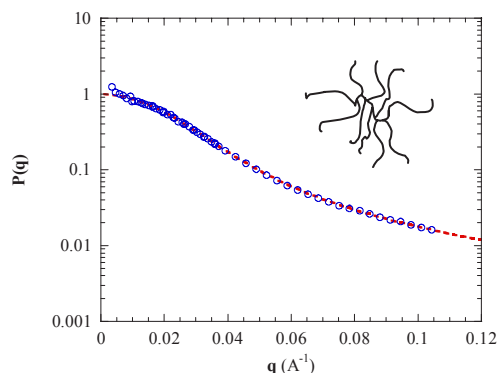
Branched macromolecules exhibit specific solution and melt properties due to a higher segment density compared to linear chains of equivalent molar mass and same chemical composition. Polymacromonomers (PM) are characterized by a regular branching interval and exhibit narrowly distributed molar masses when polymerized under “living” conditions. They can thus be considered as model compounds. Our aim is to describe in a quantitative way the PM conformation using Small Angle Neutron Scattering (SANS) and deuteration, a technique that has been already used to measure the extension of the backbone due to side chains [1].

In order to control the final PM (Fig.1) and allow precise SANS experiments, ring-opening metathesis polymerization has been successfully performed on both labeled and unlabeled PS macromonomers fitted with norbornenyl unsaturation [2]. In order to investigate the influence of the side chain length on the PM conformation as well as on its dynamic behavior. PM with different branch lengths have been prepared, such as PM A or PM B (-H or -D) (Fig.1).


 Figure 1. Poly(ω -norbornenyl polystyrene) PM

The structure of labeled PM has been investigated as a function of its environment: good or Θ solvent of polystyrene PS branches (98 % PM weight) and melts of PM in PM or in linear PS. The SANS measurements evidence that our PM adopt different conformations. The latter roughly varies from a spherical distribution to a tubular symmetry, depending upon the lengths of the side chain and of the backbone, as well as upon the solvent or the matrix used. Different geometric models have been applied to fit experimental form factors $P(q)$, measured by SANS, such as cylinder or star models [3, 4]. At small scale (large q), experimental curves are well fitted, for Θ solvent

(Fig. 2) as well as for molten state (Fig. 3). However, in both cases, the model does not provide the exact description of the conformation. Suitable models should be more complex than a tube or a sphere and should involve the degree of interpenetration of branches.


 Figure 2. $P(q)$ as a function of q for solution 1% PM A-D / cyclohexane \circ , non-oriented cylinder model with $R = 3.1$ nm and $L = 17.3$ nm ---

 Figure 3. $P(q)$ as a function of q for blend 2% PM A-D / linear PS 700k : extrapolation to 0% \square , non-oriented cylinder model with $R = 3.1$ nm and $L = 19.2$ nm ---

Comparison between different blends (PM in linear PS) demonstrates that the matrix affects the conformation. Blends of a labeled PM (A-D or B-D) with unlabeled linear PS ($M_w = 700000$ g.mol⁻¹) have been investigated for different volume fractions. For blends with short branches PM A-D, a clear increase in intensity at low q values is visible in the $q^2I=f(q)$ plot (Fig.3). Note that in such plot, the presence of a peak that is indicative of a high internal density of branched polymers

unlike the case of linear polymers. The low q intensity increase may result from partial immiscibility between labeled and unlabeled macromolecules. However, blends of the same linear PS with long branches B-D show no increase in their low q intensity. This suggests that the specific architecture of short branches PM affects the free energy of mixing. Further experiments have been performed to demonstrate the temperature parameter does not affect the phase separation.

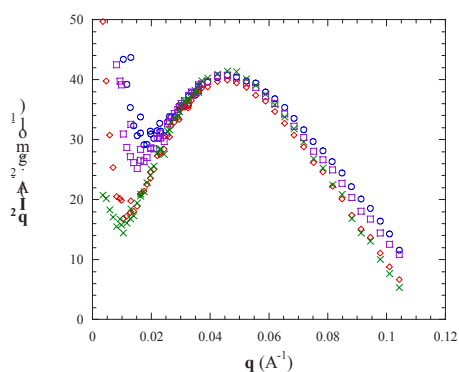


Figure 4. $q^2 I$ as a function of the scattering vector q for blends PM A-D / linear PS 700k: $\phi = 10\%$ \circ , 7% \square , 5% \diamond , 2% \times

Besides, rheological investigation has been performed to define dynamics of the PM relaxation, which strongly differs from that of linear polymers. The latter exhibit for large chain (more than 180 units in PS, i.e. a mass $>M_e = 18000 \text{ g.mol}^{-1}$) a characteristic time much longer than the maximum time of the free chain. In oscillatory mechanical measurements, the decrease of the storage modulus to zero at low frequencies is shifted to lower frequencies, and a flat region called entanglement plateau appears. This plateau is visible on the curves of storage modulus versus the frequency ($G'(\omega)$) for the *linear* PS of large mass. For PMs, since all PS branches have molar masses below or equal to the entanglement molar mass M_e , no plateau region was really expected. However, a weak shoulder is observed for PM with the longest side chains (namely PM B-H and PM B-D). This indicates some interpenetration between adjacent macromolecules.

References

- [1] S. Lecommandoux, F. Chécot, R. Borsali, M. Schappacher, A. Deffieux, A. Brûlet, J.P. Cotton, *Macromol.*, **2002**, 35, 8878
- [2] V. Héroguez, Y. Gnanou, M. Fontanille, *Macromol.*, **1997**, 30, 4791
D. Grande, J.L. Six, S. Breunig, V. Héroguez, M. Fontanille, Y. Gnanou, *Polym. Adv. Technol.*, **1998**, 9, 601
- [3] G. Fournet, *Bull. Soc. Fr. Minéral. Crist.*, **1951**, 74, 39-113
- [4] H. Benoît, *J. Polym. Sci.*, **1953**, 11, 507

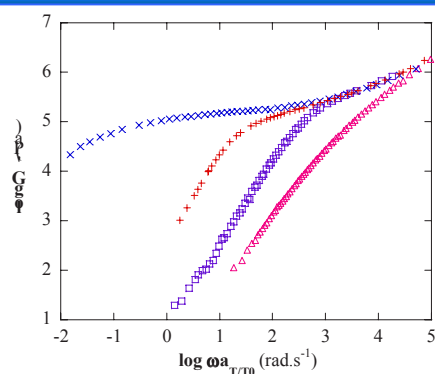


Figure 5. Master curves of G' linear PS 700k \times , PS 70k $+$, PM B-H \square and PM A-H \triangle

This is confirmed by the fact that, the shorter the side chains, the smaller the rubbery plateau. Thus branches seem responsible for the specific response of our PM. These findings are in good agreement with previous studies in literature. They are also consistent with the film-forming property: films of PM with short branches are too brittle to handle, whereas those with long branches enabled to obtain films of thickness around 0.5 mm. Furthermore, blends of 50% PM / 50% linear PS 70k exhibited an intermediate viscoelastic behavior between those of linear polymers and PM. To understand better these rheological behaviors, we are currently investigating the relaxation of the chain conformation after a quick elongation step of PM/linear blends films (Fig. 5).

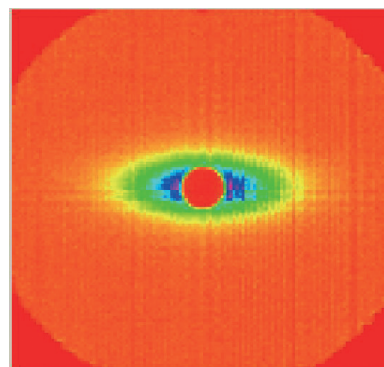


Figure 5. Intensity map of scattering of a sample (Blend 2% PM B-D / linear PS 700k elongated by a facteur 2.5, after a relaxation time = 0s)

AQUEOUS SUPRAMOLECULAR POLYMER FORMED BY AN AMPHIPHILIC PERYLENE DERIVATIVE

Alix Arnaud^a, Joël Belleney^a, François Boué^b, Laurent Bouteiller^a,
Géraldine Carrot^b, Véronique Wintgens^c.

^a Laboratoire de Chimie des Polymères, UMR 7610, Université Pierre et Marie Curie, Paris;

^b Laboratoire Léon Brillouin, CEA-Saclay, Gif-sur-Yvette;

^c Laboratoire de Recherche sur les Polymères, 2-8 rue Henri Dunant, Thiais.

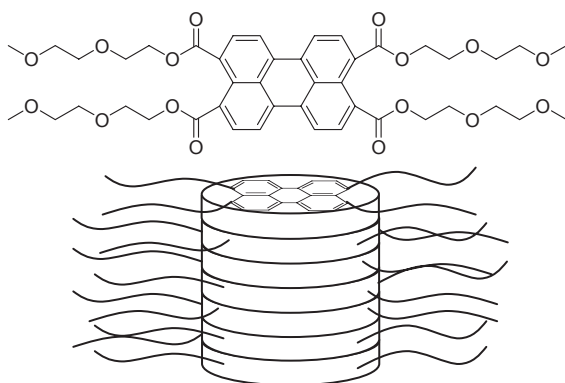


Figure 1: Structure of **Pery-2**.

Supramolecular polymers are reversible one-dimensional assemblies, driven by dynamic non-covalent intermolecular interactions.¹ Apart from biological systems, such self-assemblies are mostly known in organic and non-polar solvents, and interesting material properties have been demonstrated in the case of specific monomers such as ureido-pyrimidones or bis-ureas that can self-organize into very long chains. These materials combine conventional polymer properties with reversibility and responsiveness. It is a challenging objective to expand this innovative theme to aqueous medium. Thus, we designed an amphiphilic molecule affordable in large scale, via easy synthesis and purification.² This perylene derivative exhibits a large hydrophobic aromatic core, surrounded by four hydrophilic arms (Figure 1). Such a design provides one-dimensional assembly in water, through intermolecular π -stacking and/or hydrophobic interactions. The four hydrophilic arms are expected to hinder side aggregation of such assemblies and to ensure their water-solubility.

Qualitative evidence of self-assembly

Spectroscopic evidence (¹H NMR, UV absorption and fluorescence) show that **Pery-2** is molecularly dissolved in chloroform, but self-associated in more polar solvents such as ethanol and water (Figure 2). Moreover, the relative viscosity of aqueous solutions increases significantly with the concentration of **Pery-2**.² This macroscopic

observation is in agreement with a polymer-like behavior of **Pery-2** in water.

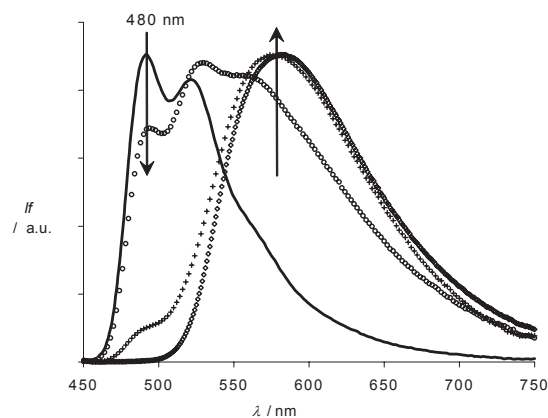


Figure 2. Fluorescence spectra of **Pery-2** in water, at 25°C (—: $4 \cdot 10^{-7}$ M, \circ : 10^{-5} M, $+$: 10^{-4} M, \diamond : 10^{-2} M). Excitation at 425 nm. Arrows indicate the direction of change with increasing concentration.

Shape of the supramolecular aggregates

Solutions of **Pery-2** (in D₂O at 25°C) were studied using small-angle neutron scattering (SANS) to demonstrate the expected wire-like structure. For the three concentrations, the scattered intensity is proportional to the concentration (Figure 3a). Therefore, it is reasonable to assume that no inter-object correlations are visible: the signal is proportional to the signal of one single object in this q range. At intermediate scattering vector, the qI product shows a plateau corresponding to a q^{-1} dependence well known as the signature of rod-like objects (Figure 3b). However, when q tends towards zero, the qI product increases. This shows a stronger q dependence for I , attributed to larger additional aggregates.

A model of infinite rigid rods with circular cross section and a uniform scattering length density profile was used. Fitting the scattering curves according to equations (1) and (2) provides the characteristics of the fibrillar objects.

$$I = \frac{\pi}{q} \overline{\Delta b^2} M_L \left[2 \cdot \frac{J_1(qr)}{qr} \right]^2 \quad (1)$$

$$(qI)_{q \rightarrow 0} = (qI)_o \exp\left(-\frac{r^2 q^2}{4}\right) \quad (2)$$

c is the rod concentration ($\text{g}\cdot\text{cm}^{-3}$), M_L is the mass per unit length of the rod ($\text{g}\cdot\text{\AA}^{-1}$), Δb is its specific

contrast (i.e. the difference in density of scattering length between **Pery-2** and the solvent D_2O), r is the radius of the cross section, and J_1 is the Bessel function of the first kind.

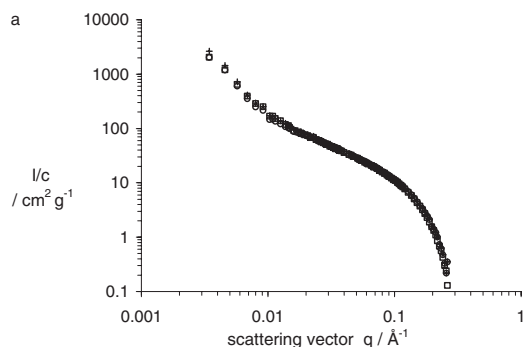


Figure 3a. SANS data (PACE) for solutions of **Pery-2** in D_2O , at 0.5% (o), 1% (+) and 2% (\square) at 25°C . (a): I/c vs. q , (b): qI vs. q , curves were fitted according to equation (1).

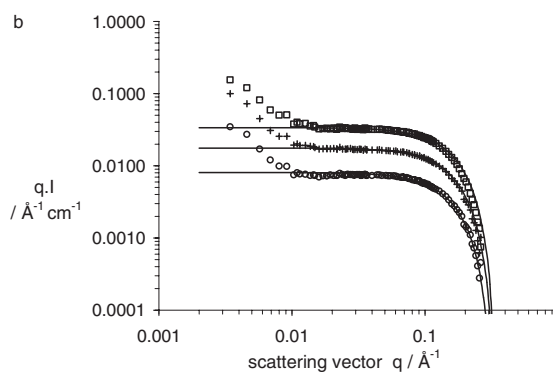


Figure 3b. shows satisfying fits for $q \geq 0.01 \text{ \AA}^{-1}$, establishing a constant rod diameter ($2r = 24 \text{ \AA}$) over this range of concentration. A 24 \AA diameter is coherent with the largest dimension of **Pery-2**. This confirms that the rod is a one-dimensional assembly of stacked molecules of **Pery-2**, i.e. a supramolecular polymer in water.

Strength of the association

A model involving an infinite number of equilibria has been used to describe the formation of the long supramolecular chains, with a dimerization (K_2) and multimerization (K) constant.² Then, the free monomer concentration (M_1) can be numerically calculated from the mass balance equation. NMR and fluorescence data were used to determine these association constants. The knowledge of the association constants makes it possible to compute the degree of polymerization of the supramolecular polymer versus concentration (Figure 4). Average chains of 50 to 100 units can be obtained at reasonable concentrations.

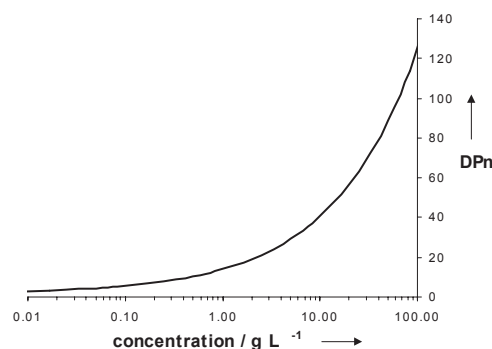


Figure 4. Calculated number average degree of polymerization of **Pery-2** versus concentration, in water.

References

1. L. Brunsveld, B. J. B. Folmer, E.W.Meijer, R.P.Sijbesma, *Chem. Rev.* **2001**, *101*, 4071-4097
2. A. Arnaud, J. Belleney, F. Boué, L. Bouteiller, G. Carrot, V. Wintgens, *Angew. Chem. Int. Ed.* **2004**, *43*, 1718-1721

SWELLING AND COLLAPSE OF A WEAK POLYELECTROLYTE AS A FUNCTION OF PH

P. Topham¹, c. J. Crook¹, J. R. Howse^{1,2}, A. J. Ryan¹, A. J. Parnell², L. Ruiz-Pérez², R. A. L. Jones²,
M. Geoghegan², A. Menelle³

¹ Department of Chemistry, University of Sheffield, Sheffield S3 7HF, UK

² Department of Physics and Astronomy, University of Sheffield, Sheffield S3 7RH, UK

³ Laboratoire Léon Brillouin (CEA-CNRS), CEA- Saclay, 91191 Gif sur Yvette Cedex

Progress in the application of soft condensed matter to areas of nanotechnologies depends in large part in the development of “smart” polymers with the capacity to respond to their environment. Weak polyacids and polybases contain no fixed charges along the chain and so present an interesting class of material in their own right as this absence of fixed charges allows a reasonable amount of control over the polymer conformation. We have synthesized polybase chains tethered to a silicon substrate using a “grafting from” method, in which the polymer chains grow from a self-assembled monolayer coated surface. (Diethylamino)ethyl methacrylate was grown directly from the functionalised surface using atom transfer radical polymerization (ATRP). Full details of the poly[(diethylamino)ethyl methacrylate] (PDEAEMA) synthesis are given elsewhere [1] and in a forthcoming publication.

Although polyelectrolyte brushes have been studied by a variety of techniques [2] including ellipsometry [3], neutron reflectometry is perhaps the technique most suited to studying their conformation. We have used this technique on the EROS reflectometer to study PDEAEMA grafted from silicon wafers. The PDEAEMA was immersed in deuterated water with small amounts of NaOH or HCl added to control the pH between 3 and 10. In acidic conditions, the PDEAEMA is stretched; Coulombic repulsion between charges located along the chain control the structure of the normally hydrophobic polymer. In the presence of added salt, charges are stripped from the brush, causing collapse of the now-hydrophobic chains.

In Figure 1 we show neutron reflectivity data for a PDEAEMA brush, which was measured to be 13 nm thick dry (in air). The data are plotted in the Porod form of k against $R.k^4$ in order to better reveal the quality of the fits (a variation of less than three orders of magnitude in comparison to six orders with a simple reflectivity plot). The data were fitted using a downhill simplex routine using a depth profile consisting of a trilayer structure. The fits are of a very high quality with $\chi^2 < 2$ in each case.

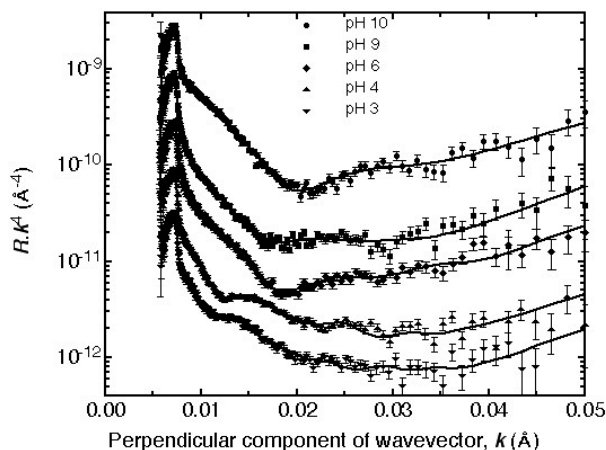


Figure 1. Reflectivity data and fits for a PDEAEMA brush in D₂O for various values of pH. The data for pH = 9, 6, 4, and 3 are staggered by factors of 3 for clarity.

Depth profiles (as a function of distance from the substrate) obtained from these data are shown in Figure 2.

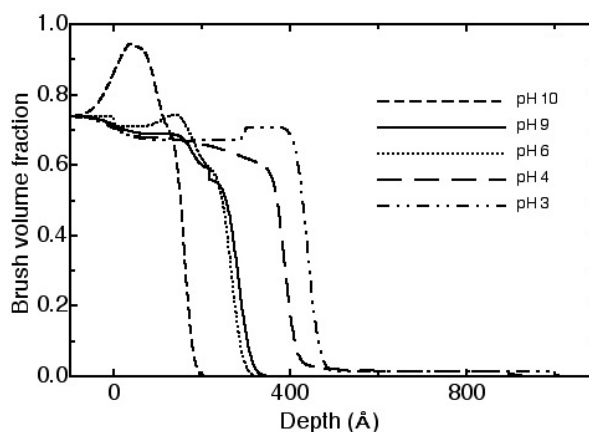


Figure 2. Volume fraction-depth profiles for a PDEAEMA brush as a function of pH (the fits are presented in Figure 1). A clear swelling of the brush with decreasing pH is visible. Note that initiator and oxide layer are not visible in these profiles; the k -range of the experiment was not sufficient to visualise these rather thin layers

In order to consider the effect of brush thickness on the conformation, we considered a thicker brush (28 nm dry thickness). In this case the brush

structure shows a more pronounced structure with a large depletion in the near-substrate region, with the brush swelling by a factor of four in comparison with a factor of a little over two in the depth profiles shown in Figure 2. These depth profiles are shown in Figure 3. The fits were of a similar quality to those in Figure 1, with χ^2 again less than 2 in all cases. It must be pointed out that in both cases there is a small amount of brush that is strongly extended. This effect is real because of the existence of short wavelength fringes in the neutron data, which must correspond to extended layers.

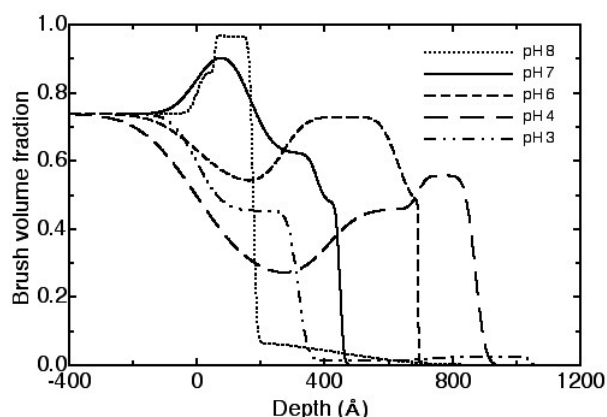


Figure 3. Volume fraction-depth profiles for a PDEAEMA brush as a function of pH. This brush exhibits more dramatic swelling than that shown in Figure 2.

Grafting densities for brushes of this nature are very difficult to experimentally determine [3], and we have been unable to determine the grafting density for these PDEAEMA brushes. Without this information, an explanation for the dramatically different profiles displayed in Figures 2 and 3 must remain speculative. Basic polymer physics would suggest that the thicker grafted layer (Figure 3) is in a “mushroom” conformation, whereby the brush stretches away from the surface before adopting a random walk conformation. We note that the

nomenclature “brush” is often used for grafted polymers, but is used uniquely to differentiate the polymer layer from the mushroom regime. Given that the polymer layer detailed in Figure 3 stretches significantly more than that in Figure 2, this polymer must be of a greater molecular weight if it is adopting a mushroom conformation.

We have performed scanning force microscopy measurements to examine the brush surface and observed that the brush does not completely cover the entire surface (in both samples); there were “holes” in the brush layer of typically $\sim 1 \mu\text{m}$ diameter. The consequence for the analysis of the neutron reflectometry data is that the brush can swell laterally, and the neutron depth profile does not necessarily constitute a lateral average of the total material. To obtain the best possible fits to the data, the requirement that the total brush mass be conserved was relaxed. In fact, a one parameter fit with conserved mass is provided elsewhere [1]. Although the fits are substantially weaker than those presented here, the conclusions are not significantly altered; the degree of swelling discussed here is still observed.

To summarise; we have used ATRP to study the swelling of a polyelectrolyte brush as a function of pH. The synthesis was capable of providing a reasonably uniform film over the large length scales necessary for neutron reflectometry measurements ($\sim 3 \text{ cm}$). The polymer swells to a thickness of around a factor of three from its dry thickness. Such brushes may have applications in technologies where pH responsive behaviour is particularly desirable such as controlled drug delivery.

Funding for the experiments on EROS was provided to LRP and MG by the European Commission under the “Large Research Infrastructure” contract HPRI-CT-2002-00170.

References

- [1] A. J. Ryan, C. J. Crook, J. R. Howse, P. Topham, R.A.L. Jones, M. Geoghegan, A. J. Parnell, L. Ruiz-Pérez, S. J. Martin, A. Cadby, A. Menelle, J. R. P. Webster, A. J. Gleeson, W. Bras, *Faraday Disc.* 128 in press.
- [2] J. Rühle, M. Ballauff, M. Biesalski, P. Dziezok, F. Gröhn, D. Johannsmann, Houbenov, N, Hugenberg, R. Konradi, S. Minko, M. Motornov, R. R. Netz, M. Schmidt, C. Seidel, M. Stamm, T. Stephan, D. Usov, H. Zhang, *Adv. Polym. Sci.* 165 (2004) 79.
- [3] M. Biesalski, D. Johannsmann, J. Rühle, *J. Chem. Phys.* 120 (2004) 8807.

POLYMER-POLYMER ADHESION OF UNCROSSLINKED ELASTOMERS STUDIED BY NEUTRON REFLECTIVITY

R. Schach*, C. Creton, Y. Tran

Physico-chimie des Polymères et des Milieux Dispersés. UMR 7516

Ecole Supérieure de Physique et de Chimie Industrielles

10, rue Vauquelin - 75231 Paris Cedex 05 – France

*Thèse financée par la Manufacture Française des Pneumatiques Michelin, commencée en janvier 2003

The polymer-polymer adhesion of uncrosslinked elastomers (i.e. polymers with a glass transition temperature below room temperature) used in the tire industry is directly related to the cohesion of the different layers of a tire before the final crosslinking process, and is a key parameter for these materials. Despite this industrial relevance, only few studies have been carried out on the so-called “tack”, and so many aspects of the problem remain poorly understood.

To understand these adhesion phenomena, we need to link the structure and the mechanical properties of the interface between two polymers. In the case of elastomers, these studies present major challenges. On the one hand, the interface and the bulk contributions to adhesive strength must be separated. On the other hand, the structure of the interface (essentially, the degree of interpenetration of polymer chains) and the stress necessary to extract the chains to separate the interface (which is likely to depend on friction coefficients) have to be distinguished. Thus, a precise knowledge of the structure of the interface is a necessary step to infer adhesion measurements in a less speculative way.

When two polymers are put into contact at a temperature higher than their glass transition temperature, they either diffuse into each other over long distances as a function of the contact time, if they are fully miscible, or they reach an equilibrium degree of interpenetration when they are immiscible. The adhesion between two polymers is directly related to this interpenetration width, and hence to the degree of miscibility.

Neutron reflectivity is very well suited to measure the interfacial width between two polymers. Interfaces between two glassy polymers have been extensively studied [1]. Adhesion experiments and neutron reflectivity studies confirmed that the interpenetration of two polymers is one of the most important parameters of these systems [2,3]. The aim of our work is to exploit this experimental technique to elastomer/elastomer interfaces.

These experiments have never been performed on elastomers because of the extreme difficulty of

preparing samples. To conduct neutron reflectivity experiments, double layers of polymers are needed. Usually, this double layers are obtained by the flotation technique : a first film, prepared by spin-coating on silicon substrate, pick up a second film which was also spin-coated and was floated off its substrate onto a deionized water surface. Unfortunately, this technique cannot be applied to elastomers, because of mechanical properties of these polymers. Actually, as elastomers are “liquids” contrary to glassy polymers, an elastomer film floated on water will flow and is not stable.

We investigated here the adhesion between a cis 1,4 polybutadiene (PB) and several other elastomers (styrenebutadiene rubber (SBR), polyisobutylene (PIB) and poly-dimethylsiloxane (PDMS)). In order to satisfy the contrast conditions for neutron reflectivity studies, deuterated PB (PB-d, purchased from Polymer Source) was required. We also used four different SBR with various degrees of immiscibility with the PB. SBR samples were specially synthesized by Michelin with a narrow polydispersity : three SBR with a glass transition temperature of -35°C and three different molecular weights, 80000 g/mol, 160000 g/mol and 240000 g/mol (the higher the molecular weight and the more the SBR is immiscible with the PB) and a SBR with a glass transition temperature of -50°C and a molecular weight of 160 000 g/mol (this fourth elastomer has a lower styrene content than the 3 others and is less immiscible with PB). These four elastomers are weakly immiscible with the PB. The PDMS and the PIB can be considered as polymer models strongly immiscible with the PB.

We aim to determine the interpenetration depth at thermodynamic equilibrium between deuterated polybutadiene (PB-d) and the other elastomers by neutron reflectivity. A method to prepare double layers of elastomers was hence developed. The floating technique was a little modified. A first film of polybutadiene was prepared by spin-coating a solution of the polymer in toluene on silicon substrate. A double layer of polymethylmetacrylate (PMMA) and elastomer

(SBR, PIB or PDMS) was then spin-coated by using toluene as PMMA solvent and carbon tetrachloride as elastomer solvent and PMAA non-solvent. As PMMA is a glassy polymer at room temperature, this double layer can be easily floated. The double layer is then transferred on the first film to obtain a triple layer PMMA/elastomer/PB-d. Finally, the excess PMMA is rinsed with acetone which is a good solvent of PMMA but a non-solvent of the other polymers. This last step permits to remove the PMMA and to obtain a double layer of elastomers. Ellipsometry measurements were carried out at each step to verify the thicknesses of the resulting layers.

Neutron reflectivity experiments have been performed on the EROS spectrometer at the LLB to determine the interfacial width of these samples. The interfacial width is the sum of two contributions : the actual interpenetration of the polymers and the thermally excited capillary waves [4]. The relative contribution can be calculated using the results of Buff [5] for the capillary waves and Broseta [6] for the interpenetration. Finally, we find the deconvoluted interpenetration profiles (figure 1).

A wide range of interpenetrations is observed. For very immiscible systems such as the PDMS/PB interface, the interpenetration width, about 15 Å, is very weak whereas for SBR/PB systems (SBR with the glass transition temperature of -50°C), it is more than 200 Å. Actually, the key parameter is the comparison between the interpenetration and the size of the polymer. For example, the SBR with a T_g of -35°C and a molecular weight of 80 000 g/mol shows an interpenetration greater than its radius of gyration which is approximately 150 Å. Thus, the interface between the PB and this SBR at thermodynamic equilibrium may be probably as

strong as the bulk. On the other hand, the SBR with a molecular weight of 240 000 g/mol shows an interpenetration of half its radius of gyration. This interface is expected to be less strong than the bulk. Of course interpenetration depth is only half the story since the stress that can be transferred across the interfaces depends probably of the friction coefficients at the monomer level. These friction coefficients have been measured for some glassy polymer pairs [7,8] but remain unknown for elastomer systems.

In conclusion, we have shown that the measurement of the interfacial width for elastomers/elastomers interfaces at thermodynamic equilibrium is possible and we expect that this information will be invaluable to interpret further adhesion experiments on same systems.

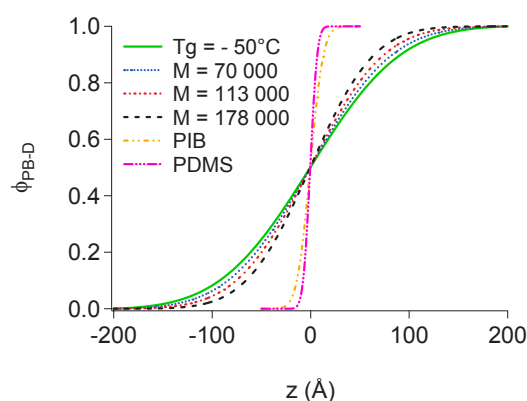


Figure 1. Interpenetration profiles of PB and six different elastomers. The PDMS/PB interface shows an interpenetration width of 15 Å, the PIB/PB 30 Å, the three SBR with a T_g of -35°C 145 Å, 165 Å and 185 Å (the wider interface corresponding to the lower molecular weight) and the SBR with a T_g of -50°C has an interpenetration width of 205 Å.

References

- [1] M. Stamm and D. W. Schubert, *Annual Review of Materials Science* **25**, 325-356 (1995)
- [2] R. Schnell, M. Stamm, and C. Creton, *Macromolecules* **31**, 2284-2292 (1998).
- [3] R. Schnell, M. Stamm, and C. Creton, *Macromolecules* **32**, 3420-3425 (1999).
- [4] K.R. Shull, A.M. Mayes, T.P. Russel *Macromolecules* **26**, 3929 (1993)
- [5] F.P. Buff, R.A. Lovett and F. H. Stillinger *Physical Review Letters* **15**, 621 (1965)
- [6] D. Broseta, G.H. Fredrickson, E. Helfand, L. Leibler (1990) *Macromolecules* **23**, 132
- [7] J. Washiyama, E. J. Kramer, and C. Y. Hui, *Macromolecules* **26**, 2928-2934 (1993).
- [8] J. Washiyama, E. J. Kramer, C. Creton, and C. Y. Hui, *Macromolecules* **27**, 2019-2024 (1994).]

ATOM TRANSFER RADICAL POLYMERIZATION FROM SILICA NANOPARTICLES : FOLLOWING CHEMICAL SYNTHESIS USING S.A.N.S.

A. El Harrak^{1*}, G. Carrot¹, J. Oberdisse², J. Jestin¹, F. Boué¹

¹ Laboratoire Léon Brillouin (CEA-CNRS), CEA- Saclay, 91191 Gif sur Yvette Cedex

² Groupe de Dynamique des Phases Condensées, UMR 5581, Université Montpellier II, 34095 Montpellier Cedex 05

At LLB, we develop a chemistry group to synthesize new materials for which neutron techniques are particularly useful (this includes labeling using deuteration). The present work is an intricate combination of chemistry synthesis and neutron scattering. The aim is to produce grafted nanoparticles, and consecutive nanomaterials, which are studied by SANS at the different steps of the procedure. We wish to keep the nanoparticles in a state of individual dispersion. Connection is systematically done between the information provided by SANS and our effort in improvement of the synthetic process.

The effort in synthesis was to use and develop the rather new “grafting from” method, combined with controlled polymerizations -in our case atom transfer radical polymerization (ATRP)- It consists in grafting first an initiator molecule, making polymerization start from the particle surface, under controlled conditions (“living polymerisation”) [1]. Moreover, grafting the initiator is done in two steps to avoid steric hinderances encountered for large molecules, These three key features yield a high degree of grafting and good control in the chain growth. Another new feature of the work is avoiding aggregation for each reaction step: we kept the nanoparticles in the same solvent to avoid drying of the particles or changes in the solvent quality. For each step, aggregation has been followed using SANS. First, SANS showed that the silica particles staid well-dispersed after the two grafting steps (functionalization and over-grafting). The polymerization (here we take the example of styrene) was done after adding so-called “sacrificial initiator”, free in solution, because of the small concentration of grafted initiator The backdraw is that we generate free chains in the solution but they can be separated by centrifugation or filtration.

During and at the end of polymerisation, the chemical tests were carefully performed, most of them at the lab. The fact that the semi logarithmic plot of monomer conversion with time

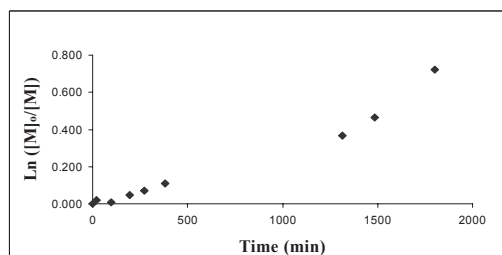


Figure. 1. Logarithm of monomer conversion versus time.

is linear (see Fig. 1) attest a good control of the polymerisation rate. Size Exclusion Chromatography (SEC) was performed on the free chains which showed masses (100 000) of the same order as the grafted chains (130000): the latter were separated from the silica surface by etching with Fluorhydric acid. The slight difference suggests steric congestion of initiators at the surface of the particles, which remains a point to improve. But the rather narrow chain mass distribution ($M_w/M_n \sim 1.3$) confirms the control and leads to well characterized particles.

We also used off-lab techniques: e.g. thermogravimetry (burning the polymer at high T) to check the amount of grafted polystyrene (after removing the “free chains”) The grafted / free chains ratio is of the order of grafted/free initiator ratio, but lower.

Now that advanced chemical characterisation is satisfactory, we can use SANS to follow the polymerization. A first new information is the level of aggregation of silica beads(Fig.2). To measure it, we matched the scattering length density of the solvent to the one of the polymer, using a mixture of hydrogenated /deuterated solvent.

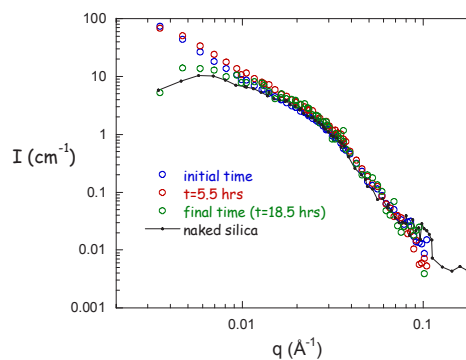


Figure 2: Scattered signal from silica only (polymer matching) at 3 times of polymerisation.

The full line is the scattering curve for silica before the reaction. At the initial step, when no polymer has yet been formed, the low- q scattering, indicates the presence of large aggregates, probably because the presence of styrene has reduced the polarity of the solvent (at this stage particles are stabilised by electrostatic repulsion). At the end of polymerization, the low- q signal decreases (i.e. the aggregates size decreases) and becomes very close to the signal of the naked silica. In summary, grafting polymer on silica spheres has reduced aggregation and stabilized the colloidal dispersion. (probably because of repulsion between the polymer grafted brushes).

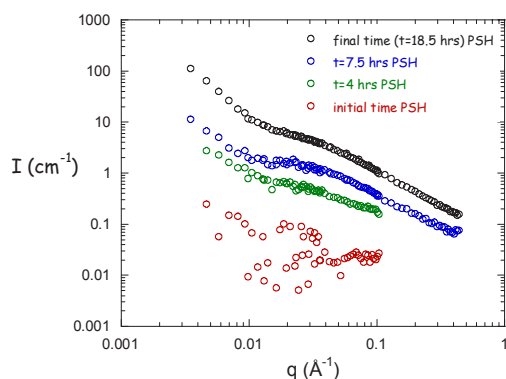


Figure 3. Scattered intensity by hydrogenated styrene grafted on nanoparticles in silica matching conditions at different stages of the polymerization.

We can also follow the structure and conformation of the grafted polymer layer. We used here the possibility of matching the solvent to silica beads. The figure 3 presents the scattering curves for grafted particles with hydrogenated polymer, from initial to final stage. The first curve (initial time) verifies the correct matching conditions (flat signal without polymer). When the polymerization process starts, the low- q intensity increases. This is a qualitative indication of the presence of polymer. At large q , the signal slowly decreases, with a slope (around 1.65) characteristic of polymer scattering in this q -range. We also observe a shoulder at lower $q \sim 0.02 \text{ \AA}^{-1}$. If the grafted particles scatter like hollow spheres, this shoulder could be the signature of the grafted polymer. A shift of the shoulder position towards the low- q values should then indicate the growth of the polymer layer

References

- [1] G. Schmidt, M.M. Malwitz, *Curr Opin Colloid Interface Sci* **2003**, *8*, 103.
- [2] A. El Harrak, G. Carrot, J. Oberdisse, C. Eychenne-Baron, F. Boué, *Macromolecules*, **2004**, *37*, 6376-6384.
- [3] A. El Harrak, G. Carrot, J. Jestin, J. Oberdisse, F. Boué, to appear in *Polymer*.

around the particle. And this shift is actually observed in experimental data. Nevertheless, this shoulder could also be due to the scattering of the free polymer chains present in the sample. Simple subtraction of the signal of a solution of such free chains is unaccurate for sure, because it ignores all kind of interactions between free and grafted chains. Therefore, to progress in this way, we used centrifugation to remove free chains (for the same sample presented, before centrifugation, in Fig. 3). The shoulder is still present (lower curve of Fig.4), and even more clear cut, a proof that it was not due to free chains. Fig.4 also shows a sample synthesized with deuterated monomer, for which contrast with solvent is larger. The shoulder is still observed in that case, at the same q value. Such joint information for two contrasts yields an unambiguous SANS signature of hollow spheres of polymer-grafted-silica particles. However, refined analysis using fitting models requires to account for aggregation which occurs during reaction. The corresponding calculation are on the way. The next important step is to define new physical and chemical routes to maintain colloidal stability through the different steps of the grafting procedure, a task which will combine both types of knowledge in our team.

Another extension of this work is to produce, and characterize films of polymer where those nanoparticles are embedded in the same polymer than the grafted one.

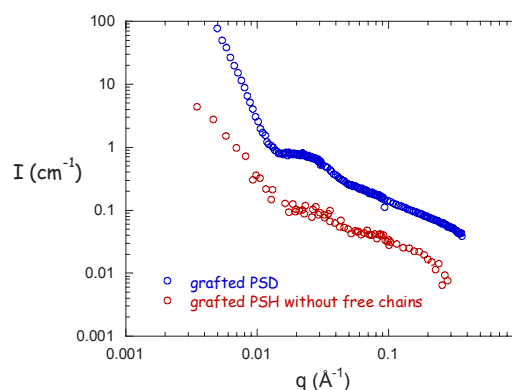


Figure 4. $I(q)$ in silica matching conditions at final polymerisation stage, for normal polystyrene after removing free chains (PSH, red) and deuterated polystyrene (PSD, blue).

HIGHLY STRETCHED POLYMER BRUSHES WITH A LOW SWELLING CAPACITY

C. Devaux¹, F. Cousin², J-P. Chapel¹¹Laboratoire des Matériaux Polymères et des Biomateriaux, UMR CNRS 5627, Université Claude Bernard Lyon 1, ISTIL, 43, Boulevard du 11 Novembre 1918, 69622 Villeurbanne cedex, France}²Laboratoire Léon Brillouin, CEA-CNRS, CEA Saclay, 91191 Gif sur Yvette, France

Polymer chains in thin films are seen in a tremendous number of systems and devices of modern material science and technology. The need for controlled (thickness, Mw, conformations...), stable and reproducible thin films is then essential. We have developed an overall strategy to built-up chemisorbed thin films with tunable architectures grown directly from silica surface through controlled macromolecular chemistry [1]. The process is split in two distinct steps : (i) deposition of an initiator monolayer using "reactive" Langmuir-Blodgett deposition technique that allows the control of the chain lateral grafting density σ (up to 1.0 chain/nm²) (ii) the nitroxide mediated free radical polymerization of styrene that allows the control of chain length N. It induces a direct control of both brush thickness h and chain stretch S. The active chain ends enables to reinitiate the polymerization.

We describe here neutron reflectivity measurements performed on the EROS reflectometer on our controlled brushes in order to (i) test the homogeneity of the chains growth *during* the polymerization process and (ii) to measure the conformation of the brushes in good solvent. The brush preparation and characterization were achieved according to methods previously reported. The brush thicknesses were obtained in air through ellipsometric measurements with a 15-20 Å layer of native silica and a 10-15 Å layer of grafted initiator. All reflectivity curves have been fitted by model reflectivity curves calculated by the standard optical matrix method including SiO₂ and initiator layers. Best fits between calculated and experimental spectra were obtained by minimizing least squares χ^2 .

Homogeneity of the brushes

Taking profit from high neutronic contrast between deuterated and hydrogenated PS, we have designed a DPS/HPS copolymer brush to check *a posteriori* the homogeneity of the chain growth front *during* the polymerisation from the surface. It is linked to the width of the interdiffusion layer of the DPS/HPS interface. The bilayer was build up from two polymerization runs in a row a first one with deuterated styrene (N= 95) followed by a second

one with hydrogenated styrene (N=90). The DPS and (DPS+HPS) dry thicknesses obtained by ellipsometric measurements were respectively 230Å and 420Å. Neutron reflectivity measurements, carried out in the dry state, are presented on figure 1. There are irregular Kiessig Fringes arising from the three layers structure (HPS, DPS and the total PS layer). Best fits are obtained with a PSH and a PSD layer of 250Å and 180Å respectively with an interdiffusion layer of 25 Å. σ_{int} is get unambiguously from the progressive apparition or disappearance of the fringes when the interdiffusion layer is shifted shift from 0Å to 50Å. The value of 25Å for σ_{int} on a total layer of 430Å underline the homogeneity of the brush growth and the possibility to build multilayers with well defined interfaces.

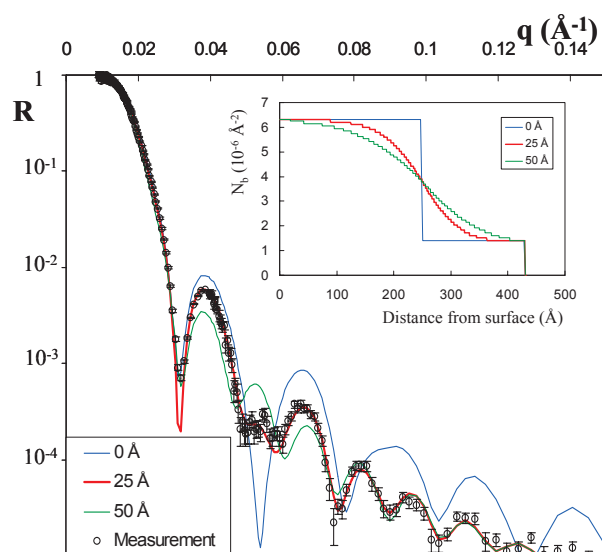


Figure 1. Reflected curve of the PDH/PSD layer. Fits correspond to the profiles showed in the insert.

Conformation of the brushes

Three samples were made with quite high grafting density in which we vary either σ test at constant N, either N at constant σ ($\sigma=0.5\text{chain/nm}^2$, N=120; $\sigma=1\text{chain/nm}^2$, N=120; $\sigma=1\text{chain/nm}^2$, N=270).

Figure 2.a presents the results obtained for dry layers. Fits have been realized with a zero roughness interface and with a polymeric volume

fraction Φ of 1. We get $h = 110 \text{ \AA}$, 220 \AA and 470 \AA respectively for the three layers. We check thus that thickness the thickness h scales linearly with either the chain length N and the grafting density σ ($h \propto N\sigma$) in bad solvent (air). As σ is quite high, the chains are then already extended in air.

Though the brush structure does not depend on N , we studied the influence of σ on swollen brushes for the samples with $N = 120$ in good solvent (deuterated toluene). The reflected curves are presented on figure 2.b where they are compared to the calculated ones obtained for the unswollen brushes. Three features enables to conclude qualitatively on the swollen brush conformations: (i) brushes are partially swelled. The polymer/solvent contrast has decreased as the reflectivity is weaker than in the unswollen case. (ii) The Kiessig fringes are still visible but less marked. The polymer layer has hence finite size but the density profiles are no longer step-like. (iii) The solvent has enlarged the thickness of the layers as the Kiessig fringes are shifted towards lower q . Their thickness is roughly the same as the fringes minima are located at the same q .

Reflected curves have been fitted by a continuous profile of swelled chains which ensures polymer conservation from dry to swollen state (divided in layers of 10 \AA). Profiles are shown in the insert. The thickness for which Φ reaches 0 is the same for both samples ($\approx 300 \text{ \AA}$). This value corresponds nearly to the fully extended PS chain (L_0). The volume fraction Φ_s at the surface ($z=0$) keeps for the highest grafting density the unusual value of 0.85, to our knowledge the highest value ever reported in literature. As the chains are already very stretched the dry state when increasing σ , the solvent has some difficulty to penetrate the layer leading to a somehow low swelling capacity.

This has a direct impact on the swelling laws. In a good solvent, the chains adopt an extended conformation consecutive to the solvent-polymer interactions determined by a balance between the interactions that promote stretching and the associated loss of chain conformational entropy [2]: h/N scales with $\sigma^{1/3}$ for moderate densities

($\sigma < 0.2 \text{ chain/nm}^2$) [3] as the chains adopt an extended conformation consecutive to the solvent-polymer interactions. But for our dense brushes, $h_s/N \propto \sigma^n$ with $n=0.5$, a result generally obtained in Θ conditions. The very high grafting density which reduces the brush swelling capacity as toluene is a good solvent of PS at room temperature.

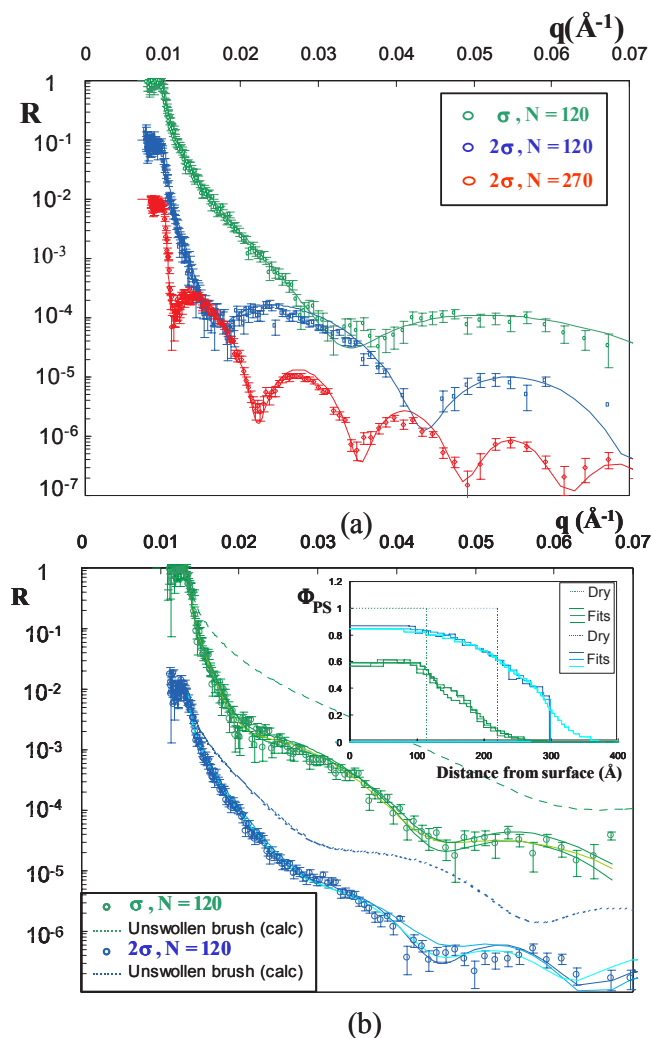


Figure 2. (a) Experimental reflected curves and corresponding fits for dry brushes. (b) Experimental reflected curves, corresponding fits for the swollen brushes and calculated curves for unswollen brushes. Insert present volume fraction profiles.

References

- [1] Devaux C., Beyou E., Chaumont P., Chapel JP., *Eur. Phys. J. E.*, 2002, 7(4), 345.
- [2] Brown H.R., Char K., Delin V.R., *Macromolecules*, 1990, 23, 3385.
- [3] Auroy P., Auvray L., Léger L., *Phys. Rev. Lett.*, 1991, 66, 719.

NEW STRUCTURAL MODEL FOR NAFION® MEMBRANES

 Laurent Rubatat¹, Olivier Diat² and Gérard Gebel²
¹Simon Fraser Univ. Vancouver

²UMR SprAM 5819, DRFMC/CEA Grenoble

Proton Exchange Membrane Fuel Cells are considered to be the most promising system for electric power generation. The heart of these cells is made of a polymeric solid electrolyte which has to satisfy several features: high ionic (protonic) conductivity (10^{-2} - 10^{-1} S.cm⁻¹), excellent chemical and electrochemical stability (>5000 h), low permeability to reactants ($p < 10^{-15}$ m²s⁻¹Pa⁻¹), and stable mechanical properties over a wide range of water content (0-30% wt) and temperature (0-100°C)

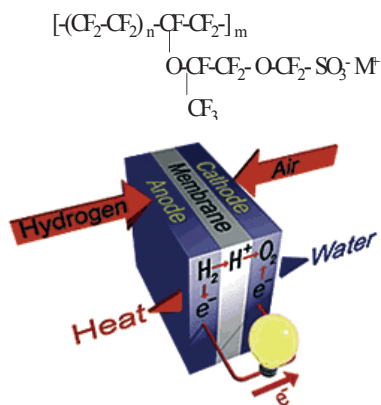


Figure 1. Schematic view of a Hydrogen fuel cell.

Nafion¹™, a perfluoro-sulfonated ionomer membrane is the benchmark material in terms of performance and stability, at least in stationary operation conditions. Although numerous studies are performed on alternative membranes, blends and composites (organic-inorganic system), all results are systematically compared to Nafion membranes. However the Nafion structural models are mainly based on the Eisenberg² description which considers ionic clusters dispersed in a hydrophobic polymeric matrix (in order to reduce the total free energy of the system). Based on the assumption that this cluster picture is correct, different models³ of aqueous membrane swelling were developed to explain data from structural studies, aqueous sorption and swelling, ionic conductivity, etc. A considerable effort has been made in the last few years in order to understand the underlying conduction processes, with the objective to ameliorate the membrane performances for industrial applications. However, few studies have been designed to explore the structural and transport evolution at different

length scales taking into account the complete hydration processes

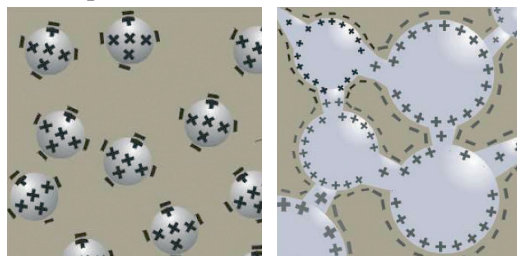


Figure 2. Representation of dry (left) and swollen (right) ionic clusters in an ionomer bulk system.

Recent developments in x-ray and neutron scattering techniques permit us to obtain high resolution data over an extended angular range and to define more accurate model. In parallel, the application of microscopy techniques such as the atomic force or electronic microscopies also reveal important information about the membrane structure. It is clear that both the microscopy and scattering data must be correlated to validate the proposed models. From this analysis, a new structural model of Nafion⁴ (applicable to other perfluorinated ionomer systems) has recently been developed in our laboratory. It describes Nafion membrane as an aggregation of polymeric chains forming elongated objects (simplified as cylinders), embedded in a continuous ionic medium. At larger scales, those aggregates form bundles, characterised by an orientation order between the aggregates. This new insight of a multi-scale structure can explain the membrane swelling process from dry state to the colloidal suspension, in a continuous way.

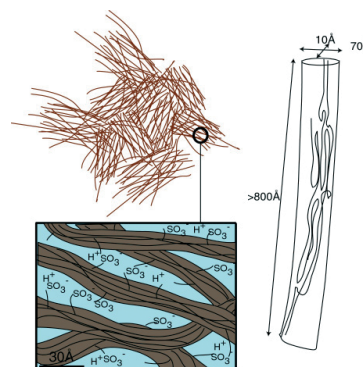


Figure 3. New insight of a Nafion membrane multi-scale structure.

Neutron scattering was chosen to take advantage of the contrast variation method and was a key experiment in our study. Using SANS a partially deuterated solvent and a highly protonated counter-ion such as TMA⁺ (non-transient contrast agent), it was previously demonstrated that the counter-ions condense at the polymer-solvent interface and that the highly swollen membrane spectra can be to some extent simulated by a core-shell cylindrical form factor (polymeric core surrounded by a counter-ions shell⁵).

Therefore, SANS combined with contrast variation is a suitable technique to determine the distribution of the counter-ions in NafionTM and to determine the shape of the polymeric aggregates. In this new model, the water medium is described as a 3D continuous media (as a function of water sorption) rather than confined water molecules in a channel and micelles network (Gierke's model).

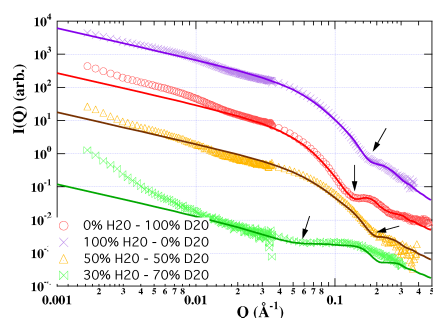


Figure 4. Scattering curves from an hyper-swollen Nafion membrane for different H₂O/D₂O ratios. Black curves correspond to theoretical form factors.

On the other hand, membrane drawing experiments have confirmed the “cylinder” model and the structure orientation effect on the protonic conductivity have been measured. SAXS and SANS studies on stretched Nafion films were analysed thanks to a basic deformation model taking into account randomly oriented set of bundles (assuming cubic shape) at the origin. Those results have been correlated with birefringence measurements⁶.

References

1. from du Pont de Nemours
2. Eisenberg, A. *Macromolecules* **1970**, *3*, 147-154.
3. Schlick, S. *Ionomers: Characterization, Theory and Applications*; CRC Press: Boca Raton, 1996.
4. Rubatat, L. et al *Macromolecules* **2002**, *35*, 40-50-4055; *Macromolecules* **37** (2004) 7772.
5. Rollet, A.-L. et al *J.Phys.Chem.B* **2002**, *106*, 3033-3036.
6. P.C. Van der Heijden et al *J. Polym. Sci.: Polym. Phys.* **42** (2004) 2857. *J. Nucl. Inst. Meth. B* submitted.

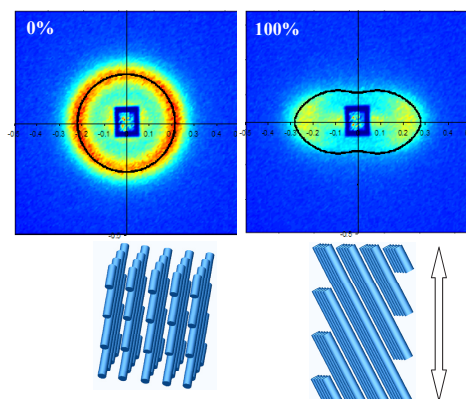


Figure 5. 2D scattering pattern from a Nafion membrane at rest (left) and under stretching (right). Taking into account a simple model of a distorted bundle of rod-like aggregates, the position of the ionomer peak as a function of the azimuthal angle (black lines) is simulated and superimposed to the experimental spectra.

The results of this study allow us to propose some modification of ionomer systems in order to improve performances in fuel cell. Moreover, the associated dynamical processes are expected to occur at different time scales: internal motion of protons along aggregates, motion from one aggregate to another, from one bundle to another, and through the whole membrane.

The relaxation times associated to the proton dynamics in these systems are consequently expected to range from the picosecond (local jump of a proton between two sulfonated groups) to few tenths of seconds (macroscopic conductivity through the whole membrane).

A complete study of the dynamics, using various complementary techniques, is necessary in order to verify that they correlate with what we know about the structure. Quasi-elastic neutron scattering, neutron spin echo, back scattering studies, gradient field-pulsed NMR and field cycling NMR relaxometry will be conducted to understand the multi-scale ionic and water transport in this kind of material. This understanding is crucial to be able to model the water management in fuel cells

LOCAL DYNAMICS OF BULK AND NANOPARTICLE FILLED POLY(VINYL ACETATE) OBSERVED BY QUASIELASTIC NEUTRON SCATTERING

Chuhong Zhang, Valeria Arrighi*

Chemistry, School of Engineering and Physical Sciences, Heriot-Watt University, Edinburgh EH14 4AS – UK

The addition of nanoparticles to polymers leads to changes in the physical and mechanical properties of the matrix. This effect depends on parameters such as particle size, shape and distribution, state of dispersion in the matrix, particle-particle as well as particle-matrix interactions.

One of the major consequences of adding particulate fillers to a polymer is the formation of an "interphase", *e.g.* the bound rubber in rubber/filler composite. Changes in chain dynamics at the polymer-filler interface play an important role in the reinforcement effect [1-2] but aggregation of filler particles arising from filler-filler interactions probably also contributes to the reinforcement [3].

While many studies of filled polymers have focused on the mechanical and rheological behaviour, there have been fewer measurements attempting to investigate the changes in chain dynamics, at the microscopic level. Our aim has been to characterize the local polymer dynamics in filled systems, using quasielastic neutron scattering (QENS) [4,5], hoping to combine microscopic information with macroscopic behaviour.

Polymer motion is per se a complex issue. The large size of any polymeric chain means that molecular motion occurs over a wide range of distances and frequencies. It is therefore crucial, in dynamic studies, to use a combination of experimental methods in order to probe a wide dynamic range. This is particularly true for quasielastic neutron scattering and much can be gained in this case by using a range of instruments differing in energy resolution and energy window.

The aim of the measurements carried out on MIBEMOL was to complement existing data collected on the backscattering spectrometers IN10 (ILL) and IRIS (ISIS) (Table 1). The system chosen for the study is poly(vinyl acetate) (PVAc, $M_w = 237,100$ g/mol, $M_w/M_n = 2.64$). Fumed silica particles with specific surface area equal to 90 (A90) and 300 (A300) m^2/g were used as filler.

At temperatures below the glass transition ($T_g = 314$ K), rotational motion of the methyl groups dominates the PVAc dynamics. Previous measurements carried out on IRIS with the PG004 analyser had shown that the motion of the CH_3 groups can be modeled by the rotational rate distribution model (RRDM). However, a Q and temperature dependent background was observed,

which suggested the existence of a fast process. This was confirmed by the time-of-flight data collected on MIBEMOL. As shown in Figure 1, at $T < T_g$, the MIBEMOL data consist of three components: (a) a fast process which has a Lorentzian shape, (b) a slower process due to the CH_3 motion and (c) an elastic component.

Table 1. Characteristics of neutron spectrometers.

Instrument	Energy resolution (FWHH)	Energy range	Q range
IN10	1 μ eV	-13 ~ 13 μ eV	0.5 \AA^{-1} ~ 1.96 \AA^{-1}
IRIS	PG004: 54.5 μ eV ($< T_g$)	-4 ~ 4 meV	0.3 \AA^{-1} ~ 3.7 \AA^{-1}
	PG002: 15 μ eV ($> T_g$)	-0.2 ~ 1.2 meV	0.25 ~ 1.9 \AA^{-1}
MIBEMOL	$\lambda_i = 6$ \AA : 107 μ eV	-1 ~ 10 meV	0.72 \AA^{-1} ~ 1.95 \AA^{-1}
	$\lambda_i = 3$ \AA : 850 μ eV	-5 ~ 50 meV	0.92 \AA^{-1} ~ 3.90 \AA^{-1}

FWHH= full width at half height, $Q = 4\pi/\lambda \sin(\theta/2)$, λ =neutron wavelength, θ = scattering angle.

The intermediate scattering function, $I(Q,t)$, obtained via inverse Fourier transform, shows that there is good overlap between data obtained from IRIS and MIBEMOL (Figure 2). A CONTIN analysis of the overlapped $I(Q,t)$ data indicates that the distribution of relaxation times is made up of two distinct processes.

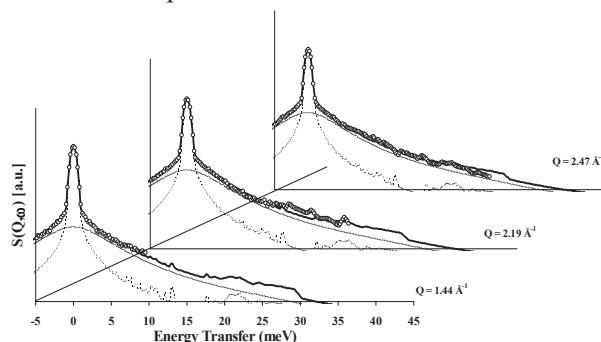


Figure 1. QENS spectra of PVAc (FWHH=850 μ eV) at 150 K: data points (\circ) and fits (continuous line). The dotted line is the contribution from CH_3 motion and the dashed line shows the fast process.

Above the glass transition, measurements carried out on IN10 and IRIS (PG002), enabled us to probe the segmental motion of the PVAc chains and its temperature dependence. The QENS spectra were fitted using a Kohlrausch-Williams-Watts (KWW) function, convoluted with the instrumental resolution plus a flat background. This procedure leads to two parameters: the shape parameter β ($\beta=0.58$, independent of temperature) and the characteristic time τ_{KWW} . The latter was

found to vary as Q^{-n} , with n close to 2, independent of temperature, as expected for a diffusive process. The temperature dependence of τ_{KWW} is expressed by the Vogel-Fulcher-Tammann (VFT) equation, in agreement with results from other techniques such as dielectric spectroscopy.

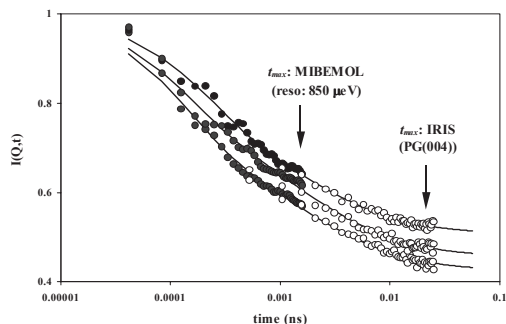


Figure 2. $I(Q,t)$ data of PVAc at 150 K and $Q = 1.68, 1.91$ and 2.13 \AA^{-1} (top to bottom) from MIBEMOL (\bullet) and IRIS (PG004) (\circ). The lines are fits to the experimental data using a two-process model.

Similarly to the QENS data at $T < T_g$, the higher temperature QENS spectra from the IRIS spectrometer had revealed the existence of a Q and temperature dependent background. By combining results from the analyses below and above T_g , the fast process observable on MIBEMOL was found to follow an Arrhenius temperature dependence with an activation energy of 1.9 kJ/mol.

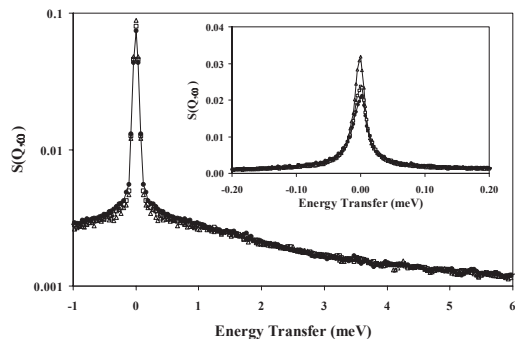


Figure 3. Normalized QENS spectra from MIBEMOL (FWHH: $107 \mu\text{eV}$) of PVAc (\bullet) and PVAc containing 40 wt% A90 (\square) and A300 (Δ) at 1.68 \AA^{-1} and 400 K. Inset: normalized QENS spectra of the same samples from IRIS (PG002) at 1.58 \AA^{-1} and 478 K.

The QENS measurements carried out on PVAc samples containing A300 and A90 indicated that the addition of the filler particles has a negligible effect on the sub- T_g dynamics. However, at $T > T_g$,

there exists a portion of chains with reduced mobility compared to the pure polymer and it increases with increasing the particle surface area and filler content. The dynamic restriction is evident at all resolutions (Figure 3). The QENS spectra of the filled samples show bimodal dynamics *i.e.* a portion of the chains has unperturbed dynamics while a smaller fraction seems to be “immobile” within the timescale of the experiment. This immobile fraction is believed to be related to the “bound” polymer layer that is chains strongly interacting with the surface.

The density of states spectra obtained on MIBEMOL indicate some interesting features. As shown in Figure 4 two distinct peaks can be observed, centered at ca. 18 and 32 meV for both bulk and filled PVAc at $T < T_g$. The position of the latter peak is close to the value calculated from the attempt frequency of the fast process ($\Gamma_\infty = 30.2 \text{ meV}$) obtained from the analysis of the MIBEMOL QENS spectra. The intensity of the two peaks decreases with increasing the filler surface area. At 400 K ($T > T_g$), the density of states of pure and filled polymers show significant differences. For pure PVAc, an additional broad peak, probably ascribed to the vibrational modes associated with the backbone, appears at higher energy but it is almost unnoticeable in the filled PVAc samples (Figure 4).

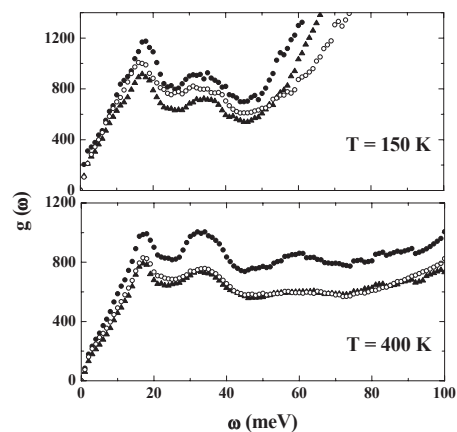


Figure 4. Hydrogen-weighted vibrational density of states for PVAc (\bullet) and PVAc filled with 40% (w/w) A90 (\circ) and A300 (\blacktriangle) at 150 K and 400 K (MIBEMOL, FWHH: $107 \mu\text{eV}$)

References

1. Litvinov, V.M. in *Organosilicon Chemistry II – From Molecules to Materials*, N. Auner and J. Weis eds.; VCH, 1996, 779.
2. Mansencal, R.; Haidar, B.; Vidal, A.; Delmotte, L.; Chezeau, J.-M. *Polym. Int.* 2001, **50**, 387.
3. Mele, P.; Marceau, S.; Brown, D.; de Puydt, Y.; Alberola, N.D. *Polymer* 2002, **43**, 5577.
4. Arrighi, V.; Higgins, J.S.; Burgess, A.H.; Floudas, G. *Polymer* 1998, **39**, 6369.
5. Gagliardi, S.; Arrighi, V.; Ferguson, R.; Telling, M. T. F. *Physica B-Condensed Matter* 2001, **301**, 110.



5 - LIFE SCIENCES

This chapter reports on the research activities on Life Sciences. It collects results obtained during the past two years by LLB scientists as well as scientists collaborating with LLB. Some results have been selected to appear as “Highlights” at the end of the chapter.

Our research activities in the Life Sciences are to characterize the movements and dynamic structural equilibria of proteins, including fast internal motions, domain motions and global unfolding and refolding transitions, to understand how the primary sequence of the protein controls these dynamic properties and to relate the specific structural dynamics to the specific functional properties of the proteins. Neutrons produced by present research-oriented sources typically have wavelengths on the order of angstroms, and energies of tens of wavenumbers, and hence are well-suited for probing the structures and motions of molecules. Neutrons scatter from nuclei, both coherently and incoherently. Coherent scattering provides information on structure and collective dynamics, and incoherent scattering on single particle motion. The large difference in scattering cross-sections between hydrogen and deuterium provides a powerful method for accentuating (or masking) the scattering from particular parts of a system by selective deuteration. Neutron scattering has been demonstrated to be a powerful tool for characterizing the structures and dynamics of biological molecules. We present recent results of applications of a wide variety of neutron scattering measurements (small-angle scattering for structure; quasi-elastic scattering, spin echo for dynamics). Theoretical molecular models for interpreting the data are presented in the chapter dedicated to Theory. The thesis work of V. Hamon is an example of collaboration between experimentalists and theoreticians (see Highlight in chapter Theory).

The research activities have progressed along the lines described previously:

- studies of conformation of proteins in solution (native and unfolded states)
- relationship between structure, dynamics and function of biological macromolecules and role of hydration water in this relationship with orientation to complex systems

Role of hydration water

Hydration water plays a major role in the stability, dynamics and function of biological macromolecules. The knowledge of structure and dynamics of hydration water is needed to get a better understanding of the role of water in biology. Water in various systems from model systems to complex ones like DNA and entire cells has been studied.

Water as a monolayer at the hydrophilic surface of a porous Vycor glass

Nanosecond-time-scale measurements of local rotational and translational dynamics of interfacial, non-crystalline, water from 77 to 280 K have been done. These experimental dynamic results meet calorimetric and diffraction data to show that after exhibiting a glass transition at 165 K, interfacial water experiences a first order liquid-liquid transition at 240 K from a low density to a high density liquid. This is the first direct evidence of the existence of a liquid-liquid transition involving water (see Highlight). Collaboration J.-M. Zanotti, M.-C. Bellissent-Funel (LLB), S.H. Chen (MIT)

Water in assemblies of identical small peptides

A chain of five alanins has been hydrated, at various levels of hydration, providing with 1 to 25 water molecules. At high level of hydration, the H-bond lifetime is slightly longer than that observed in bulk water. Higher the hydration and higher the diffusion that tends asymptotically to the self-diffusion in bulk water. As obtained in previous works, the residence time is almost constant with a value similar to that bulk water at a temperature 30 K lower.

(see Highlight). Collaboration D. Russo (postdoctorant, Berkeley), P. Baglioni (Florence), J. Teixeira (LLB)

Water in ds-DNA and ss-DNA

Analysis of quasielastic neutron scattering data of hydrated samples of ds-DNA and ss-DNA indicates that in the ds-DNA sample one can distinguish two types of protons—those belonging to water molecules strongly attached to the ds-DNA surface and another fraction belonging to water that has an isotropic diffusion. For

ss-DNA, on the other hand, no indication was found of motionally restricted or confined water. Further, the fraction of protons strongly attached to the ds-DNA surface corresponds to 0.16 g H₂O/g ds-DNA, which equals the amount of water that is released by ds-DNA upon thermal denaturation, by differential scanning calorimetry. These results represent, thus, a completely independent measurement of water characteristics and behavior in ds- and ss-DNA at critical hydration values, and therefore substantiate the previous suggestions/conclusions of the results obtained by calorimetry.

(see Highlight). Collaboration M. Bastos, V. Castro, G. Mrevlishvili (Porto), J. Teixeira (LLB)

Water in entire cells

Although water (which constitutes around 80% of a cell) plays a crucial role in nearly all biochemical processes, the properties of water in the cytoplasm are still under much discussion. Former NMR experiments had suggested a very different cytosolic environment in *Haloarcula marismortui* (*Hm*) and *Halobacterium salinarum* (*Hs*). Both are extreme halophiles, but hydration interactions appeared to be much stronger in *Hm* than in *Hs*.

Deuterated *Haloarcula marismortui* cells were cultivated, and whole cell pellets were prepared to measure cellular water dynamics. Quasielastic measurements were performed on Muses for a Q value of 1.7 Å⁻¹ and a significant difference can be observed between the water in the cells and the buffer (a high concentration of salts in D₂O). By fitting the curves with a stretched exponential, one gets for intracellular water a characteristic diffusion time which is a factor ten longer than for bulk water.

(see Highlight). Collaboration K. Wood, B. Franzetti, G. Zaccai (Grenoble), D. Oesterhelt (Martinsried), M. Ginzburg and B.-Z. Ginzburg (Jerusalem), S. Longeville(LLB), M.-C. Bellissent-Funel (LLB)

Dynamics and function of biological systems

The dynamical transition temperature

The physical origin of the dynamical transition still remains a matter of debate. Several models to analyze the temperature dependence of the mean square displacement $\langle u^2 \rangle$ have been proposed. Recently, in a series of recent papers, the hypothesis was developed that the strong increase in the $\langle u^2 \rangle$ around 200 K could at least partially arise from an increase in the low energy part of the density of states. Studies are under way to try to discriminate between mode softening and anharmonic contributions in the dynamical transition.

S. Longeville, J.-M. Zanotti (LLB)

Effects of co-solvents on β -lactoglobulin dynamics

Quasi-elastic and elastic neutron scattering preliminary measurements performed on Mibemol spectrometer, have shown that the β -lactoglobulin (β -LG) is a very rigid protein (picosecond time scale). Indeed, the evolutions of the $\langle \mu^2 \rangle$ as a function of temperature for the dry and wet protein (0.7g D₂O/g protein) are exactly the same. No dynamical transition was observed on the hydrated β -LG around 220 K as usually observed on other globular proteins.

Collaboration C. Loupiac (ENSBANA,Dijon), J.-M. Zanotti (LLB)

Dynamics of Aquaporin-1 (AQP1)

Aquaporin-1 (AQP1) is a small membrane protein that functions as a selective water channel in different cell types, including red blood cells. Its structure is now known at 2.2 Å and molecular dynamics simulations suggest that water dipole rotation during passage in the pore of the channel is essential for water selectivity and proton impermeability. Our aim is to investigate AQP1 dynamics *in vitro*, using neutron scattering and contrast matching strategy with hydrogen-deuterium substitution. A first series of experiments by neutron scattering has been carried out on AQP1 *via* elastic scans on MIBEMOL spectrometer (LLB). The high hydrophobicity of AQP1 allowed its partial purification with native membranes from human red blood cells, before freeze-drying. Mean square displacements (MSDs) of the hydrogen population were determined for D₂O-hydrated membrane powder (0.38 g D₂O/g dry sample), compared to controlled dehydrated sample. The extracted MSDs in D₂O-hydrated sample reveal an increase beginning at ~ 230 K called the "dynamical transition", comparable to other membrane proteins like bacteriorhodopsin but with a smoother transition. For a better comparison with dynamic behaviour of other membrane proteins, sample preparation is under improvement. AQP1 is purified in detergent by chromatography to avoid contamination from red blood cell lipids, before reconstitution in deuterated liposomes to match the membranes. Quasi-elastic and inelastic neutron scattering measurements in the intermediate temperature range will also be carried out to provide more information on the nature of the movements occurring in this regime.

S. Combet-Jeanceneil, J.-M. Zanotti and M.-C. Bellissent-Funel (LLB)

Influence of concentration on the diffusion process of myoglobin and haemoglobin

The interior of cells is often filled with a very wide variety of "objects" with respect to the size and shape. Proteins are present *in-vivo* in a very crowded environment, with sometimes volume fraction up to $\Phi \sim 0.3$. This environment can affect some physical, chemical or biological properties of the macromolecules. As a particular aspect, diffusion mechanism in highly concentrated protein solutions is of high interest, with the aim to address the question of transport properties and the possible diffusion assisted or limited biochemical reactions. Combined SANS and NSE analyses of protein solution have been used to analyze the effect of non-specific protein-protein interactions on myoglobin diffusion. Direct protein-protein interactions are modeled using DLVO potential. The diffusion mechanisms can be measured up to volume fractions of $\Phi \sim 0.4$. From the volume fraction dependence of $D_s^s(\Phi)/D_0$ we have extracted i: the magnitude of the short range hydrodynamic interaction which are related to the local viscosity, ii: computed the protein friction, iii: shown that theories for hydrodynamic interaction failed for describing the $H(Q \rightarrow \infty)$ but give a qualitatively correct description of the wave vector dependence. When compared to the results of $D_s^l(\Phi)/D_0$ our results show that hydrodynamic interactions are the leading interactions that drive the macromolecular mobility even over long distances. These results are the first attempt to measure the wave vector dependent solvent mediated interactions in protein solutions.

Collaboration S. Longeville (LLB), W. Doster (Munich)

Protein folding

A complete understanding of protein folding requires the physical characterization of both native and denaturated states and the evaluation of the thermodynamic parameters of the system. This involves obtaining information concerning the structure and dynamics of proteins denaturated under various conditions (temperature, pH, chemicals). The application of hydrostatic pressure to a protein solution also provides a controlled manner to alter these physical properties. Thus, characterisation of the denaturated states of proteins is important for a complete understanding of the factors stabilising their folded conformation. Small-angle scattering, of either neutrons or X-rays, is a very powerful tool giving structural information at low and medium resolution. Complementary information from circular dichroism, fluorescence and differential scanning calorimetry is used.

Effects of high pressure on β -lactoglobulin structure

Studies of high pressure on the structure of this milk protein are interesting for the food industry as a way to make gel with new properties and texture. The effect of high pressure (50 MPa to 450 MPa) on the structure of the protein has been obtained from measurements of the radius of gyration and analysis of the initial forward scattering intensity by SANS on PACE spectrometer at LLB. At pressures lower than 200 MPa, the change of radius of gyration is about 0.15 nm. According to other studies with only pH change, where the β -LG goes from dimer to monomer, one expects that the dissociation should at least be linked to a change of 0.7 nm of the radius of gyration. So one can say that the protein unfolds under this range of pressure but the dimer does not dissociate. Beyond 200 MPa aggregation occurs between partially unfolded dimers and the gelation process is initiated

Collaboration C. Loupiac (ENSBANA, Dijon), M. Bonetti (SPEC, CEA), S. Pin (Laboratoire Claude Fréjaques, CEA), P. Calmettes (LLB)

Effects of high pressure on BPTI (bovine pancreatic trypsin inhibitor) structure and dynamics (Part of Thesis work of M.-S. Appavou)

BPTI is a small protein, formed by 58 amino acids (6,5 kDa). The structure is well known, and contains both alpha-helix and beta-sheet patterns. Its heat-induced irreversible transition temperature occurs between 80 and 90°C.

Under pressure, a first structural transition has been observed between 3 and 6 kbar. The global shape of the protein studied by SANS starts to exhibit changes at 3 kbar, and the secondary structure studied by FTIR changes from 5kbar. This first transition concerns the breaking of α -helices, turned into unordered structures. A second structural transition occurs at about 14 kbar and is related to the change of unordered structures, accompanied by the formation of into β -sheets. This second structural transition has only been studied by FTIR. Such a transition presents, moreover, a great interest for the understanding of mechanisms involved into the amyloid diseases (due to beta-sheet formation).

In the same context as described above, the protein has been investigated by QENS (IN5,ILL; NEAT, HMI) to characterise the evolution of the dynamics during the heat and pressure induced denaturation. Changes have been observed around 3 kbar, and a clear transition occurs between 5 and 6 kbar. Data are analysed

with theoretical laws developed for polymeric systems, from which geometry of motions and distribution of relaxation times of various parts of the protein are obtained. One foresees to carry out experiments at higher pressures.

With SANS (NEAT, HMI), we get some structural information, enabling us to link structure and dynamics over the whole denaturation process. A new high-pressure cell (up to 14 kbar), suitable for SANS measurements and developed at LLB, will be used, This high-pressure range has not yet been investigated by SANS.

Collaboration M.S. Appavou, G. Gibrat, B. Annighofer, M.-C. Bellissent-Funel (LLB), M. Plazanet (ILL), A. Buchsteiner, J. Pieper (HMI, Berlin)

Complex systems

Fibronectin matrix assembly by endothelial cells as a function of fibronectin conformations.

Fibronectin is a high molecular weight multidomain glycoprotein which is distributed in a soluble form in plasma and most body fluid. Fibronectin is also found in a polymerized form as part of the extracellular matrix (ECM) of various connective tissues. Recently, one has obtained and characterised in terms of size, volume fraction and shape by angle neutron scattering experiments three different fibronectin conformations: a flexible string of 56 globules, a globular shape, at large scale with a low protein density inside the globule (Gaussian local structure), a still open conformation, at large scale with a very low density. In the absence of endogenous fibronectin synthesis, the cells are able to form fibrillar matrix with the different exogenous fibronectins. The extended and the globular conformations are assembled into extensive fibrillar network, where as the string of beads conformation is assembled into different short fibrils (figure). The cell adherence and the spreading are increased at the same level independently of the exogenous fibronectin conformation. These data show that the cell capability to form a fibronectin network with exogenous protein is principally due to the fibronectin conformation. These results are consistent with the hypothesis that cells stretch mechanically fibronectin during fibrillogenesis.

Collaboration B. Thiébot, M.-F. Breton, (Cergy-Pontoise), J. Pelta (Cergy-Pontoise and LLB), D. Lairez (LLB)

Structure of proteins-polyelectrolyte complexes

Small Angle Neutron Scattering (SANS) has been used to reveal the inner structure of complexes that can be formed when proteins (here lysozyme) and polyelectrolyte of opposite charges are mixed.

In a first time, we mix lysozyme protein with a fully deuterated synthetic polyelectrolyte (PSSNa) to reveal both the structure of lysozyme and PSS chains within the complexes for different PSS chain length and lysozyme/PSS chains ratios. We identify three main complexes types that are in accordance with the macroscopical mechanical properties. For large lysozyme/PSS ratios we get: (i) dense aggregates with short PSS chains and (ii) a PSS network cross-linked by lysozyme for long chains. (iii) for low lysozyme/PSS ratio, lysozyme is unfolded and behaves as an excluded volume chain. We get a costructure formed by the two chainlike objects.

In a second time, in collaboration with an external team (INRA), we study a system of biological interest formed by lysozyme and pectin. Though matching contrast is not possible here, we reveal the structure of complexes on the basis of the study of the first part. A data treatment enables us to get the inner volume fraction of complexes and to link it with the electrostatic interactions.

(see Highlight). Collaboration F. Cousin, J. Gummel, C. Huchon, F. Boué (LLB), I. Schmidt, M. Axelos (INRA, Nantes)

Conclusion

In the post genomic area, one is aware that proteomics will be central to the functional genomics efforts. In the field of proteomics, neutrons can be decisive to solving conformations of big biological assemblies. For this purpose, efforts must be devoted to get fully and specifically deuterated biological samples. Fully deuterated C-phycoyanin protein samples have been obtained in big amount from cultures of cyanobacteria in D₂O (Stage of DESS of A. Ould-Ouali, in collaboration with A. Boussac and D. Kourilovsky, SBE, DSV, Saclay). Location of protons and water molecules in a deuterated crystal of C-phycoyanin is now possible (collaboration with ILL) as well as studies of internal slow collective motions in big protein samples using spin-echo techniques.

A new contract for the CRG IN13 is in preparation. This involves the collaboration between LLB, IBS (Grenoble) and INFM (Italy). The CRG IN13 must restart on January 2005.

On January 2003, the Department of Life Sciences of CNRS has renewed (for four years) the GDR-1862 entitled 'Fonction et Dynamique des Macromolécules Biologiques' (Director: M.-C. Bellissent-Funel, Co-Director: J. Parello). In the frame of the GDR successful research activities have been undertaken. The last ones concerned "Journées Thématiques: *Molécules de l'Adhérence Cellulaire: Forces et Dynamique*, (Institut Curie and ENS, Paris, January 2004).

One has to notice the fruitful collaborations in Life Sciences, at the French and European level, with the following organisms: SBE (Service de Bio-Energétique), CEA, Saclay, IBS and ILL, Grenoble; INRA, Nantes; University of Cergy-Pontoise; University of Porto, Portugal; Technical University of Munich, HMI, Berlin.

1. Experimental evidence of a liquid-liquid transition at 0 K in interfacial water 117
J.-M. Zanotti, M.-C. Bellissent-Funel, S.-H. Chen
2. Hydration water dynamics of hydrophobic oligopeptide 119
D. Russo, P. Baglioni, E. Peroni, J. Teixeira
3. Hydration of ds-DNA and ss-DNA 121
M. Bastos, V. Castro, G. Mrevlishvili, J. Teixeira
4. Diffusion of water in halophilic archaea 123
K. Wood, S. Longeville, B. Franzetti, M.-C. Bellissent-Funel, D. Oesterhelt, G. Zaccai, B.-Z. Ginzburg
5. Structure of proteins-polyelectrolyte complexes 125
F. Cousin, J. Gummel, I. Schmidt, C. Huchon, F. Boué, M. Axelos

resolution (Inset Fig.4) i.e. shorter time (QENS, ANL/IPNS) confirms this point.

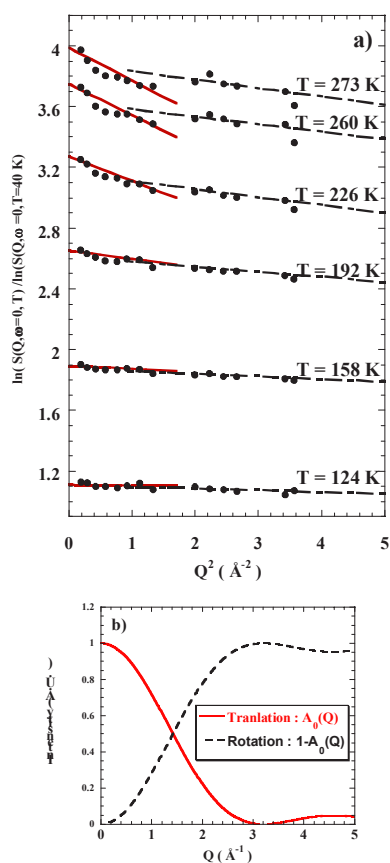


Figure 3. a) Normalized $\ln S(Q, \omega=0)$ vs Q^2 at selected temperatures in the range 77 K, 280 K (IN16, ILL). At high temperature, two distinct linear regions may clearly be defined. b) The translational and rotational contributions to the scattered intensity are strongly Q dependent, making it possible to discriminate between them. From the data in the low Q range [0.1\AA^{-1} - 1.0\AA^{-1}] of Fig. 3a, we extract a first characteristic mean square displacement, $\langle u^2 \rangle_{\text{Trans}}$, related to the water molecule long range diffusion. From the data in the higher Q range [1.1\AA^{-1} - 1.9\AA^{-1}] we define $\langle u^2 \rangle_{\text{Rot}}$, a mean square displacement related to the local molecular reorientations.

The existence of a liquid-liquid transition is a key element in discriminating between the different scenarios proposed for the peculiar properties of liquid water. In spite of strong similarities between interfacial water and bulk water (structure, calorimetric $T_g = 165 \text{ K}$ [3]) the extrapolation of the interfacial water 240 K liquid-liquid transition to the existence of a liquid-liquid transition in

bulk liquid water would be speculative. Nevertheless, the evidences presented here of a liquid-liquid transition involving water is a real breakthrough and is of general interest. Beyond the fundamental interest above, the finding of liquid water at temperatures as low as 165 K is relevant to fields as different as material science (cement technology, nuclear waste confining materials, geology) and biology (dynamics of hydration water).

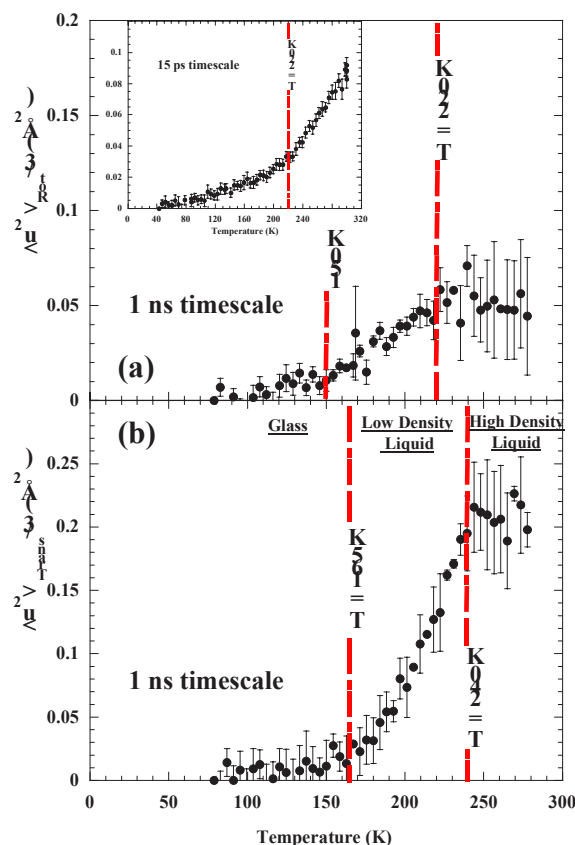


Figure 4. Temperature dependence of rotational and translational mean-square displacements of interfacial water $\langle u^2 \rangle_{\text{Rot}}$ (a) and $\langle u^2 \rangle_{\text{Trans}}$ (b) have been extracted from the two Q ranges defined in Fig. 3. Inset: lower resolution (shorter times) experiment (QENS, ANL/IPNS) confirming the saturation effect observed on IN16 due to the “high density” water fast dynamics above 240 K. The different transitions (see text) detected in water rotational (a) and translational (b) behaviours are noted by red dash lines. As expected in water, where translational dynamics is driven by hydrogen bond life time (i.e. rotational behaviour), any transition in the long range translational behaviour is preceded by a transition in the water molecules rotational behaviour.

References:

- [1] O. Mishima and H. E. Stanley, *Nature*, **396**, 329-335 (1998).
- [2] J.-M. Zanotti, M.-C. Bellissent-Funel and S.-H. Chen, *Europhys. Lett.*, submitted.
- [3] V. Velikov, S. Borick, and C.A. Angell, *Science*, 294,2335 (2001).

HYDRATION WATER DYNAMICS OF A HYDROPHOBIC OLIGOPEPTIDE

D. Russo¹, P. Baglioni², E. Peroni² and J. Teixeira³¹ University of California, Berkeley, USA² Department of Chemistry, University of Florence, Italy³ Laboratoire Léon Brillouin (CEA/CNRS), Saclay

The role of water on the structure and activity of proteins, DNA and other biological macromolecules is certainly important, although not easily to comprehend.

Depending on its situation, water forms hydrogen bonds, occupies small cavities (pools) or participates to the so-called hydrophobic interaction. The more interesting and realistic approach is the study of aqueous solutions of bio-molecules but, in such samples, the interesting local behaviour is hidden by the molecules of the solvent. Consequently, most of the detailed studies of the behaviour of hydration water have been performed with hydrated powders. Even in this way the results are ambiguous because molecules at different sites contribute in different ways to a global result that is only the average of all the possible motions. The ideal issue would be the selective deuteration of parts of the bio-molecule as it is currently done for example in the study of polymers but, notwithstanding undeniable progresses, this issue remains rare, expensive and not always possible.

We decided to circumvent the problem by the study of a synthesized uniform oligomer formed by five monomers of alanin, which is one of the simplest hydrophobic amino-acids with α -helix potential (figure 1).

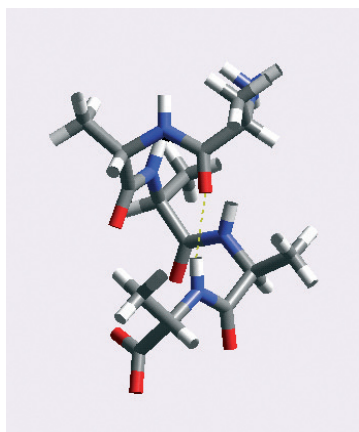


Figure 1. Representation of the structure of penta-alanin (a β -sheet). The broken line represents an internal hydrogen bond.

Quasi-elastic scattered intensity is almost totally due to different motions of hydrogen atoms in water molecules and the minor contribution of the

peptide corresponds in intensity to that of three hydrogen atoms.

In a general way, we analysed the scattering function, $S(Q, \omega)$, with the following expression subsequently convoluted with the instrumental resolution:

$$S(Q, \omega) = A\delta(\omega) + X [B(Q)\delta(\omega) + (1-B(Q))L2(Q, \omega)] * [C(Q)\delta(\omega) + (1-C(Q))L1(Q, \omega)]$$

In this expression the first term accounts for the elastic scattering of the peptide and X is the fraction of water contributing to different motions. They are separated into two terms, one representing rotational diffusion, the second the translational diffusion.

Different levels of hydration have been measured according to the following Table:

Hydration (%)	0	7	30	50	90
N total of molecules of water/peptide	0.84	2.8	9.24	14.84	25.84

The dry oligomer contains almost 1 water molecule per peptide. Its dynamics reduces to rotational motions due to the breaking of hydrogen bonds. The signal is a single Lorentzian with a Q independent half-width (0.10 meV). The characteristic time is of the order of 2 ps which corresponds to a life time of hydrogen bonds almost two times longer than in bulk water.

At 7% hydration, there are two more water molecules present. They go preferentially to the only hydrophilic sites at the extremities of the peptide. Their motion is confined and is well described by a model of diffusion inside a sphere of small radius [1] as illustrated in figure 2 by the Q dependence of the elastic incoherent structure factor (EISF).

At higher levels of hydration, the translational diffusion is apparent and two Lorentzian quasi-elastic components are necessary to fit the data. The rotational component, yields a value for the hydrogen-bond lifetime equal to 1.3 ps, slightly larger than that (1.1 ps) observed in bulk water at the same room temperature [2]. The half-width of

the Lorentzian $L_l(Q, \omega)$ is plotted in figure 3 for different levels of hydration and compared with bulk water.

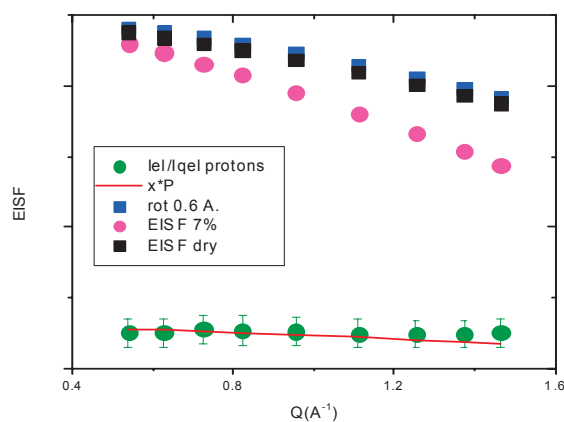


Figure 2. Representation of the Q dependence of the EISF for the dry and 7% hydrated peptide.

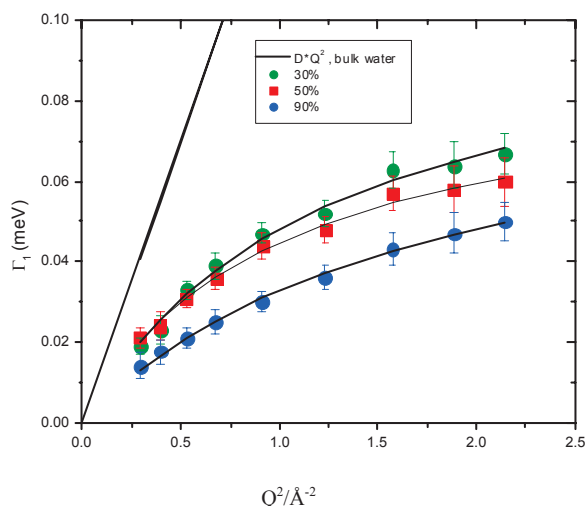


Figure 3. Half width at half maximum of the translational Lorentzian at different levels of hydration plotted as a function of Q^2 . The solid line represents DQ^2 for bulk water.

The Table below summarizes the self-diffusion, D , and the residence time, τ_0 , that can be deduced from the Q dependence of the half-width, Γ_1 ,

within a model of jump for the molecular diffusion:

$$\Gamma = DQ^2 / (1 + DQ^2\tau_0)$$

Higher the hydration and higher the diffusion which tends asymptotically to the self-diffusion in bulk water. Instead, the residence time remains almost constant and much longer than in bulk water, i.e. a behaviour similar to bulk water at a temperature around 30 K lower, as reported previously [3]. The constant jump length, which corresponds to the distance between two neighbouring hydrogen atoms, indicates that the mechanism of diffusion by rotational jumps is always the same.

Hydration	D (10^{-6} cm^2s^{-1})	τ_0 (ps)	Jump length
30 %	7.7	7.4	1,5
50 %	13.1	7,4	1,6
90 %	13.6	6,1	1,5
bulk water	22.0	1.2	1.6

This detailed study of the hydration of pentalanine shows that the dynamical contribution of the first hydration water, of a completely hydrophobic environment, is characteristic of a slow rotational motion with a relaxation time of 2.2 ps.

The addition of two more hydration water molecules shows that the rotational motion of the first water is coupled with diffusive motion. The dynamical profile is described, in first approximation, through a rotational jump model.

At higher levels of hydration, the mobility of water is quite similar to that of bulk water, i.e. translational diffusion by rotational jumps. The 23 water molecules that correspond to the full hydration of the peptide minus the three first hydration waters diffuse in a free way along the peptide. The residence time between successive jumps and the resulting self-diffusion is that of bulk water at a temperature 30° lower.

References

- [1] F. Volino and A.J. Dianoux, *Mol. Phys.* **41**, 271 (1980)
- [2] J. Teixeira, M.-C. Bellissent-Funel, S.-H. Chen and A. J. Dianoux, *Phys. Rev.* **A31**, 1913 (1985)
- [3] M.-C. Bellissent-Funel, K. F. Bradley, S.-H. Chen, J. Lal and J. Teixeira, *Physica A* **201**, 277 (1993)

HYDRATION OF ds-DNA and ss-DNA

M. Bastos¹, V. Castro¹, G. Mrevlishvili¹ and J. Teixeira²¹ Centro de Investigação em Química, Universidade do Porto, P-4169-007 Porto, Portugal² Laboratoire Léon Brillouin (CEA-CNRS), CEA- Saclay, 91191 Gif sur Yvette Cedex

Hydration of DNA plays an important role in its structure, conformation and function, particularly in the process of recognition of drugs. The B form of DNA contains a relatively large number of water molecules: around 18 per nucleotide. Depending on their position along the double helix, the behaviour of each water molecule is different, especially the dynamics of diffusion and rotation.

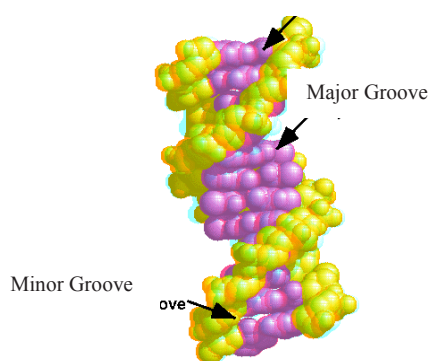


Figure 1. Schematic view of the B form of ds-DNA showing the two grooves.

Studies performed by X-rays have shown that the minor groove (fig. 1) is hydrated in an extensive and regular manner with a spine of first and second hydration shells. In contrast, the hydration of the major groove is reduced to a monolayer [1]. Differential scanning calorimetry studies of samples of double stranded (ds) and single stranded (ss) DNA [2] show that part of the hydration water does not freeze when cooled down at low temperatures. This amount of "unfreezable" water is equal to 0.55 g H₂O/g ds-DNA and 0.40 g H₂O/g ss-DNA. Logically, the difference between these two quantities (0.15 g H₂O/g DNA) corresponds exactly to the dehydration of ds-DNA at the transformation double-stranded helix → single-stranded chains. This difference is also equal to the hydration change during the thermal denaturation of ds-DNA. All these features were interpreted as suggesting that the thermal transition from double helix to single strand is accompanied by a disruption of the ordered part of the water present in the hydration shell of the double helix. Incoherent quasi-elastic neutron scattering probes the dynamics of hydrogen atoms and is an ideal technique to study the behaviour of hydration water.

It is assumed that different hydrogen atoms can be classified into three classes:

- a fraction p belonging to DNA, which are immobile in the experimental time window.
- a fraction $(1-p)q$ belonging to water molecules strongly attached to DNA.
- the fraction $(1-p)(1-q)$ of remaining hydrogen atoms, belonging to water molecules that can diffuse and rotate in the vicinity of the DNA.

The resulting scattering function $S(Q, \omega)$ is:

$$S(Q, \omega) = [p + (1-p)A_0(Qa)]\delta(\omega) + (1-p) \times (1-A_0(Qa))[qL_1(\omega) + (1-q)L_2(\omega)]$$

where $L_1(\omega)$ and $L_2(\omega)$ represent respectively a narrow and a broad Lorentzian functions, $\delta(\omega)$ is the Dirac distribution and $A_0(Qa)$ represents the confined diffusion of the atom within a sphere of radius a , according to a model due to F. Volino and A.J. Dianoux [3]:

$$A_0(Qa) = [3j_1(Qa)/(Qa)]^2$$

where $j_1(Qa)$ is the first order spherical Bessel function.

Two different configurations, corresponding to two instrument resolutions of the spectrometer Mibémol allow the evaluation of the two Lorentzians. With the lowest resolution, the only motions that can be observed are those of the class c) of hydrogen atoms. In this case, atoms of class b) are seen as if they were immobile and the scattering function is:

$$S(Q, \omega) = [P + (1-P)A_0(Qa)]\delta(\omega) + (1-P) \times (1-A_0(Qa))L_2(\omega)$$

where $P = p + q(1-p)$.

The first term is an experimental elastic incoherent structure factor (EISF). Its asymptotic value at large values of Q is equal to P and, because p is deduced from the chemical composition, the different fractions of water molecules are experimentally determined. The molecular motions are deduced from the width of the Lorentzians. In figure 2 the experimental EISF for hydrated ds-DNA and ss-DNA are plotted as a function of Q .

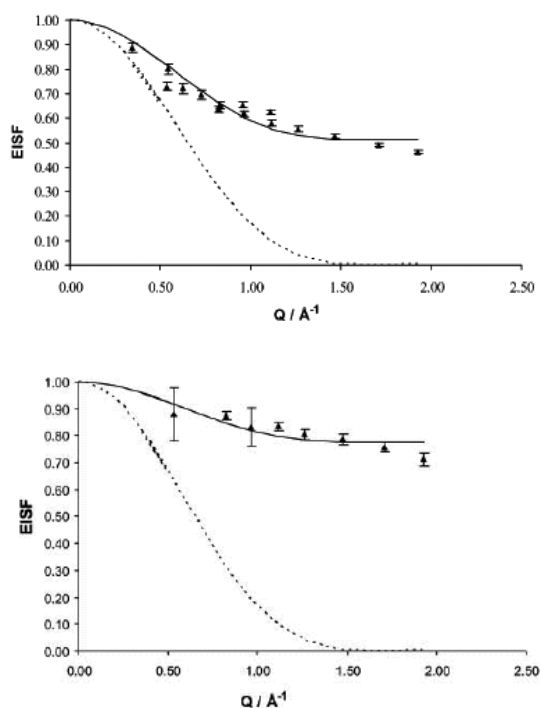


Figure 2. EISF for ds-DNA (upper plot) and ss-DNA (lower plot). Symbols are experimental points, the solid lines are the experimental fit and the dotted lines represent the function $A_0(Q, \omega)$ with $a=2.8 \text{ \AA}$.

The following values of p and q can be deduced:

	ds	ss
p	0.32	0.78
q	0.28	0.0

The half-width at half-maximum $\Gamma_{1/2}$ of the Lorentzian $L_2(Q, \omega)$ is plotted in Figure 3 for ds-DNA. The effect of confinement is clearly seen, because at small values of Q the line-width goes to a constant value. The model of confined motion [3] gives the value of the self-diffusion constant $D = 2.37 \times 10^{-5} \text{ cm}^2 \text{ s}^{-1}$, very close to the self-diffusion of bulk water, but the radius of the sphere of confinement is $a=2.8 \text{ \AA}$, what means that the dynamics of the water molecules is reduced to rotational and diffusive motions along distances of the order of magnitude of the molecular size.

References

- [1] S.K. Pal, L. Zhao and A.H. Zewail, *Proc. Natl. Acad. Sci. USA* **100**, 8113 (2003).
- [2] G.M. Mrevlishvili, A.P.S.M.C. Carvalho, M.A.V. Ribeiro da Silva, T.D. Mdzinarashvili, G.Z. Razmadze and T.O. Tarielashvili, *J. Therm. Anal. Cal.* **66**, 133 (2001).
- [3] F. Volino and A.J. Dianoux, *Mol. Phys.* **41**, 271 (1980)

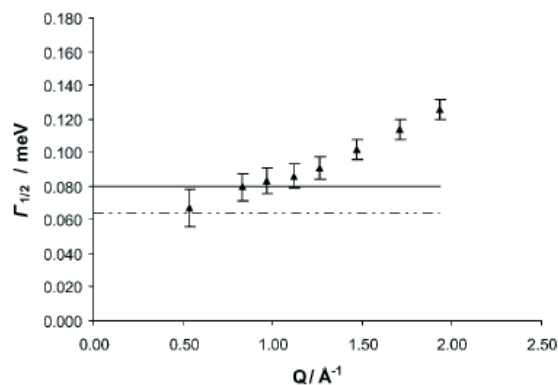


Figure 3. Half-width at half-maximum of the broader Lorentzian for ds-DNA.

Instead, the Lorentzian $L_1(Q, \omega)$ is absent for the sample ss-DNA, what corresponds to the absence of water molecules strongly bounded and is in agreement with the value of $q=0$ deduced from the Q dependence of the EISF.

Finally, the value $q=0.28$ obtained for ds-DNA (see Table above) corresponds to $0.16 \text{ g H}_2\text{O/g DNA}$, i.e. almost exactly the value deduced by calorimetry for the water release in the transformation ds-ss.

We conclude that, at this limiting hydration value (B-DNA) two types of water molecules are present in ds-DNA. About 72% of hydration water is confined, probably inside the grooves, with a local diffusion coefficient D not very different from that of bulk water. The remaining hydration water (28%) is strongly attached to the ds-DNA. Its dynamic is very slow, probably reduced to reorientations resulting from hydrogen bond dynamics. This water is lost upon ds-DNA thermal denaturation, demonstrating that the thermal transition between ds-DNA and ss-DNA is accompanied by disruption of the ordered water fraction in the inner hydration of the double helix and stresses the importance of hydration effects on the maintenance of the double-helix structure.

DIFFUSION OF WATER IN HALOPHILIC ARCHAEA

K. Wood^{1,2}, S. Longeville³, B. Franzetti⁴, M.-C. Bellissent-Funel³, D. Oesterhelt², G. Zaccai^{1,4}, M. and B.-Z. Ginzburg⁵

¹ Institut Laue Langevin, Grenoble

² MPI für Biochemie, Martinsried, Germany

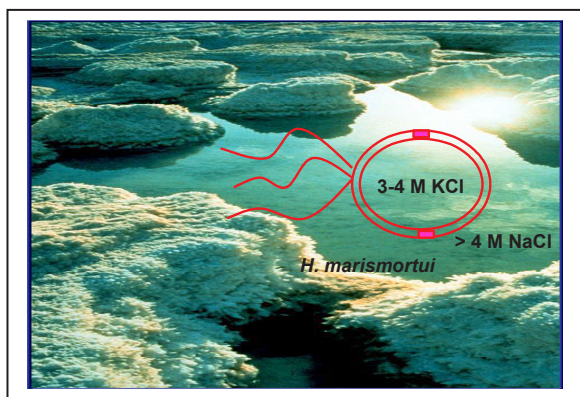
³ Laboratoire Léon Brillouin (CEA/CNRS), Saclay

⁴ Institut de Biologie Structurale (CEA/CNRS/UJF), Grenoble

⁵ Institute of Life Sciences, Hebrew University, Jerusalem, Israel

Although acknowledged as an essential part of all cells, very little is known about the properties of intra-cellular water. Most cell functions require the diffusion of either macromolecules or smaller solutes through the highly crowded aqueous cell compartments. What are the characteristics of this intra-cellular water? In what way does its interactions with many surfaces modify its dynamics?

These questions have mostly been studied by NMR and dielectric measurements and the values found by different groups have been subject to much controversy. Previous work by Ginzburg and collaborators concluded on a very different cytosolic environment for *Haloarcula marismortui* (*Hm*) compared to other organisms [1].



The “Dead” sea, where *Haloarcula marismortui* thrive in 4 molar salt

Neutron scattering has been used to investigate water dynamics since the early days of the method [2]. More recently it has been used to probe confined water [3], water associated with proteins [4], and the average internal dynamics of proteins in whole cells [5]. Here it provides a particularly well-adapted tool to probe the dynamics of water in the highly crowded cytoplasm ‘in vivo’.

Spin echo spectroscopy is unique in providing information directly in the time domain, as compared to other types of neutron spectroscopy where the signal is measured in energy. The

instrument resolution is not convoluted with the signal, but simply multiplied and we can directly observe the distribution of characteristic times in the sample.

In spin echo spectroscopy the polarisation measured is proportional to the coherent contribution minus one third of the incoherent contribution. Using a completely deuterated system is therefore of great interest. Since the signal is dominated by coherent scattering, it is possible to clearly identify the water peak around 1.9 \AA^{-1} . In such a complex system as a biological cell, it is important to be sure the signal measured is in fact dominated by water, and by choosing Q values on this peak means that the signal mainly arises from the diffusion of D_2O molecules.

Hm are halophilic archae (organisms which are neither eukaryotes, nor bacteria, but share characteristics with both of these organisms) living in almost saturated salt. Mechanisms for adaptation to such salt concentrations have created much interest [6]; *the aim of this project is to study the dynamics of water in this almost saturated in salt cytoplasm.*

To take full advantage of the spin echo technique, we have succeeded in cultivating deuterated *Hm* cells. These were then harvested, washed in a deuterated buffer, and layered in an aluminium sample holder. This fully deuterated system was then measured on g1bis at the LLB, to determine the dynamics of water in the cytoplasm. The spectra were compared to that of the deuterated buffer in which the cells are washed, to check that the effect observed is not only due to the high salt concentration.

We first checked that the D_2O peak is present in the cell samples (see figure 1) and then performed quasi-elastic spectra at Q values on the D_2O peak.

The buffer, which is almost saturated in NaCl, is slightly slowed down in comparison to pure D_2O (see figure 2). The intracellular water is however slowed considerably more: a fit with a stretched exponential yields a characteristic diffusion time which is a factor of ten longer than for that of bulk.

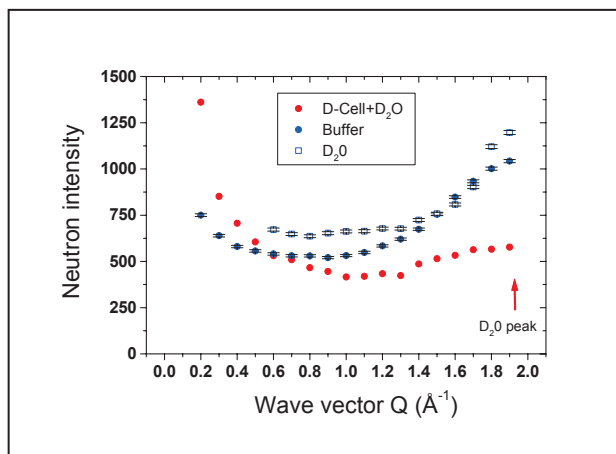


Figure 1. scattering function measured on g1bis. (pure D₂O in empty blue squares, buffer (D₂O with 4M NaCl) in full blue diamonds, and Hm cells in red.)

The feasibility of this study has been shown in this experiment, and we now expect to improve statistics with a larger quantity of deuterated cells in future beam time, and also to examine the Q dependence of the characteristic diffusion time.

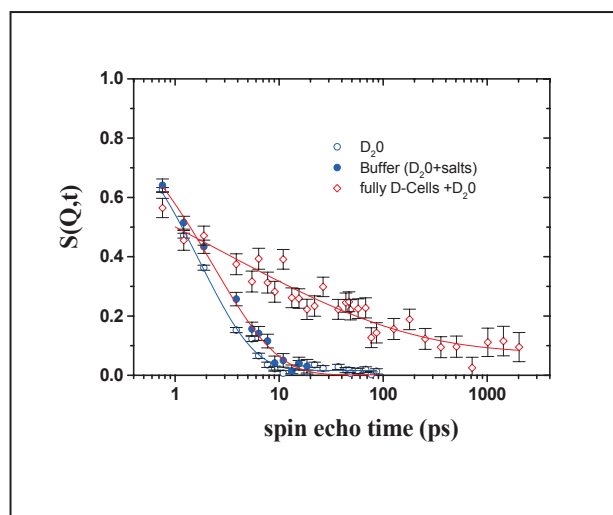


Figure 2 : spectra at $Q = 1.7 \text{ \AA}^{-1}$ on g1bis, pure D₂O in empty blue circles, buffer (D₂O with 4M NaCl) in full blue circles, and Hm cells in red.

Our next aim is to determine if this slowing down of water is specific to these archaic halophiles, or if it is a general property of intracellular water.

References

- [1] Ginzburg B.Z. (1991). Bioenergetics of H.halobium and H. marismortui, In:General and applied aspects of halophilic microorganisms. F.Rodriguez-Valera ed. Plenum Press New York.
- [2] Egelstaff P.A. (1965) Thermal Neutron Scattering. Academic Press. London and New York.
- [3] Bellissent-Funel MC. (2003) Status of experiments probing the dynamics of water in confinement. *Eur Phys J E Soft Matter*. 12(1):83-92
- [4] Bellissent-Funel M. C., Teixeira J., Chen S. H., Dorner B., Middendorf H. D., Crespi H. L. (1989). Low-frequency collective modes in dry and hydrated proteins. *Biophys. J* 56, 713-716.
- [5] Tehei M, Franzetti B, Madern D, Ginzburg M, Ginzburg BZ, Giudici-Ortoni MT, Bruschi M, Zaccai G. (2004) Adaptation to extreme environments: macromolecular dynamics in bacteria compared in vivo by neutron scattering. *EMBO Rep*. 5(1), 66-70
- [6] Irimia A, Ebel C, Madern D, Richard SB, Cosenza LW, Zaccai G, Vellieux FM. (2003) The Oligomeric states of Haloarcula marismortui malate dehydrogenase are modulated by solvent components as shown by crystallographic and biochemical studies. *J Mol Biol*. 21;326(3):859-73.

STRUCTURE OF PROTEINS-POLYELECTROLYTE COMPLEXES

F. Cousin¹, J.Gummel¹, I. Schmidt², C. Huchon¹, F. Boué¹, M. Axelos²¹Laboratoire Léon Brillouin, CEA-CNRS, CEA Saclay, 91191 Gif sur Yvette, France²INRA, Laboratoire de Physico-Chimie des Macromolécules, Rue de la Géraudière, BP 71627, 44316 Nantes cedex 03, France

We wish here to show how useful can be the combination of a “in-house” work, which involves synthetic polyelectrolyte material allowing deuteration labelling, with the work of an external team, at INRA, on natural polyelectrolytes, namely polysaccharide.

Understanding the mechanisms driving the formation of complexes of polyelectrolytes and proteins of opposite charges complexes is of a fundamental importance as such complexes are often encountered in biological or industrial situations [1]. The sum of interactions in the system is generally dominated by electrostatic interactions and their screening by salt, but hydrophobic interactions or Van der Waals interactions can also be involved. This results in a large variety of morphologies for the macroscopic structures of complexes solutions. The system can be monophasic or diphasic. Such phases can be either clear, either turbid, either form a solid-like precipitate. From a rheological point of view, phases can be either fluid, either form a gel.

There is nevertheless a lack of knowledge on the local structure of both polyelectrolytes and proteins in the inner complexes, *i.e* at the protein scale, as complexes are essentially experimentally studied by means of rheology, pH titration, titrimetry, turbimetry, light scattering. We show here that Small Angle Neutron Scattering (SANS) is a powerful relevant technique to reveal the structure of the complexes as it provides a direct access to the different length scales of the system sizes.

As a protein, we used here lysozyme, a small globular protein positively charged in acidic medium (its isoelectric point is 11.2). As polyelectrolytes, we used two different negatively charged polyions:

(i) first we use a synthetic deuterated polyelectrolyte (PSSNa) to unravel the main features of the structures that can be obtained. The contrast method allows to get the specific structures of the individual components within the complexes. (ii) In a second time, we focus on the influence of the electrostatic parameters that control the inner structures of complexes made with biological polysaccharides (pectin) that are of an industrial interest for food formulation.

Revealing the main features of complexes: PSSNa and lysozyme: using deuteration to play on contrasts.

In this first part lysozyme is mixed with PSSNa, a polyelectrolyte with an hydrophobic backbone and a small stiffness. At the pH of our study (4.5), each repetition unit bears a negative charge. In all experiments described, PSSNa chains are in semi-dilute regime and the negative charges provided by PSSNa are in excess compared to the positive charges provided by lysozyme.

PSSNa chains are fully deuterated. Solutions of lysozyme and PSSNa are firstly prepared by dissolution in an acetate/acetic acid buffer ($5 \cdot 10^{-2}$ mol/L) that maintains the pH at 4.5. Both solutions are then mixed and homogenized with a vortex for few seconds and left at least two days before SANS measurements. For each lysozyme/PSSNa ratio two samples were prepared : one in D₂O that matches the neutronic PSSD contrast and one in a 57%/43% H₂O/D₂O mixture that matches lysozyme neutronic contrast.

When mixture is achieved a turbid solution that strongly scatters light is instantaneously obtained. If the excess charge is low (here [lysozyme] = 40g/L; [PSSNa] = 0.1Mol/L that corresponds to [+]/[-] = 0.3), solutions remains turbid with time. Complexes made with short chains length are fluid though they form gels with long chains. If the excess charge is large ([lysozyme] = 20g/L; [PSSNa] = 0.3Mol/L that corresponds to [+]/[-] = 0.05), samples progressively become clear with time. Samples that were originally gelled turn back liquid. The scale time of this clarification lies from some hours to a few days.

Figure 1 presents spectra obtained for a low excess of charge. For small chains (N=120), the spectrum of protein within the complexes (Fig 1.a, blue curve), is similar to the one of protein alone at large q (see form factor). But it shows a peak at $q \sim 0.2 \text{ \AA}^{-1}$. Its abscissa corresponds to protein-protein contact. At lower q the strong slope part can actually be divided in two regions : a q^{-4} law characteristic of scattering from the surface of a large dense object, followed at the lowest q by a $q^{-2.5}$ suggesting a fractal structure. Complexes look as compact objects made of several hundreds of

proteins arranged at larger scale in a kind of ramified clusters. Spectrum where polyions are

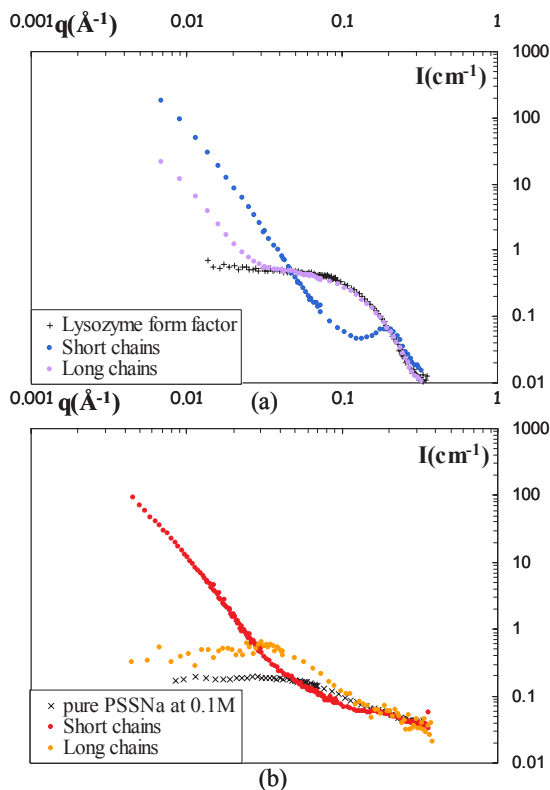


Figure 1. low charge excess ([lysozyme] = 40g/L; [PSSNa] = 0.1Mol/L) (a) Lysozyme signal (b) PSSNa signal

seen inside the complexes (Fig 1.b, red curve) is strikingly different from the one for pure polyions : the corresponding structure of the polyion solution has vanished. Conversely, it is quite similar to the scattering from protein: this indicates that lysozyme and protein are indeed embedded together inside the large dense complexes. Complexes are formed of dense 3-D objects made of several hundreds of proteins in which the polyelectrolyte plays the role of stickers between proteins. For long chains ($N = 620$), the protein signal (Fig 1.a, purple curve) is completely different as for short polyions: there is no more correlation peak at $q \sim 0.2 \text{ \AA}^{-1}$ thus no more contact. Dense aggregates have vanished, as confirmed by the low q law ($q^{-2.5}$) typical of fractal clusters, the latter are connected into a macroscopic gel. Looking now at the scattering from polyions (Fig 2.b, orange curve), we see that for long chains, it is close to the pure polyion one, with a similar maximum. The proteins are stuck on the polyions, which still form a chain network as in polyelectrolyte semi-dilute solution. However the maximum abscissa is lower here: this suggests a shrinking of the chains provoked by the proteins. We propose that part of the chain length is now looped around the protein. Complexes behave like

charged polymeric networks in which proteins play the role of crosslinkers.

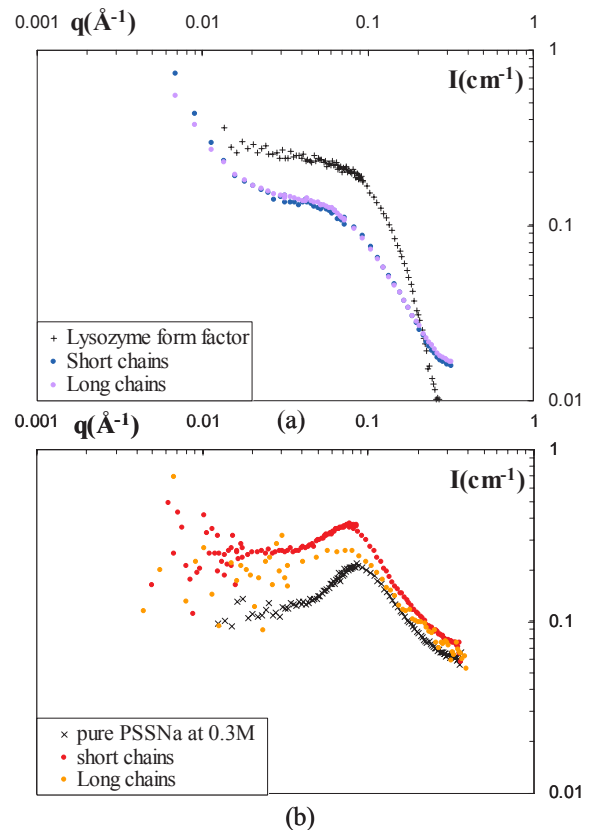


Figure 2 : low charge excess ([lysozyme] = 20g/L; [PSSNa] = 0.3Mol/L) (a) Lysozyme signal (b) PSSNa signal

Figure 2 present spectra obtained for a large excess of charge. All samples have turned clear. The chain length is no longer important. The most striking is the scattering of protein at large q (Fig 2.a), which varies as $q^{-1.7}$ instead of q^{-4} . This is typical of excluded volume chain, and is often observed for unfolded protein. Indeed, FTIR spectroscopy confirm that the α -helix 1654cm^{-1} peak is now absent (it is shifted towards 1645cm^{-1}). Looking at polyelectrolyte (Fig 2.b), we again see a “solution-like” organization, with a maximum shifted to low q compared to pure polyion solutions as in Fig. 1b. This can here also be due to some shrinking of the chain. A second striking fact is the location of this peak. It is located at the same q as the shoulder shown in the protein signal (Fig.2a) The two chainlike objects are now organized in a costructure. For a strong excess of charge, we realize the best situation for the PSSNa to interact with the lysozyme. It can bring its hydrophobic regions in contact with the protein hydrophobic ones and then unfold it.

Inner structure of complexes: what we can see without deuteration, the pectin example.

In this second part lysozyme is mixed with pectin, a polysaccharide with a hydrophilic backbone and

a large stiffness. Its charge density can be changed through a chemical composition of the backbone : each monomer can bear either a methyl group either a dissociable carboxylic group that provide a negative charge for $\text{pH} > 3$. In all experiment described pectin chains are in dilute regime. In order to vary the strength of electrostatic interactions, we vary either the pH to vary lysozyme charges at constant pectin charge (it has a global net charge $Z = +15$ at $\text{pH} 3.5$, $Z = +10$ at $\text{pH} 5$ and $Z = +8$ at $\text{pH} 7$), either the degree of methylation (DM) to vary pectin charged at constant pH.

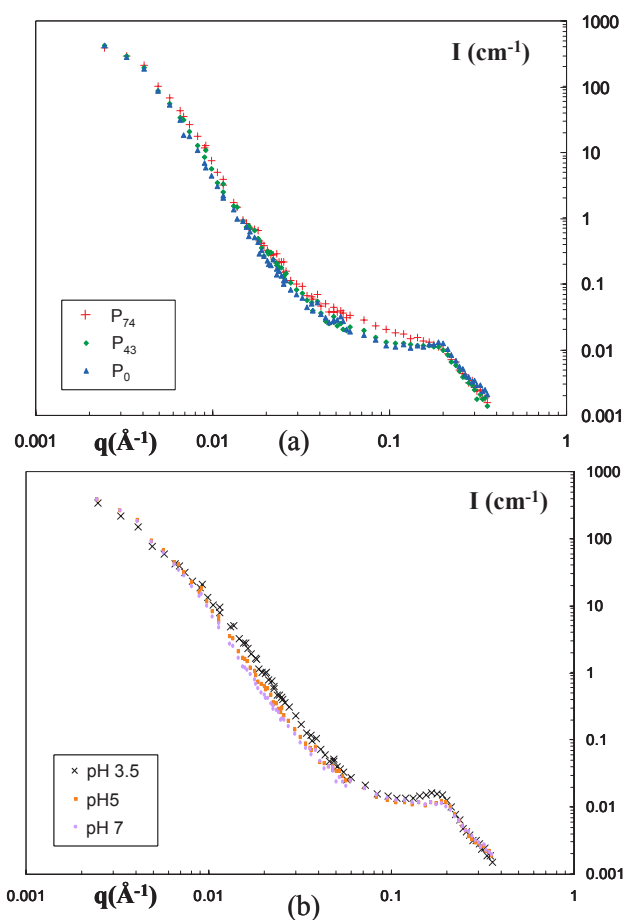


Figure 3. (a) Pectin charge variation signal (b) Lysozyme charge variation

Samples are realized with the same method as lysozyme/PSSNa mixtures. Here we use a mixture of KH_2PO_4 and $\text{Na}_2\text{HPO}_4 \cdot 2\text{H}_2\text{O}$ with a global ionic strength of $2.5 \cdot 10^{-2}$ mol/L. pH is adjusted with NaOH. All samples have been realized in pure D_2O with $\Phi_{\text{lysozyme}} \sim \Phi_{\text{pectin}} = 0.003$. Whatever the conditions, a turbid solution that strongly scatters light is instantaneously obtained. If left at rest, some samples demix between a turbid liquid phase and precipitate on a scale time of a week. The complexes size slowly grows with time, up to final sedimentation. Mixtures of complexes are thus out

of equilibrium on such a time scale and the kinetics of their evolution is a two-steps process: (i) a first fast complexation of lysozyme and pectin followed by (ii) a slow aggregation. All SANS measurements have been performed after two days on macroscopically homogeneous solutions. Figure 3 presents all SANS spectra obtained by varying pH and DM. They all present the same features as spectrum measured on lysozyme/PSSNa mixtures for short chains and low excess charges. $I(q)$ decreases as q^{-4} at large q due to the globular form factor of the lysozyme. There is a correlation peak that corresponds to protein-protein contact around 0.2 \AA^{-1} . All spectra present a correlation peak that corresponds to protein-protein contact. At low q , the intensity scatters again as q^{-4} . As one probes scales much larger than the lysozyme scale, this q^{-4} behaviour, typical of scattering form factor of a 3-D shaped object, arises from the form factor of the 3-D shaped complexes. At very small q , the q^{-4} scattering law vanishes and the intensity present a shoulder.

In order to go further and to get the size and inner volume fraction of the complexes, we plot $I(q)q^4$ as a function of q (figure 4). Two plateaus appear. For each q range where $I(q)$ scatters as q^{-4} , the Porod law can be applied. $I(q)q^4/2\pi$ should present a plateau that equals $\Delta\rho^2 S/V$ where S/V is the total specific area of the objects probed at the scale of the q range. At large q , it provides the specific surface of lysozyme within the complexes. At low q , the plot of $I(q)q^4 / 2\pi$ presents two features : a peak followed by a plateau (figure 4). The peak position is linked to the complex size and the plateau value to its specific surface. Assuming spherical complex, the peak arises at the maximum of $P_{\text{comp}}(q)q^4$ where $P_{\text{comp}}(q)$ is the form factor of a spherical complex of radius R_{comp} . The maximum enables to get R_{comp} .

$$P_{\text{comp}}(q) = \left(3 \frac{(\sin qR_{\text{comp}} - qR_{\text{comp}} \cos qR_{\text{comp}})}{(qR_{\text{comp}})^3} \right)^2 \quad (1)$$

From the plateau value of $Iq^4/2\pi$ the complexes contrast $\Delta\rho_{\text{comp}}^2$ can be deduced by assuming complexes as perfect monodisperses spheres. The Porod radius R_p of complexes (where the specific area of complexes is $3/R_p$) equals its real radius R_{comp} . If Φ_{comp} is the volume fraction occupied by the complexes, we get :

$$\Delta\rho_{\text{comp}}^2 = Iq^4 R_{\text{comp}} / ((1-\Phi_{\text{comp}})\Phi_{\text{comp}} 2\pi 3)$$

The contrast $\Delta\rho_{\text{comp}}^2$ can be written as a function of the volume fraction of lysozyme Φ_{lyso} and of pectin Φ_{pectin} and their respective neutron length densities ρ_{lyso} and ρ_{pectin} and we obtain the volume fraction of water in complexes $\Phi_{\text{D20,comp}}$:

$$\Phi_{D2O_comp} = \frac{1}{1 + \frac{Iq^4 R_{comp}}{2\pi^3} - (\Phi_{lyso} + \Phi_{pectin})} - (\Phi_{lyso} + \Phi_{pectin}) \quad (2)$$

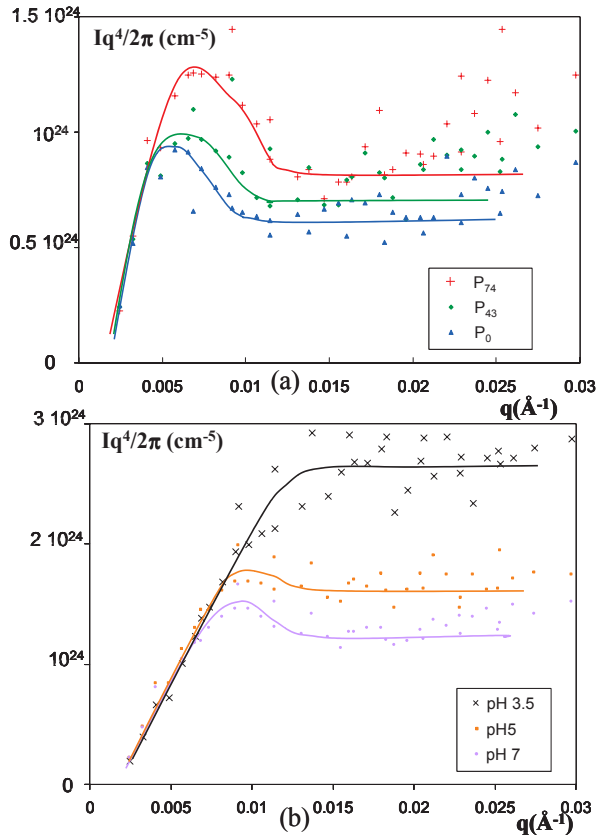


Figure 4 : $I(q)q^4$ versus q (low q) (a) Pectin charge variation signal (b) Lysozyme charge variation. Lines are guides for the eye.

As complexes are dense spheres, the intensity scattered by the complexes writes :

$$I(q) \text{ (cm}^{-1}\text{)} = \Phi V_{comp} \Delta\rho_{comp}^2 P_{comp}(q) S_{comp}(q) \quad (3)$$

where n is the object density (cm^{-3}), $\Delta\rho_{comp}^2$ the contrast (cm^{-4}), V_{comp} the complexes volume (cm^3), $P_{comp}(q)$ the form factor and $S_{comp}(q)$ the structure factor. $S_{comp}(q)$ can thus be valued from $I(q)$. $P_{comp}(q)$ is calculated according to equation 1. $S_{comp}(q)$ is linked to the interactions between

complexes. Whatever the system, it is superior to 1 and strongly increases when $S(q)$ tends to 0, indicating then a high compressibility in the complexes solution. There are thus **effectives attractions** between the complexes. The interactions strength can be valued through the compressibility. The latter evaluation is achieved by the measure of the correlation length of the density fluctuations in the system, Ξ , fitting to $S(q) \sim 1/(1 + q^2\Xi^2)$ at low q . Table 1 gives values ranging from 450Å to 150Å.

Sample	Φ_{comp}	R_{comp} (Å)	Ξ (Å)
pH 3.5	~ 0.35	~ 230	450
pH 5	0.25	280	310
pH 7	0.21	310	320
P_0	0.17	480	175
P_{43}	0.17	420	230
P_{74}	0.175	400	160

Table 1. Structural parameters of complexes

These results can then be used to understand the formation of complexes. We can see the complex as a network of pectin chains cross-linked by lysozyme. The latter controls the number of cross-links ν in the network. Like in a charged polymer gel, the swelling trend due to repulsion between charged units is limited by the network elastic modulus, proportional to ν . The inner volume fraction of complexes, i.e. gel swelling appears controlled by lysozyme, hence by ν , and not by pectin electrostatic repulsion. Pectin charge density plays nevertheless a huge role on the final size of complexes and on their effective interactions. This can be due to the fact that increase of pectin charge density: (i) increases complex radius by increasing electrostatic interactions with positive charges at the nucleation stage (ii) decreases attraction between larger complexes by increasing the electrostatic repulsive part of the interaction potential in a later maturation stage.

Reference

[1] C.Tribet, Surfactant Science Series “Physical chemistry of polyelectrolytes”, T. Radeva Ed., M. Dekker, 99, 2000 chap 19, 687.

6 - MODELLING

6 - MODELLING

In this modelling section, we present recent development of the theoretical and numerical tools that have been developed at the LLB to predict, calculate, reduce and interpret neutron scattering spectra. The ability of neutron scattering to bring key evidences and answers to a large spectrum of scientific domains is strongly correlated with the progress made in various fields of modelling. Except pure theory that is the ultimate modelling tool, these scientific and technical efforts can be separated in three main categories:

- Provide efficient User Interfaces to fitting programs for neutron users (FULLPROF SUITE)
- Develop more realistic models and simulations (MATERIAL SCIENCE)
- Perform accurate simulations of physical systems (MOLECULAR DYNAMICS)

This chapter spans the whole spectrum of LLB research activity, from hard-condensed matter theory to material science and Molecular Dynamics simulations in life sciences. The “Magnetism and Superconductivity” chapter has described the experimental results obtained in the field of High T_C superconducting-materials. The scientific research at LLB is closely connected to the theoretical efforts performed in-house, see below and Highlight F. Onufrieva. A team from the “Centre de Biophysique Moléculaire” of Orléans had joined the LLB in order to combine, in an efficient way, Molecular Dynamics and experimental neutron scattering data in Life Sciences. Indeed, The LLB access to the new LINUX cluster farms has provided an inexpensive source of interactive, single-processor flops (floating-point operations per second), a source of batch flops during off hours and a source of multiprocessors for parallel Molecular Dynamics simulations. This new type of hardware calls for improved software methods. Take a look at the last paragraph of this introduction and at Highlight G. Kneller.

THEORY OF STRONGLY CORRELATED ELECTRONIC SYSTEMS

a) Chemical reactions and electronic transfer reactions

Electron Transfer (ET) reactions are central to many biological processes and are also of interest to the growing community interested in molecular electronics. Traditional theoretical descriptions of ET in condensed phases have focused on systems either in the high temperature limit, where nuclei can be treated classically, or in the low temperature and small electronic coupling limit, in which case nuclear modes are approximately harmonic and Fermi's Golden rule is valid. Exact, fully quantum mechanical description of complex systems in more general temperature and coupling regimes is not computationally feasible, and as a result, many studies of these regimes have utilized semiclassical approximations. Equally important is the fact that traditional rate expressions, based on the assumptions of small and constant electronic coupling or the assumption of nuclear thermal equilibrium, cannot be relied upon in the case of ultrafast ET reactions.

Understanding the role that these resonances play in chemical reactions is crucial to our basic understanding of all chemical reactivity. See Highlight S. Aubry.

b) Superconductivity

In transition-metal oxides, d-electrons experience competing forces: Coulombic repulsion tends to localize individual electrons at atomic lattice sites, while hybridization with the oxygen p-electrons tends to delocalize the electrons. These strong correlations between electrons are a central unifying factor in a wide range of phenomena, such as high temperature superconductivity, colossal magnetoresistance, the quantum Hall effect, heavy fermions and Coulomb blockade in single-electron transistors. In a large number of systems, non-Fermi liquid behaviour is replacing the Fermi liquid paradigm. The current theoretical research at the LLB focuses mainly on transitions between different ground states of a many-particle system as function of doping either with holes or with electrons. Prominent examples are phase transitions between a magnetic state at low doping and a nonmagnetic one and then a superconducting state at higher doping in the High T_C superconducting-materials. The correlation problem can be attacked with various demanding numerical and field-theoretical techniques: Exact diagonalization, Quantum Monte Carlo, Mori Zwanzig projection technique, cumulant techniques, Dynamical mean field theory and so on. See Highlight F. Onufrieva.

CRYSTALLOGRAPHY AND DATA REDUCTION IN DIFFRACTION : Recent improvements of the FULLPROF SUITE and the new FULLPROF STUDIO for visualising crystal and magnetic structures

Juan Rodríguez-Carvajal, Lab. Léon Brillouin, CEA/Saclay 91191 Gif sur Yvette Cedex, FRANCE,
Laurent C. Chapon, ISIS facility, RAL-CCLRC, Chilton, Didcot, Oxfordshire, UNITED KINGDOM,
Javier González-Platas, Departamento de Física Fundamental II, Universidad de La Laguna Tenerife, SPAIN,
Aziz Daoud-Aladine, Paul Scherrer Institut, SINQ CH-5232 Willigen, SWITZERLAND,
Thierry Roisnel, Lab. de Chimie du Solide et Inorganique Moléculaire, UMR6511, CNRS-Univ. Rennes I, FRANCE,
Carlos Frontera, Instituto de Ciencia de Materiales de Barcelona (CSIC), Universidad Autónoma Bellaterra, SPAIN

The **FULLPROF SUITE** is a combination of data analysis and simulation programs among which the couple **WINPLOTR** and **FULLPROF** [1-2] constitutes one of the most popular Rietveld refinement tools. These programs are used worldwide for the analysis of powder diffraction data. The treatment of incommensurate magnetic structures is one of the specialities of **FULLPROF** that other programs cannot handle [3]. During the last two years we have improved the Crystallographic FORTRAN Modules Library (**CRYFML**) [4], which is the development framework of the full suite of programs we are distributing. Here we provide a detailed summary of the recent work done in different parts of the source code. See also Highlight M. Casas-Cabanas.

a) FullProf

During 2004, the collaboration between the LLB and ISIS, the English spallation source, concerning data analysis has been strongly developed and enhanced. Several improvements concerning the analysis of Time of Flight (TOF) powder and single crystal diffraction data have been introduced in **FULLPROF**. In particular the number of different scale factors for treating single crystal data coming from different detectors has been increased up to 24; this allows a quite easy calibration of the detector banks of instruments like SXD at ISIS using a standard single crystal sample.

In powder diffraction, we have improved the calculation of the peak shape functions that allows robust and faster refinements. The technique of simulated annealing to solve crystal and magnetic structures has also been adapted to TOF using multi-banks data. The extraction of integrated intensities, to be used in simulated annealing work, has been improved and adapted to the fact that the most important data from the point of view of structure determination are those of low Q (high TOF) appearing usually at the end of the TOF data files.

In 2004, a new kind of analysis concerning anomalous powder diffraction using synchrotron radiation has been introduced within **FULLPROF**. Thanks to the collaboration with Hervé Palancher and Jean Louis Hodeau (Laboratoire de Cristallographie, CNRS, Grenoble) we have developed new tools for exploiting the information contained in X-ray powder diffraction patterns as a function of the energy. At present **FULLPROF** is able to output calculated and observed “difference anomalous diffraction patterns” and “anomalous Fourier difference maps”. These tools are extremely important when one seeks, for instance, the cationic distribution of different chemical species in zeolites.

b) CrysFGL

The incorporation of Laurent C. Chapon from ISIS to the team working around the **FULLPROF SUITE** has boosted the development of graphics support for diffraction data analysis within suite. A new Fortran library, called **CRYSFGL**, to access OpenGL has been written (Laurent C. Chapon) implementing everything concerned with atoms and magnetic moments. The library uses the symmetry parts of **CRYFML**, to generate all atoms/magnetic moments in a given crystal. The library implements linked list of atoms, magnetic moments and bonds allowing a dynamic loading (construction and destruction) of the different objects in complete interactivity with the user. **CRYSFGL** should be linked with one of the Fortran implementations of OpenGL existing in the market.

At present we can either use GLUT, which is completely free, or Winteracter (**WCRYSFGL**). Programs to visualise structures can be easily developed by using **CRYSFGL**. The first application we have developed is **FULLPROF STUDIO** (Laurent C. Chapon), which allows an automatic representation of the crystal and/or magnetic structure solved/refined by using **FULLPROF**.

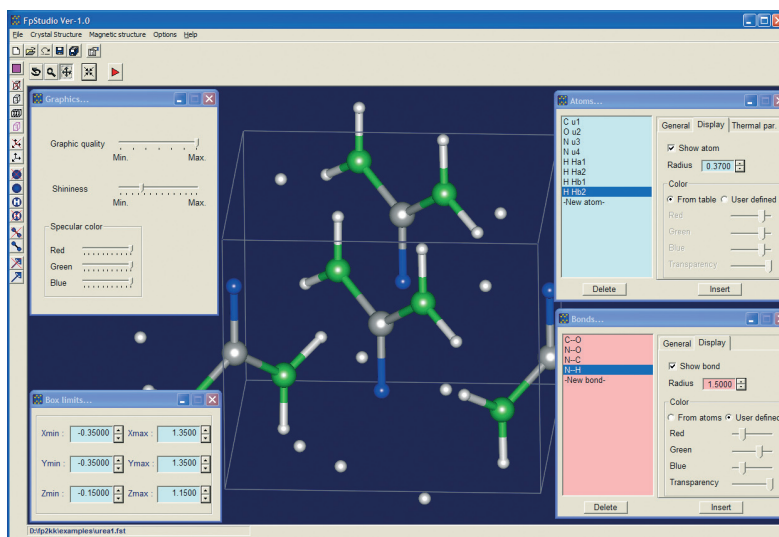


Figure 1: General view of FullProf Studio during a session on the urea structure

This application has been developed as a tool so simplify and understand what is happening in the course of a structure solution by simulated annealing or a refinement by least squares, however high quality graphics can be generated selecting the appropriate parameter in the **FULLPROF STUDIO** menu. Examples of such graphics visualisations are provided in the following figures and pages.

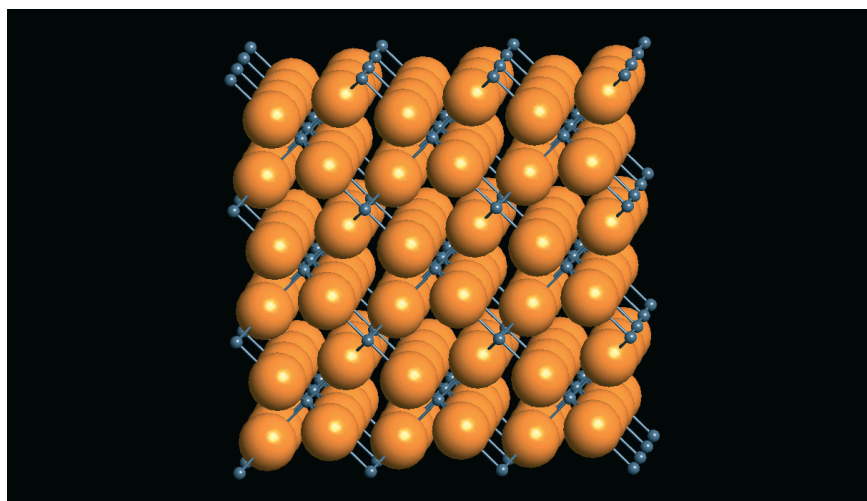


Figure 2: Oxygen packing representation of rutile TiO_2 structure

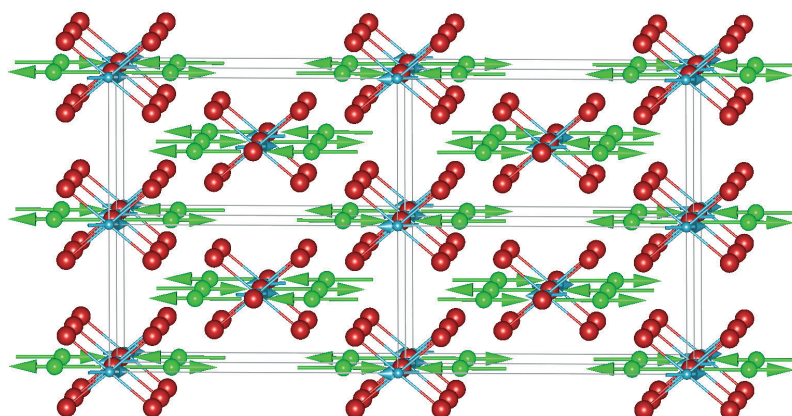


Figure 3: Magnetic structure of $\text{Ho}_2\text{BaNiO}_5$ as saved in a bitmap picture.

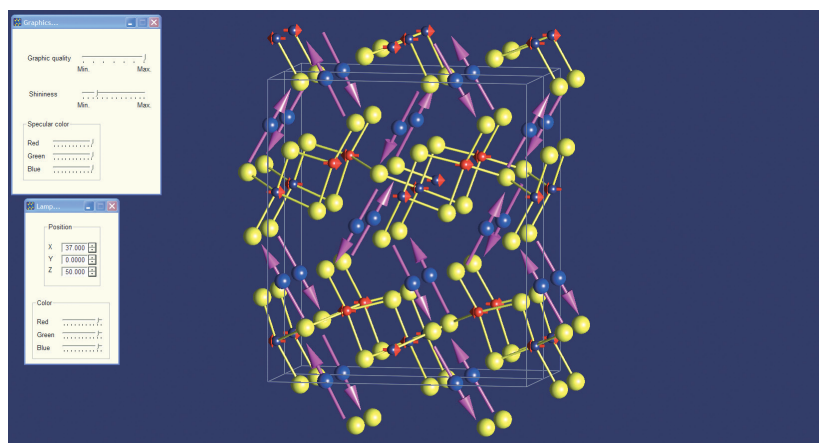


Figure 4. Changing the orientation of the illuminating lamp and graphic quality in a representation of the magnetic structure of $\text{Ho}_2\text{Cu}_2\text{O}_5$.

Other important changes have been performed within the graphical interface program, **WINPLOTR** - instrumental resolution function files, TOF, access to **FULLPROF STUDIO**, access to the new version of DICVOL 2004, Fourier filtering, etc.- and **BASIREPS**, a program for calculating basis functions of irreducible representations of space groups. See the documents within the **FULLPROF SUITE** [2] for details.

c) CrysFML

The first version of **CRYSFML** contained procedures for reading data files of many different formats, string utilities for handling the reading in free format, generation and reading of CIF files, mathematical procedures, and modules for generating space groups from their Hermann-Mauguin, user-defined generators or Hall symbols for whatever setting. Also reflection handling modules for generating reflections in selected regions of reciprocal space and for calculating structure factors were incorporated into the library. More recently we have developed a special module for calculating structure factors of incommensurate crystal structures. This is under testing and we seek the creation of a general module handling symmetry in high dimensional spaces (Aziz Daoud-Aladine).

We have also developed a module, called “Molecular_Crystals”, that is able to handle all geometrical aspects of molecules in crystals. This is the basis for the new rigid body option to be implemented in **FULLPROF** and also for the Molecular Editor (EdMol, Javier González-Platas) and Structure Determination program (StructRes, Javier González-Platas & Juan Rodríguez-Carvajal) that we are currently developing. The molecules can be described using different options, in particular the Z-matrix formalism: the free parameters are the distances, bond angles and torsion angles. This is extremely useful for the structural analysis of pharmaceutical compounds.

References on Crystallography and data reduction in diffraction

- [1] “WinPLOTR: a Windows tool for powder diffraction patterns analysis” T. Roisnel and J.Rodríguez-Carvajal, *Materials Science Forum* **378-381**, 118-123 (2001).
- [2] “Recent developments of the program FullProf”, Juan Rodríguez-Carvajal, *Commission for Powder Diffraction, IUCr Newsletter* **26**, 12-19 (2001).
The complete FULLPROF SUITE can be obtained from <ftp://ftp.cea.fr/pub/llb/divers/fullprof2k/>.
- [3] “Magnetic structure determination from powder diffraction. Symmetry analysis and simulated annealing” J.Rodríguez-Carvajal, *Materials Science Forum* **378-381**, 268-273 (2001).
- [4] “Crystallographic Fortran Modules Library (CrysFML). *Computing Commission, IUCr Newsletter* **1**, 50-58 (2003), this document is freely accessible via the Internet at <http://www.iucr.org/iucr-top/comm/ccom/newsletters/2003jan/>.

MATERIAL SCIENCES : Monte Carlo modelling of recrystallisation processes in metals and alloys

Quantitative predictions on the microstructure and properties of metals and alloys are on the verge to be obtainable now for computer simulations of recrystallization processes [1]. Simulations can be used to predict the average texture and grain size that strongly affect mechanical behaviour [2]: refining the grain size is a low-cost way to increase both the strength and the toughness of metals. Simulations are a promising

tool to improve our understanding of the recrystallization phenomenon, a highly complex process from a microstructural point of view. The main driving force acting in these processes is the stored energy, resulting from plastic deformation, that can be evaluated from neutron scattering or Electron Back Scattering Diffraction (EBSD) techniques. The microstructural evolution inherent in recrystallization depends on the grain boundary properties, which are sensitive to their detailed crystallographic character. Computer simulation techniques that can take in account the full range of grain boundary behaviour are of great interest.

In order to simulate the recrystallization process, Monte Carlo modelling has been applied to the case of wire-drawn copper deformed to a moderate strain. Several nucleation hypotheses have been introduced and tested into the model.

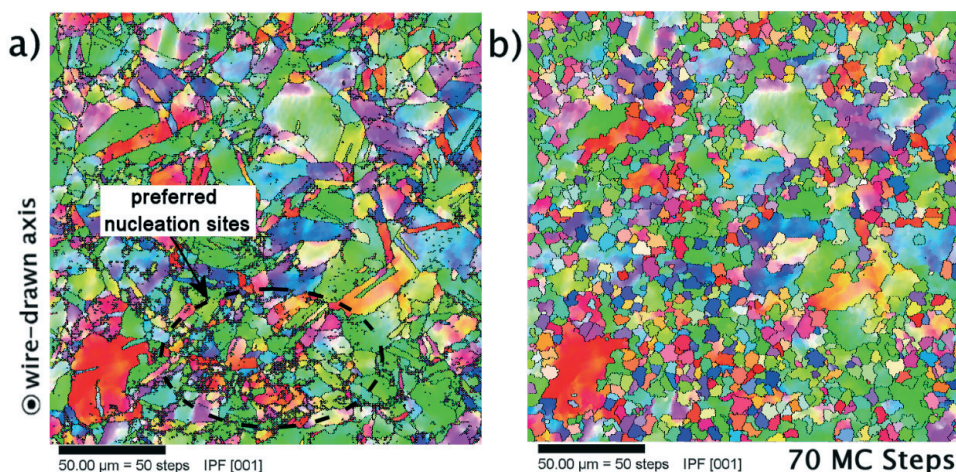


Figure. 5 a) Experimental microstructure of the deformed state measured with EBSD in wire-drawn copper.
b) Microstructure evolution after 70 MC Steps using the nucleation hypothesis connected to the sites with strong misorientation and high stored energy values.

It has been shown that nucleation taking into account the sites associated with the highest stored energy and highest local misorientation leads to the best results in terms of recrystallization microstructure and texture. An important number of new orientations - that come only from annealing twinning - are not reproduced with the model, indicating the major role of this particular mechanism during the recrystallization process. Similar studies have been also performed in cold-rolled IF-Ti steel [3].

- [1] *Monte Carlo Modelling of Recrystallization Mechanisms in Wire-Drawn Copper from EBSD Data*, Ph. Gerber, J. Tarasiuk, D. Solas, S. Jakani, M.-H. Mathon and T. Baudin, *Material Science Forum*, 467 (2004), 635
- [2] *Prédiction de cornes d'emboutissage à partir de données EBSD mesurées dans le cas du cuivre pur* Ph. Gerber, T. Baudin, R. Chiron, B. Bacroix, *MATÉRIAUX & TECHNIQUES - N°10-12 (2004)*, 1
- [3] *Monte Carlo modelling of recrystallization process in cold rolled IF-Ti steel* A. Samet-Meziou, Ph. Gerber, J. Tarasiuk, T. Baudin and R. Penelle, *Material Science Forum*, 467-470 (2004), 635

LIFE SCIENCES : Molecular dynamics simulations in Life Sciences

G.R. Kneller and K. Hinsén, Lab. Léon Brillouin, CEA/Saclay 91191 Gif sur Yvette Cedex, France
G. Sutmann, John von Neumann Institut für Computing, Forschungszentrum Jülich, Germany
J.-J. Lacapère, U410 INSERM, Faculté de Médecine Xavier Bichat, 16 rue Henri Huchard, Paris, France
B. Brutovský, Department of Biophysics, P.J. Šafárik University, Jesenná 5, Košice, Slovakia

a) Interface between Molecular Dynamics simulations and Neutron scattering

nMOLDYN is an interactive analysis tool for Molecular Dynamics trajectories, with an emphasis on quantities related to neutron scattering. The software is developed since several years and a first version has been published in 1995 [1]. nMOLDYN calculates intermediate scattering functions and dynamic structure factors, the EISF, velocity autocorrelation functions and densities of state, angular velocity autocorrelation functions, and mean square displacements. A recent addition is the analysis of molecular trajectories by autoregressive models, which permits in particular the calculation of memory functions. There are also several trajectory transformation functions and visualization aids [2].

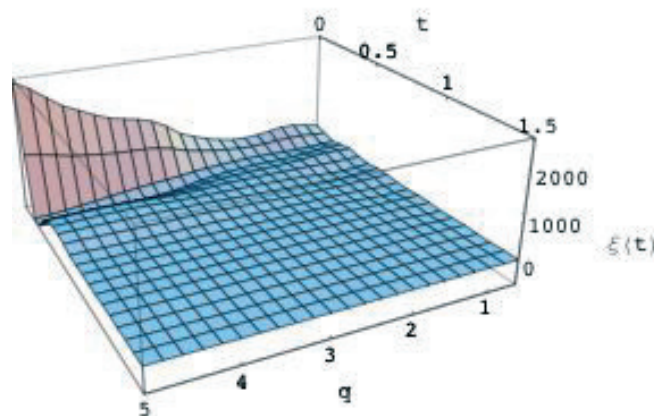


Figure 6. The memory function $\xi(q, t)$ of the coherent intermediate scattering function.

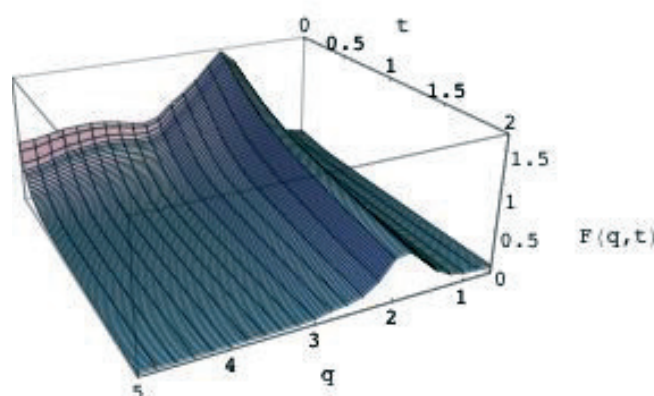


Figure 7. The coherent intermediate scattering function $S_{\text{coh}}(q, t)$.

b) Proteins dynamics: Microhydrodynamics and Fractional Brownian Motion

A characteristic feature of protein dynamics is the presence of a wide range of time scales. Correlation functions describing relaxation processes in proteins exhibit a non-exponential decay. We find that fractional Brownian dynamics is a good model for the internal dynamics of lysozyme in solution as obtained from Molecular Dynamics simulations [3]. Both the dynamic structure factor and the associated memory function fit well the corresponding analytical functions calculated from the model.

In the framework of the bilateral PROCOPE-program (2001-2003), a new collaboration was started with G. Sutmann from *Jülich* on the study of Brownian motion on the molecular level [4]. The idea is to use a new method to compute memory functions from Molecular Dynamics simulations [5] in order to perform systematic studies of the transition from deterministic Hamiltonian mechanics to Brownian dynamics and on hydrodynamic interactions on the microscopic level.

c) Protein structure prediction from electron microscopy data

Electron microscopy provides structural information about biological systems that cannot be studied by X-ray crystallography. However, the resolution of the resulting electron density maps is too low to create models at the atomic level. We have developed a computational method to predict atomic protein structures from electron microscopy data for the frequent case in which an atomic-scale structure is available for another conformation of the same protein [6]. This structure is deformed iteratively until it is compatible as far as possible with the experimental electron density map. The deformation algorithm is based on an evaluation of the local flexibility in different parts of the protein from a simple harmonic potential for a reduced protein model [7].

d) Development of molecular simulation software

In parallel to working on new computational methods for the simulation of molecular systems, we have developed a range of simulation software to make our methods (and others) accessible to the scientific community. This software is continuously maintained and extended, and is freely available for downloading.

The Molecular Modelling Toolkit [8] is a molecular simulation library that provides many standard simulation algorithms (Molecular Dynamics, energy minimization, normal modes) as well as those developed by our group. It also provides lower-level building blocks for implementing new methods, such as the definition of molecules, their manipulation, energy evaluation, and trajectory management. In addition to being used directly by simulation scripts, it can also serve as a basis for writing interactive simulation tools. Scientific Python [9] is a more general library for scientific computing. It contains all the code that is of use in more application areas than only molecular modelling. It provides standard numerical algorithms (e.g. interpolation, least-squares fits) and provides support for geometry, visualization, I/O, GUIs, and parallel computing.

e) Parallel software engineering for scientific computing

Many molecular simulation techniques require a lot of CPU time. Since parallel computers are by now nearly ubiquitous in research environments, and since many molecular simulation algorithms have been parallelized or are very easy to parallelize, one would expect parallel computing to be a standard tool in the molecular simulation community. However, parallel programming is very difficult and time consuming, which discourages most computational scientists from writing their own parallel code.

A big part of the complexity is due to the dominant parallel programming model, message passing. This model offers detailed low-level control over communication to the programmer, but also makes him responsible for all the details, in particular synchronization between processors. Moreover, the most popular message passing protocol, MPI, works only with low-level data structures; transferring complex data such as a protein structure is a very difficult task.

By combining the Bulk Synchronous Parallel model (BSP) with the high-level Python language, a parallel programming environment was produced that permits rapid development through interactive testing and debugging and lets the programmer work on a higher level of communication specification [10]. Moreover, the use of the BSP model eliminates many sources of errors in parallel programming, in particular deadlocks.

f) Development of efficient Molecular Dynamics algorithms

We have recently developed a Molecular Dynamics simulation algorithm in which intermolecular are computed by switching periodically between explicit evaluation and linear prediction from previous values [11,12]. For the moment the method been applied to a simple model liquid consisting of several hundred oxygen molecules in the liquid state. The method yields an effective speed-up of 6-7, keeping all essential structural and dynamical features of the simulated system. The work has been performed in the framework of a Marie Curie Fellowship under contract number HPMF-CT-2000-00470.

References of Molecular dynamics simulations in Life Sciences

- [1] *nMOLDYN: A Program Package for a Neutron Scattering Oriented Analysis of Molecular Dynamics Simulations*, Comp. Phys. Comm. **91**, 191-214 (1995).
- [2] *nMOLDYN: A Program Package for a Neutron Scattering Oriented Analysis of Molecular Dynamics Simulations*, T. Róg, K. Murzyn, K. Hinsen, and G. R. Kneller, J. Comp. Chem. **24**, 657-667 (2003) and <http://dirac.cnrs-orleans.fr/nMOLDYN/>
- [3] *Fractional Brownian dynamics in proteins*, G.R. Kneller and K. Hinsen, J. Chem. Phys., in print
- [4] *Mass and size effects on the memory function of tracer particles*, G.R. Kneller, K. Hinsen, and G. Sutmann, J. Chem. Phys. **118**(12), 5283-5286 (2003)
- [5] *Scaling of the memory function and Brownian motion*, G.R. Kneller and G. Sutmann, J. Chem. Phys. **120**, 1667 (2004)
- [6] *Normal mode based fitting of atomic structure into electron density maps: application to SR Ca-ATPase*, K. Hinsen, N. Reuter, J. Navaza, D. L. Stokes, and J.-J. Lacapère, accepted by Biophys. J.
- [7] *Harmonicity in slow protein dynamics*, K. Hinsen, A.J. Petrescu, S. Dellerue, M.C. Bellissent-Funel, and G.R. Kneller, Chem. Phys. **261**, 25-37 (2000)
- [8] *The Molecular Modeling Toolkit: A New Approach to Molecular Simulations*, K. Hinsen, J. Comp. Chem. **21**, 79-85 (2000), <http://dirac.cnrs-orleans.fr/MMTK/>
- [9] *Scientific Python*, K. Hinsen, <http://dirac.cnrs-orleans.fr/ScientificPython/> 473-484 (2003)
- [11] *Accelerating molecular dynamics simulations by linear prediction of time series*, B. Brutovsky, T. Mülders, and G.R. Kneller, J. Chem. Phys. **118**(14), 2003.
- [12] *Linear Prediction of Force Time Series to Accelerate Molecular Dynamics Simulations*, Special Issue, Comp. Phys. Comm., in print (to appear in 2005).

6 - MODELLING

1. The weakly coupled Rotor-Morse oscillator system: A toy model for selective chemical dissociation. **140**
S. Aubry and A. Memboeuf
2. Spin dynamics of the electron-doped high T_c superconducting cuprates **143**
F. Onufrieva and P. Pfeuty
3. Faults, a new program for refinement of powder diffraction patterns from layered structures **144**
M. Casas-Cabanas, J. Rodríguez-Carvajal, M.R. Palacín
4. Dynamics of lysozyme under pressure seen by molecular simulation and neutron scattering **146**
G.R. Kneller, K. Hinsén, V. Hamon, M.-C. Bellissent-Funel

THE WEAKLY COUPLED ROTOR-MORSE OSCILLATOR SYSTEM: A TOY MODEL FOR SELECTIVE CHEMICAL DISSOCIATION.

S. Aubry and A. Memboeuf

Laboratoire Léon Brillouin, CEA Saclay, 91191-Gif-sur-Yvette, France

In his famous pioneering work published in 1940, Hendrik Kramers understood chemical reactions, as the climbing of an energy barrier between two energy wells in a large configuration space where the first well represents the state of the reactant molecules and the second well those of the product molecules. In standard theories, chemical reactions are still essentially governed by the thermal (Brownian) motion in a potential of a point defined by the reaction coordinates which represents the configuration of the whole system. Many detailed investigations have been performed during the last decades for specific chemical reactions where energy landscape, basin and saddle point in energy (transition states) were accurately calculated.

However, these models assume that the diffusion process in the phase space is incoherent and ignore possible coherent phenomena which could bias the reaction process. Actually, numerous studies show that the polyatomic molecules seen as a set of non-linear coupled oscillators is not an ergodic system, but instead, they form a mixed phase space with regular and chaotic regions [1,2]. Particularly, it is now well-known that spontaneous energy localization may occur in complex molecular systems. Transitions from normal modes (extended motions) to local modes were first observed spectroscopically in molecules. These local modes in finite size systems are known to exist as well in infinite discrete and nonlinear lattices [3,4]. They appear as localized oscillations with large amplitudes well above the thermal noise and may persist out of thermal equilibrium over unexpected long life time. Their existence requires both the discreteness and the nonlinearity of the system but does not require its spatial periodicity. Many open problems concern DNA transcription through bubble opening, protein folding and biological machines which involve bond breaking/formation with a high degree of selectivity and specificity in conformational changes. Energy localisation phenomena could play an essential role in these processes.

There are several major problems to understand before practical application to those complex systems. How such localized energy packet could be spontaneously created and how it could be

transported selectively from one place to another without being spread out thus favouring specific

reactions? Assuming that a local mode has been already produced by another mechanism (for example energy has been released at a specific location by ATP), our aim is to show on a simple toy model that then a coherent energy transfer may occur spontaneously at a selected site and induce a chemical reaction.

Local modes in complex system may be viewed as (almost) isolated nonlinear oscillators, the frequency of which depends on their amplitude. Their stability require in principle that they are nonresonant with the normal modes of the system but nevertheless coherent energy transport requires (special) resonances. Indeed, when two resonant harmonic oscillators are weakly coupled, it is well-known that any amount of energy injected on the first one is completely transferred to the second one after it is completely transferred (and subsequently oscillates back and forth). In contrast, such resonant energy transfer generally cannot occur for two weakly coupled anharmonic oscillators because the frequencies of these oscillators do not remain equal during the whole transfer. However, there are special situations where the anharmonic oscillators are well tuned one with each other (and are said to be conjugated). Beside the condition of linear resonance at the initial time, a precise condition is required on the nonlinearity [5]. Then, when a selected amount of energy is injected on the first one, this energy is completely transferred to the second one after some time while the frequencies of the two nonlinear oscillators both vary but persistently remain equal. We called this phenomena Targeted Energy Transfer (TET).

Applying our theory, we have shown that such a situation is met when a rotor chosen with an appropriate inertia momentum and an appropriate angular momentum is weakly coupled with a Morse oscillator [6]. TET trajectories of this nonintegrable model can be analytically calculated with a very good accuracy. Numerical simulations shown fig1 confirms that when the TET conditions are fulfilled, there is initially almost complete energy transfer according to the theory, but in addition due to the nonintegrability

of the model, this energy transfer is followed by transient chaotic oscillations which rapidly ends by the ejection of the particle in the Morse potential at

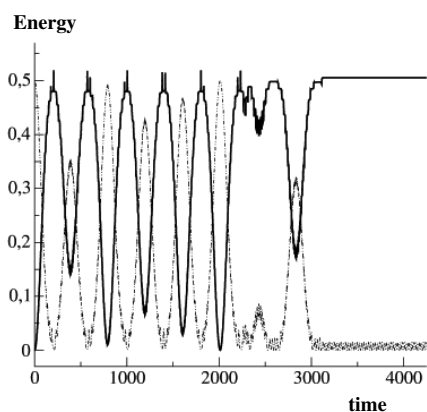
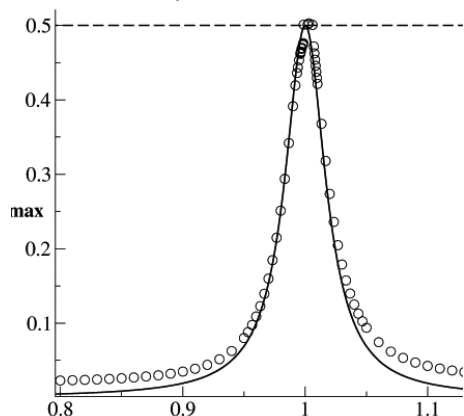


Figure 1. Energy of the Rotor (dot-dashed line) and of the Morse oscillator (full line) versus time when the oscillator is appropriately tuned for TET. After a chaotic transient, the particle is ejected with a nonzero velocity (and proved to never return)

infinity. Considering this potential is those of a chemical bond, we thus obtain a selective



chemical dissociation. Selectivity in energy appears fig.2 which shows the maximum energy transferred as a function of the initial velocity of the rotor. Only when the appropriate initial energy is selected, energy transfer is substantial and sufficient to induce chemical dissociation. Moreover, no chemical dissociation occurs when the rotor is not conjugate with the Morse oscillator.

Surely, this model suffers of many flaws and would need improvements for application to real systems. The main criticism is that it discards the dense set of resonances with the normal modes which could be expected from the surrounding environment. However, as noted above, if the nonlinearities of all the normal modes are not well-tuned (i.e. are nonconjugate with the rotor), they could be simply considered as a phonon bath generating a damping term in the dynamical equations of the system. We plan in the future to generalize the tuning conditions for TET in presence of damping and then to show that selective energy transfer and chemical dissociation may then persist in that case.

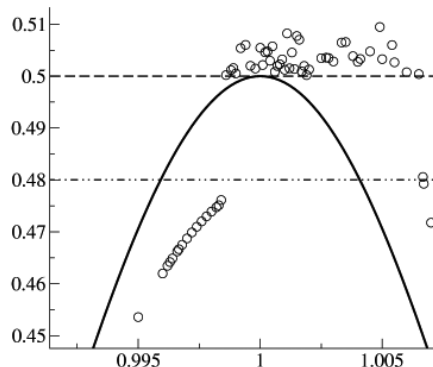


Figure 2. Comparison of the theoretical curve (full line) and the numerical results (open dots) of the maximum energy transferred to the Morse oscillator as a function of the initial velocity of the rotor(left) and magnification of the tip of the peak (right).Chemical dissociation occurs in the narrow interval where the transferred energy becomes larger than $\frac{1}{2}$

In summary, this toy model demonstrates the possibility to produce highly selective chemical reactions which do not obey to the standard theory of (incoherent) thermally activated process. We believe more generally that essential and highly

specific reactions in biosystems could be triggered by a fine molecular machinery based on similar coherent energy transfers between specific local modes.

References

- [1] <http://tccc.iesl.forth.gr/cecam2004/cecam2004.html> ; H. Ishikawa, R. W. Field, S. C. Farantos, M. Joyeux, J. Koput, C. Beck and R. Schinke, *Ann. Rev. Phys. Chit.***50**, 443 (1999)
- [2] M. Joyeux, S.C. Farantos and R. Schinke, *J. Phys. Chem. A***106** 5407 (2002).
- [3] S. Aubry, *Physica* **103D**, 201 (1997)
- [4] S. Flach and C. R. Willis, *Phys. Rep.***295**, 181 (1998)
- [5] AKMT01 S. Aubry, G. Kopidakis, A-M. Morgante and G. Tsironis, *Physica* **B296** (2001), 222-236
- [6] A. Memboeuf and S. Aubry, preprint submitted to *Physica D* (2004)

SPIN DYNAMICS OF THE ELECTRON-DOPED HIGH T_C SUPERCONDUCTING CUPRATES

F. Onufrieva and P. Pfeuty

Laboratoire Léon Brillouin, CEA Saclay, 91191-Gif-sur-Yvette, France

It is crucial to understand the differences between hole and electron-doped high T_C superconducting cuprates. The spin dynamics has been studied intensively in hole-doped cuprates and it is only recently that the first inelastic neutron results were obtained for the electron-doped cuprate $\text{Nd}_{1.85}\text{Ce}_{0.15}\text{CuO}_4$ in both the normal and the superconducting state, with an impressive difference from what is found with hole doping. The resonance peak that is the most prominent feature of the hole-doped cuprates is not observed and the spin response which is also peaked at antiferromagnetic wave vector has an extremely narrow q width (one order of magnitude smaller than in hole doped cuprates). The spin gap is extremely small. It has been proposed by theoreticians at LLB that the basic difference between electron and hole doped cuprates is the proximity of the two electronic systems to two different critical situations (for the corresponding

free Fermion system on a square lattice), one related to saddle point electrons (electronic topological transition) and the other to the nodal electrons (antiferromagnetic nesting). These two borderline situations behave as quantum critical points (QCP) and it is shown that the narrow q width and the low spin gap are the signature of the proximity to one of the QCP while the resonance peak is a signature of a proximity to the other one. This is illustrated in Figure 4[a,b] which shows the calculated electron-hole spin excitation continuum in the superconducting state, for hole and electron-doped cuprates, with very striking predicted differences in the energy and wave vector scales. The same simple conceptual framework is actually developed to explain the differences in the anomalies of the electronic spectral functions between hole and electron-doped cuprates as measured by photoemission.

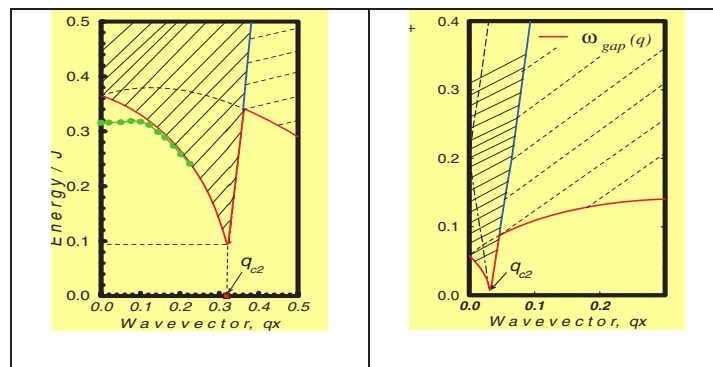


Figure 4[a,b]: Calculated electron-hole continuum, at low energy and in the vicinity of the antiferromagnetic wave vector, in the d-wave superconducting state for hole doping in 4-a [left figure] and for electron doping in 4-b [right figure]. The red line corresponds to a true gap, the blue line to a pseudogap and the green line to the resonance peak dispersion (only present for hole doping).

Reference:

F. Onufrieva and P. Pfeuty, Phys.Rev.Lett. 92 247003 (18 Juin 2004).

FAULTS, A NEW PROGRAM FOR REFINEMENT OF POWDER DIFFRACTION PATTERNS FROM LAYERED STRUCTURES

M. Casas-Cabanas^{1,2}, J. Rodríguez-Carvajal^{2,*}, M.R. Palacín¹

¹Institut de Ciència de Materials de Barcelona (CSIC), Campus UAB E-08193 Bellaterra, Catalonia, Spain.

²Laboratoire Léon Brillouin (CEA-CNRS), CEA/Saclay, 91191 Gif-sur-Yvette Cedex, France.

Layered systems include a large number of mineral families and synthetic compounds of great technological importance. It is well known that their structural features, including those associated to certain defects, are directly related to their physical-chemical properties. Indeed the microstructural characterization of these materials is of essential importance and requires the determination of parameters specific to different types of defects, such as the proportions in which they occur and their exact location.

So far, a widely used tool to interpret the diffraction data of one-dimensionally disordered systems is the DIFFax program [1], which allows the simulation of their powder X-ray and neutron diffraction patterns. As approximate or merely qualitative results sometimes are not sufficient for a thorough microstructural characterization, a computerized comparison of the DIFFax calculated intensities with experimental data has been developed. The resulting code is the FAULTS program, which can be used for the refinement of layered structures containing coherent planar faults.

Program specifications

As DIFFax, FAULTS is a Fortran program except that it is written in the new standard Fortran 95. The program FAULTS conserves the kernel of DIFFax, which has been transformed into a Fortran 95 module, and adds other modules from the Crystallographic Fortran Modules Library (CrysFML) [2]. It can be used to refine XRD and NPD patterns of crystal systems with any type of coherent planar defect, such as twins and stacking faults.

The refinable parameters are read by FAULTS from a free format input data file, similar to that of DIFFax, where the structure is described in terms of layers of atoms which interconnect via stacking operations that occur with a certain probability. Each value used to describe the structure is associated to a refinement code that allows the possibility of constraints. The high and low limits of free parameters as well as the nature of the boundary conditions are provided by the user.

The experimental XRD or NPD patterns can be read from many different formats and background treatment can be achieved by linear interpolation or by polynomial fitting.

Another major feature of FAULTS is the implementation of a more adequate isotropic size broadening treatment which takes into account the Gaussian (HG) and Lorentzian (HL) contributions to the FWHM in addition to the consideration of a finite number of layers per crystallite already present in DIFFax. The profile calculated by DIFFax is convoluted with a Voigt function taking into account the size and instrumental effects. The FWHM of the Gaussian (H_G) and Lorentzian (H_L) components of the size/instrumental peak profile have an angular dependence given by equations (1) and (2):

$$H_G^2 = U \tan^2 \theta + V \tan \theta + W + \frac{4 \ln 2 \lambda^2}{\pi D_g^2 \cos \theta} \quad (1)$$

$$H_L = X \tan \theta + \frac{2 \lambda}{\pi D_l \cos \theta} \quad (2)$$

Were U , V , W , X , D_g and D_l are refinable parameters. Of course it is better knowing a priori the parameters constituting the instrumental resolution function (IRF) and fixing them. This treatment allows a successful description of the separate contributions to line broadening of instrumental features, the finite crystallite size and planar defects.

The refinement can be carried out using local optimisation algorithms, like Nelder-Mead simplex [3], or global ones, as Simulated Annealing [4] or Multilevel Clustering [5, 6], all of them implemented in CrysFML [2].

The quality of the agreement between observed and calculated profiles is given by a set of indices such as the conventional R_p and R_{WP} values, or χ^2 , that are calculated at the end of each refinement cycle.

FAULTS refinement of the XRD pattern of two different Ni(OH)₂ samples

Ni(OH)₂ is used as a battery positive electrode material. It presents better electrochemical activity when the particle size is small [7] and it is believed that defects also contribute positively to its behaviour.

The refinement of experimental patterns corresponding to two different Ni(OH)₂ samples has been carried out using the FAULTS program assuming the existence of stacking faults and using the Nelder-Mead simplex calculation. These samples were prepared by two different synthetic routes in order to achieve different microstructural characteristics, i.e. size and amount of defects. Both X-ray diffraction patterns were obtained with a Siemens D-500 diffractometer with Cu-K α radiation and a step size of 0.03° (2 θ). In order to avoid preferential orientation effects, the samples were side loaded in the sample holder.

Sample A was synthesized by addition of 1M nickel nitrate solution to 28% NH₄OH solution at 60°C. The mean particle diameter is around 430Å as determined by TEM. Sample B was synthesized by addition of 1M nickel sulphate solution to 2N NaOH solution at 70°C. The mean particle diameter is around 139Å.

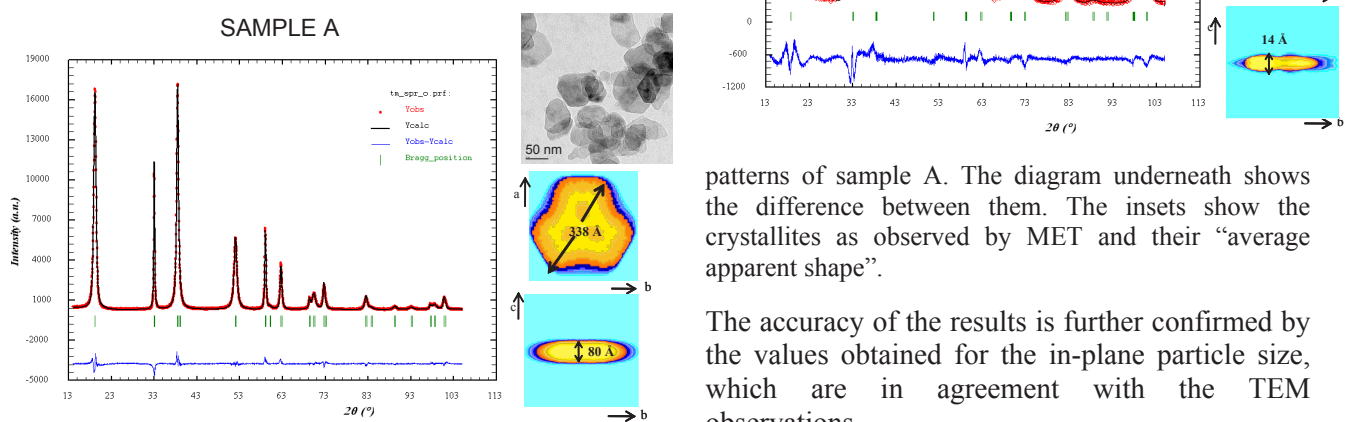


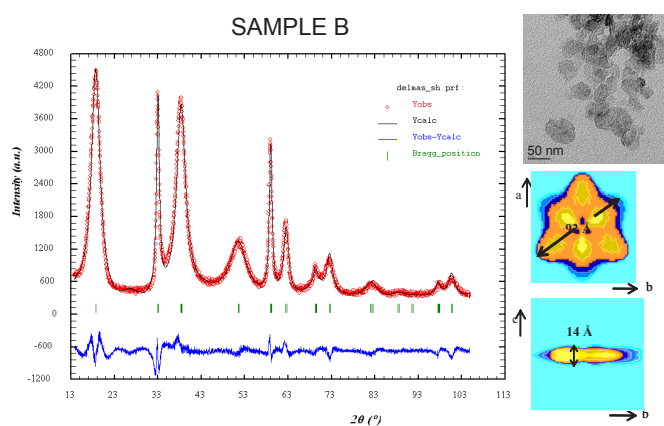
Figure 1. Comparison of observed and calculated patterns of sample A. The diagram underneath shows the difference between them. The insets show the crystallites as observed by MET and their “average apparent shape”.

References

1. M.M. Treacy, J.M. Newsam, M.W. Deem, 1991, *Proc. R. Soc. London Ser. A*, **433**, 499-520.
2. J. Rodríguez-Carvajal and J. González-Platas, 2003, *IUCr CompCom Newsletter*, **1**, 50-58.
3. J.A. Nelder, R. Mead, 1965, *The computer journal*, **7**, 308-313.
4. S. Kirkpatrick, C. D. Gelatt, Jr., M. P. Vecchi, 1983, *Science*, **220**, 671-680.
5. Boender, C.G.E., A.H.G. Rinnooy Kan, G.T. Timmer, L. Stougie, 1982, *Mathematical Programming*, **22**, 125-140.
6. Csendes, T., 1988, *Acta Cybernetica*, **8**, 361-370.
7. McBreen J. 1990, *Modern aspects of electrochemistry*, **21**. Plenum Press
8. Rodríguez-Carvajal J., 1993, *Physica B*, **192**, 55-69.

In the case of sample A, obtained R_p value is 7.61%. The results indicate the presence of 2% deformation faults. A comparison between the calculated, the observed and difference powder patterns is shown in figure 1, as well as a MET image and the “average apparent shape” of the crystallites obtained with the program FullProf [8]. For sample B the obtained R_p value is 6.83%. The results indicate the presence of 20% growth faults and 25% deformation faults. A comparison between the calculated, the observed and difference powder patterns is shown in figure 2, as well as a MET image and the “average apparent shape” of the crystallites obtained with the program FullProf [8]. An important part of the anisotropic broadening comes from the size effect (refined number of layers \approx 7.4).

Figure 2. Comparison of observed and calculated



patterns of sample A. The diagram underneath shows the difference between them. The insets show the crystallites as observed by MET and their “average apparent shape”.

The accuracy of the results is further confirmed by the values obtained for the in-plane particle size, which are in agreement with the TEM observations.

These results show that the synthetic method of sample B leads to a smaller and more defective Ni(OH)₂. Further electrochemical studies are to be performed in order to establish the relationship between amount and type of defects and electrochemical activity of these materials.

DYNAMICS OF LYSOZYME UNDER PRESSURE SEEN BY MOLECULAR SIMULATION AND NEUTRON SCATTERING

G.R. Kneller^{1,2}, K. Hinsén¹, V. Hamon², M.-C. Bellissent-Funel¹

¹Laboratoire Léon Brillouin (CEA-CNRS) CEA-Saclay, F-91191 Gif-sur-Yvette Cedex, France}

²Centre de Biophysique Moléculaire (CNRS UPR 430) Rue Charles Sadron, 45071 Orléans Cedex 2

1. Motivation

The motivation of the study presented here is to investigate how hydrostatic pressure influences the internal dynamics of proteins below the denaturation threshold. Combining molecular dynamics simulations and quasielastic neutron scattering, we study the internal dynamics of lysozyme in solution for pressures between 1 atm and 3 kbar. Both techniques give access to the internal dynamics of condensed matter on the nanosecond time scale and length scales between 1 Å and 100 Å. The analysis of the simulations yields valuable complementary information to the experimental data which helps to interpret the latter and to develop models for the internal dynamics of proteins.

2. Simulation

We performed Molecular Dynamics simulations of one single lysozyme molecule in a solvent of 3403 water molecules, yielding a total number of 12169 atoms in the simulation box. In order to mimic the experimental conditions of constant temperature and pressure, all simulations have been performed in the thermodynamic NpT ensemble [1,2] using an integration time step of 1 fs and applying periodic boundary conditions. We used the AMBER94 potential [3] to describe the interactions in the system. To be able to compute purely quasielastic neutron scattering spectra, global protein motions have been subtracted from the trajectories, which have been saved for further analysis. The length of the production runs varied between 1 and 1.2 nanoseconds, yielding a frequency resolution of $\Delta f \approx 5 \cdot 10^8 \text{ Hz} \cong 2.06 \text{ } \mu\text{eV}$. The molecular dynamics simulations and the analyses have been performed with the programs MMTK and nMoldyn, respectively [4,5].

3. Experiments

The experiments described in the following have been performed on the time-of-flight spectrometer IN5 of the Institut Laue-Langevin in Grenoble [6]. The experiments were performed on a lysozyme solution of 60 mg/ml, using a deuterated acetate buffer (50 mM and pH 4.6). We used a pressure cell made of a titane-zirconium alloy whose scattering is purely incoherent. The experiments were performed at pressures of 1 atm and 3 kbar, with a resolution

of 8 μeV (HWHM). The preparation of the samples and the data analysis is briefly described in [6], and a more detailed description will be published in a forthcoming article [7]. In contrast to the simulations, the experimental spectra contain contributions from internal protein motions and from

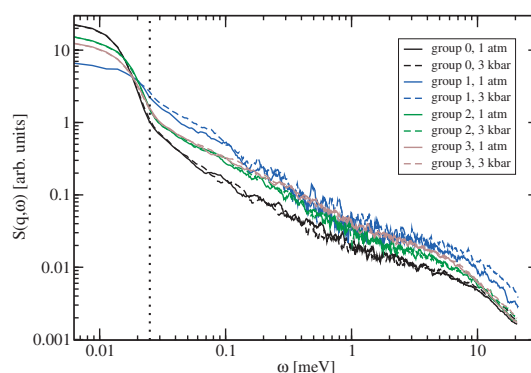


Figure 1. Experimental QENS spectra for lysozyme in solution from IN5. The broken line indicates the range of the contribution due to global translational protein motions.

4. Results

We found that the experimental quasielastic spectra and their simulated counterparts do not show a significant change upon the application of pressures up to 3kbar (see Fig.1). The detector groups 0,1,2,3 correspond, respectively, to $q_{el} = 3.9, 6.7, 9.7, 11.9 \text{ nm}^{-1}$. A zoom on the experimental structure factor for the extreme pressures of 1 bar and 3 kbar at small energy transfers is shown in Fig.2. One recognises that the intensity of the quasielastic is slightly increased at 3 kbar. To understand the result we write the measured dynamic structure factor as a convolution product: $S_{meas}(q, \omega) = R(\omega) \otimes S_{cm}(q, \omega) \otimes S_{int}(q, \omega)$. Here $S_{cm}(q, \omega)$ and $S_{int}(q, \omega)$ are, respectively, the dynamic structure factors describing translational diffusion and internal motions in the protein, and $R(\omega)$ is the resolution function of the instrument. One supposes that internal and global protein motions are uncorrelated. It is worthwhile noting that rotational diffusion can be neglected on the time scale of the spectrometers we used. The dynamic structure describing internal motions splits into an elastic part

and a contribution which describes diffusive and vibrational motions,

$$S_{\text{int}}(q, \omega) + EISF(q)\delta(\omega) + S'_{\text{int}}(q, \omega) \quad (1)$$

Here $EISF(q)$ is the elastic incoherent structure factor. Consequently, $S_{\text{meas}}(q, \omega)$ takes the form

$$S_{\text{meas}}(q, \omega) = R(\omega) \otimes S_{\text{cm}}(q, \omega) \otimes (EISF(q)\delta(\omega) + S'(q, \omega)) \quad (2)$$

The inset of Fig. 2 shows the normalised EISF obtained from the simulations described above at $p = 1$ atm and $p = 3$ kbar. At high pressure the EISF decreases less rapidly with q , which indicates that the atomic fluctuations are reduced. This effect can explain qualitatively the slight increase of $S_{\text{meas}}(q, \omega = 0)$. A more detailed study, accounting for a narrowing of $S_{\text{cm}}(q, \omega)$ due to a reduction of the protein diffusion constant in water under pressure

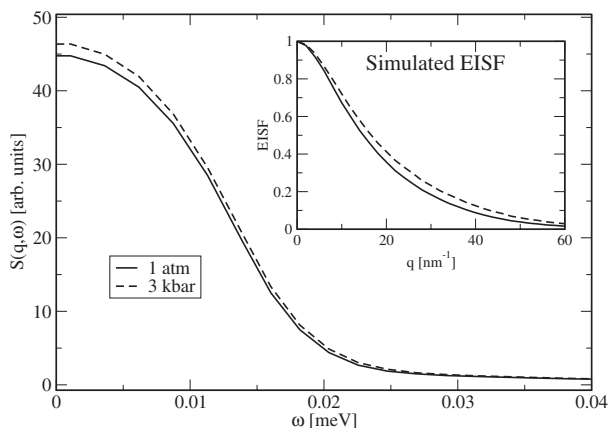


Figure 2. Comparison of $S(q, \omega)$ for $p = 1$ atm and $p = 3$ kbar at small energy transfers and $q = 4 \text{ nm}^{-1}$. The inset shows the *simulated* normalized EISF at the same pressures.

References

- [1] H.C. Andersen, J. Chem. Phys. **72**, :2384-2393, 1980.
- [2] S. Nosé, J. Chem. Phys. **81**, 511-519, 1984.
- [3] W.D. Cornell et al, J. Am. Chem. Soc, **117**:5179, 1995.
- [4] K. Hinsen, J. Comp. Chem., **21**:79-85, 2000.
- [5] T. Rog, K. Murzyn, K. Hinsen, and G.R. Kneller, J. Comp. Chem., **24**, :657-667, 2003.
- [6] G.R. Kneller, M.-C. Bellissent-Funel, and V. Hamon, Technical Report 8-04-286, Institut Laue-Langevin, 2004.
- [7] V. Hamon, M.-C. Bellissent-Funel, K. Hinsen, and G.R. Kneller. Manuscript in preparation.

To investigate the influence of pressure on the internal dynamics of lysozyme and the influence on the position fluctuations, we analysed the frequency spectrum of the average velocity autocorrelation function (density of states) of the hydrogen atoms. The latter yield the dominant contribution to the neutron scattering spectra. The DOS is related to the mean-square position fluctuations

$$\langle \mathbf{u}^2 \rangle(\omega_c) = \lim_{t \rightarrow \omega} \frac{6}{\pi} \int_0^{\omega_c} d\omega \frac{1 - \cos \omega t}{\omega^2} g_{\text{vv}}(\omega) \quad (3)$$

One recognises that the low frequency part of the DOS contributes most to the position fluctuation. Fig. 3 pressure has an impact on the low frequency part of the DOS (inset), which leads in turn to a reduction of the position fluctuations and confirms the effect seen in the EISF and in the experimental spectra. Pressure has thus an impact on the internal dynamics and the position fluctuations of lysozyme, but the effect is not pronounced in the quasielastic

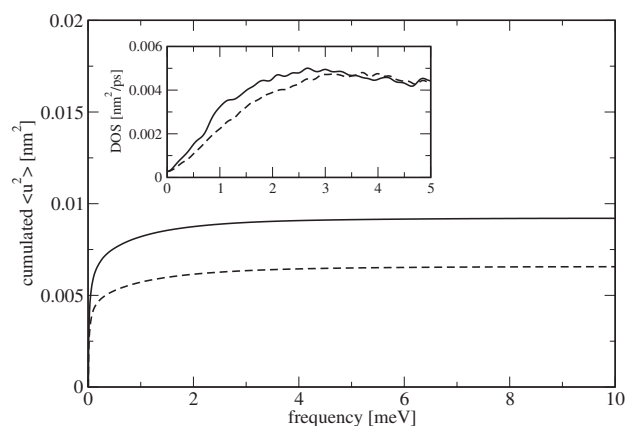


Figure 3. Cumulated position fluctuation as a function of frequency and corresponding density of states (inset).

7 - TECHNICAL AND INSTRUMENTAL DEVELOPMENTS

7 - TECHNICAL AND INSTRUMENTAL DEVELOPMENTS

In the last 2 years the investments on the development of new spectrometers has been limited. The 2 main developments are connected with Small Angle Neutron Scattering and 2 new spectrometers are being built. Other instrumental developments have consisted in incremental improvements of existing spectrometers. They either allow to obtain “soft gains” and to improve the flux of the spectrometer by factors of the order to 2-3 or consist in providing to the users improved sample environments.

Spectrometers

SANS - Reflectivity

- PAPYRUS
One of the existing SANS spectrometer (PAPOL) has been upgraded in order to make it suitable for the technique of GISANS (Grazing Incidence Small Angle Neutron Scattering). This spectrometer is optimized for the study of magnetic thin film nanostructures and can use a polarized neutron beam. Two persons are now fully dedicated to this spectrometer. More details can be found in the following highlight.
- TPA
The study of new composite systems require Very Small Angle Neutron Scattering. Thus the spectrometer TPA (Très Petits Angles) is being development at the guide position G5bis. This spectrometer is optimized for the measurement of anisotropic large size nano-systems ($2 \cdot 10^{-4} \text{ \AA}^{-1} < Q < 10^{-1} \text{ \AA}^{-1}$) (see following highlight).
- EROS
The Time of Flight reflectometer EROS has benefited from incremental developments. A new multi-discs chopper system has been installed. It allows to work with a constant instrumental resolution over the entire Q-range. The collimation part of the spectrometer has been completely redesigned to make it shorter. The fabrication of the new collimator is under way. Large gains in flux are expected (up to 50 for a significant λ range).

Material science

- Textures
The sample environment of the texture spectrometer 6T1 has been significantly improved. A furnace is now available which allows to perform in-situ experiments. An in-situ traction machine has also been designed in collaboration with the LPMTM Univ. Paris XIII (see following highlight).
- Strains
The strain spectrometer DIANE has been upgraded so as to able to accommodate very heavy samples (~500kg) adapted to the study of “industrial” objects. An Euler cradle is now also available (which can handle pieces up to 20 kg).

Diffraction

- Powder diffraction

The high resolution powder diffractometer 3T2 has been redesigned in order to be able to accommodate a completely new detector system (detectors twice as high and twice the number of detectors). The gains in measuring time should be of the order of 5 (gains obtained in detection surface). The different pieces (collimators; detectors) of this new detector have been tested individually ; they should be setup during 2005.



The new collimators - detectors block for the spectrometer 3T2 (seen from the sample position)

This new system will allow :

- an improved flexibility (intensity/resolution)
- The possibility to study monoclinic structures with $V_0 \leq 1200 \text{ \AA}^3$
- to study microstructures as a function of the temperature
- to study complex systems such as : molecular compounds, bio-materials, cement...

- Single Crystal diffraction

A new method of type "Quasi Laue single crystal diffraction" has been tested on 5C1 by using a large PSD system (see CAP 2010). The first tests have been satisfactory. The new principle of measurement will be evaluated further during the year 2005. Large gains in measuring time are expected (from 5 up to 10).

Sample environments

High pressures

Various techniques have been developed to study neutron scattering under high pressures combined with applied magnetic field and/or uniaxial stress. New "hybride" pressure cells with diamond, sapphire and moissanite anvils are compatible with neutron instrumentation at the LLB and X-ray scattering facilities at the ESRF, allowing to carry out X-ray and neutron studies on the same sample. These pressure cells are used at the LLB on a number of spectrometers (powder diffraction G61, single crystal diffraction)

An example of the use of such cells is presented below :

New Medium Pressure (3 GPa) Cell for Single Crystal Diffraction in LLB

(B. Annighöfer, A. Gukasov)

A new hydrostatic pressure cell has been developed for single crystal diffraction experiments (see Fig. 1). The design of the cell allows a maximum pressure of 3 GPa, with the inner diameter of 4 mm and the maximum height of 8 mm. The cell is compatible with a superconducting magnet of 7.5 Tesla.

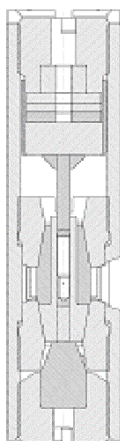


Figure 1: Pressure cell.

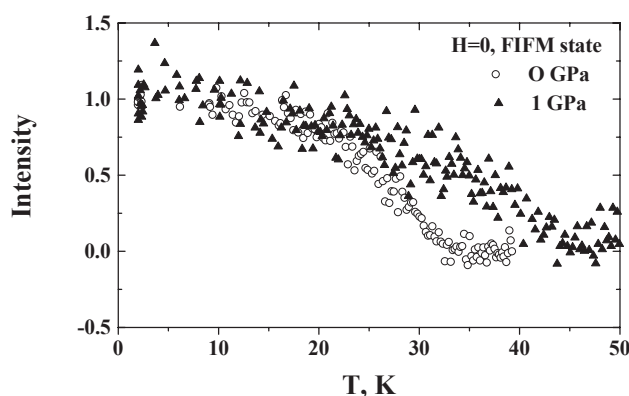


Figure 2. Temperature dependence of the (110) reflection in the FIM state under different pressures.

Test measurements have been carried out on a single crystal of bilayer manganite $(La_{0.4}Pr_{0.6})_{1.2}Sr_{1.8}Mn_2O_7$, which exhibit a field induced ferromagnetic-metallic (FIFM) phase transition. Without field, this material shows no spontaneous ferromagnetic ordering, and keeps its insulating state down to 2 K. A magnetic field of several teslas (at 2 K) triggers the onset of a long range ferromagnetism, simultaneously with the insulator-metal transition. This field-induced ferromagnetic (FIFM) state behaves like an ordinary ferromagnetic state and disappears at Curie temperature $T_C=32$ K. Fig. 2 shows that the pressure of 1 GPa increases the Curie temperature of the FIFM state from 32 to 45 K.

Pressure cells for biological studies

M.S. Appavou, G. Gibrat, B. Annighofer, M.-C. Bellissent-Funel (LLB)

This pressure cell has been especially developed for studying the protein folding and to comparing structural conformation and dynamics of native and pressure denatured states in solution. It has been optimised to allow both SANS and TOF experiments. With this cell, pressure experiments on NEAT spectrometer (HMI, Berlin) have been successively performed at a given pressure using SANS and TOF configurations of NEAT spectrometer.

This cell is made with a Cu-Be alloy (98%Cu-2%Be). The neutron scattering characteristics of this alloy are given in table 1. The cell has an internal diameter of 10 mm and an external diameter of 28 mm. It allows a maximum pressure of 600 MPa and can contain up to 7.4 ml of solution. A cylindrical insert is put inside the sample chamber to reduce the sample volume. The pressure transmitting media used is D_2O . (See photograph below)



New cells for the study of biological samples have been developed.

Element	σ_{coh} (barn)	σ_{inc} (barn)	σ_{abs} at $\lambda = 1.8 \text{ \AA}$ (barn)
Cu	7.49	0.55	3.78
Be	7.63	$1.80 \cdot 10^{-3}$	$7.60 \cdot 10^{-3}$
Alloy	7.49	0.54	3.7

Table 1 : Neutron scattering cross sections of the components of the cell.

Non magnetic environment for 4F1

The spectrometer 4F1 has been modified to remove all the magnetic elements so as to be able to set-up a large cryomagnet.

Polarization analysis option is installed on the thermal beam triple axis spectrometer 2T. Unfortunately, the current setup is not fully operational as an insufficient flipping ratio is measured. This further depends on the incident wave-vector angle apparently due to a lack of neutron guide field between the monochromator and the sample. Additional tests are required to sort out that problem. They have been postponed due to reduced number of days of running reactor and the surcharge of the spectrometer.

Guide systems

The guide G1, G2 and G6 in the plugs have been replaced by $2\theta_c$ super-mirrors. Most guides have thus benefited from a measurable increase in flux (see report in the next pages). Some spectrometers do not show any gains because some of the main guides still use simple Ni coatings. During 2005, the guide G6 should be upgraded with $2\theta_c$ super-mirrors. The main benefit will be for the spectrometer G61.

Future developments

- A new PSD detector will be installed on 5C2 during the year 2005 to improve the collection rate of the spectrometer.
- The spin-echo MUSES will benefit from a multi-detector system increasing the collected solid angle.
- In the long term, a new time of flight spectrometer is being designed. The funding for this new spectrometer has however no been secured yet.

- 1 Papyrus : a dedicated tool to study surfaces at the nanoscale **155**
G. Chaboussant, F. Cousin, S. Gautrot, H. Glattli, J. Jestin, F. Ott, M. Viret
2. Very small angle neutron scattering spectrometer (TPA) **158**
J. Oberdisse, R. Kahn, V. Thévenot, A. Gabriel, P. Permingeat, D. Lairez, B. Hannighofer, S. Désert, A. Brûlet
3. Technical developmentS dedicated to “in situ” temperature analysis of crystallographic textures by neutron diffraction **160**
Ph. Gerber, J.P. Ambroise, M.H. Mathon
4. Neutron holographic study of palladium hydride **162**
L. Cser, G. Krexner, M. Prem, I. Sharkov, Gy. Török
5. Replacement of first elements of Guides 1 to 6 **164**
A. Menelle
6. Report on a first neutron test of a new D position-sensitive detector of thermal neutrons **165**
A. Kuklin, G.Eckold , V.Gordeliy, S.Kutuzov, A.Islamov, A.Smirnov, P.Utrobin, A.Bogdzal, N.Alekseev, V.Comparat, A.Pelissier, J. Ballon, J. Teixeira , G.Koskas, A.Gabriel

PAPYRUS: A DEDICATED TOOL TO STUDY SURFACES AT THE NANOSCALE

G. Chaboussant¹, F. Cousin¹, S. Gautrot¹, H. Glattli¹, J. Jestin¹, F. Ott¹, M. Viret²

¹ Laboratoire Léon Brillouin (CEA/CNRS), CEA Saclay, F-91191, France

² SPEC, CEA, Ormes les Merisiers, France.

PAPYRUS, formerly PAPOL [1], is a spectrometer that has been modified to perform Grazing Incidence Small Angle Neutron Scattering (GISANS). It is primarily devoted to the study of surface and interface at the nanometer scale [2,3,4].

GISANS (and SANS) can be performed using a $\lambda=8\pm 0.5\text{\AA}$ neutron beam ($3.10^5\text{ n/cm}^2/\text{s}$) with polarization option (94% polarization, 45% transmission). It allows to work in the Q-range $0.02\text{-}3\text{ nm}^{-1}$ thanks to a $64\times 64\text{ cm BF}_3$ detector grid (128x128 cells) and an adjustable sample-to-detectors distance (min 80cm, max 380cm).

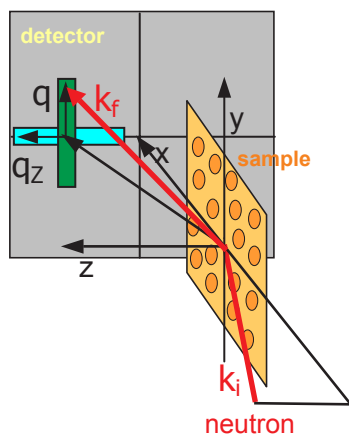


Figure 1. GISANS geometry. The accessible Q range is $10^{-2} < q_y < 3\text{ nm}^{-1}$. Scattering in the off-specular GISANS plane (green area) allows to probe objects with typical size between 5 and 100 nm. In the specular direction (q_z), typical sizes between 600 nm and $60\text{ }\mu\text{m}$ can be probed (blue area).

PAPYRUS can also be used as a standard polarised neutron reflectivity instrument, probing structural and magnetic depth profile.

The GISANS configuration, schematically represented in Figure-1, is particularly useful for the study of domain formation in magnetic thin films, organized nanostructures (nanowires, nanodots) and soft matter materials. By detecting off-specular scattering perpendicular to the incident plane (q_y direction, green area in Figure-1) one can bring information on the lateral (planar) correlations between nanometer scale objects deposited on a surface or confined at interfaces with typical size between 5 and 100 nm. Off specular scattering in the incident plane (light blue area) also brings information about lateral

structures (in the plane of the surface) but with typical length scales from 600nm to $60\text{ }\mu\text{m}$ [5,6,7]. The period 2003-2004 has seen a refit of the instrument with several new features. The 7m long collimation has been improved, a 3m neutron guide and a new slit system are now in place, leading to a best q_z resolution of about 0.02 nm^{-1} , essentially limited by the resolution of the detector grid. The sample table area is now motorized in four directions (vertical, rotation, translation, tilting) and allow accurate reflectivity measurements as well as GISANS measurements in horizontal geometry which is the most convenient for liquid samples.

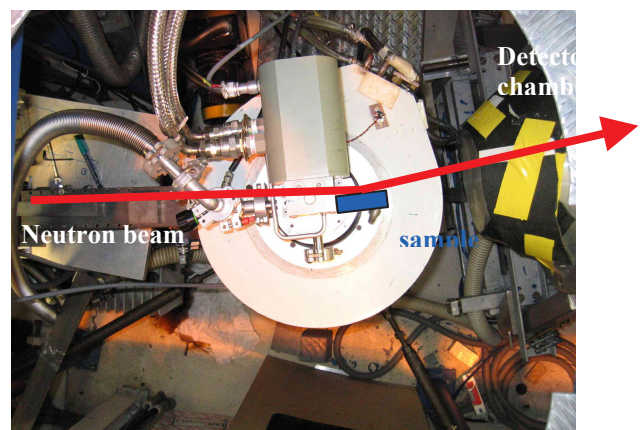


Figure 2. Partial view of PAPYRUS with the neutron guide on the left hand side and the detector chamber on the right hand side.

A variety of sample environment (cryomagnet, displax, electromagnet, etc.) can now be accommodated (see Figure 2). The background noise from the detector chamber has been reduced (0.5 count/cell/hour). In addition, new instrument developments in 2005 will include a new beam stop system and a polarization analysis option. To illustrate the GISANS capabilities, a selection of recent achievements using PAPYRUS are given below.

Domain formation in AFM Fe/FeF₂ bilayers

Neutron off-specular scattering is a technique which can be used for the study of the formation of magnetic domains at the interfaces of bilayer systems like Fe/FeF₂. This material consists of a 100nm FeF₂ layer, deposited on a MgO substrate and capped with a 80nm Fe layer and a thin non-magnetic Al layer. We show that it is possible to

study the exchange coupling within the single magnetic interface between the Fe layer and the antiferromagnetic FeF₂ layer (T_N = 80K).

Figure-3 shows two polarised neutron scattering intensity maps obtained with UP and DOWN polarisations, close to the critical angle and at low temperature (13K) and weak negative magnetic field (-30G) after Zero field cooled under a positive magnetic field of H=+1kG.

Beside the specular reflectivity which is identical for “up” and “down” configurations, a strong off-specular peak is observed at higher Q_z values. This off-specular intensity is strongly temperature dependent (not shown) and suggests that it is of magnetic origin. It is also visibly strongly dependent on the polarisation as illustrated in the horizontal slice shown in Figure-4.

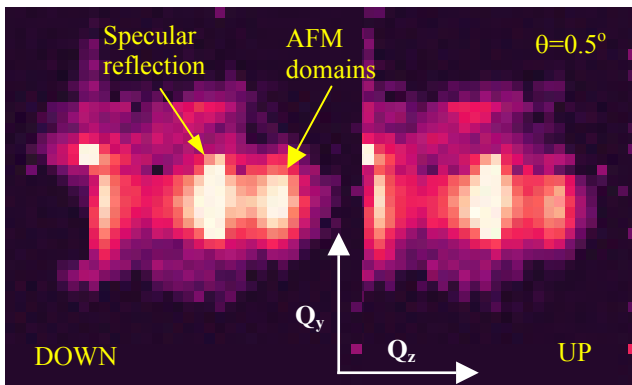


Figure 3. Scattering intensity maps with “up” and “down” neutron polarisation of Fe/FeF₂ layers obtained with $\theta_1 = 0.5^\circ$, T=13K and H=-30G applied field.

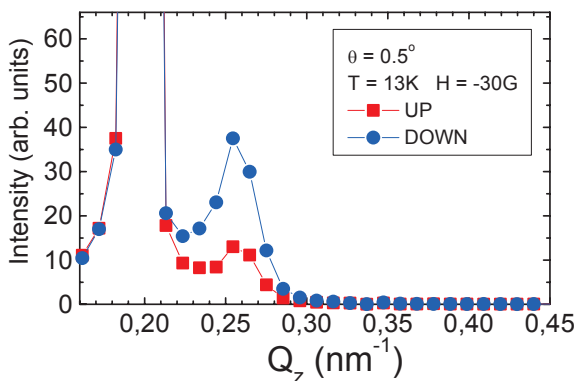


Figure 4: Scattering intensity maps with “up” and “down” neutron polarisation of Fe/FeF₂ layers obtained with $\theta_1 = 0.5^\circ$, T=13K and H=-30G applied field.

Magnetic off-specular scattering in the Q_z direction is attributed to the formation of magnetic domains at the interface between the two magnetic layers [8,9] while reducing the magnetic field from a fully polarized state to the remanent state.

Magnetic (Fe) nanodots in insulating matrix

Figure-6 shows an example of a GISANS measurement taken at T=210K and H=1T on an array of Fe nanodots (60 nm in diameter and 100nm separation) grown on porous Al₂O₃ membranes (Figure 5).

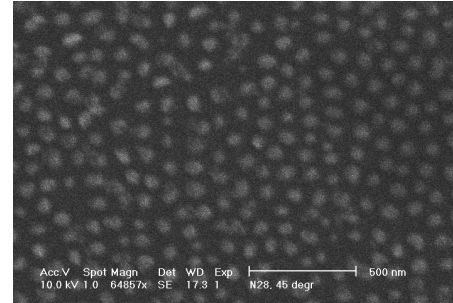


Figure 5. Fe (60nm) nanodots observed by SEM

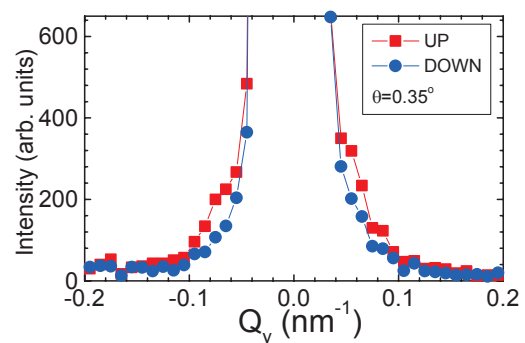
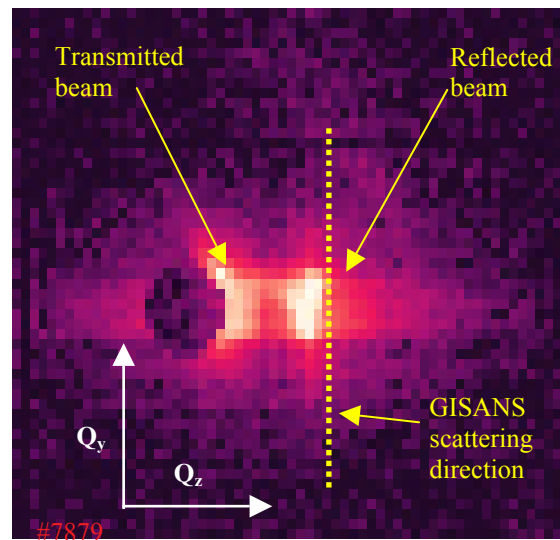


Figure 6: Top: Colour image of Fe nanodots scattering at $\theta=0.35^\circ$, T=210K and H=1T applied field. Bottom: Slice along Q_y close to the specular reflection for UP and DOWN polarisation.

Off-specular scattering is observed in the Q_y direction corresponding to in-plane properties of the sample. Up and Down polarisation measurements at remanence and under 1T (Figure 6) shows that some extra scattering of magnetic origin develops symmetrically on each side of the specular reflection. It is thus possible to

measure the local magnetization of nanodots deposited on a surface. It also shows that the magnetisation of the Fe dots is close to saturation as expected at low temperature. In principle one could infer the magnetic form factor of such dots and to determine their vortex state. However, more work is needed to improve the resolution and signal-to-noise ratio in order to quantitatively study such nanostructures.

PAPYRUS for soft matter

GISANS can also be a powerful tool for soft matter applications to study the structure of objects weakly organized on a surface, especially for systems whose surface properties are driven by the bulk properties (micelles adsorption for example) [10]. We present here an experiment **in liquid environment** that allow to get both the signal from the objects organized on the surface and the signal from the objects in bulk solution.

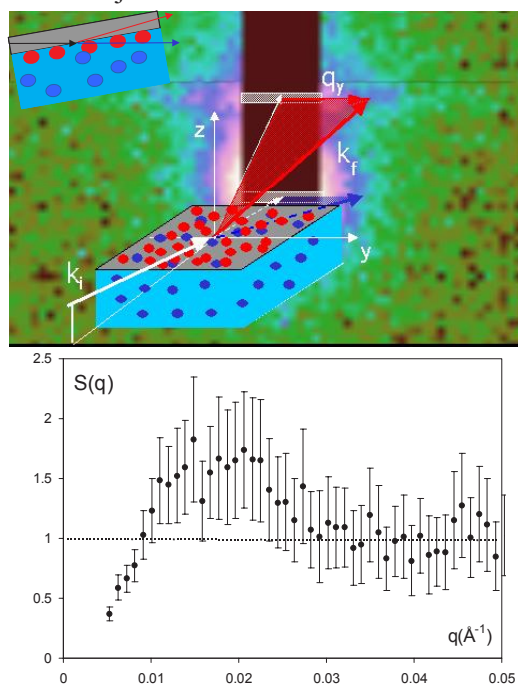


Figure 7. Top: principle scheme of GISANS in liquid environment : the signal of the red spheres attached on surface (GISANS) is located in the plane of specular reflectivity. The signal of the blue spheres in bulk solution (SANS) is located around the direct beam. Bottom: Structure factor of spheres at the surface.

We have designed for this purpose a model system to test the experiment feasibility on PAPYRUS. A layer of monodisperse nanospheres of SiO_2 ($\langle R \rangle = 135 \text{ \AA}$) has been grafted on a silicon wafer.

References

- [1] H. Glättli *et al*, *Physica B* **213-214**, 887 (1995).
- [2] G. H. Vineyard, *Phys. Rev. B* **26**, 4146 (1982).
- [3] S. K. Sinha *et al*, *Phys. Rev. B* **38**, 2297 (1988).
- [4] R. Pynn, *Phys. Rev. B* **45**, 602 (1992).
- [5] C. Fermon *et al*, *Physica B*, **267**, 162 (1999).

The surface of the wafer is in a first step functionalized by terminal amines functions that provide positive charges to the surface at neutral pH. The silica nanospheres, negatively charged at pH 7, interact then electrostatically with the surface. As this interaction is irreversible, it is possible to place the wafer containing the same nanospheres in bulk solution without degrafting the surface nanospheres. The system enables thus to continuously tune the ratio of spheres at the surface to the spheres in volume.

The nanospheres layer at the silicon surface has been characterized by neutron specular reflectivity on EROS spectrometer (LLB). It was shown that the layer is homogenous and rather dense with a surface fraction Φ_s of about ~ 0.4 .

The GISANS measurement has been realized at the silicon/ D_2O interface and is presented in figure 7. The neutron beam crosses through the silicon and is partially reflected by the silicon/ D_2O interface. The signal from the spheres at surface (red spheres on picture) is located in the plane of the specular reflectivity and the signal from the spheres in the bulk (blue spheres on picture) around the direct beam as in classical SANS.

In the experiment described here, the spheres in bulk were diluted enough to identify the signal of SANS to the form factor of spheres ($\Phi = 0.001$). Dividing the GISANS signal by the one of SANS provides then the structure factor of spheres at surface (figure 7, bottom). The structure factor shows a repulsive liquid-like order of the nanosphere at the surface. This is in accordance to our expectations as spheres mutually electrostatically repel in solution during the grafting stage. The correlation peak enables to get the mean distance between spheres ($\sim 370 \text{ \AA}$) and to recover the same surface fraction as (Φ_s about ~ 0.4) as obtained by specular reflectivity.

This experiment has revealed the feasibility of soft matter experiment on PAPYRUS. Especially the typical acquisition time (about 12 hours) is reasonable regarding to the volume of spheres at surface (about 0.01 mm^3). Plus, this is to our knowledge the first time that both the structure of objects at interface and the structure of objects in bulk are simultaneously measured.

- [6] F. Ott *et al*, *Physica B*, **297**, 189 (2001).
- [7] M. Pannetier *et al*, *Physica B*, **335**, 54 (1999).
- [8] E. Kentzinger *et al*, *Physica B*, **335**, 82 (2003).
- [9] B.P. Toperverg, *Physica B*, **297**, 160 (2001).
- [10] P. Müller-Buschbaum *et al*, *Physica B* **350**, 207 (2004).

VERY SMALL ANGLE NEUTRON SCATTERING SPECTROMETER (TPA)

J. Oberdisse, R. Kahn, V. Thévenot, A. Gabriel, P. Permingeat, D. Lairez, B. Annighöfer
S. Désert, A. Brûlet

Laboratoire Léon Brillouin (CEA/CNRS), Saclay

More and more studies of large-scale objects (> 50 nm) are needed nowadays. The very small angle neutron spectrometer (Très Petits Angles, TPA) will be dedicated to the study of such nanostructures, usually found in branched polymers, organized multi-component systems (such as vesicles), reinforced rubber, cell membranes in biology, clays, porous systems, alloys in metallurgy...

TPA is developed to reach lower scattering vectors than those obtained by classical small angle scattering spectrometers. The scattering vector range will be from $2 \cdot 10^{-4}$ to 10^{-1} \AA^{-1} . The principles of this new spectrometer are the same as for conventional small angle spectrometers: small apertures collimation and two dimensional detector but with a high resolution. In order to achieve the $2 \cdot 10^{-4} \text{ \AA}^{-1}$ wave vector and keep a "reasonable" flux, the overall length of the apparatus will be 2 x 6 m. It is installed at the end of a cold neutron bender, G5bis.

The fabrication of a large multi-detector with small pixel size (< mm) is far from easy. There-fore, it has been decided to use a commercial

image plate (MAR345), equipped with a neutron converter. Its dimensions (2300 x 2300 pixels of 100 or 150 μm each) give access to high resolution. The drawback is its sensitivity to γ radiations, which imposes special care such as the use of lead and heavy concrete shielding and requires new technical studies on the spectrometer elements.

The wavelength selection will be achieved by a monochromator with double super-mirrors $3\theta_c$ (15% FWHM). The characteristics of these super-mirrors are especially interesting for our purpose: better transmission (+20%) compared to velocity selector, no direct view of the guide and weaker γ production. A mechanical apparatus, now under construction, will allow the monochromatic beam position to be kept constant while changing the wavelength from 4 to 15 \AA .

The detector tank in which the detector will be located is under study. Once finished, its fabrication (6 months) and on site installation are foreseen in 2005. Figure 1 is a scheme of the TPA.

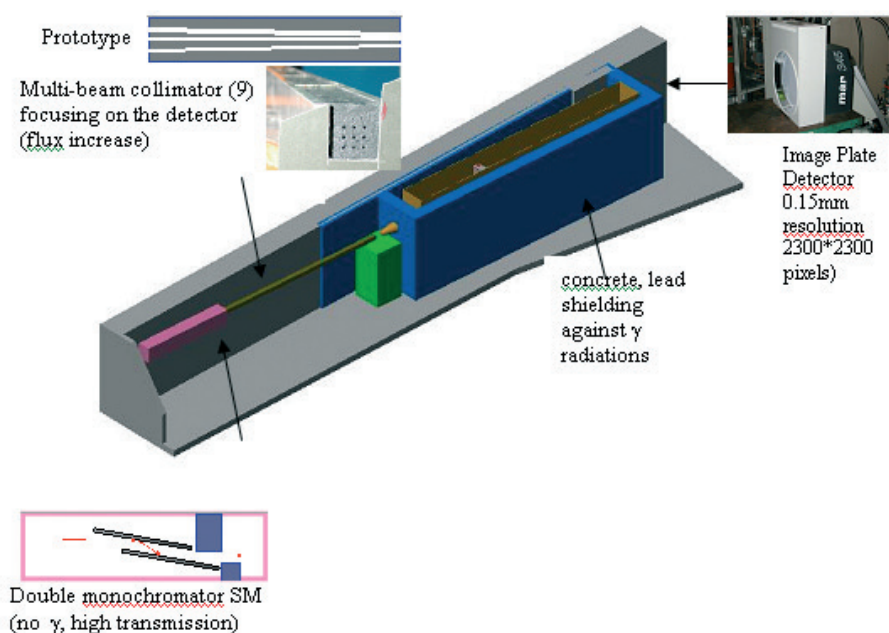


Figure 1. Principle of the Très Petits Angles (TPA) spectrometer. q range : $2 \cdot 10^{-4} - 10^{-1} \text{ \AA}^{-1}$.

At the present time, the sample-to-detector distance is 4 m and the wavelength is 7.5 Å. This non optimized setup already gives access to the smallest scattering vectors possible at LLB. Data are in good agreement with those from D11 at ILL (40 m collimation, detector at 36 m from the sample). Even if the latter enables lower scattering vectors, TPA has a much better resolution (figure 2).

The weak neutron flux is a limitation of this type of spectrometer. To compensate, different focalisation systems can be implemented: Fresnel

lenses, magnetic lenses ... At LLB, a multi beam collimator prototype, made of 9 cylindrical holes along a 1 m long boron carbide with a 1 m focalisation length, has been successfully tested. Figure 3 shows the results obtained with this multi-beam collimator compared to equivalent simple collimation and figure 4 shows the spatial distribution of neutrons for various detector positions from the exit of the collimator up to the focal plane. Further multi-beam collimators will be tested and collaboration on this topic has started in 2004 in the frame of the European project NMI3.

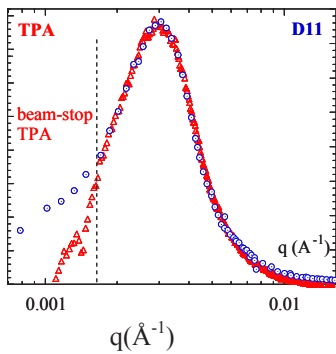


Figure 2. Comparison of resolution between D11 ILL in its very small angle configuration (blue points) and TPA in a non optimised configuration (red points) .

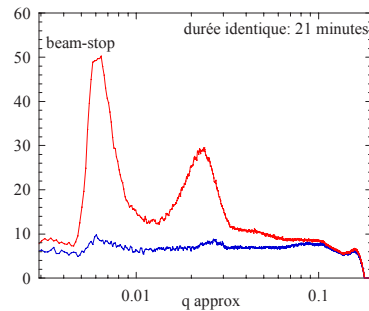


Figure 3. Scattering intensity by a lamellar phase with the 9 multi-beam collimation prototype (red curve) and with simple collimation (blue curve) on TPA.

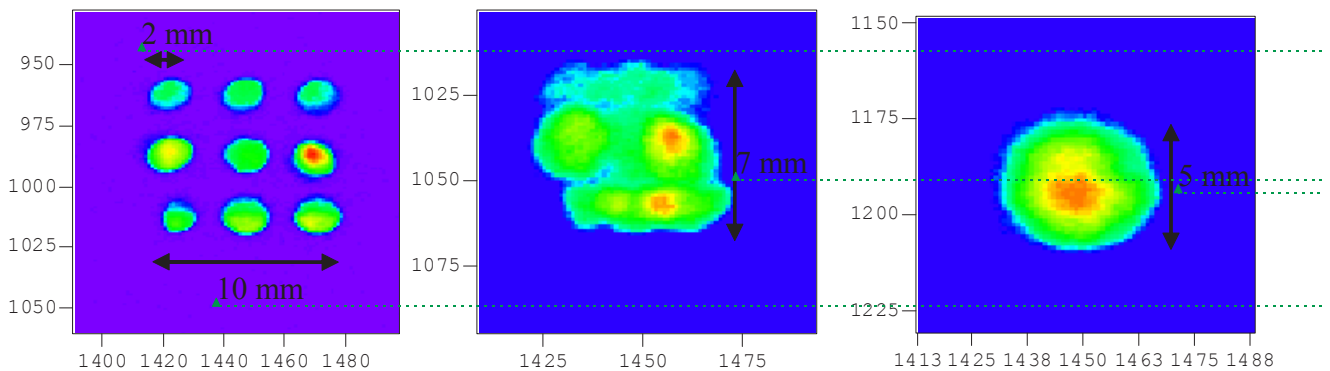


Figure 4. Spatial distribution of neutron flux after the multi-beam collimator for various detector positions: (A) at the exit of the collimator, (B) at 50 cm and (C) at the focal plane (100 cm).

TECHNICAL DEVELOPMENTS DEDICATED TO “IN SITU” TEMPERATURE ANALYSIS OF CRYSTALLOGRAPHIC TEXTURES BY NEUTRON DIFFRACTION

Ph. Gerber, J.P. Ambroise, M.H. Mathon

Laboratoire Léon Brillouin, UMR 12, CEA (DSM/DRECAM)-CNRS, CEA Saclay, 91191 Gif sur Yvette, France

The mechanical, physical and chemical properties of polycrystalline materials are strongly correlated to the distribution of crystallographic orientations. Controlling the crystallographic textures is crucial for the optimization of these properties and requires to precisely follow their development during each step of any industrial thermomechanical process. Neutron diffraction is particularly well-fitted with crystallographic textures analysis. This technique enables the achievement of good statistical measurements resulting from the large size of the investigated volume, consequence of the neutrons high penetration. The minority texture components are easily characterized, which makes it possible to follow the evolutions of the preferential components as of the first stages of their development.

A special furnace adapted to the texture measurement has been recently developed to allow “in situ” experiments on the 4-circles diffractometer 6T1. The furnace was built by Pyrox company and the technical improvements (heating elements, the coolant system, the regulation, ..) as its adaptation on the Euler’s cradle were carried out by J.P. Ambroise.

The furnace (Fig. 1 and 2) is centred on the goniometer. It is constituted of heating elements achieved on molybdenum (1) that provides a maximum temperature of about 1000°C with a ramping rate of 300°C/min. The sample (2) is fixed on the sample mounting rod (3) with vanadium wires. The temperature is controlled by three thermocouples (4) displaced into the furnace (5), in close contact with the sample. Under normal conditions and without any readjustment, the temperature typically displays drifts that not exceed 1°C, even over several days. Vanadium foil is placed over the sample and acts as a heat shield. An aluminium sphere with a perfectly homogeneous thickness lower than 1 mm, constitutes the external envelope of the furnace and ensures its sealing. At the bottom of the device, a pump-out port for pumping high vacuum produces a controlled atmosphere of 10⁻³ Torr. Finally, a cooling water system minimizes heat transfers towards the Euler’s cradle.

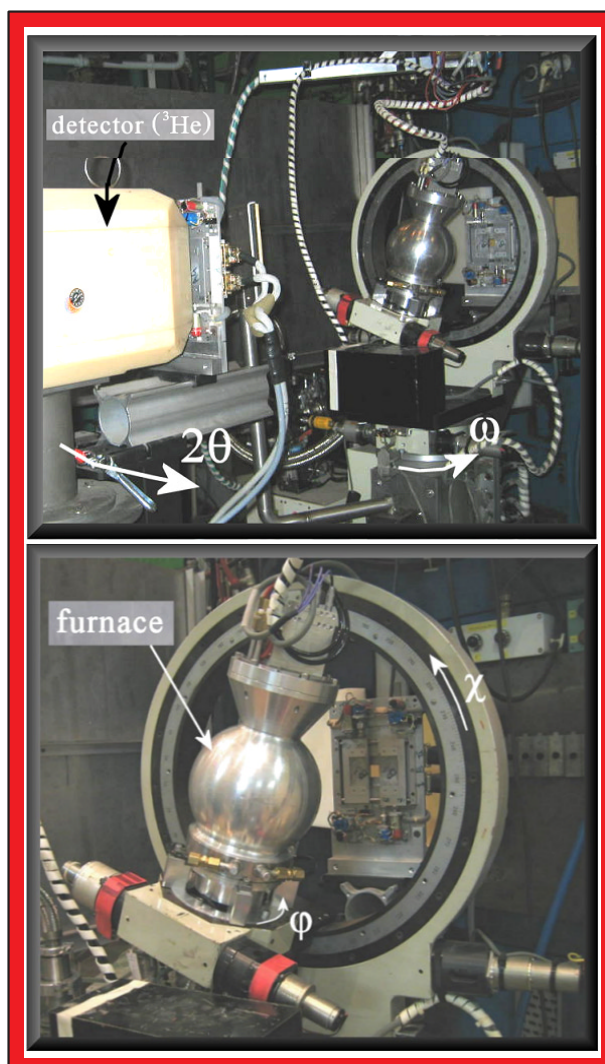


Figure 1 : Presentation of the furnace installed on the 4 circles 6T1 diffractometer

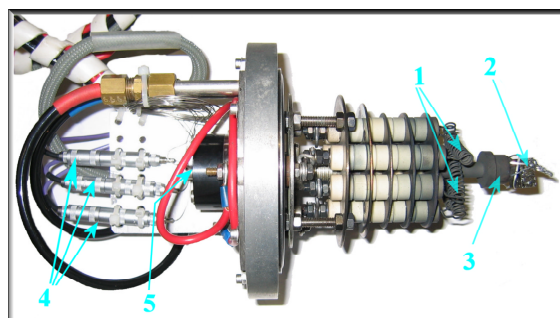


Figure 2. Upper and internal part of the furnace.

This new furnace equipment allows the study of the texture development during annealing process at high temperatures in plastically deformed materials and/or phase texture transformation. In order to analyze the texture evolution versus the annealing time, the experiment is performed following a specific pole related to one major crystallographic orientation that appears or disappears during annealing. With a single-detector, recording time accuracy between 1 and 20 sec is possible. This time scale is compatible with the phenomena of recrystallization. One of the most important goal of recrystallization-of-deformed-materials science is to predict the overall kinetics, *i.e.* to forecast the time and temperature conditions under which the process will occur for a material. For example, static recrystallization has been analyzed in wire-drawn copper deformed for various strain levels (true strain between $\epsilon=0.73$ to 2.84).

It has been determined in copper from neutron diffraction measurements, that the wire-drawn texture is composed of unbalanced $\langle 111 \rangle$ fiber (major orientation) and $\langle 100 \rangle$ fiber (minor one) [1,2]. According to the recrystallization textures analysis in copper wires, it appears that the deformation texture becomes sharper with increasing strain. During recrystallization, the $\langle 100 \rangle$ fiber is reinforced while the $\langle 111 \rangle$ fiber decreased drastically [2]. Hence, during “in situ” annealing at constant temperatures, the recrystallization kinetic can be followed through the decrease of the diffracted intensity at the $\{111\}$ pole figure center. Note that the process could be followed through the increase of the diffracted intensity related to the $\langle 100 \rangle$ fiber and it should give the same results. For a given temperature, the reaction advancement factor $R(t)$ of the recrystallization process is calculated by the relation:

$$R(t) = \frac{I(0) - I(t)}{I(0) - I(\infty)} \quad (1)$$

with $I(0)$, $I(t)$ and $I(\infty)$ are diffracted intensities respectively at the initial deformed state, at a given time t and at the end of the recrystallization process. The Figures 3a and 3b present the $R(t)$ evolution for two different deformation rates ($\epsilon=1.27$ and 2.84) and different temperatures. They present a classical sigmoidal shape with an incubation time followed by an increase of the recrystallization rate (linear region) and finally, a decrease of the recrystallization

rate corresponding to the impingement of growing grains. Assuming that the growth of the grains is thermally activated, the activation energy associated to the recrystallization process, can be deduced from the results obtained at different annealing temperatures, according to Arrhenius equation:

$$a(t) = C.e^{\frac{-E_a}{kT}} \quad (2)$$

E_a is the activation energy of the recrystallization process in J/mol. k is the Boltzmann constant equal to 8.314 J/K.mol and for a given temperature, C is a constant related to the incubation time.

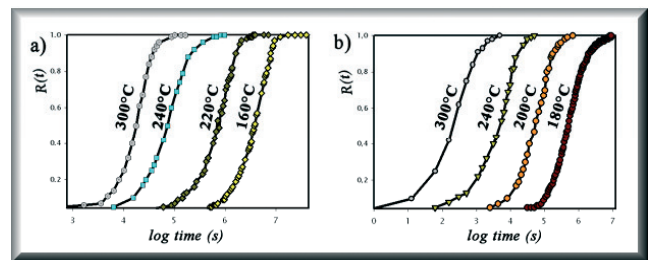


Figure 3 : Recrystallization kinetics of copper for two deformation rate a) $\epsilon=1.27$. b) $\epsilon=2.84$.

For the first time, the relation between E_a and the level of strain has been expressed. The figure 4 shows an exponential decay of the activation energy upon increasing strain. The fast decrease is rapidly slow down at the highest level of reduction and value of $E_a \approx 45$ KJ/mol is reached for a strain level equal and higher 2.29. The lower values of E_a obtained for higher deformation levels can be explained by the larger vacancies content that promotes easier boundary motion during recrystallization. These E_a values will be introduced in statistical models in order to predict the microstructure and texture evolutions during recrystallization.

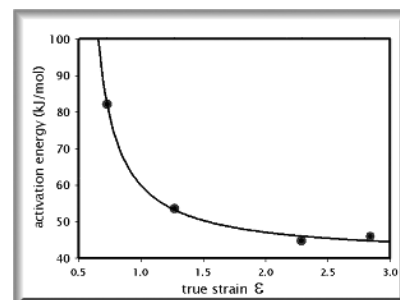


Figure 4. Evolution of activation energy E_a as function of the true strain.

References

[1] S. Jakani, M.H. Mathon, M. Benyoucef, Ph. Gerber, T. Baudin, C.H. de Novion, J. of Neutron Research, **126** (2004) 249.
 [2] Ph. Gerber, S. Jakani, M.H. Mathon, T. Baudin, accepted for publication in *Mat. Science For*

NEUTRON HOLOGRAPHIC STUDY OF PALLADIUM HYDRIDE

L. Cser¹, G. Krexner², M. Prem³, I. Sharkov⁴, Gy. Török¹¹ Central Research Institute for Physics – Budapest P.O.B. 49, H-1525, Hungary² Institute of Experimental Physics, University of Vienna, Boltzmanngasse 5, A-1090 Vienna, Austria³ Laboratoire Léon Brillouin (CEA-CNRS), CEA- Saclay, 91191 Gif sur Yvette Cedex⁴ St.Petersburg State University, Institute of Physics, Chair of Optics and Spectroscopy, Ulyanovskaja str.1, 198904 St.Petersburg, Russia

Holography was invented by Dénes Gábor [1] in an attempt to construct an electron microscope attaining atomic resolution without image distortions due to electromagnetic lenses. Despite the widespread use of holographic techniques in the wavelength range of visible light, which followed the development of highly coherent laser beams, the original idea to record images on an atomic scale could be realized only about 40 years later. During the last decade holographic techniques based on electrons (i.e. matter waves) were successfully extended to electromagnetic waves (X-rays and γ -rays) readily available from synchrotron radiation. A major part of this work has been reviewed e.g. in [2].

Limitations in applying the above techniques arise in the case of electrons from their extremely strong interaction with condensed matter restricting them essentially to the investigation of surfaces. X-rays, on the other hand, while being able to penetrate more deeply into matter, exhibit variations of sensitivity covering several orders of magnitude over the periodic table impeding their use for many systems involving particular combinations of elements. Neutrons, in principle, are not subject to these drawbacks. However, for various reasons, partly related to the limited intensity of presently available neutron beams, their application was not considered feasible. Only recently [3] experimental setups were put forward permitting to transfer certain conceptions developed in the context of X-ray holography to the case of neutrons.

Holographic imaging techniques are based on the recording of the interference pattern of two coherent waves originating from the same source. The first wave, that reaches the detector directly, serves as the reference wave; the second one is scattered by the object of interest and subsequently interferes with the reference wave. In the context of holography with atomic resolution basically two techniques are in use which are called the *inside source* and the *inside detector* setup, respectively.

In the case of neutrons [3,4,5], the inside-source concept requires a point-like source of spherical neutron waves within the sample. Hydrogen nuclei (i.e. protons) are extremely well suited to serve this

purpose due to their large incoherent elastic scattering cross section (~ 80 barns) for thermal neutrons. Metal-hydrogen systems, therefore, are a natural choice in studying various features of this novel technique. The feasibility of *Neutron Inside Source Holography* was first demonstrated in an experiment on a mineral containing substantial amounts of hydrogen by a Canadian group at Chalk River [6] and is applied in the present experiment on the metal-hydrogen system PdH [7]. The second method, *Neutron Inside Detector Holography*, requires the application of strongly neutron-absorbing isotopes which act as point-like detectors within the sample. It was successfully applied by the present authors in an experiment at the ILL in Grenoble recording the holographic image of a lead single crystal containing a small fraction of neutron-absorbing cadmium [8].

In the present investigation a holographic image of palladium nuclei in a PdH_{0.78} single crystal was recorded [7]. The sample was a slightly irregular-shaped slab with the dimensions $\sim 2.8 \times 15 \times 8$ mm³. It was covered with a thin copper film whose thickness (~ 30 μ m) was sufficient to avoid hydrogen loss. Hydrogen is well known to occupy octahedral interstitial sites in the *fcc* palladium lattice. The palladium nuclei play the role of the object while the hydrogen nuclei (i.e. protons) serve as point-like neutron sources inside the sample.

The experiment was done with the goal to overcome certain technical problems in order to open the way towards a wider range of applications. A particular challenge of the experiment consisted in the extraordinarily strong variations of the scattering intensity due to the size and irregular shape of the sample exceeding the weak holographic modulation ($\sim 10^{-3}$) by several orders of magnitude. This problem, however, could be solved by the application of suitable filtering and image processing techniques. In addition, it was shown that the problem of Bragg peak contaminations encountered in the first inside-source measurements [6] can be completely avoided by choosing an experimental setup where the sample is rotated about two perpendicular axes

while the detector is kept fixed at a scattering angle where the momentum transfer does not fulfil the Bragg condition [5]. In the same way contributions of Debye-Scherrer rings due to the copper coating could be circumvented and, more generally, this technique can be applied to any sample environment.

The experiment was carried out at the 6T2 four-circle diffractometer at the LLB Saclay, using a neutron wavelength of $\sim 0.9 \text{ \AA}$. The sample was mounted on the cradle of the diffractometer and rotated about the angle χ through a range of 45° and about the angle ϕ through a range of 350° . The angular step-width was 5° for both rotations leading to a mesh of $10 \times 71 = 710$ pixels forming the hologram. Due to the strong scattering from hydrogen the mean free neutron path in the sample was only several *mm* and, consequently, the geometry of the sample is strongly influencing the recorded hologram (cf. Fig.1). However, since the wavelengths of the holographic intensity modulations are typically much shorter, the shape function can be removed by appropriate filtering without disturbing the holographic information. A mathematical reconstruction of the positions of the Pd atoms occupying crystal lattice sites around the hydrogen probe nuclei is shown in Fig.2.

The above results demonstrate that neutron holography indeed may serve as a novel tool to investigate structural properties of metal-hydrogen systems and can be expected to yield reliable information on the positions of atoms in crystal lattices. The experience gained in the present experiment suggests, however, that the availability of more sophisticated image processing techniques is likely to become an important issue in practical applications.

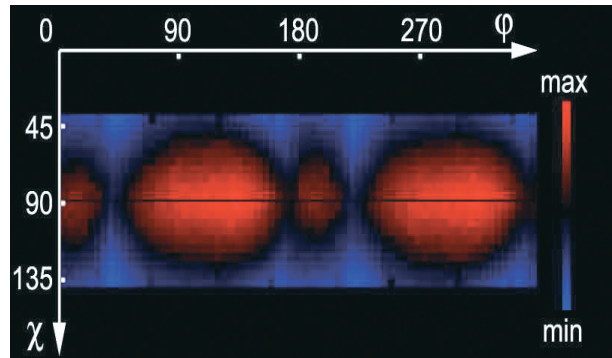


Figure 1. The raw hologram of the $\text{PdH}_{0.78}$ single crystal extended by symmetry operations to the whole range of the angle χ . The strong intensity variation due to the shape of the sample is clearly visible.

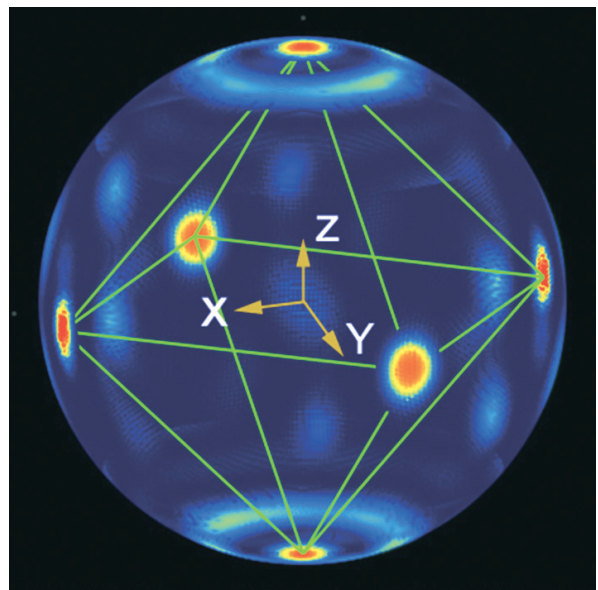


Figure 2. The restored holographic image of the local environment of a hydrogen nucleus. The three-dimensional octahedral arrangement of the Pd atoms is clearly visible. The hydrogen (not shown here) is located at the centre. The axes of the coordinate system are parallel to crystallographic [100] directions.

References

- [1] D. Gabor, *Nature* **161** (1948) 777
- [2] C. S. Fadley et al., *J.Phys.: Cond.Matter* **13** (2001) 10517
- [3] L. Cser, G.Krexner, and Gy.Török, *Europhys. Lett.* **54** (2001) 747.
- [4] L. Cser, G. Krexner, and Gy. Török, *Appl. Phys. A* **74** (2002) [Suppl1] s215-s217
- [5] L. Cser, B. Faragó, G. Krexner, I. Sharkov, and Gy. Török, *Physica B: Cond.Matter* **350** (2004) 113.
- [6] B. Sur, R.B.Rogge, R.P.Hammond, V.N.P.Anghel, and J.Katsaras, *Nature* **414** (2001) 525
- [7] L. Cser, Gy. Török, G. Krexner, M.Prem, and I. Sharkov, *Appl.Phys.Lett.* **85** (2004) 1149.
- [8] L. Cser, Gy. Török, G. Krexner, I. Sharkov, and B. Faragó, *Phys.Rev.Lett.* **89** (2002) 175504.

REPLACEMENT OF FIRST ELEMENTS OF GUIDES 1 TO 6

A. Menelle

Laboratoire Léon Brillouin (CEA/CNRS), CEA Saclay, F-91191 Gif sur Yvette, France

During summer 2003, the ring system in charge of the tightness of the 8F and 9F channels has been modified. This operation requires to remove the two beam plugs. This difficult operation took place on schedule between June and September 2003 without any noticeable incident.

The beam plugs contains the first two meters of the guides G1 to G6. Their quality is the key point of the neutron flux available on the instruments in the hall of guides. These elements, installed in 1984 have lost their original quality (especially on 8F). We took this opportunity to replace them by new elements better adapted to the new characteristics of the guides. Elements of G3, G4 and G5 have been replaced by identical elements, but G1, G2 and G6 have been replaced by elements coated with supermirrors.

After the restart of the reactor we have measured substantial improvements of flux on the instruments in the hall of guides. These improvements are very dependant on the wavelength and can reach 100% at 2 nm. A mean increase of 35% has been recorded on the instruments installed on G1 and G2. On G3 and G4, the increase of flux is 11%. Guides G5 and G6 were less degraded, and instruments installed on these guides have recover their usual flux. The replacement of the first elements of G6 by elements coated by supermirror has been done in order to anticipate the change of the entire guide G6 by supermirror elements that will take place in July 2005. Only at that moment important gain of flux on this guide will be measured.

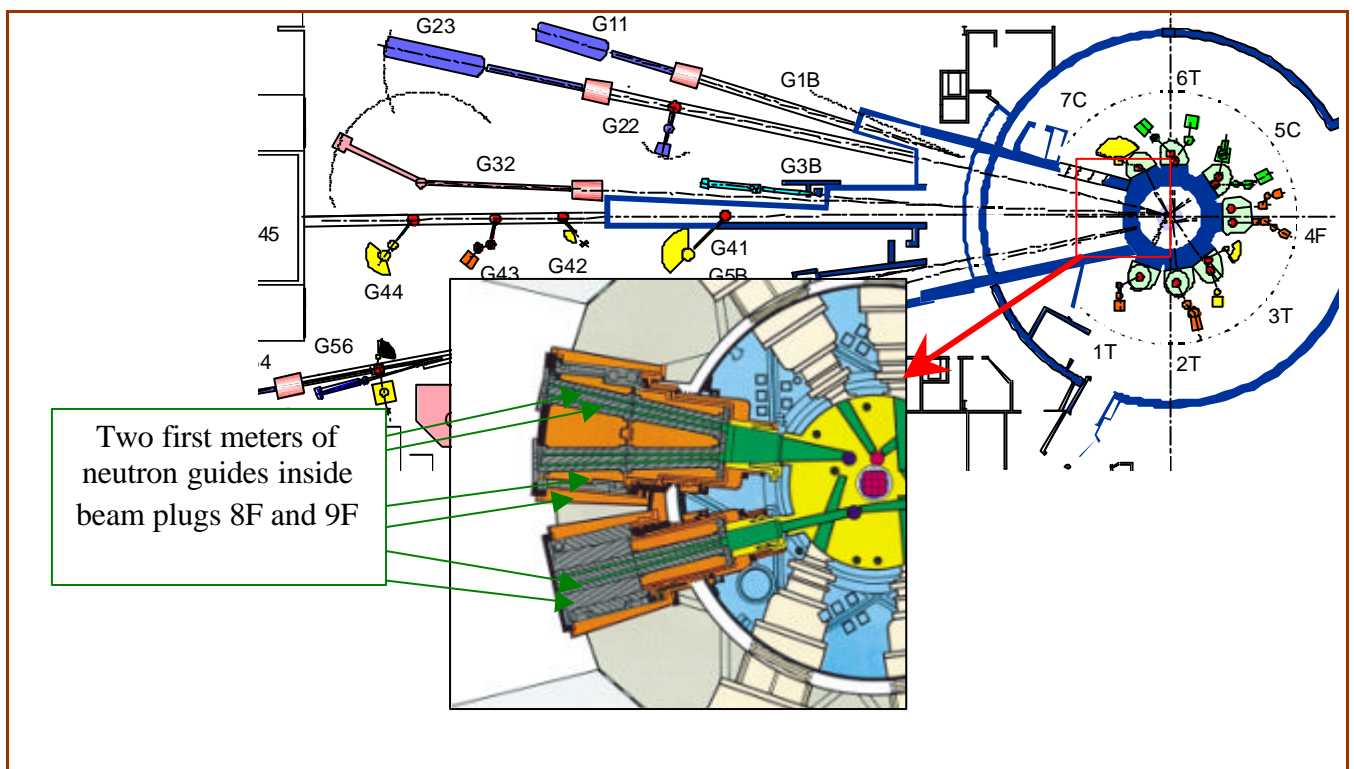


Figure. General layout of the guides elements within the 8F and 9F beam plugs.

REPORT ON A FIRST NEUTRON TEST OF A NEW 2D POSITION-SENSITIVE DETECTOR OF THERMAL NEUTRONS

A.Kuklin, G.Eckold , V.Gordeliy, S.Kutuzov, A.Islamov, A.Smirnov, P.Utrobin, A.Bogdzal, N.Alekseev, V.Comparat, A.Pelissier, J. Ballon, J. Teixeira , G.Koskas and A.Gabriel

The small angle neutron scattering time-of-flight spectrometer “YuMO” at the high flux reactor of IBR-2 (Dubna) has been operating successfully since 1984.

Recently, the Franck Laboratory for Neutron Physics (FLNP), in collaboration with the company 2D at Grenoble and the University of Goettingen have developed a new 2D position sensitive detector (PSD) with a central hole. The data acquisition is based on the delay line technique. This PSD will be installed at the YuMO spectrometer (Fig.1).

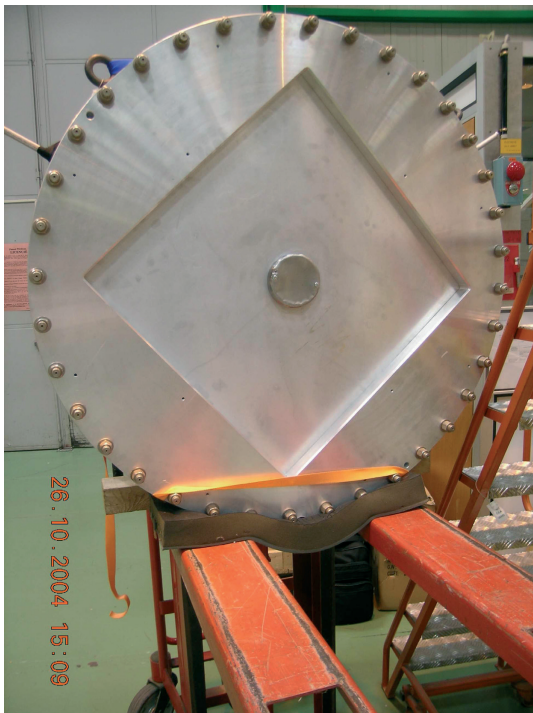


Figure 1. Main view of detector

The first neutron test of this detector has been performed at the beam-line G5-6 of the LLB. The detector was filled at a test pressure equal to 1 bar for CF₄ and 0.1 bar for ³He. For the estimation of the parameters of the detector we used several Cd-plates with different slit-sizes: 15, 12 and 10 mm as shown in Fig.2.

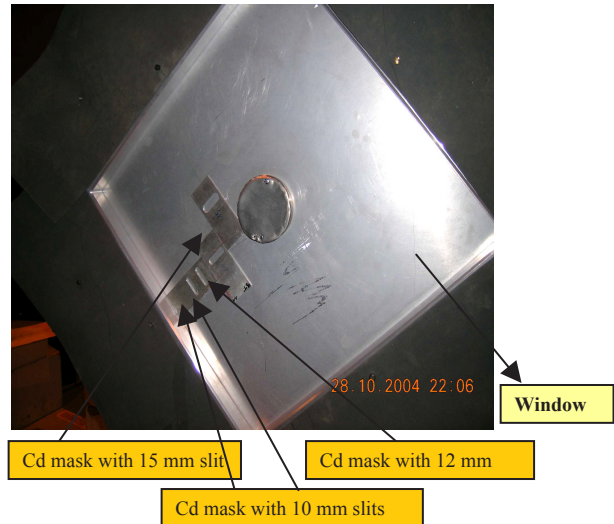


Figure 2. View of Cd slits during neutron test in LLB

The results of the tests of the detector are depicted in Fig.3. The final results yield the following information about the main parameters of the detector: standard deviation of the efficiency: 12% and positional resolution of the order of 3 mm.

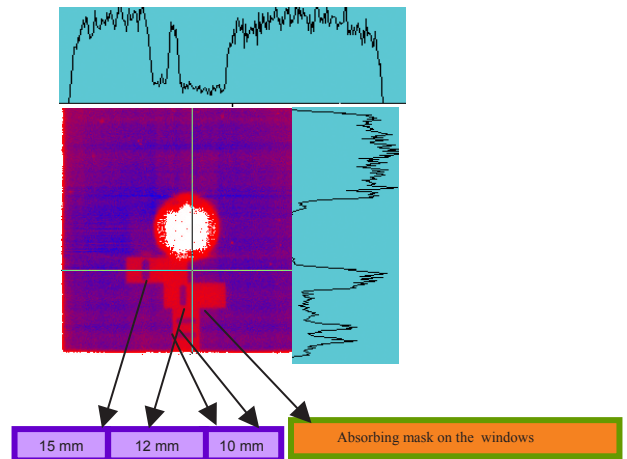


Figure 3. Main test result

Acknowledgments

We are very grateful to the staff of LLB for his help and support in the preparation and during the tests.

EXPERIMENTAL PROGRAMME AND USER ACTIVITIES

Operation of the Orphée Reactor and LLB facility in 2003-2004

The Orphée reactor is one of the most recent medium power reactors in Europe and has a very efficient operation. However, despite all its merit, Orphée-LLB suffers in the last years from severe budget cuts and will operate in a reduced mode for two years, in 2004-2005. In 2003, the LLB associates (CEA and CNRS) decided to reduce the operation of the Orphée reactor to 114 days per year (FPED, Full Power Equivalent Days) for the next two years due to budgetary problems. This reduction followed the 2001 agreement on the 180 days per year operation in 2001-2003, already for budgetary cuts. In former times, the agreement between the two associates (CEA and CNRS) had fixed this number of operating days to 210 days during the previous period, i.e. 1999-2000. In fact, the reactor operation has slightly exceeded these nominal numbers in the 2000-2002 years, leading to a real availability greater than 100% (see table 1). The normal operation mode of the Orphée reactor for its first eighteen (18) years in 1981-1998 was fixed to 245 days.

Year	1998	1999	2000	2001	2002	2003	2004
Reactor Days (EFPD)	218	205	213	186	183	163	118
% Availability	99,4	96,8	101,4	103,3	101,6	90,5	103,3

Table 1. Operation of the LLB-Orphée reactor for the last seven years, given in Equivalent Full Power Days (EFPD). The nominal operation mode was of 245 days up to 1997, of 210 days in 1998-2000, of 180 days in 2001-2003 and of 114 days in 2004. The low figure in 2003 is due to the extended summer stop to finish the refurbishment of the 8F-9F beam tubes feeding the cold neutron spectrometers in the guide hall.

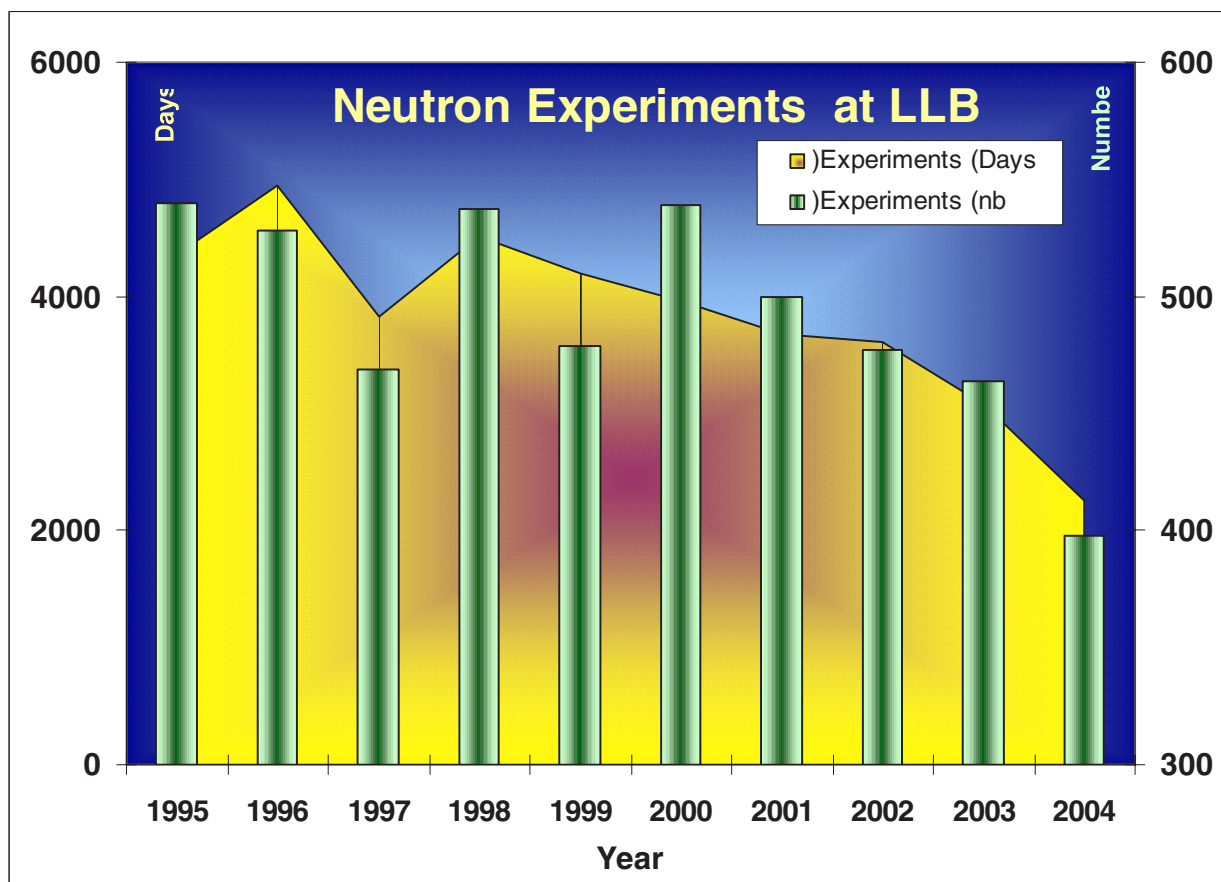


Figure 1. Graph of the number of experiments (green bars and right scale) and experiment days (yellow curve and left scale) performed at LLB-Orphée during the last ten years. The curves followed closely the number of operation days of the Orphée reactor (table 1).

The number of experiments and experiment days performed at LLB in 2003-2004 scaled closely with this **24% decrease of the available beam time**, compared to the previous two-year period: An average of **2670 experiment days per year in 2003-2004** (3080 exp. days in 2003 and 2260 exp. days in 2004) is to be compared with an average of 3400 experiment days per year in 2001-2002 (3340 exp. days in 2001 and 3440 exp. Days in 2002). The smoothed average over the last six years amounts to 3380 experiment days per year in 1999-2004.

The number of experiments decreased comparatively in a smaller proportion: an average of **431 experiments per year in 2003-2004** (464 experiments in 2003 and 398 in 2004) to compare with an average of 489 experiments in 2001-2002 (500 experiments in 2001 and 477 in 2002), leading to an 11% decrease only. The smoothed average over the last six years amounts to 476 experiments per year in 1999-2004.

Bibliometry of the LLB

The 2003-2004 period can be considered as record years for the LLB publications in high impact journals and reviews as it can be appreciated in the table 2 below.

Journals and Reviews	Impact Factor	2003-2004	2001-2002	1999-2000	TOTAL
Acta Materialia	2.65	1	2	-	3
Advanced Materials	5.57	-	-	1	1
Angewandte Chemie -International Edition	8.25	1	-	1	2
Applied Physics Letters	3.84	2	-	-	2
Biophysical Journal	4.63	4	4	1	9
Chemistry of Materials	3.69	4	3	3	10
Faraday Discussion	3.26	1	-	-	1
Inorganic Chemistry	2.94	3	1	-	4
Journal of Applied Crystallography	2.58	6	1	1	8
Journal of Chemical Physics	3.14	6	6	9	21
Journal of Materials Chemistry	2.74	1	-	-	1
Journal of Physical Chemistry A	2.53	2	-	-	2
Journal of Physical Chemistry B	3.38	6	5	-	11
Journal of Rheology	2.57	1	-	-	1
Journal of the American Chemical Society	6.07	1	1	-	2
J. of the Chemical Society, Dalton Trans.	2.82	1	1	-	2
Langmuir	2.97	6	2	9	17
Macromolecules	3.73	6	12	9	27
Microporous and Mesoporous Materials	2.50	1	-	-	1
Nature	27.96	2	2	1	5
Physical Review B.	3.19	46	40	43	129
Physical Review Letters	6.67	29	18	29	76
Science	23.33	1	1	1	3
Publications	Total	131	99	108	338

Table 2. Publication records of the LLB in the last six years, in high impact journals (IF > 2.5)

The French and European LLB users have been extremely productive and have written more papers in Physical Review Letters than ever. The production in the various areas of expertise of the LLB, like crystallography, material science, soft condensed matter and biology, is very satisfactory. These bibliometric benchmarks prove that Science made at the LLB is very well appreciated on an international level and we will not enter any kind of arguing on budget-averaged or flux-averaged figures of merit of the neutron

sources in Europe or abroad. The LLB is a top-level neutron facility and a laboratory of excellence. The LLB can even play its role in the worst conditions and keep a very high level of quality production.

Beyond childish quarrels and short-sighted arguments, we would like to pinpoint that most of the educational tasks, like training schools, thesis and post-doc works are better done in medium-power installations where scientific and technical staff have less pressure on their shoulders and that these day-to-day “underground” tasks are often under-evaluated even if they are most important to prepare the medium-term future of science. There is a reservoir of a dozen thesis students working currently at the LLB and we can estimate that every year more than a dozen thesis works are defended all over Europe that have crucially depended on the neutron beamtime delivered on LLB spectrometers. It is plain obvious that these figures played a key role in the battle fought by the LLB to convince its ruling authorities that LLB played, plays and will play a role in science and education : Now, The LLB has a clear future in the French and European neutron landscape for the next ten years.

Beam time allocation, experimental programme and user activities

The four review committees of the selection panel of the LLB comprise fifty (50) international scientists (see table at the end of the section) who meet twice a year at the LLB and have the difficult job of assessing the scientific quality and timeliness of submitted proposals and to advise on the allocation of beam time. The four committees report to the LLB direction that regulates the beam time allocation.

The LLB is the French Neutron Facility. Therefore, the major part of experiments allocated at the LLB in 2003-2004 has been given to French teams coming from all over the country. The French experiments stand for nearly two-thirds (2/3) of the total beam time allocated during this two-year period.

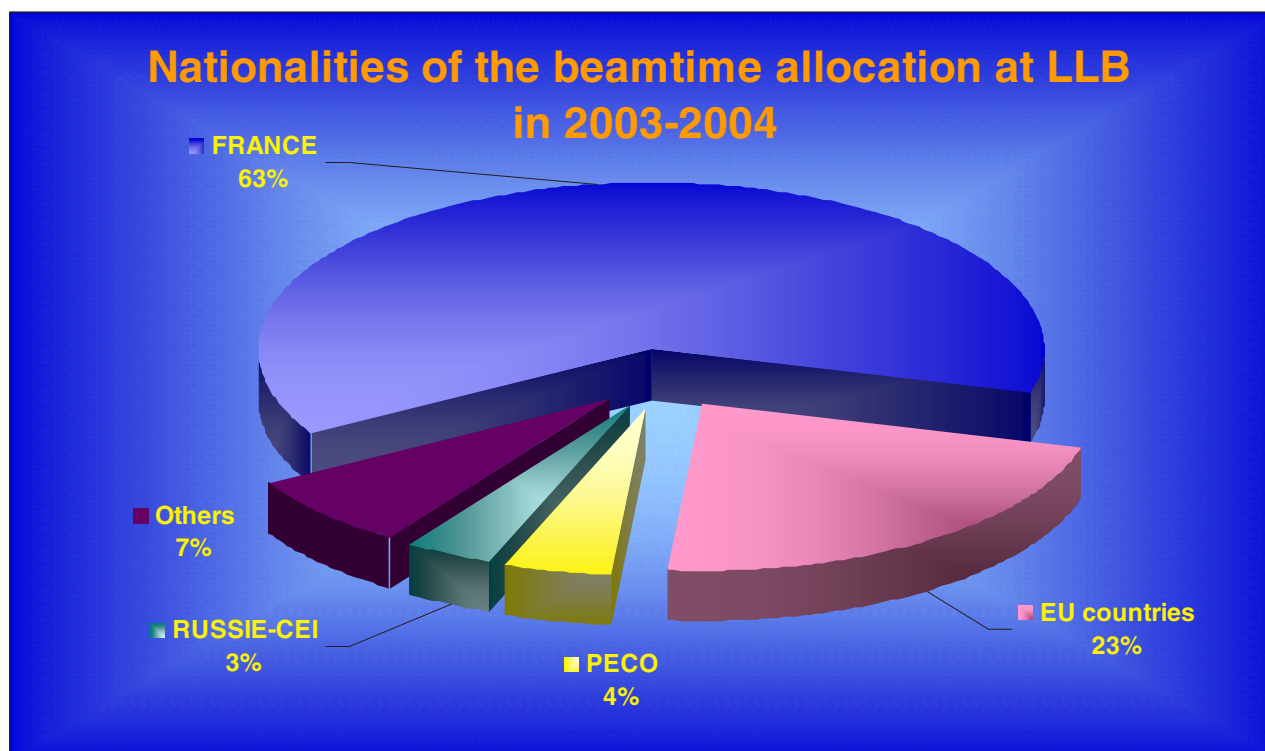


Figure 2. Beam time allocated at LLB-Orphée in 2003-2004 as a function of the nationality of the neutron teams involved in the accepted proposals .

The neutron teams from European and associated PECO (“Pays d’Europe Centrale et Orientale”) countries have benefited of more than one fourth (1/4) of the total beam time allocation, part of this use being supported by the European support for large-scale facilities (see next sub-section). The rest of the beam time

has been given mainly to Russia and for a non-negligible fraction (7%) to the remaining countries (USA, Japan, Switzerland, see beam time allocation subsection for a detailed analysis by countries).

Overall, the four review committees of the selection panel examined nine hundred thirty-four (934) proposals requesting 7778.5 days of beam time for 2003-2004, out of which seven hundred sixteen (716) proposals received beam time, allocating 4297 days on the twenty-three (23) LLB instruments.

The distribution of beam time requested and allocated amongst the different European and other countries is shown in the table 3.

Nearly two-thirds of the allocated beam time goes to the French proposals covering all domains of science and nearly all regions of France. One fourth of the beam time is devoted to European proposals coming from the major “neutron-wise” countries, i.e. Germany, Great Britain, Spain, Austria and Italy. Half of this European beam time goes to German experiments in long term collaborations, initiated on all instruments and not only on the CRG ones.

Country	Proposals 2003-2004	Experiments 2003-2004	Beamtime asked (days)	Beam time all. (Days)	Beam time asked (%)	Beam time all. (%)
France	550	451	4,588.0	2,681.5	59.0%	62.4%
FRANCE	550	451	4,588.0	2,681.5	59.0%	62.4%
Germany	96	76	785.5	504.0	10.1%	11.7%
Austria	12	8	109.0	65.0	1.4%	1.5%
Italy	50	30	372.0	149.5	4.8%	3.5%
Great-Britain	16	8	93.0	40.5	1.2%	0.9%
Spain	16	14	121.0	69.0	1.6%	1.6%
Others	30	22	226.0	136.0	2.9%	3.2%
EU countries	220	158	1,706.5	964.0	21.9%	22.4%
Poland	31	19	325.5	147.0	4.2%	3.4%
Hungary	4	2	37.0	8.0	0.5%	0.2%
Czech Rep.	3	2	32.0	13.0	0.4%	0.3%
Others	6	5	40.0	21.0	0.5%	0.5%
PECO	44	28	434.5	189.0	1.4%	1.0%
Russia	35	30	259.0	140.0	3.3%	3.3%
Ukraine	10	2	134.0	9.0	1.7%	0.2%
RUSSIE-CEI	45	32	393.0	149.0	5.1%	3.5%
United-States	27	22	277.0	170.0	3.6%	4.0%
Japan	18	10	154.0	68.0	2.0%	1.6%
Switzerland	2	2	17.5	10.5	0.2%	0.2%
Magrheb	14	9	103.0	36.0	1.3%	0.8%
Others	14	4	105.0	29.0	1.3%	0.7%
Others	75	47	656.5	313.5	8.4%	7.3%
TOTAL	934	716	7,778.5	4,297.0	100%	100%

Table 3. Compilation of the proposed and accepted experiments at LLB by the four series of selection panels done in 2003-2004 with the corresponding beam time demand and allocation in days and percentage for France, the EC countries, PECO and Russia and the rest of the world. The main “neutron-wise” countries have been highlighted.

Collaborations with Austria and Italy suffered with the closedown of the corresponding CRG instruments. On the contrary, the collaborations with Russia and PECO countries are still very active and count for nearly five percent of the allocated beam time, comparable with the rest of the internationally allocated beam time. This is the last report where these PECO countries appear, as they have been integrated in the European Community in 2004. We have stick to this definition in this report for consistency and comparison with the previous report (See also next sections).

European access programme: Bye-Bye HPRI in the FP5 and Welcome to NMI³ in the FP6

Since 1993, the LLB is a large-scale facility for the transnational access of European users in the framework of the Human Capital and Mobility (HCM, 1993-1997) and Training and Mobility of researchers (TMR, 1996-2000) programmes of the European Commission. In 1999, The LLB applied successfully in the FP5 scheme for the new HPRI European programme opened also to associated countries (e.g. central Europe). In 2003, the LLB has applied successfully in the FP6 scheme to continue in participating to the transnational access of European users to large-scale facilities in the Neutron-Muon Integrated Infrastructure Initiative, NMI³ in the forthcoming years (http://neutron.neutron-eu.int/n_nmi3). The LLB is particularly keen to attract new user groups from EC or associated countries and those wishing to apply neutron techniques to novel scientific areas. Researchers wishing to apply under the EC programme can do so via the normal LLB proposal mechanism. The LLB will provide travel and subsistence cost for up to two researchers in an accepted experiment.

As for the FP5 access programme, the first contract HPRI-CT-1999-0032 started on 1 February 2000 for three years until 31 January 2003. The initial plan was to deliver five hundred and ten (510) days of beam time for seventy (70) projects involving one hundred (100) individual users. The LLB has signed a new overlapping contract in 2002, HPRI-CT-2001-0170 for two years until February 2004. This contract concerned one hundred and eighty-five (185) days of beam time for twenty-five (25) projects involving thirty-seven (37) individual users. This second contract has ended up the transnational access programme of the FP5 scheme. The total FP5 access programme was planned for 695 days of beam time.

The access really delivered by the LLB during the total four-year period amounted in fact up to seven hundred and thirty-five (735) days of beam time, delivered to one hundred and twenty-eight (128) projects and concerned one hundred and eighty-seven (187) individual users coming from EC countries or associated countries. Amongst the 128 projects, 88 projects came from EC countries, i.e. roughly two-thirds of the total and 40 projects from associated countries. Nationalities involved in the access programme reflect closely the ones active in the global access described in the preceding section, i.e. Germany, Italy, Spain and Greece for EC and Poland and Hungary for associated countries at the time of the contracts.

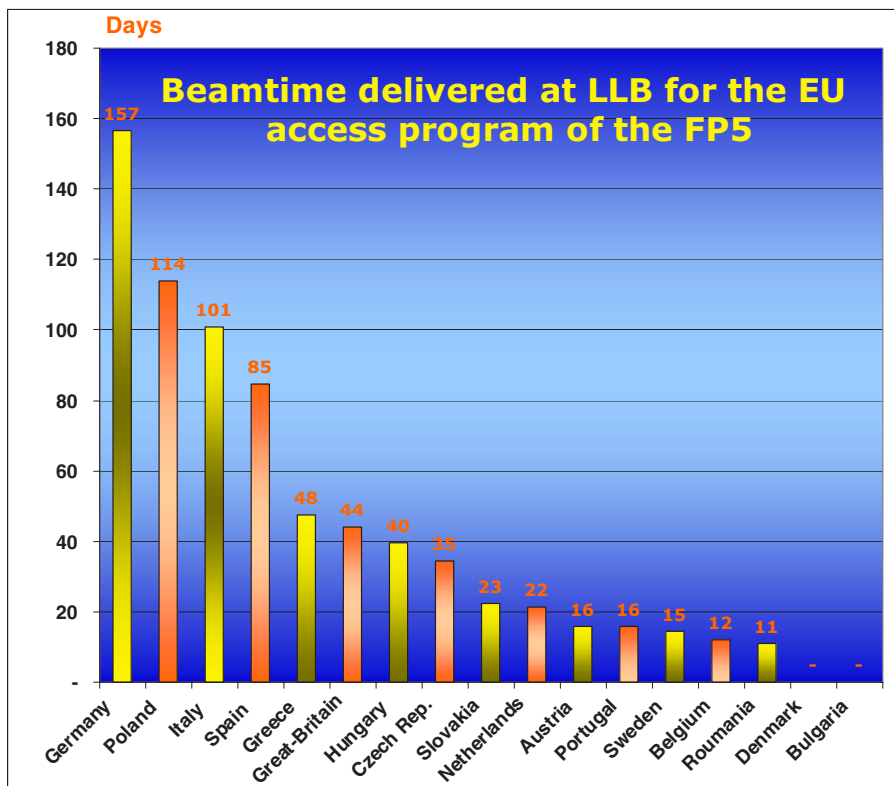


Figure 3. Beam time delivered at LLB-Orphée in 2003-2004 in the framework of the transnational access program supported by the European FP5 scheme for large scale facilities, as a function of the nationality of the neutron researchers invited by the LLB.

Selection panel and Beam time allocation

There are three different complementary ways of submitting a proposal to the LLB:

- Standard submission of a research proposal, twice a year in Spring and Fall
- Long term research project over three (3) years, twice a year in Spring and Fall
- Fast access procedure for short experiment or test, without time restriction.

Special access for proprietary research and industrial users and firms are considered separately.

More detailed information on applications for beam time and deadlines are given on the LLB web site at <http://www-llb.cea.fr>

Proposals for experiments are selected and beam time allocations are made through peer review. Review committees of specialists from France and the most parts of European countries have been set up in the following scientific areas:

- Session A for physical chemistry and biology
- Session B for structural studies and phase transitions
- Session C for Magnetism and superconductivity
- Session D for disordered systems and material science.

The relative importance of these four committees of the selection panel at LLB is depicted in the figure 4 below this paragraph. The largest committee of the LLB is the one dealing with magnetism and superconductivity, domain where the LLB expertise is acknowledged worldwide. The three other committees are roughly equivalent in importance and share the rest of the allocated beam time, each of them getting around 20% of the total beam time. Each session of the Selection Panel comprises typically nine (9) members (3 French members, 3 foreign members and 3 LLB members).

The list of the selection panel for Fall 2004 is given at the end of this section.

The review committee meet twice a year, some six weeks after the deadline for submission of proposals (1 April in spring and 1 October in fall). Accepted proposals submitted by April receive beam time in the second half of the year and those submitted by October, in the first half of the following year.

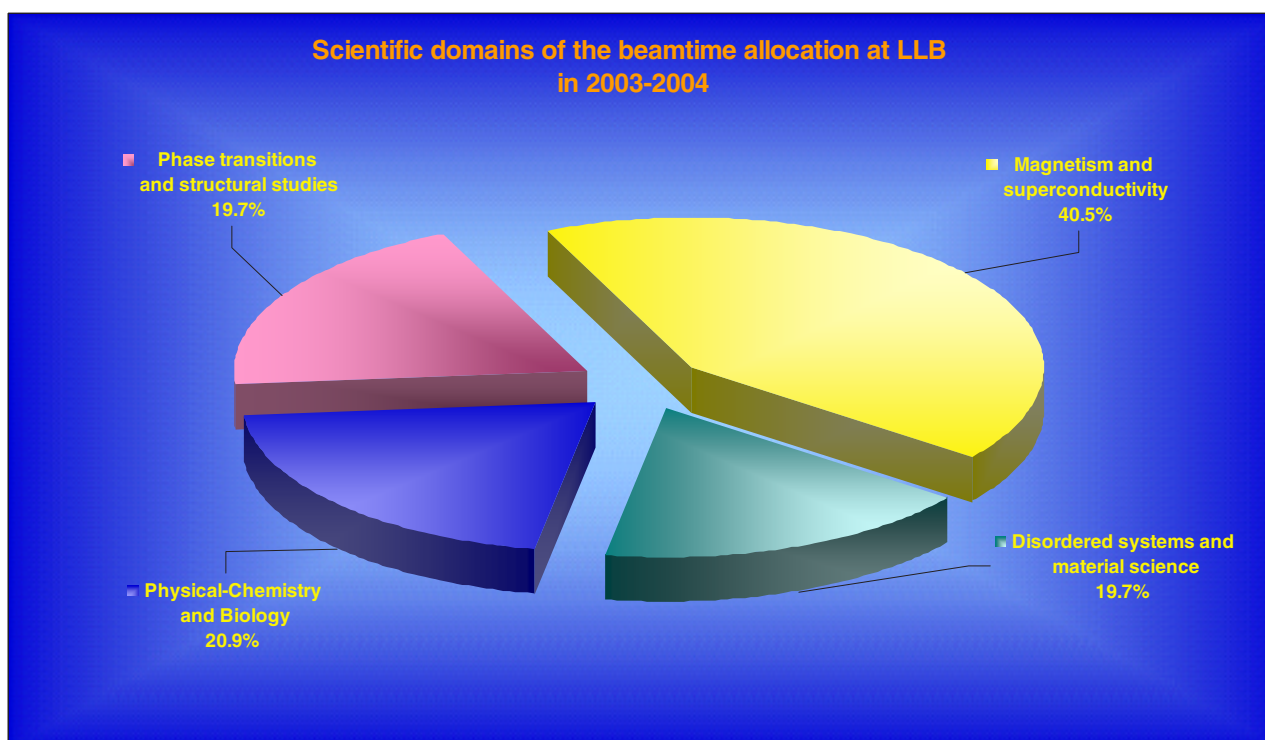


Figure 4. Repartition of the beam time delivered at LLB-Orphée in 2003-2004 amongst the four committees of the selection panel with the corresponding percentage.

The LLB has discontinued in 2003 the fall user meeting and the system of Round Tables and User Selection panels put in place in 1996. The “Tables Rondes du LLB” are splitted into a selection committee meeting (twice a year) and thematic workshops called “Rencontres de StAubin” organised in close collaboration with the new French synchrotron SOLEIL that will be soon in operation on the Saclay Plateau. These workshops will focus on the major scientific areas of the LLB and of SOLEIL and will emphasise the complementarity of the two scattering techniques.

The four selection committees allocated the neutron beam time on the 23 spectrometers of the LLB with an average overload factor of 1.81 in 2003-2004. The spectrometers are grouped in five major categories: structure determination (on powders or single crystals), dynamical studies, Small Angles Neutron Scattering (SANS), Materials science (including nanomaterials and metallurgy) and High Resolution (in time, energy or reciprocal space).

Group	Proposals 2003-2004	Beamtime 2003-2004	Session A	Session B	Session C	Session D	TOTAL Alloc.	F_over
Structure	310	2,570	19	436	872	39	1,366	1.88
Dynamics	157	1,691	7	341	626	31	1,005	1.68
SANS	238	1,303	466	12	49	124	650	2.00
Materials	104	1,152	154	-	209	313	676	1.71
High Res.	125	1,063	253	58	43	248	601	1.77
TOTAL	934	7,778.5	898.0	846.5	1,798.5	754.0	4,297	1.81

Table 4. Compilation of the proposed experiments at LLB by the four series of selection panels done in 2003-2004 with the corresponding beam time demand and allocation in days by the four committees: Session A stands for physical chemistry and biology, Session B for structural studies and phase transitions, Session C for Magnetism and superconductivity, Session D for disordered systems and material science.

Last column displays the overload factor in the five instrument categories and the global overload factor calculated on the beam time allocation.

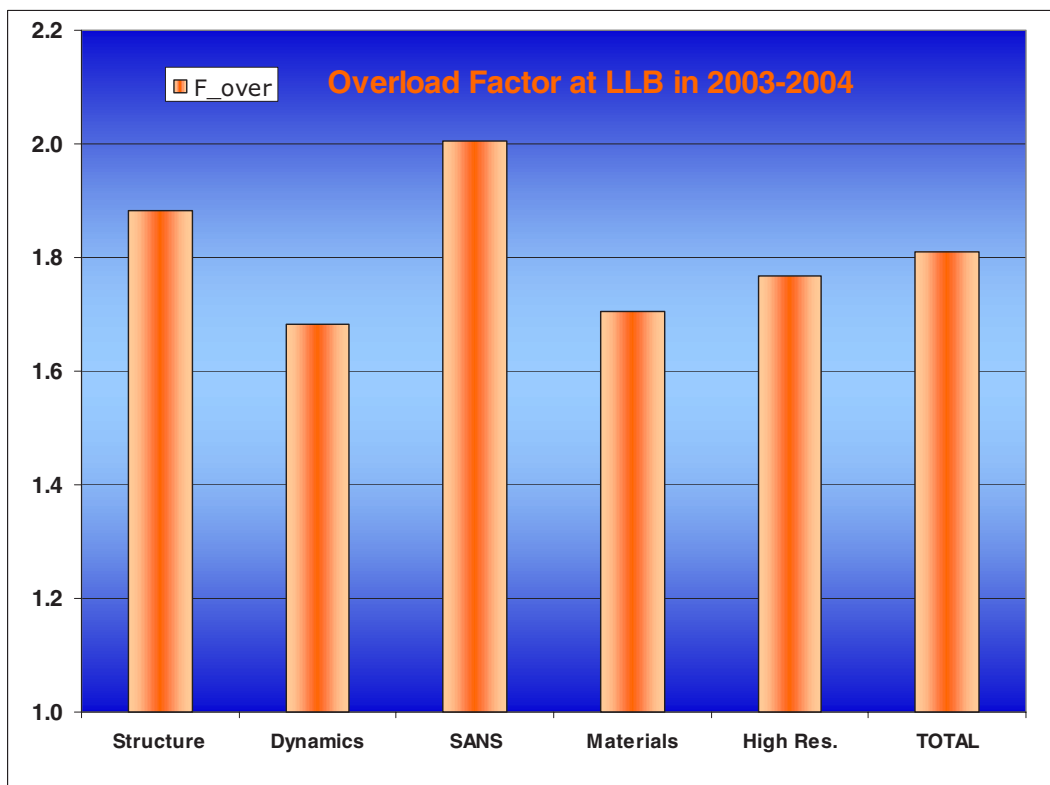


Figure 5. Overload factor of the various instrument groups at LLB 2003-2004 calculated on the beam time demand and allocation.

EXPERIMENTAL PROGRAMME AND USER ACTIVITIES

Experiments at LLB are performed on various types of spectrometers. The five main groups are concerned with structure determination (on powders or single crystals), dynamical studies, Small Angles Neutron Scattering (SANS), Materials science (including nanomaterials and metallurgy) and High Resolution (in time, energy or reciprocal space).

The structural and dynamical studies have an allocated beam time of more than one thousands experimental days per two years. The three smaller groups of instruments deal with SANS, material science and High Resolution. They get an allocation of around six hundreds experimental days per two years.

LLB 2003-2004	Proposal number	Beamtime Asked (days)	Allocated Session A	Allocated Session B	Allocated Session C	Allocated Session D	TOTAL Allocated
5C1	29	409	-	-	188	-	188
5C2	30	521	-	205	38	-	243
6T2	40	456	-	58	156	-	214
3T2	78	353	-	107	94	5	206
G4.1	73	357	5	34	169	11	219
G4.2*	19	114	4	23	51	-	78
G6.1	41	360	10	9	176	23	218
Structures	310	2 570	19	436	872	39	1 366
1T1*	38	379	7	64	113	-	184
2T1	46	528	-	40	201	24	265
4F1/4F2	68	708	-	160	312	7	479
G4.3*	5	76	-	77	-	-	77
G4.5	-	-	-	-	-	-	-
Dynamics	157	1 691	7	341	626	31	1 005
PACE	94	553	232	-	-	19	251
PAXE	76	386	96	8	7	75	185
PAXY	68	364	139	4	42	31	215
SANS	238	1 303	466	12	49	124	650
6T1	17	314	-	-	-	201	201
G5.2*	20	225	-	-	-	97	97
G2.4	25	222	6	-	151	-	157
G3.Bis	31	228	133	-	26	10	169
G5.5	11	163	15	-	32	5	52
Materials	104	1 152	154	-	209	313	676
7C2	45	317	25	14	10	148	197
G4.4	1	3	-	-	-	-	-
G1.Bis*	27	295	91	7	14	64	176
Spin Echo	2	35	21	-	-	-	21
TV	50	413	116	37	19	36	208
High Res.	125	1 063	253	58	43	248	601
TOTAL	934	7 779	898	847	1 799	754	4 297

Table 5. Compilation of the proposed and accepted experiments at LLB by the four series of selection panels done in 2003-2004 with the corresponding beam time demand and allocation in days and percentage for the five groups of dedicated spectrometers for Structure, Dynamics, SANS, Materials science and High Resolution spectroscopy.

Instrument operation in 2003-2004

The instrumental operation at LLB in 2003-2004 was smooth and efficient. Despite all the pressure on its future, The LLB has continued in 2003-2004 to upgrade its instrument park, especially on the material science spectrometer 6T1 for textures and the cold neutron triple-axis spectrometer 4F2. The LLB has progressed in the development of the Very small angle spectrometer TPA and finished the definition of the spectrometer (see instrumentation section). The spectrometer will be finished in the forthcoming years. The high-resolution powder diffractometer 3T2 will be completely rebuilt and upgraded by the end of 2005. Upgrade of the time of flight reflectometer G3.Bis "Eros" has also started and will be rapidly evolving in the next years before the transfer of the spectrometer on the Mibemol position.

The two graphs below show the beam time really delivered and the experiments performed over the last two years on the different types of spectrometers.

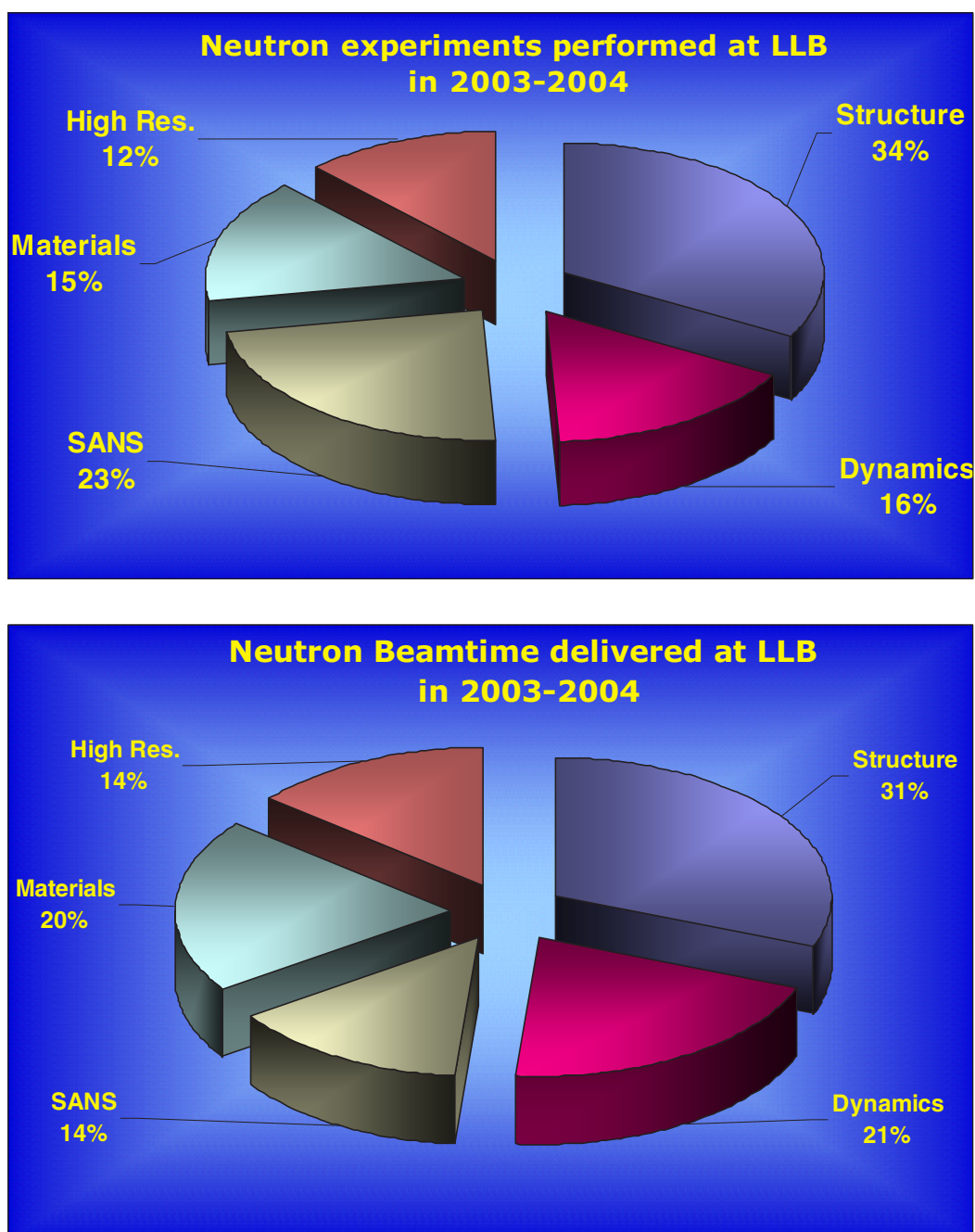


Figure 6. Repartition of the experiments performed and of the beam time delivered at LLB-Orphée in 2003-2004 amongst the five instrumental groups of spectrometers with the corresponding percentage.

The LLB spectrometers are grouped in five major categories: structure determination (on powders or single crystals), dynamical studies, Small Angles Neutron Scattering (SANS), Materials science (including nanomaterials and metallurgy) and High Resolution (in time, energy or reciprocal space). The two graphs below show the beam time really delivered and the experiments performed over the last four years on the different types of spectrometers. An average plot serves as a reference.

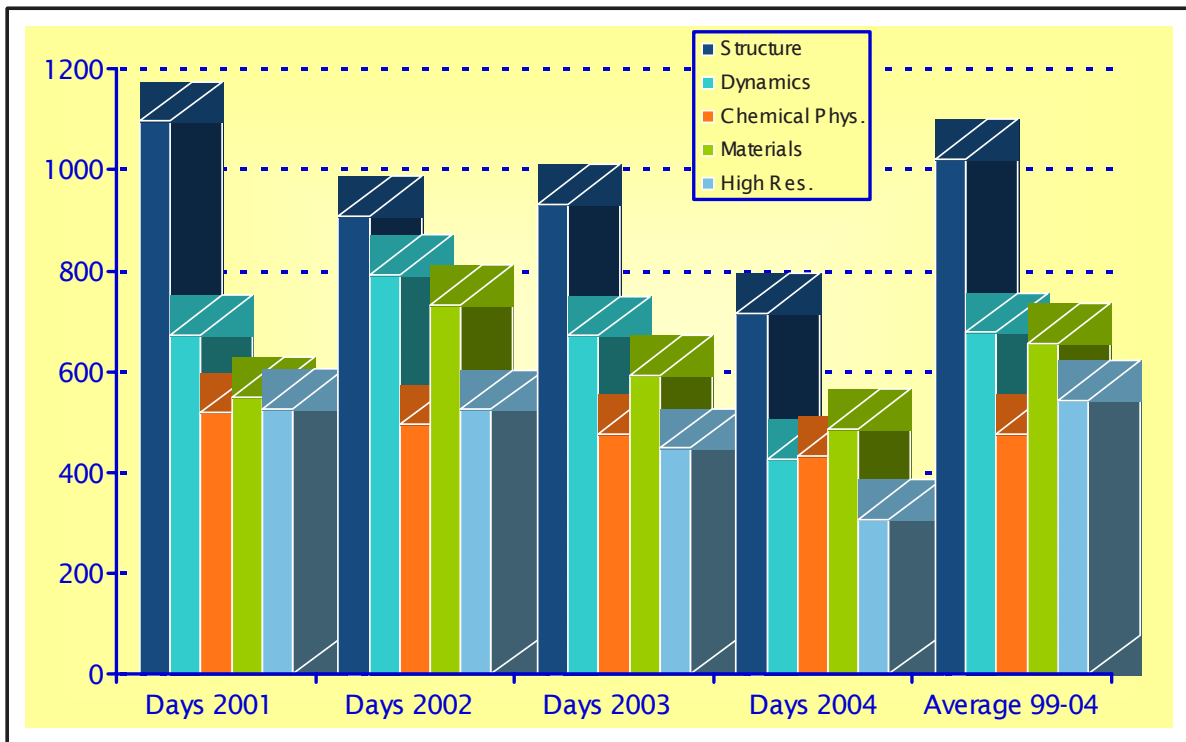
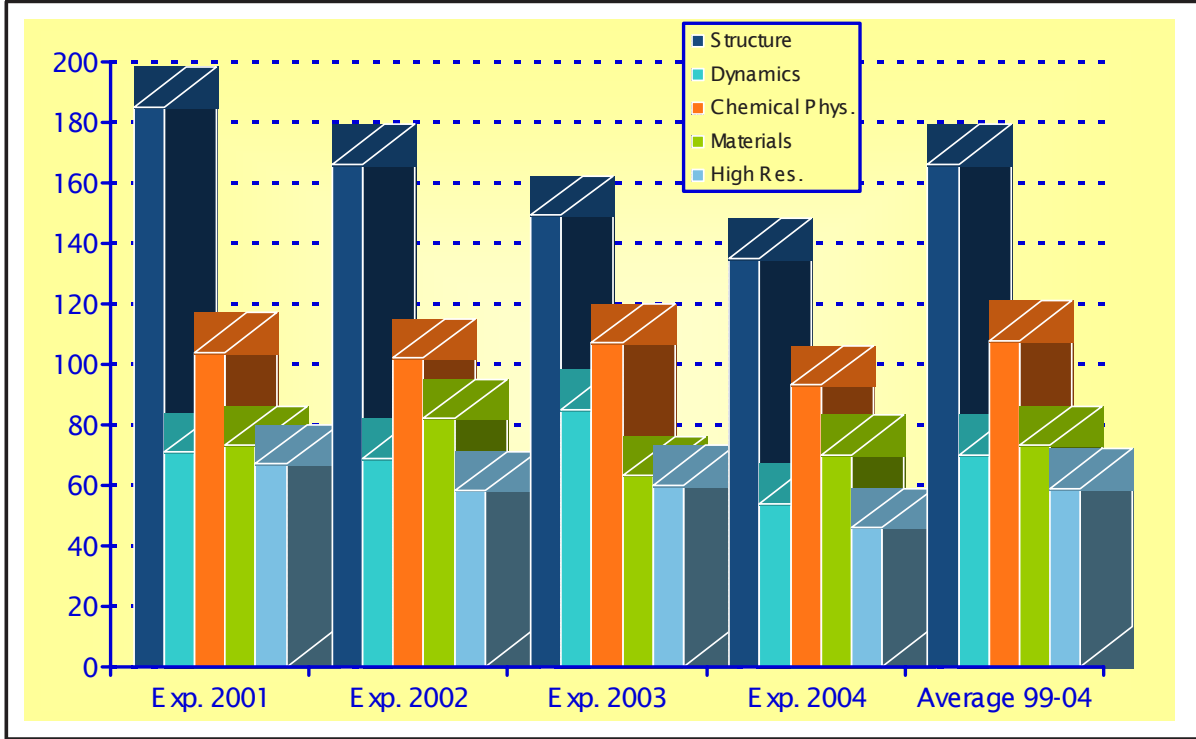


Figure 7. Graphs of the beam time (lower figure) delivered at LLB-Orphée over the last four (4) years and of experiments (upper figure) done in the same period as a function of the instrumental group (listing at the section end). The last data show the average over the last six years.

EXPERIMENTAL PROGRAMME AND USER ACTIVITIES

The two tables below show the beam time really delivered and the experiments performed over the last four years on the different types of spectrometers. The beam time percentage serves as a reference.

LLB Spectrometer	Experiments 2001-2002	Exp. Days 2001-2002	Beamtime 2001-2002	Experiments 2003-2004	Exp. Days 2003-2004	Beamtime 2003-2004
5C1	24	313	4.3%	28	246	4.6%
5C2	38	342	4.7%	31	259	4.9%
6T2	31	332	4.6%	29	264	4.9%
3T2	69	309	4.2%	66	235	4.4%
G4.1	77	328	4.5%	73	238	4.5%
G4.2*	67	224	3.1%	20	169	3.2%
G6.1	45	336	4.6%	37	237	4.4%
Structure	351	2 184	30.0%	284	1 648	30.9%
1T1*	26	218	3.0%	22	154	2.9%
2T1	31	328	4.5%	31	273	5.1%
4F1/4F2	59	670	9.2%	75	568	10.6%
G4.3*	20	214	2.9%	10	101	1.9%
G4.5	4	36	0.5%	1	3	0.1%
Dynamics	140	1 466	20.1%	139	1 099	20.6%
PACE	64	316	4.3%	63	240	4.5%
PAXE	66	306	4.2%	75	255	4.8%
PAXY	76	351	4.8%	62	257	4.8%
SANS	206	973	13.4%	200	752	14.1%
6T1	21	351	4.8%	16	242	4.5%
G5.2*	40	325	4.5%	25	256	4.8%
G2.4	37	252	3.5%	33	217	4.1%
G3.Bis	44	360	4.9%	28	173	3.2%
G5.5	13	146	2.0%	31	193	3.6%
Materials	155	1 434	19.7%	133	1 081	20.3%
7C2	45	340	4.7%	39	208	3.9%
G4.4	7	279	3.8%	1	7	0.1%
G1.Bis*	25	192	2.6%	24	207	3.9%
Spin Echo	7	118	1.6%	5	83	1.6%
TV	41	301	4.1%	37	251	4.7%
High Res.	125	1 230	16.9%	106	756	14.2%
TOTAL	977	7 286	100%	862	5 336	100%

Table 6. Compilation of performed experiments at LLB in 2003-2004 : comparison with the corresponding beam time use and performed experiments in 2001-2002 for the five instrumental groups of spectrometers with the corresponding percentage.

The Graph and the table below show the beam time really delivered and the experiments actually performed over the last two and the last four years for the various countries. The beam time percentage serves as a reference.

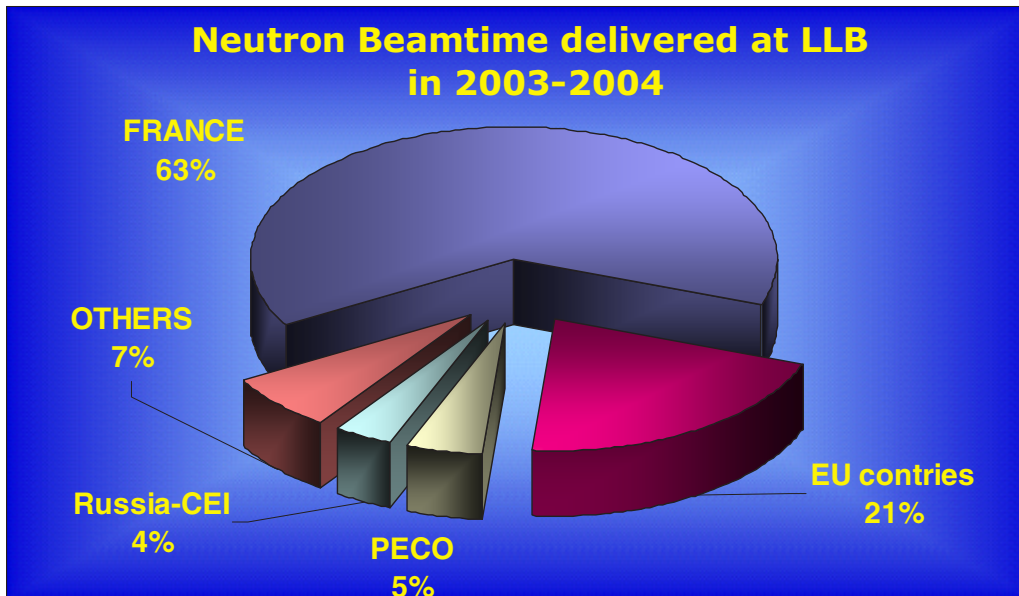


Figure 8. Repartition of the experiments performed and of the beam time delivered at LLB-Orphée in 2003-2004 amongst the five instrumental groups of spectrometers with the corresponding percentage.

Country	Experiments 2001-2002	Exp. Days 2001-2002	Beamtime 2001-2002	Experiments 2003-2004	Exp. Days 2003-2004	Beamtime 2003-2004
FRANCE	648	4 722	64.8%	564	3 414	64.0%
FRANCE	648	4 722	64.8%	564	3 414	64.0%
Germany	76	600	8.2%	85	544	10.2%
Austria	19	229	3.1%	11	75	1.4%
Italy	30	215	2.9%	33	180	3.4%
Great-Britain	22	185	2.5%	7	46	0.9%
Spain	17	112	1.5%	16	107	2.0%
Others	47	274	3.8%	25	156	2.9%
EU countries	211	1 615	22.2%	177	1 106	20.7%
Poland	19	214	2.9%	25	205	3.8%
Hungary	10	74	1.0%	5	29	0.5%
Czech Rep.	8	57	0.8%	3	21	0.4%
PECO	37	345	4.7%	33	255	4.8%
Russia	37	272	3.7%	36	187	3.5%
Russia-CEI	37	272	3.7%	36	187	3.5%
United States	12	89	1.2%	17	129	2.4%
Switzerland	6	66	0.9%	1	8	0.1%
Japan	11	76	1.0%	12	99	1.9%
Other countries	15	100	1.4%	23	138	2.6%
OTHERS	44	331	4.5%	53	374	7.0%
TOTAL	977	7 284	100%	862	5 335	100%

Table 7. Compilation of the proposed and accepted experiments at LLB by the four series of selection panels done in 2003-2004 with the corresponding beam time demand and allocation in days and percentage for France, the EC countries, PECO and Russia and the rest of the world. The main “neutron-wise” countries have been highlighted.

Listing of the selection panel Fall 2004

TABLE RONDE A : Physico-chimie, Biologie				
<i>Organisateurs : L. Noirez</i>				
Représentants LLB	Représentants français		Représentants européens	
F. Boué	J. Combet	ICS Strasbourg	M. Geoghegan	Université de Sheffield
J.-M. Zanotti	O. Diat (Président)	CENG Grenoble	T. Hellweg	Technische Univ. Berlin
	M. Ferrand	CENG Grenoble	P. Mariani	Université d'Ancone
	I. Grillo	ILL Grenoble	P. Stepanek	IMC, Prague
	S. Lecommandoux	LCPO Pessac		

TABLE RONDE B : Etudes Structurales, Transitions de Phase				
<i>Organisateurs : F. Bourée, H. Moudden</i>				
Représentants LLB	Représentants français		Représentants européens	
J.-M. Kiat	T. Fernandez-Diaz	ILL, Grenoble	F. Frey	Université Munich
	S. Klotz	Université P. et M. Curie, Paris	M. Braden (Président)	Université Cologne
	M. Latroche	CNRS, Thiais	J.-M. Perez-Mato	Université Bilbao

TABLE RONDE C : Magnétisme, Supraconductivité				
<i>Organisateurs : P. Bourges, G. Chaboussant</i>				
Représentants LLB	Représentants français		Représentants européens	
A. Goukassov	M. D'astuto	Université Paris VI	J.-L. Garcia-Munoz	ICMAB, Barcelone
M. Hennion	C. Dufour	Université Nancy I	G. Mc Intyre (Président)	I.L.L., Grenoble
	A. Ivanov	I.L.L., Grenoble	P.G. Radaelli	ISIS, Oxfordshire
	C. Martin	CRISMAT Caen		

TABLE RONDE D : Systèmes désordonnés, Matériaux				
<i>Organisateurs : B. Beuneu, C.-H. de Novion</i>				
Représentants LLB	Représentants français		Représentants européens	
G. Pepy	M. Bée	Univ. Joseph Fourier, Grenoble	I. Cabaco-Fialho (Pdte)	CFAUL, Lisbonne
	O. Castelnau	LPMTM, Villetaneuse	H.-G. Priesmeyer	Université de Kiel
	P. Vajda	Ecole Polytechnique, Palaiseau		

Table 8. Table of the members of the four selection committees of LLB in Fall 2004

The LLB instrument suite of scheduled neutron spectrometers for external users

STRUCTURE	TYPE	SPECTRUM	DOMAIN
3T2	High resolution 2-axis	Thermal	Powder
G4.1	Multidetector 2-axis-	Cold	Powder
G4.2	High resolution 2-axis	Cold	Powder
G6.1	Multidetector 2-axis	Cold	High pressure
5C1	2-axis	Hot, polarised	Magnetism
5C2	4-cercles	Hot	Single crystal
6T2	4-cercles and 2-axis	Thermal	Single crystal
DYNAMICS	TYPE	SPECTRUM	DOMAIN
1T1	3-axis	Thermal	Excitations
2T1	3-axis	Thermal, polarised	Excitations
4F1	3-axis	Cold, (pol. opt.)	Excitations
4F2	3-axis	Cold	Excitations
G4.3	3-axis	Cold	Excitations
G4.5 Neutronography	(HPRI users only)	Cold	Imaging
SMALL ANGLE	TYPE	SPECTRUM	DOMAIN
G1.2 PACE	Annular Detector	Cold	Large scale
G2.3 PAXY	XY Detector	Cold	Large scale
G5.4 PAXE	XY Detector	Cold	Large scale
MATERIAL SCIENCE	TYPE	SPECTRUM	DOMAIN
6T1	4-cercles for textures	Thermal	Material science
G5.2 DIANE	2-axis	Cold	Material science
G3 bis EROS	XY Detector (TOF)	Cold	Soft matter
G2.4. PRISM	2-axis	Cold, polarised	Magnetism
G5.5 PAPOL	XY Detector	Cold, polarised	Large scale
HIGH RESOLUTION	TYPE	SPECTRUM	DOMAIN
7C2	Multidetector 2-axis	Hot	Liquids & disorder
G4.4	2-axis TOF	Cold	Diffuse scattering
G1 bis MUSES	High flux Spin Echo	Cold, polarised	Quasi-elastic
G3.2 MESS	Spin Echo	Cold, polarised	Quasi-elastic
G6.2 MIBEMOL	Time of flight (TOF)	Cold	Quasi-elastic

Table 9. The details of the five main categories of the LLB instrument suite.

PUBLICATIONS 2003-2004

PUBLICATIONS – 2003-2004
PAPERS PUBLISHED IN SCIENTIFIC PERIODICALS
AND CONFERENCE PROCEEDINGS

- Abete, T. ; de Candia, A. ; Lairez, D. ; Coniglio, A.**
Percolation model for enzyme gel degradation
 Physical Review Letters, 2004, **93** 228301
- Aguado, F.; Rodriguez, F.; Valiente, R.; Senas, A.; Goncharenko, I.**
Three-dimensional magnetic ordering in the Rb_2CuCl_4 layer perovskite - structural correlations
 Journal of Physics: Condensed Matter, 2004, **16** 1927-1938
- Alamo, A.; Lambard, V.; Averty, X.; Mathon, M.H.**
Assessment of ODS-14%Cr ferritic alloy for high temperature applications
 Journal of Nuclear Materials, 2004, **329** 333-337
- Albergamo, F.; Bossy, J.; Glyde, H.R.; Dianoux, A.-J.**
Elementary excitations in liquid ^4He confined in MCM-41
 Physical Review B, 2003, **67** 224506
- Alekseev, P.A.; Mignot, J.M.; Nefedova, E.V.; Nemkovskii, K.S.; Lazukov, V.N.; Sadikov, I.P.; Ochiai, A.**
Nature of the magnetic excitation spectrum in $(\text{Sm}, \text{Y})\text{S}$: CEF effects or an exciton
 JETP Letters, 2004, **79** 81-84
- Alekseev, P.A.; Mignot, J.M.; Nemkovskii, K.S.; Nefedova, E.V.; Shitsevalova, N.Yu.; Paderno, Yu.B.; Bewley, R.I.; Eccleston, R.S.; Clementyev, E.S.; Lazukov, V.N.; Sadikov, I.P.; Tiden, N.N.**
Yb-Yb correlations and crystal-field effects in the Kondo insulator YbB_{12} and its solid solutions
 Journal of Physics. Condensed Matter, 2004, **16** 2631-2646
- Alekseev, P.A.; Mignot, J.M.; Nemkovskii, K.S.; Shitsevalova, N.Y.; Bewley, R.I.; Lazukov, V.; Nefedova, E.V.; Sadikov, I.P.; Toden, N.N.**
Cooperative and local properties in the Kondo insulator YbB_{12}
 Journal of Magnetism and Magnetic Materials, 2004, **272** 75-76
- Alleno, E.; Godard, C.; Andre, G.; Dhar, S.K.; Pattalwar, S.M.; Bonville, P.**
Magnetic structure in the zero-applied-field reentrant superconductor $\text{ErNi}_{1.96}\text{Fe}_{0.04}\text{B}_2\text{C}_{0.99}$
 Physical Review B, 2003, **68** 214518
- Almasy, L.; Cser, L.; Jancso, G.**
Kirkwood-buff integrals in aqueous solutions of 3-methylpyridine
 Journal of Molecular Liquids, 2003, **101** 89-98
- Almazy, L.; Jancso, G.**
Small-angle neutron scattering and kirkwood-buff integral study of aqueous solutions of pyridine
 Journal of Molecular Liquids, 2004, **113** 61-66
- Altissimo, M.; Di Fabrizio, E.; Ott, F.; Petrillo, C.; Sacchetti, F.**
Fresnel zone plates as neutron optical elements
 Nuclear Instruments and Methods in Physics Research A, 2004, **529** 148-151
- Altissimo, M.; Petrillo, C.; Sacchetti, F.; Ott, F.; Di Fabrizio, E.**
Zone plate for thermal neutron focusing : design, fabrication and first experimental tests
 Microelectronic Engineering, 2004, **73** 644-650
- Ammar, A.; Ménétrier, M.; Villesuzanne, A.; Matar, S.; Chevalier, B.; Etourneau, J.; Villeneuve, G.; Rodríguez-Carvajal, J.; Koo, H.-J.; Smirnov, A.I.; Whangbo, M.-H.**
Investigation of the Electronic and Structural Properties of Potassium Hexaboride, KB_6 , by Transport, Magnetic Susceptibility, EPR, and NMR Measurements, Temperature-Dependent Crystal Structure Determination, and Electronic Band Structure Calculations
 Inorganic Chemistry, 2004, **43** 4974-4987
- Angilella, G.G.N.; Pucci, R.; Varlamov, A.A.; Onufrieva F.**
Effects of proximity to an electronic topological transition on normal-state transport properties of the high- T_c superconductors
 Physical Review B, 2003, **67** 134525
- Arcos, D.; Rodríguez-Carvajal, J.; Vallet-Regí, M.**
Silicon Incorporation in hydroxylapatite obtained by controlled crystallization
 Chemistry of Materials, 2004, **16** 2300-2308
- Arcos, D.; Rodríguez-Carvajal, J.; Vallet-Regí, M.**
The effect of the silicon incorporation in hydroxylapatite
 Solid State Sciences, 2004, **6** 987-994
- Arcos, D.; Rodríguez-Carvajal, J.; Vallet-Regí, M.**
Neutron scattering for the study of improved bone implants
 Physica B, 2004, **350** E607-E610
- Arnaud, A.; Belleney, J.; Boué, F.; Bouteiller, L.; Carrot, G.; Wintgens, W.**
Aqueous supramolecular polymer formed an amphiphilic perylene derivative
 Angewandte Chemie-International Edition, 2004, **43** 194-202
- Arnold Z.; Prokhnenko, O.; Ritter, C.; Goncharenko, I.; Kamarad, J.**
Existence of incommensurate spiral magnetic structure in Y_2Fe_{17} under high pressure
 Journal of Magnetism and Magnetic Materials, 2004, **272** E1589-E1590
- Aubry, S. Kopidakis, S.**
A nonlinear dynamical model for ultrafast catalytic transfer of electrons at zero temperature
 International Journal of Modern Physics B, 2003, **17** 3908-3921
- Autret, C.; Martin, C.; Hervieu, M.; Maignan, A.; Raveau, B.; André, G.; Bouree, F.; Jirak, Z.**
 $\text{Pr}_{0.5}\text{Sr}_{0.5-x}\text{Ba}_x\text{MnO}_3$: Size and mismatch effects on structural and magnetic transitions
 Chemical Materials, 2003, **15** 1886-1896
- Autret, C.; Martin, C.; Hervieu, M.; Retoux, R.; Raveau, B.; André, G.; Bourée, F.**
Structural investigation of Ca_2MnO_4 by neutron powder diffraction and electron microscopy
 Journal of Solid State Chemistry, 2004, **177** 2044-2052
- Autret, C.; Martin, C.; Hervieu, M.; Maignan, A.; Raveau, B.; André, G.; Bourée, F.; Jirak, Z.**
From A-type antiferromagnetism to ferromagnetism in half-doped perovskite manganites
 Journal of Magnetism and Magnetic Materials, 2004, **270** 194-202
- Autret, C.; Martin, C.; Retoux, R.; Maignan, A.; Raveau, B.; André, G.; Bouree, F.; Jirak, Z.**
Coexistence of ferromagnetism and antiferromagnetism in the $L_{0.08}\text{Ca}_{1.92}\text{MnO}_4$ series
 Journal of Magnetism and Magnetic Materials, 2004 **284** 172-180
- Axelos, M.A.V.; Boue, F.**
Foams as viewed by small angle neutron scattering
 Langmuir, 2003, **19** 6598-6604
- Ayari, A.; Danneau, R.; Requardt, H.; Ortega, L. ; Lorenzo, J.E. ; Monceau, P.; Currat, R.; Brazovskii, S.; Grübel, G.**
Sliding-induced decoupling and charge transfer between the coexisting Q_1 and Q_2 charge density waves in NbSe_3
 Physical Review Letters, 2004, **93** 106404

- Babushkina, N.A.; Chistotina, E.A.; Gorbenko, O.Y.; Kaul, A.R.; Kugel, K.I.; Kurbakov, A.I.; Trunov, V.A.; Andre, J.**
Phase separation induced by oxygen isotope substitution in manganites of the $Sr_{1-x}Sr_xMnO_3$ system
Physics of the Solid State, 2004, **46** 1884-1890
- Baczmanski, A.; Braham, C.**
Elastoplastic properties of duplex steel determined using neutron diffraction and self-consistent model
Acta Materiala, 2004, **52** 1133-1142
- Baczmanski, A.; Levy-Tubiana, R.; Fitzpatrick, M.E.; Lodini, A.**
Elastoplastic deformation of Al/SiC_p metal-matrix composite studied by self-consistent modelling and neutron diffraction
Acta Materiala, 2004, **52** 1565-1577
- Baczmanski, A.; Levy-Tubiana, R.; Fitzpatrick, M.E.; Lodini, A.**
Phase stresses in Al/SiC_p metal matrix composite determined by modelling and neutron diffraction
Journal of Neutron Research, 2004, **12** 5-8
- Bailleul, M.; Ott, F.; Fermon, C.**
Interaction between magnetostatic waves and neutrons in magnetic thin films
Physica B, 2003, **335** 68-71
- Bako I.; Grosz T.; Palinkas G.; Bellissent-Funel M.-C.**
Ethylene glycol dimers in the liquid phase : a study by X-ray and neutron diffraction
Journal of Chemical Physics, 2003, **118** 3215-3221
- Bako, I.; Schubert, G.; Megyes, T.; Palikas, G.; Swan, G.I.; Dore, J.; Bellissent-Funel, M.-C.**
Structural investigation of liquid formic acid by neutron diffraction. II: Isotopic substitution for $DCOD[H/D]$
Chemical Physics, 2004, **306** 241-251
- Bako, I.; Radnai, T.; Bellissent-Funel, M.C.**
Investigation of structure of liquid 2,2,2-trifluoroethanol: Neutron diffraction.; molecular dynamics.; and ab initio quantum chemical study
Journal of Chemical Physics, 2004 **121** 12472-12480
- Barbier, V.; Hervé, M.; Sudor, J.; Brulet, A.; Hourdet, D.; Viovy, J.L.**
*Thermally induced gelation of poly(acrylamide) grafted with poly(*N*-isopropylacrylamide): a small-angle neutron scattering study*
Macromolecules, 2004, **37** 5682-5691
- Bastos, M.; Castro, V.; Mrevlishvili, G.; Teixeira, J.**
Hydration of ds-DNA and ss-DNA by neutron quasi-elastic scattering
Biophysical Journal, 2004, **86** 3822-3827
- Battle, P.D.; Grey, C.P.; Hervieu, M.; Martin, C.; Moore, C.A.; Paik, Y.**
Structural chemistry and magnetic properties of La_2LiRuO_6
Journal of Solid State Chemistry, 2003, **175** 20-26
- Beaufils, S.; Cormier, L.; Bionducci, M.; Ecolivet, C.; Calas, G.; Le Sauze, A.; Marchand, R.**
Medium-range order in alkali metaphosphate glasses and melts investigated by reverse Monte Carlo simulations and diffraction analysis
Physical Review B, 2003, **67** 104201
- Bellissent-Funel, M.C.**
Status of experiments probing the dynamics of water in confinement
European Physical Journal E, 2003, **12** 83-92
- Bellissent-Funel, M.C.; Doster, W.; Gähler R.; Koper, I.; Longeville, S.; Petry, W.**
Performance of neutron resonance spin-echo in biology
Neutron news, 2003, **14** 35-38
- Bellissent-Funel, M.-C.**
Internal motions in proteins : a combined neutron scattering and molecular modelling approach
Pramana - Journal of Physics, 2004, **63** 91-97
- Bellissent-Funel, M.C.; Teixeira J.**
Structural and dynamic properties of bulk and confined water
Drugs and the Pharmaceutical Science, 2004, **137** 33-62
- Belloni, L.; Delsanti, M.; Fontaine, P.; Muller, F.; Guenoun, P.; Mays, J.W.; Boesecke, O.; Alba, M.**
Counterion distribution in urchinlike charged copolymer micelles
Monte Carlo simulation and small angle x-ray scattering
Journal of Chemical Physics, 2003, **119** 7560-7567
- Belushkin, A.V.; Kuzmin, E.S.; Shvetsov, V.N.**
Status of the FLNP project on neutron position-sensitive detectors
Nuclear Instruments and Methods in Physics Research Section A, 2004, **529** 249-253
- Ben Salah, M.; Vilminot, S.; Richard-Plouet, M.; Andre, G.; Mhiri, T.; Kurmoo, M.**
 $Co_5(II)(OH)_6(SO_4)_2(H_2O)_4$: the first ferromagnet based on a layered cobalt-hydroxide pillared by inorganic center dot center dot center dot $OSO_3-Co(H_2O)_4O_3SO$ center dot center dot center dot
Chemical Communications, 2004, n°22 2548-2549
- Ben Salah, M.; Vilminot, S.; Andre, G.; Richard-Plouet, M.; Bourée-Vigneron, F.; Mhiri, T.; Kurmoo, M.**
Synthesis, nuclear, and magnetic structures and magnetic properties of $[Mn_3(OH)_3SO_4]_2(H_2O)_2$
Chemistry - A European Journal, 2004, **10** 2048-2057
- Bendiab, N.; Almairac, R.; Rols, S.; Aznar, R.; Sauvajol, J.-L.; Mirebeau, I.**
Structural determination of iodine localization in single-walled carbon nanotube bundles by diffraction methods
Physical Review B. Condensed Matter, 2004, **69** 195415
- Benyoucef, M.; Jakani, S.; Baudin, T.; Mathon, M.H.; Penelle, R.**
Study of deformation microstructure and static recovery in copper after cold drawing
Materials Science Forum, 2004, **467** 27-32
- Berret, J.-F.; Hervé, P.; Aguerre-Chariol, O.; Oberdisse, J.**
Colloidal complexes obtained from charged block copolymers and surfactants : a comparison between small-angle neutron scattering, Cryo-TEM, and simulations
Journal of Physical Chemistry B, 2003, **107** 9111-8118
- Berret, J.F.; Oberdisse, J.**
Electrostatic self-assembly in polyelectrolyte-neutral block copolymers and oppositely charged surfactant solutions
Physica B, 2004, **350** 204-206
- Bertagna, V.; Menelle, A.; Petitdidier, S.; Levy, D.; Saboungi, M.L.**
A neutron reflectivity of silicon oxide thin films
Proceedings of the Electrochemical Society, 2003, 525-532
- Bertagna, V.; Erre, R.; Saboungi, M.L.; Petitdidier, S.; Levy, D.; Menelle, A.**
A neutron reflectivity study of ultrathin SiO_2 on Si
Applied Physics Letters, 2004, **84** 3816-3818
- Beta, I.A., Li, J.C.; Bellissent-Funel, M. -C.**
A quasi-elastic neutron scattering study of the dynamics of supercritical water
Chemical Physics, 2003, **292** 229-234
- Beta I. A., Michalarias, I.; Ford, R.C.; Li, J.C., Bellissent-Funel, M.-C.**
Quasi-elastic neutron scattering study of hydrated DNA
Chemical Physics, 2003, **292** 451-454
- Bleuel M.; Demmel F.; Gähler R.; Golub R.; Habicht K.; Keller T.; Klimko S.; Koper I.; Longeville S.; Prokudaylo S.**
Future developments in resonance spin echo.
Lecture Notes in Physics, 2003, **601** 176-200
- Block, T.; Felser, C.; Jakob, G.; Ensling, J.; Mühlhng, B.; Gütllich, P.; Cava, R.J.**
Large negative magnetoresistance effects in $Co_2Cr_{0.6}Fe_{0.4}Al$
Journal of Solid State Chemistry, 2003, **176** 646-651

- Bogdanova, A.N.; Irodova, A.V.; Andre, G.; Bouree, F.**
The ZrV_2D_6 crystal structure
Journal of Alloys and Compounds , 2003, **356** 50-53
- Bogdanova, A.N. ; André, G.**
Phase transformations in the solid solutions ZrV_2H_x at high hydrogen concentrations ($4 < x < 5$)
Journal of Alloys and Compounds, 2004, **379** 54-59
- Böhmert, J. ; Viehri, H.-W. ; Ulbricht, A.**
Correlation between irradiation-induced changes of microstructural parameters and mechanical properties of RPV steels
Journal of Nuclear Materials, 2004, **334** 71-78
- Bombardi, A.; Paolasini, L.; Carretta, P.; Rodriguez-Carvajal, J.; Millet, P.; Caciuffo, R.**
Magnetic order in a $S=1/2$ frustrated antiferromagnet on a square lattice
Journal of Magnetism and Magnetic Materials, 2004, **272** E659-E660
- Bombardi, A.; Rodriguez-Carvajal, J.; Di Matteo, S.; de Bergevin, F.; Paolasini, L.; Carretta, P.; Millet, P.; Caciuffo, R.**
Direct determination of the magnetic ground state in the square lattice $S=1/2$ antiferromagnet $Li_2VO_2SiO_4$
Physical Review Letters, 2004, **93** 027202
- Bonetti, M.; Calmettes, P.; Bervillier, C.**
Study of supercritical krypton by small-angle neutron scattering : analysis of the cross-over region
Journal of Chemical Physics , 2003, **119** 8542-8548
- Bonetti, M.; Calmettes, P.**
High-pressure cell for small- and -medium-angle neutron scattering measurements up to 300 Mpa
Review of Scientific Instruments, 2004, **75** 440-444
- Bono, D.; Mendels, P.; Collin, G.; Blanchard, N.; Bert, F.; Amato, A.; Baines, C.; Hillier, A.D.**
 μ SR study of the quantum dynamics in the frustrated $S = 2/3$ Kagomé bilayers
Physical Review Letters, 2004, **93** 187201
- Bono, D.; Mendels, P.; Collin, G.; Blanchard, N.**
Intrinsic susceptibility and bond defects in the novel two dimensional frustrated antiferromagnet $Ba_2Sn_2ZnCr_{7p}Ga_{10-7p}O_{22}$
Physical Review Letters, 2004, **92** 217202
- Bono, D.; Mendels, P.; Collin, G.; Blanchard, N.; Baines, C.; Amato, A.**
A local study of dynamic and static magnetism in the Kagome bilayer compound $Ba_2Sn_2ZnCr_{6.8}Ga_{3.2}O_{22}$
Journal of Physics. Condensed Matter, 2004, **16** S817-S822
- Bouad, N.; Chapon, L.; Marin-Ayral, R.M.; Bouree-Vigneron, F.; Tedenac, J.**
Neutron powder diffraction study of strain and crystallite size in mechanically alloyed PbTe
Journal of Solid State Chemistry , 2003, **173** 189-195
- Boué, F.**
Les polymères comme matériaux désordonnés : l'apport de la diffusion de neutrons
Journal de Physique IV , 2003, **111** 211-241
- Bourgeois, L.; Ecolivet, C.; Toudic, B.; Bourges, Ph.; Breczewski, T.**
First one-dimensional stress-strain experiments inside an aperiodic inclusion compound : Evidence of depinning effects
Physical Review Letters, 2003, **91** 025504
- Bourgeois, L.; Toudic, B.; Ecolivet, C.; Ameline, J.C.; Bourges, P.; Guillaume, F.; Breczewski, T.**
Interactions in self-organized nanoporous organic crystals
Physical Review Letters, 2004, **93** 026101
- Bourges, P.; Hennion, B.**
2T : High-flux triple-axis spectrometer with polarization-analysis option
Neutron news , 2003, **14** 13-16
- Bourges, P., Sidis, Y., Braden, M., Nakajima, K., Tranquada, J.M.**
High-energy spin dynamics in $La_{1.69}Sr_{0.31}NiO_4$
Physical Review Letters , 2003, **90** 147202
- Buyer, F.; Gérardin, C. ; Fajula, F. ; Putaux, J.-L. ; Chopin, T.**
Role of double-hydrophilic block copolymers in the synthesis of lanthanum-based nanoparticles
Colloids and Surfaces A, 2003, **217** 179-184
- Braden, M.; Friedt, O.; Sidis, Y.; Bourges, P.; Pfeuty, P.; Maeno, Y.**
Magnetic excitations in 214-ruthenates.
Lecture Notes in Physics , 2003, **603** 15-31
- Braden, M.; Friedt, O.; Sidis, Y.; Bourges, P.; Pfeuty, P.; Nakatsuji, S.; Mao, Z.; Kikugawa, N.; Minakata, M.; Maeno, Y.**
Magnetic excitations in 214-ruthenates
Physica C, 2003, **388-389** 489-490
- Braden, M., Steffens, P., Sidis, Y., Kulda, J., Bourges, P., Hayden, S., Kikugawa, N., Maeno, Y.**
Anisotropy of the incommensurate fluctuations in Sr_2RuO_4 : a study with polarized neutrons
Physical Review Letters, 2004, **92** 097402
- Braden, M.; Etrillard, J.; Gukasov, A.; Ammerahl, U.; Revcolevschi, A.**
Neutron diffraction study of the lattice distortion related to charge ordering in $Sr_{14}Cu_{24}O_{41}$
Physical Review B, 2004, **69** 214426
- Branca, C.; Magazù, S. ; Maisano, G.**
Fragility characterization of disaccharide/water glass-forming systems by QENS
Chemical Physics, 2003, **292** 341-345
- Bréard, Y.; Michel, C.; Hervieu, M.; Nguyen, N.; Ducouret, A.; Hardy, V.; Maignan, A.; Raveau, B.; Bourée, F.; André, G.**
Spin Reorientation Associated with a Structural Transition in the Iron Oxycarbonate $Sr_4Fe_2O_6CO_3$
Chemistry of Materials, 2004, **16** 2895-2905
- Bruno, G.; Ceretti, M.; Girardin, E.; Giuliani, A.; Manescu, A.**
Relaxation of residual stress in MMC after combined plastic deformation and heat treatment
Scripta Materialia, 2004, **51** 999-1004
- Buhler, E.; Boué, F.**
Chain persistence length and structure in Hyaluronan solutions : ionic strength dependence for a model semirigid polyelectrolyte
Macromolecules, 2004, **37** 1600-1610
- Celli, M.; Magli, R.; Guarini, E.; André, G.; Zoppi, M.**
Long-range pair potential from the low-density $S(k)$ of ^4He around 6K
Physica B, 2004, **350** E1059-E1061
- Ceolin, R.; Lopez, D.O.; Barrio, M.; Tamarit, J.L., Espeau, P.; Nicolai, B.; Allouchi, H.; Papoular, R**
Solid state studies on C-60 solvates formed with n-alkanes: orthorhombic C_{60} center dot 2/3 n-nonane
Chemical Physics Letters, 2004, **399** 401-405
- Chaboussant, G.; Sieber, A.; Ochsenbein, S.; Güdel, H.-U.; Murrie, M.; Honecker, A.; Fukushima, N.; Normand, B.**
Exchange interactions and high-energy spin states in Mn_{12} -acetate
Physical Review B, 2004 **70** 104422
- Chaboussant, G.; Basler, R.; Gudel, H.U.; Ochsenbein, S.; Parkin, A.; Parsons, S.; Rajaraman, G.; Sieber, A.; Smith, A.A.; Timco, G.A.; Wimpenny, R.E.P.**
Nickel pivalate complexes: structural variations and magnetic susceptibility and inelastic neutron scattering studies
Dalton Transactions, 2004, **17** 2758-2766
- Chaboussant, G.; Ochsenbein, S.T.; Sieber, A.; Güdel, H.-U.; Mutka, H.; Müller, A.; Barbara, B.**
Mechanism of ground state selection in the frustrated molecular spin cluster V_{15}
Europhysics Letters, 2004, **66** 423-429

- Chevire, F. ; Tessier, F. ; Marchand, R.**
New scheelite-type oxynitrides in systems TWO_3N-AWO_4 ($R=rare-earth\ element; A=Ca,Sr$) from precursors obtained by the citrate route
 Materials Research Bulletin, 2004, **39** 1091-1101
- Chevrier G., Kiat J.M., Guida J., Navaza A.**
A new crystal phase of barium nitroprusside trihydrate studied by neutron diffraction at 20 K
 Acta Crystallographica, C, 2004, **60** i27-i29
- Choisnet, J. ; Caignaert, V. ; Raveau, B.**
Sodium "stuffed" $Ba_{2-x}Sr_xFe_4O_8$ ferrites : new cationic conductors
 Journal of Solid State Chemistry, 2003, **170** 435-442
- Crupi, V.; Majolino, D.; Migliardo, P.; Venuti, V.; Bellissent-Funel, M.C.**
Structure and dynamics of water confined in a nanoporous sol-gel silica glass: a neutron scattering study
 Molecular Physics, 2003 **101** 3323-3333
- Cser, L.; Torok, G.; Krexner, G.; Prem, M.; Sharkov, I.**
Neutron holographic study of palladium hydride
 Applied Physics Letters, 2004, **85** 1149-1151
- Dahmani, M. ; Ramzi, M. ; Rochas, C. ; Guenet, J.-M.**
Thermoreversible gelation in aqueous binary solvents of chemically modified agarose
 International Journal of Biological Macromolecules, 2003, **31** 147-153
- Daoud-Aladine, A.; Rodríguez-Carvajal, J.; Pinsard-Gaudart, L.; Revcolevschi, A.**
Non-collinear magnetic ordering in $R_{1/2}D_{1/2}MnO_3$ manganites
 Journal of Magnetism and Magnetic Materials, 2004, **272** E1387-E1388
- Delheusy, M.; Raty, J.Y.; Detemple, R.; Welnic, W.; Wuttig, M.; Gaspar, J.-P.**
Structure of liquid Te-based alloys used in rewritable DVDs
 Physica B, 2004, **350** E1055-E1057
- De Meyer, C.; Bourée, F.; Evans, J.S.O.; De Buysser, K.; Bruneel, E.; Van Driessche, I.; Hoste, S.**
Structure and phase transition of Sn-substituted $Zr_{(1-x)}Sn_xW_2O_8$
 Journal of Materials Chemistry, 2004, **14** 2988-2994
- Deriano, S.; Rouxel, T.; LeFloch, M.; Beuneu, B.**
Structure and mechanical properties of alkali-alkaline earth-silicate glasses
 Physics and Chemistry of Glasses, 2004, **45** 37-44
- Diat, O.; Lyonard, S.; Gebel, G.; Rollet, A.L.**
SANS analysis of perfluorinated lyotropic lamellar phase-ion condensation effect
 Physica B, 2004, **350** E959-E962
- Doan, T.D.; Ott, F.; Menelle, A.; Fermon, C.**
Polarized neutron grazing incidence diffraction on magnetic epitaxial thin films
 Physica B, 2003, **335** 72-76
- Dooglav, AV.; Egorov, AV.; Mukhamedshin, I.R.; Savinkov, A.V.; Alloul, H.; Bobroff; MacFarlan, WA.; Mendels, P.; Collin, G.; Blanchard, N.; Picard, P.G.; King, P.J.C.; Lord, J.**
Antiferromagnetic properties of a water-vapor-inserted $YBa_2Cu_3O_{6.5}$ compound studied by NMR, NQR, and μ SR
 Physical Review B, 2004, **70** 054506
- Dore, J.C. ; Garawi, M. ; Bellissent-Funel, M.C.**
Neutron diffraction studies of the structure of water at ambient temperatures, revisited [a review of past developments and current problems]
 Molecular Physics, 2004, **102** 2015-2035
- Durivault, L. ; Bourée, F. ; Chevalier, B. ; André, G., Weill, F.; Etourneau, J.; Martinez-Samper, P. ; Rodrigo, J.G. ; Suderow, H. ; Vieira, S.**
Incommensurate and commensurate magnetic structures of the ternary germanide $CeNiGe_3$
 Journal of Physics : Condensed Matter, 2003, **15** 77-90
- Durivault, L. ; Bourée, F. ; Chevalier, B. ; Isnard, O.; André, G., Weill, F., Etourneau, J.**
The Ce-Ni-Ge system : relationship between chemical composition and magnetic ordering
 Acta Physica Polonica B, 2003, **34** 1393-1397
- El Harrak, A.; Carrot, G.; Oberdisse, J.; Eychenne-Baron, C.; Boué, F.**
Surface atom transfer radical polymerization from silica nanoparticles with controlled colloidal stability
 Macromolecules, 2004, **37** 6376-6384
- Esquenet, C.; Terech P.; Boué, F.; Buhler, E.**
Structural and rheological properties of hydrophobically modified polysaccharide associative networks
 Langmuir, 2004, **20** 3583-3592
- Etrillard, J.; Bourgeois, L.; Bourges, P.; Liang, B.; Lin, C.T.; Keimer, B.**
Low-frequency structural dynamics in the incommensurate Low-frequency structural dynamics in the incommensurate $Bi_2Sr_2CuO_{6+\delta}$
 Europhysics Letters, 2004, **66** 246-252
- Etrillard, J.; Braden, M.; Gukasov, A.; Ammerahl, U.; Revcolevschi, A.**
Structural aspects of the spin-ladder compound $Sr_{14}Cu_2O_{41}$
 Physica C, 2004, **403** 290-296
- Etter, A.L.; Mathon, M.H.; Penelle, R.**
Stored energy evolution as a function of cold rolling reduction for a Fe-53%Ni alloy and an austenitic-ferritic steel
 Revue de Metallurgie-Cahiers d'Informations Technique, 2003, **100** 851-858
- Even J.; Bertault M.; Toudic B.; Cailleau H.; Girard A.; Delugeard Y.; Moussa F.**
Dynamics of the Incommensurate Phase of the Fully Deuterated Diacetylene 2,4-Hexadiynylene Bis(p-Toluene Sulfonate).
 Phase Transitions, 2003, **76** 229-237
- Fadda, G.C.; Lairez, D.; Arrio, B.; Carton, J.P.; Larreta-Garde, V.**
Enzyme-catalyzed gel proteolysis : an anomalous diffusion-controlled mechanism
 Biophysical Journal, 2003, **85** 2808-2817
- Fåk, B.; van Dijk, N.H.; Mignot, J.-M.; Charvolin, T.; Lejay, P.; Flouquet, J.**
Localized spin fluctuations in $CePd_2Si_2$
 Journal of Magnetism and Magnetic Materials, 2004, **272** E13-E14
- Falcao A. N.; Carrapico M.; Sousa J. Santos; Margaca F. M. A.; Ferreira L. M.; Carvalho F. G.; Salvado I. M. Miranda; Teixeira J.**
Investigation of Organic-Inorganic Hybrid Materials Prepared by Irradiation
 Journal of Sol-Gel Science and Technology, 2003, **26** 349-352
- Falcao A. N.; Sousa J. Santos; Carrapico M.; Margaca F. M. A.; Carvalho F. G.; Salvado I. M. Miranda; Teixeira J.**
SANS Study of Zirconia-Silica and Titania-Silica Hybrid Materials
 Journal of Sol-Gel Science and Technology 2003, **26** 345-348
- Fillaux, F.; Cousson, A.; Keen, D.**
Observation of the dynamical structure arising from spatially extended quantum entanglement and long-lived quantum coherence in the $KHCO_3$ crystal
 Physical Review B, 2003, **67** 054301
- Fillaux, F.; Nicolai, B.; Paulus, W.; Kaiser-Morris, E.; Cousson, A.**
Collective rotational tunneling of methyl groups and quantum solitons in 4-methylpyridine : neutron scattering studies of single crystals
 Physical Review B, 2003, **68** 224301

Filliaux, F.; Cousson, A.

Comment on "Quantum correlations between protons in potassium bicarbonate"

Journal of Physics. Condensed Matter, 2004, **16** 1007-1010

Filliaux, F.; Cousson, A.; Tomkinson, J.

Comment on: 'A symmetric hydrogen bond revisited: potassineutron diffraction and plane-wave DFT methods'

Chemical Physics Letters, 2004, **399** 289-291

Fitzpatrick, M.E., Lodini, A.

Analysis of residual stress by diffraction using neutron a,nd synchrotron radiation

Livre, Editeur : 2003, Taylor and Francis 320 pages

Floquet, N.; Coulomb, J.P.; André, G.

Hydrogen sorption in MCM-41 by neutron diffraction study. Characterization of the porous structure of MCM-41 and the growth mode of the hydrogen confined phases

Microporous and Mesoporous Materials, 2004, **72** 143-152

Floquet, N.; Coulomb, J.P.; Dufau, N.; Andre, G.

Structure and Dynamics of Confined Water in AlPO₄-5 Zeolite

Journal of Physical Chemistry B, 2004, **108** 13107-13115

Floquet, N.; Coulomb, J.P.; Dufau, N.; Andre, G.; Kahn, R.

Structural and dynamic properties of confined water in nanometric model porous materials (8 Å < 0 < 40 Å)

Physica B, 2004, **350** 265-269

Fogarassy, P., Turquier, F., Lodini, A.

Residual stress in plasma sprayed zirconia on cylindrical components

Mechanics of Materials, 2003, **35** 633-640

Foury -Leylekian, P.; Le Bolloc'h, D.; Hennion, B.; Ravy, S.; Moradpour, A.; Pouget, J.P.

Neutron-scattering evidence for a spin-Peierls ground state in (TMTTF)₂PF₆

Physical Review B, 2004, **70** 180405

Francoal, S.; Livet, F.; de Boissieu, M.; Yakhou, F.; Bley, F.; Letoublon, A.; Caudron, R.; Gastaldi, J.

Dynamics of phason fluctuations in the i-AlPdMn quasicrystal

Physical Review Letters, 2003, **91** 225501

Friedt, O.

Interplay between electronic, magnetic and structural instabilities in Ca_{2-x}Sr_xRuO₄ : a neutron scattering study

Thèse soutenue le 20 juin 2003 à l'Université Paris XI - Orsay

Friedt, O.; Steffens, P.; Braden, M.; Sidis, Y.; Nakatsuji, S.; Maeno, Y.

Strongly enhanced magnetic fluctuations in a large-mass layered ruthenate

Physical Review Letters, 2004, **93** 147404

Fronc, K.; Szuszkiewicz, W.; Ott, F.; Hennion, B.; Aleszkiewicz, M.; Chernyshova, M.; Kowalczyk, L.; Minikayev, R.; Paszkowicz, W.

Influence of hydrogen on magnetic properties of Fe films and multilayers

Reviews on Advanced Materials Science **8** 92-96

Frontera, C., Rodriguez-Carvajal, J.

FullProf as a new tool for flipping ratio analysis

Physica B, 2003, **335** 219-222

Frontera, C.; Rodriguez-Carvajal, J.

FullProf as a new tool for flipping ratio analysis: further improvements

Physica B, 2004, **350** E731-E733

Fuentes, M.A.; Maniadis, P.; Kalosakas, G.; Rasmussen, K.O.; Bishop, A.R.; Kenkre, V.M.; Gaididei, Yu.B.

Multipeaked polarons in soft potentials

Physical Review E, 2004, **70** 025601

Gabureac, M.; Viret, M.; Ott, F.; Fermon, C.

Magneto-resistance in nanocontacts induced by magnetostrictive effects

Physical Review B, 2004, **69** 100401

Galant, C.; Amiel, C.; Auvray, L.

Tailorable polyelectrolyte complexes using cyclodextrin polymers

Journal of Physical Chemistry B, 2004 **108** 19218-19227

Galicía J.A., Sandre O., Cousin F., Guemghar D., Ménager C., Cabuil V.

Designing magnetic composite materials using aqueous magnetic fluids

Journal of Physics : Condensed Matter, 2003, **15** S1379-S1402

Gallová, J.; Uhríková, D.; Hanulová, M.; Teixeira, J.; Balgavý, P.
Bilayer thickness in unilamellar extruded 1,2-dimyristoleoyl and 1,2-dierucoyl phosphatidylcholine vesicles: SANS contrast variation study of cholesterol effect

Colloids and Surfaces B : Biointerfaces, 2004, **38** 11-14

Gambi, C.M.C.; Giordano, R.; Chittofrati, A.; Pieri, R.; Baglioni, P.; Teixeira, J.

Counterion and temperature effects on aqueous ionic perfluoropolyether micellar solutions by small angle neutron scattering

Journal of Physical Chemistry A, 2003, **107** 11558-11564

Garamszegi, L.; Donzel, C.; Carrot, G.; Nguyen T.Q.; Hilborn, J.
Synthesis of thiol end-functional polystyrene via atom transfer radical polymerization

Reactive and Functional Polymer, 2003, **55** 179-183

Garcia-Martin, S.; Alario-Franco, M.A.; Ehrenberg, H.; Rodriguez-Carvajal, J.; Amador, A.

Crystal structure and microstructure of some La_{2/3-x}Li₃TiO₃ oxides: an example of the complementary use of electron diffraction and microscopy and synchrotron X-ray diffraction to study complex materials

Journal of the American Chemical Society, 2004, **126** 3587-3596

Gautier, P., Brunet, M., Grupp, J., Noirez, L., Anglaret, E.

Structure and texture of anisotropic nematic gels

Physical Review E, 2003, **68** (2003) 011709

Gazeau, F; Boué, F; Dubois, E; Perzynski, R

Static and quasi-elastic small-angle neutron scattering on biocompatible ionic ferrofluids : magnetic and hydrodynamic interactions

Journal of Physics : Condensed Matter, 2003, **15** S1305-S1334

Gerber, Ph.; Baudin, T.; Jakani, S.; Mathon, M.H.; Bacroix, B.

Estimation of stored energy distribution from EBSD measurements

Materials Science Forum, 2004, **467** 51-56

Gerber, Ph.; Jakani, S.; Baudin, T.; Mathon, M.H.; Penelle, R.

Recrystallization mechanisms in wire-drawn copper

Materials Science Forum, 2004, **467** 135-140

Gerber, Ph.; Tarasiuk, J.; Solas, D.; Jakani, S.; Mathon, M.H.; Baudin, T.

Monte Carlo of recrystallization mechanisms in wire-drawn copper from EBSD data

Materials Science Forum, 2004, **467** 635-640

Gil, A. ; Ole , A. ; Sikora, W. ; Szytula, A.

Neutron diffraction study of PrMn_{0.5}Sn_{1.83}

Journal of Alloys and Compounds, 2003, **360** 21-23

Gilles, F. ; Blin, J.-L. ; Mellot-Draznieks, C.; Cheetham, A.K.; Su, B.L.

Neutron diffraction evidence of double interaction between NaY zeolite and ammonia and migration of Na⁺ ions upon ND₃ adsorption

Chemical Physics Letters, 2004, **390** 236-239

Gillon, B.

Spin density maps in molecule-based magnetic materials

Neutron News, 2003, **14** n°3 17-20

- Giuliani, A. ; Albertini, G. ; Fabrizio Fiori, F.; Girardin, E.**
Residual stress analysis on AA6061+22% Al₂O₃p simple shape demonstrators of a wheel hub
Physica B, 2004, **350** E495-E498
- Givord, F.; Boucherle, J.-X.; Bulet, P.; Gillon, B.; Kunii, K.**
Non-anomalous magnetization density distribution in CeB₆
Journal of Physics : Condensed Matter, 2003, **15** 3095-3106
- Glättli, H.**
Polarised nuclei for neutron science: recent applications and perspectives
Nuclear Instruments and Methods in Physics Research A, 2004, **529** 194-198
- Golosovsky, I.V.; Kurbakov, A.I.; Mirebeau, I.; Markosyan, A.S.; Gaidukova, I.Yu.**
Magnetic behavior in the Er(Mn,Al)₂ system : Neutron diffraction study
Physical Review B, 2003, **68** 184407
- Goncharenko, I.N.; Cadavez-Peres, P.; Mirebeau, I.; Makarova, O.L.; Le Bihan, T.; Mezouar, M.**
Pressure induced magnetic collapse and hydrogen segregation in the frustrated Laves hydrides Tb(Mn_{0.88}Al_{0.12})₂H_x
Physical Review B, 2003, **68** 214418
- Goncharenko, I.N.; Mirebeau, I.; Mignot, J.-M.; Goukasov, A.**
Neutron diffraction on microsamples under high pressures
Neutron News, , 2003, **14** n°3 21-25
- Goncharenko, I.N.; Mirebeau, I.; Mignot, J.-M.; Goukasov, A.**
Neutron diffraction on microsamples under high pressures
Neutron News, 2003, **14** 21-25
- Goncharenko, I.N.**
Neutron diffraction experiments in diamond and sapphire anvil cells
High Pressure Research, 2004, **24** 193-204
- Goncharenko, I.N.; Makarova, O.L.; Ulivi, L.**
Direct determination of the magnetic structure of the delta phase of oxygen
Physical Review Letters, 2004, **93** 055502
- Gonzalez, J.; Deroller, P.; Fouret, R.; Hennion, B.**
Temperature dependence of soft modes in I-III-VI chalcopyrite semiconductors
Revista Mexicana Fisica, 2003, **49** 172-175
- Goujon, A., Gillon, B., Gukasov, A., Jetic, J., Nau, Q., Codjovi, E., Varret, F.**
Photoinduced molecular switching studied by polarized neutron diffraction
Physical Review B, 2003, **67** 220401
- Grebille, D.; Lambert, S.; Bourée, F.; Petricek, V.**
Contribution of powder diffraction for structure refinements of aperiodic misfit cobalt oxides
Journal of Applied Crystallography, 2004, **37** 823-831
- Grytsiv, A.; Rogl, P.; Andre, G.; Bouree, F.; Velikanova, T.**
Carbon-vacancy ordering in subcarbide (Cr_{0.7}Re_{0.3})₂C_{0.9}; a combined X-ray and neutron diffraction study
Journal of Alloys and Compounds, 2003, **350** L1-L3
- Grytsiv, A.; Ding, J.J.; Rogl, P.; Weill, F.; Chevalier, B.; Etourneau, J.; Andre, G.; Bouree, F.; Noel, H.; Hundegge, P.; Wiesinger, G.**
Crystal chemistry of the G-phases in the systems Ti-{Fe,Co,Ni}-Al with a novel filled variant of the ThMn₂₃-type
Intermetallic, 2003, **11** 351-359
- Habas, J.P.; Pavie, E.; Lapp, A.; Peyrelasse, J.**
Understanding the complex rheological behavior of PEO-PPO-PEO copolymers in aqueous solution
Journal of Rheology, 2004, **48** 1-21
- Habas, J.P.; Pavie, E.; Perreur, C.; Lapp, A.; Peyrelasse, J.**
Nanostructure in block copolymer solutions: Rheology and small-angle neutron scattering
Physical Review E, 2004 **70** 061802
- Hardy, V. ; Hébert, S. ; Maignan, A. ; Martin, C. ; Hervieu, M. ; Raveau, B.**
Staircase effect in metamagnetic transitions of charge and orbitally ordered manganites
Journal of Magnetism and Magnetic Materials, 2003, **264** 183-191
- Haumont R., Dkhil B., Kiat J. M., Al-Barakaty A., Dammak H., Bellaiche L.**
Cationic-competition-induced monoclinic phase in high piezoelectric (PbSc_{1/2}Nb_{1/2}O₃)_{1-x}-(PbTiO₃)_x compounds
Physical Review B, 2003, **68** 014114
- Hellweg, T.; Schemmel, S.; Rother, G.; Brulet, A.; Eckerleb, H.; Findenegg, G.H.**
De-mixing dynamics of a binary liquid system in a controlled-pore glass
European Physical Journal, 2003, **12** S1-S4 Suppl. 1
- Hennion B.; Szuszkiewicz W.; Dynowska E.; Janik E.; Wojtowicz T.**
Magnetic Characteristics of Zinc-Blende MnTe: Results of a Spin-Wave Analysis.
Journal of Superconductivity, 2003, **16** 151-154
- Henry, J., Mathon, M.-H., Jung, P.**
Microstructural analysis of 9% Cr martensitic steels containing 0.5 at.% helium
Journal of Nuclear Materials, 2003, **318** 249-259.
- Hense, H.; Witte, U.; Rotter, M.; Schedler, R.; Gratz, E.; Nowotny, H.; Loewenhaupt, M.**
Comparison of the CF-induced phonon shifts in CeCu₂ and NdCu₂
Journal of Magnetism and Magnetic Materials, 2004, **272-276** 387-388
- Hernandez, O.; Cousson, A.; Plazanet, M.; Nierlich, M.; Meinel, J.;**
The low-temperature phase of 1,3-dibromo-2,4,6-trimethylbenzene : a single-crystal neutron diffraction study at 120 and 14 K
Acta Crystallographica C, 2003, **59** o445-o450
- Hinkov, V.; Pailhès, S.; Bourges, P.; Sidis, Y., Ivanov, A.; Kulakov, A.; Lin, C.T.; Chen, D.P.; Bernhard, C.; Kelmer, B.**
Two-dimensional geometry of spin excitations in the high-transition-temperature superconductor YBa₂Cu₃O_{6+δ}
Nature, 2004, **430** 650-653
- Hofmann, M.; Campbell, S.J.; Link, P.; Goncharenko, I.; Knorr, K.**
Pressure-induced magnetic and valence transition in YbMn₂Ge
Physica B, 2004, **350** E195-E198
- Ivanov, A.; Petitgrand, D.**
Critical scattering in a quasi-two-dimensional antiferromagnet
Journal of Magnetism and Magnetic Materials, 2004, **272** 220-222
- Iwasa, K.; Kohgi, M.; Braden, M.; Mignot, J.-M.; Kitazawa, H.; Suzuki, T.**
Anomalous phonon excitations associated with strong p-f mixing effect of CeSb and CeBi
Journal of Magnetism and Magnetic Materials, 2004, **272** E65-E66
- Jakani, S.; Mathon, M.-H.; Benyoucef, M.; Gerber, Ph.; Baudin, T.; de Novion, C.H.**
Impurities effects on the stored elastic energy in cold-drawn copper wires
Journal of Neutron Research, 2004, **126** 249-254
- Jakani, S.; Mathon, M.H.; Gerber, Ph.; Benyoucef, M.; de Novion, C.H.; Baudin, T.**
Influence of oxygen content on the static recrystallization of ETP copper
Materials Science Forum, 2004, **467** 471-476

- Jankowska-Kisieli, J.; Mikke, K.; Hennion, B.**
Magnetic excitations at the Brillouin zone boundary in Mn (17%Fe, 3%Cu) alloy
Physica B, 2004, **350** E79-E81
- Jardet, K.; Favotto, C.; Bellissent, R.; Satre, P.**
Local order in liquid phases of Al-Ga-Zn alloys
Thermochimica Acta, 2003, **402** 135-143
- Javorský, P.; Schweizer, J.; Givord, F.; Boucherle, J.-X.; Andreev, A.V.; Divis, M.; Lelièvre-Berna, E.; Sechovský, V.**
Magnetic moment densities in selected UTX compounds
Physica B, 2004, **350** E131-E134
- Jayaraman, V.; Magrez, A.; Caldes, M.; Joubert, O.; Taulelle, F.; Rodriguez-Carvajal, J.; Piffard, Y.; Brohan, L.**
Characterization of perovskite systems derived from Ba₂In₂O₅. Part II: the proton compounds Ba₂In_{2(1-x)}Ti_{2x}O_{4+2x}(OH)_y [0 < x < (1-x)]
Solid State Ionics, 2004, **170** 25-32
- Jean F.; Collin G.; Andrieux M.; Blanchard N.; Forget A.; Rousseau S.; Marucco J.-F.**
Oxygen excess in Bi-2212: study of a Pb-substituted compound
Physica C, 2003, **384** 345-350
- Jean F.; Colson, D.; Collin G.; Blanchard N.; Konstantinovic, Z.; Le Bras, G.; Forget A.; Andrieux M.**
Structure and charge transfer driven by the controlled amount of additional oxygen in cation-stoichiometric Bi₂Sr₂CuO_{6+δ}
Physical Review B, 2003, **68** 174511
- Jeftić, J.; Gillon, B.; Goujon, A.; Nau, Q.; Gukasov, A.; Codjovi, E.; Varret, F.**
First study of the photo-induced metastable (paramagnetic) high-spin state in a [Fe(PtZ)₆](B₂)₂ single crystal by polarised neutron diffraction
Polyhedron, 2003, **22** 2155-2160
- Jestin, J.; Barré, L.**
Application of NMR solvent relaxation and SAXS to asphaltene solutions characterization
Journal of Dispersion Science and Technology, 2004, **25** 341-347
- Josse, M.; Dubois, M.; El-Ghozzi, M.; Avignant, D.; André, G.; Bourée, F.; Guillot, M.**
Neutron diffraction study of the magnetic structures of one-dimensional M₂TbF₆ (M=Li, K, Rb) fluorides; frustration, incommensurability and magnetic interactions
Journal of Alloys and Compounds, 2004, **374** 207-212
- Josse, M.; El-Ghozzi, M.; Dubois, M.; Avignant, D.; André, G.; Bourée, F.**
Magnetism of Tb⁴⁺ ion in fluorides: correlation with crystal-structure
Physica B, 2004, **350** E43-E45
- Joubert, J.-M.; Charton, J.; Percheron-Guégan, A.**
Investigation of structural and hydrogen absorption properties in the LaNi_{5-x}Pt_x-H₂ system
Journal of Solid State Chemistry, 2003, **173** 379-386
- Kahle, A.; Winkler, B.; Hennion, B.**
Is Faxen's correction function applicable to viscosity measurements of silicate melts with the falling sphere method?
Journal of Non Newtonian Fluid Mechanics, 2003, **112** 203-215
- Kahle, A.; Winkler, B.; Hennion, B.; Boutrouille P.**
High-temperature furnaces for dynamic neutron radiography
Review of Scientific Instruments, 2003, **74** 3717-3721
- Kallel, N.; Dezanneau, G.; Dhahri, J.; Oumezzin, M.; Vincent, H.**
Structure, magnetic and electrical behaviour of La_{0.7}Sr_{0.3}Mn_{1-x}Ti_xO₃ with 0 < x < 0.3
Journal of Magnetism and Magnetic Materials, 2003, **161** 56-65
- Kantor, A.P.; Jacobsen, S.D.; Kantor, I.Yu.; Dubrovinsky, L.S.; McCammon, C.A.; Reichmann, H.J.; Goncharenko, I.N.**
Pressure-Induced Magnetization in FeO: Evidence from Elasticity and Mössbauer Spectroscopy
Physical Review Letters, 2004, **93** 215502
- Karam, O.; Martin-Mingot, A.; Jouannetaud, M.P.; Jacquesy, J.C.; Cousson, A.**
Efficient oxidative ipso-fluorination of para-substituted phenols using pyridinium polyhydrogen fluoride in combination with hypervalent iodine (III) reagents
Tetrahedron, 2004, **60** 6629-6638
- Klotz S.; Derollez P.; Fouret R.; Braden M.; Hennion B.; Hubert Ch.; Meducin F.; Lazewski J.; Gonzalez J.**
Anomalous pressure dependence of acoustic phonons of AgGaSe₂ investigated by inelastic neutron scattering to 4.3 GPa
Physica Status Solidi B, 2003, **235** 331-336
- Knizek, K.; Hejtmanek, J.; Jirak, Z.; Martin, C.; Hervieu, M.; Raveau, B.; André, G.; Bourée, F.**
Structure, magnetism, and transport. Properties of Pr_{1-x}Sr_xMnO₃ (x=0.45-0.75) up to 1200 K
Chemistry of Materials, 2004, **16** 1104-1110
- Kober, P.; Hennion, M.; Moussa, F.; Ivanov, A.; Regnault, L.-P.; Pinsard, L.; Revcolevschi, A.**
Magnetic ground state of low-doped manganites probed by spin dynamics under magnetic field
Journal of Magnetism and Magnetic Materials, 2004, **272** 1784-1786
- Kober-Lehouelleur, P.; Moussa, F.; Hennion, M.; Ivanov, A.; Pinsard-Gaudart, L.; Revcolevschi, A.**
Magnetic ground state of low-doped manganites probed by spin dynamics in a magnetic field
Physical Review B, 2004, **70** 144409
- Kohki, M.; Iwasa, K.; Narajima, M.; Metoki, N.; Araki, S.; Bernoef, N.; Mignot, J.M.; Gukasov, A.; Sato, H.; Aoki, Y.; Sugawara, H.**
Evidence of magnetic-field-induced quadrupolar ordering in the heavy-fermion superconductor PrOs₄Sb₁₂
Journal of the Physical Society of Japan, 2003, **72** 1002-1005
- Kohki, M.; Iwasa, K.; Mignot, J.M.; Hiess, A.; Ochiai, A.; Aoki, H.**
Magnetic field effects on the one-dimensional S=1/2 antiferromagnet Yb₄As₃
Acta Physica Polonica B, 2003, **34** 1217-1220
- Kolesnikov, A.I.; Zanotti, J.M.; Loong, C.H.; Thiyagarajan, P.; Moravsky, A.P.; Loutfy, R.O.; Burnham, C.J.**
Anomalous soft dynamics of water in a nanotubes; a revelation of nanoscale confinement
Physical Review Letters, 2004, **93** 035503
- Konstantinovic, Z.; Le Bras, G.; Forget, A.; Colso, D.; Jean, F.; Collin, G.; Li, Z.Z.; Raff, H.; Ayache, C.**
Failure of the empirical OCT law in the B₂Sr₂CuO_{6+δ} compound
Europhysics Letters, , 2003, **63** 257-263
- Kopidakis, G.; Aubry, S.**
Localization and targeted transfer of atomic-scale nonlinear excitations: perspectives for applications
Advances Serie in Non Linear Dynamics, "Energy Localisation and Transfer" T. Dauxois, A. Litvak-Hinenzon, R. MacKay, A. Spanoudaki (Eds), 2004, Vol. **22**, p. 355-404 (World Scientific)
- Korobko, A.V.; Jesse, W.; Egelhaaf, S.U.; Lapp, A.; van der Maarel, J.R.C.**
Do spherical polyelectrolyte brushes interdigitate?
Physical Review Letters, 2004, **93** 177801
- Koszegi, L.**
Quenched-in stresses in FeCu(5%) alloy
Physica B, 2004, **350** E487-E490

- Kozlenko, D.P.; Jiráček, Z.; Goncharenko, I.N.; Savenko, B.N.**
Suppression of the charge ordered state in $Pr_{0.75}Na_{0.25}MnO_3$ at high pressure
Journal of Physics. Condensed Matter, 2004, **16** 5883-5895
- Kozlenko, D.P.; Goncharenko, I.N.; Savenko, B.N.; Voronin, V.I.**
High pressure effects on the crystal and magnetic structure of $La_{0.7}Sr_{0.3}MnO_3$
Journal of Physics. Condensed Matter, 2004, **16** 6755-6762
- Kreyssig, A.; Stockert, O.; Reznik, D.; Woodward, F.M.; Lynn, J.W.; Bitterlich, H.; Souptel, D.; Behr, G.; Loewenhaupt, M.**
Magnetic excitations of RNi_2B_2C single crystals with $R=Tb$ and Ho
Physica C, 2004, **408** 100-101
- Kreyssig, A.; Stockert, O.; Reznik, D.; Woodward, F.M.; Lynn, J.W.; Reichardt, W.; Souptel, D.; Behr, G.; Loewenhaupt, M.**
Low-energy phonons in $TbNi_2B_2C$ and $HoNi_2B_2C$
Physica B, 2004, **350** 69-71
- Krezhov, K.; Kovacheva, D.; Svab, E.; Bourée, F.; Stamenov, P.**
Structural distortions and charge/orbital ordering in $Bi_{0.25}Ho_{0.25}Ca_{0.5}MnO_3$
Physica B, 2004, **350** E13-E17
- Krexner, G.; Prem, M.; Beuneu, F.; Vajda, P.**
Nanocluster formation in electron-irradiated Li_2O crystals observed by elastic diffuse neutron scattering
Physical Review Letters, 2003, **91** 135502
- Ktari, L.; Dammak, M.; Hadrich, A.; Cousson, A.; Nierlich, M.; Romain, E.; Mhiri, T.**
Structural, vibrational and dielectric properties of the new mixed solution $K_{0.84}(NH_4)_{1.16}SO_4 \cdot Te(OH)_6$
Solid State Sciences, 2004, **6** 1393-1401
- Kurbakov, A.I.; Trunov, V.A.; André, G.**
Study of the effects of isotopic substitution O-16 \rightarrow O-18 in $Sr_{1-x}Sr_xMnO_3$ -type ($x=0.45$ and 0.50) manganites by powder neutron diffraction
Crystallography Reports, 2004 **49** 899-906
- Kucerka, N.; Uhríkova, D.; Teixeira, J.; Balgavy, P.**
Thickness of the phospholipid bilayer in unilamellar liposomes: small-angle neutron scattering using contrast variation
Biophysical Journal, 2004, **86** 379A
- Kucerka, N.; Uhríkova, D.; Teixeira, T.; Balgavy, P.**
Bilayer thickness in unilamellar phosphatidylcholine vesicles: small-angle neutron scattering using contrast variation
Physica B, 2004, **350** E639-E642
- Kuz'micheva, G.M.; Kurbakov, A.I.; Kostyleva, I.E.; Andreenko, A.S.; Esaulova, Yu.V.**
Crystal and magnetic structures of $RuSr_2(Nd, Ce^{4+})_2Cu_2O_{10-\delta}$
Physica B, 2004, **349** 149-155
- Lacaze, E.; Alba, M.; Goldmann, M.; Michel, J.P.; Rieutord, F.**
Dimerization in the commensurate network of 4-n-octyl-4'-cyanobiphenyl (8CB) molecules adsorbed on MoS_2 single crystal
European Physical Journal B, 2004 **39** 261-272
- Lacaze, E.; Michel, P.; Goldmann, M.; Gailhanou, M.; de Boissieu M.; Alba M.**
Bistable nematic and smectic anchoring in the liquid crystal octylcyanobiphenyl (8CB) adsorbed on a MoS_2 single crystal
Physical Review B, 2004, **69** 041705
- Lairez, D.**
Introduction à la diffusion de neutrons aux petits angles
Journal de Physique IV, 2003, **103** 253-290
- Lairez, D.; Pauthe, E.; Pelta, J.**
Refolding of a high molecular weight protein : salt effect on collapse
Biophysical Journal, 2003, **84** 3904-3916
- Lafond, A.; Leynaud, O.; André, G.; Bourée, F.; Caldes, M.; Meerschaut, A.**
The evolution of the antiferromagnetic structure of the terbium titanium oxysulfide $Tb_2Ti_2S_2O_5$ between 5K and 1.4K
Materials Science Forum, 2004, **443** 387-390
- Largeau, E.; El-Ghozzi, M.; Avignant, D.; Guillot, M.; Bourée, F.; André, G.; Cousson, A.**
Antiferromagnetic ordering in the KTb_3F_{12} mixed valence (III/IV) terbium fluoride studied by neutron diffraction and magnetic measurements
Journal of Magnetism and Magnetic Materials, 2003, **261** 93-104
- Larionova, J.; Willemin, S.; Donnadiou, B.; Henner, B.; Guérin, C.; Gillon, B.; Goujon, A.**
Crystal engineering in two- and three-dimensional system based on cyanomolybdates : structures, magnetism and intercalation properties
Journal of Physics and Chemistry of Solids, 2004, **65** 677-691
- Lasjaunias J.C., Biljakovi K., Sauvajol J.L., Monceau P.**
Evidence of 1D Behavior of He^+ Confined within Carbon-Nanotube Bundles
Physical Review Letters, 2003, **91** 025901
- Lasjaunias J.C., Biljakovi K., Sauvajol J.L., Monceau P.**
Low energy vibrational excitations in carbon nanotubes studied by heat capacity
Nanotechnology, 2003, **14** 998-1003
- Lasjaunias, J.C., Sahling, S.; Biljakovic, K.; Monceau, P.**
Unusual magnetic field-induced transition in the low temperature ($T < 1K$) SDW ground state of $(TMTSF)_2PF_6$
Journal de Physique IV, 2004, **114** 113-114
- Latroche, M.; Joubert, J.-M.; Percheron-Guégan, A.; Bourée-Vignerot, F.**
Neutron diffraction study of the deuterides of the over-stoichiometric compounds $LaNi_{5+x}$
Journal of Solid State Chemistry, 2004, **177** 1219-1229
- Latroche, M.; Paul-Boncour, V.; Percheron-Guégan, A.**
Structural properties of two deuterides $LaY_2Ni_9D_{12.8}$ and $CeY_2Ni_9D_{7.7}$ determined by neutron powder diffraction and X-ray absorption spectroscopy
Journal of Solid State Chemistry, 2004, **177** 2542-2549
- Latsyshev, Y.I.; Monceau, P.; Sinchenko, A.A.; Bulaevskii, L.N.; Brazovskii, S.A.; Kawae, T.; Yamashita, T.**
Interlayer tunnelling spectroscopy of the charge density wave state in $NbSe_3$
Journal of Physics A, 2003, **36** 9323-9335
- Lazewski J.; Parlinski K.; Szuszkiewicz W.; Hennion B.**
Lattice dynamics of HgSe: Neutron scattering measurements and ab initio studies
Physical Review B, 2003, **67** 094305/1-094305
- Lazuta, A.V.; Ryzhov, V.A.; Kurbukov, A.I.; Trunov, V.A.; Larionov, I.I.; Gorbenk, O.; Kaul, A.**
Magic hole doped composition of $^{152}Sm_{1-x}Sr_xMnO_3$ manganite: crystal structure and unusual magnetic properties in paramagnetic phase at $x=0.45$
Journal of Magnetism and Magnetic Materials, 2003, **258-259** 315-318
- Le Toquin, R.; Paulus, W.; Cousson, A.; Dhalenne, G.; Revcolevschi, A.**
Interstitial and apical oxygen order-disorder in $La_2CoO_{4+\delta}$ observed by single-crystal neutron and X-ray diffraction
Physica B, 2004, **350** E269-E272
- Lee, L.T.; da Silva, M.D.; Galembeck, F.**
Dewetting patterns of thin films of charged polymer solutions
Langmuir, 2003, **19** 6717-6722

- Lee, L.T.; Leite, C.A.P.; Galembeck, F.**
Controlled nanoparticle assembly by dewetting of charged polymer solutions
Langmuir, 2004, **20** 4430-4435
- Len, A.; Harmat, P.; Pépy, G.; Rosta, L.; Schade, P.**
Analysis of potassium inclusions in sintered tungsten wires
Journal of Applied Crystallography, 2003, **36** 621-623
- Len, A.; Pépy, G.; Rosta, L.**
Multibeam focussing in SANS technique
Physica B, 2004, **350** E771-E773
- Leone, P.; Andre, G.; Doussier, C.; Moelo, Y**
Neutron diffraction study of the.; magnetic ordering of jamesonite (FePb₄Sb₆S₁₄)
Journal of Magnetism and Magnetic materials, 2004 **284** 92-96
- Levy-Tubiana, R.; Baczanski, A.; Lodini, A.**
Relaxation of thermal mismatch stress due to plastic deformation in an Al/SiC_p
Materials Science and Engineering A, 2003, **341** 74-86
- Leyh, B.; Vangeyte, P.; Heinrich, M.; Auvray, L.; De Clercq, C.; Jérôme, R.**
Self-assembling of poly(-caprolactone)-b-poly(ethylene oxide) diblock copolymers in aqueous solution and at the silica-water interface
Physica B, 2004, **350** E901-E904
- Liang, B.; Lin, C.T**
Floating-zone growth and characterization of high-quality Bi₂Sr_{2-x}La_xCuO_{6-δ} single crystals
Journal of Crystal Growth, 2004, **267** 510-516
- Llobet, A.; Bao, W.; Moreno, N.O.; Pagliuso, P.G.; Sarrao, J.L.; Thompson, J.D.; Prokes, K.; Mignot, J.M.**
Interplay between magnetism and superconductivity in CeMn₅ heavy fermion
Journal of Magnetism and Magnetic Materials, 2004, **272** 175-176
- Llobet, A.; Gardner, J.S.; Moshopoulou, E.G.; Mignot, J.M.; Nicklas, M.; Bao, W.; Moreno, N.O.; Pagliuso, P.G.; Goncharenko, I.N.; Sarrao, J.L.;**
Magnetic structure of CeRhIn₅ as a function of pressure and temperature
Physical Review B, 2004, **69** 024403
- Longeville S.; Doster W.; Diehl M.; Gahler R.; Petry W.**
Neutron resonance spin echo: Oxygen transport in crowded protein solutions
Lecture Notes in Physics, 2003, **601** 325-335
- Longeville, S.; Doster, W.; Kali, G.**
Myoglobin in crowded solutions : structure and diffusion
Chemical Physics, 2003, **292** 413-424
- Luca, S.E.; Amara, M.; Galéra, R.M.; Givord, F.; Granovsky, S.; Isnard, O.; Beneu, B.**
Neutron diffraction studies on GdB₆ and TbB₆ powders
Physica B, 2004, **350** E39-E42
- Magazù, S. ; Branca, C. ; Migliardo, F.; Romeo, G. ; Mangione, A.**
Scattering findings on disaccharide/water mixtures
Journal of Molecular Structure, 2004, **700** 211-215
- Maitre, A.; Bourguignon, G.; Medjahdi, G.; McRae, E.; Mathon, M.H.**
Experimental study of L12 phase precipitation in the Pb-0.08wt%Ca-2.0wt%Sn alloy by resistivity and SANS measurements
Scripta Materialia, 2004, **50** 685-689
- Majerus, O.; Cormier, L.; Calas, G.; Beuneu, B.**
Temperature-induced boron coordination change in Alkali borate glasses and melts
Physical Review B, 2003, **67** 024210
- Majerus, O.; Cormier, L.; Calas, G.; Beuneu, B.**
Structural modifications between Lithium-Diborate glasses and melts: implications for transport properties and melt fragility
Journal of Physical Chemistry B, 2003, **107** 13044-13050
- Majerus, O.; Cormier, L.; Calas, G.; Beuneu, B.**
A neutron diffraction study of temperature-induced structural changes in potassium disilicate glass and melt
Chemical Geology, 2004 **213** 89-102
- Makarova O. L.; Goncharenko I. N.; Bouree F.**
Oscillating dependence between magnetic and chemical orderings in the frustrated Laves hydrides RMn₂H_x (R=Lu, Tm, Er)
Physical Review B, 2003, **6** 134418
- Makarova, O.L.; Goncharenko, I.N.; Le Bihan, T.**
Magnetic and structural instabilities in the hexagonal Laves hydride ErMn₂H_{4,6} under high-pressure
Solid State Communications, 2004, **132** 229-232
- Maluszynska, H.; Scherf, C.; Czarnecki, P., Cousson, A.**
The neutron diffraction study of pyridinium periodate at 352, 300 and 100 K
Journal of Physics : Condensed Matter, 2003, **15** 5663-5674
- Mangiapia, G.; Berti, D.; Baglioni, P.; Teixeira, J.; Paduano, L.**
Structural investigation on the Poly(vinylpyrrolidone)-Water system in the presence of sodium decyl and sodium decanesulfonate : a small angle neutron scattering study
Journal of Physical Chemistry B, 2004, **108** 9772-9779
- Maniadis, P.; Kopidakis, G.; Aubry, S.**
Quantum targeted energy transfer
Proceedings of "Localization and energy transfer in nonlinear systems" L. Vasquez, R. MacKay, M.P. Zorzano (editors), 2003, p. 268-272
- Maniadis, P., Zolotaryuka, V., Tsitonis, G.P.**
Existence and stability of discrete gap breathers in a diatomic b Fermi-Pasta-Ulam chain.
Physical Review E, 2003, **67** 046612
- Maniadis, P., Kalosakas, G.; Rasmussen, K.O.; Bishop, A.R.**
Polaron normal modes in the Peyrard-Bishop-Holstein model
Physical Review B, 2003, **68** 174304
- Maniadis, P.; Kopidakis, G.; Aubry, S.**
Quantum targeted energy transfer
In "Localization and energy transfer in nonlinear systems" L. Vasquez, R. MacKay, M.P. Zorzano (editors) (2003) p. 268-272
- Maniadis, P.; Kopidakis, G.; Aubry, S.**
Classical quantum targeted energy transfer between nonlinear oscillators
Physica D, 2004, **188** 153-177
- Maniadis, P.; Thompson, R.B.; Rasmussen, K.O.; Lookman, T.**
Ordering mechanisms in triblock copolymers
Physical Review E, 2004, **69** 031801
- Marcano, N.; Paccard, D.; Espeso, F.I., Allemand, J.; Moreau, J.M.; Kurbakov, A.; Sekine, C.; Paulsen, C.; Lhotel, E.; Gomez-Sal, J.C.**
On the structure and magnetic properties of CeNi with minor Cu substitutions
Journal of Magnetism and Magnetic Materials, 2004, **272** 468-469
- Margaca, FMA.; Moreira, M.; Teixeira, J.; Silva, RF.; Salvado, IMM.**
Porosity assessment of beta-spodumene/glass matrix composites by Small Angle Neutron Scattering
Materials Science Forum, 2004, **455** 230-234

Maschke, U.; Gogibus, N.; Ewen, B.; Wagner, T.; Noirez, L.; Benmouna, M.

Polymer dispersed liquid crystals made of deuterated polystyrene and 8CB blends: A small angle neutron scattering study
Molecular Crystals and Liquid Crystals, 2004, **413** 2171-2178

Mathon M. H.; de Carlan Y.; Geoffroy G.; Averty X.; Alamo A.; de Novion C. H.

A SANS investigation of the irradiation-enhanced a-a' phases separation in 7-12 Cr martensitic steels
Journal of Nuclear Materials, 2003, **312** 236-248.

Maury, F., Mirebeau, I.; Hodges, J.A.; Bourges, P.; Sidis, Y.; Forget, A.

Long and short range magnetic order, charge transfer and superconductivity in $YBa_2Cu_{3-x}Co_xO_7$
Physical Review B, 2004, **69** 094506

Mehaddene, T.; Kentzinger, E.; Hennion, B.; Tanaka, K.; Numakura, H.; Marty, A.; Parasote, V.; Cadeville, M.C.; Zemirli, M.; Pierron-Bohnes V.

Lattice dynamics and migration enthalpies in $CoPt_3$ and $FePd$
Physical Review B, 2004, **69** 024304

Mehaddene, T.; Zemirli, M.; Pierron-Bohnes, V.; Cadeville, M.C.; Hennion, B.; Marty, A.; Tanaka, K.; Numakura, H.

Inelastic neutron scattering and migration energies in $FePd$
Catalysis Today, 2004, **89** 313-318

Mehaddene, T.; Pierron-Bohnes, V.; Zemirli, M.; Caudron, R.; Tanaka, K.; Numakura, H.

Study of local order in $FePd$ by neutron diffuse scattering
Journal of Alloys and Compounds, 2004, **378** 294-297

Mehaddene, T.; Sanchez, J.M.; Caudron, R.; Zemirli, A.; Pierron-Bohnes, V.

Pair correlations and interaction energies in $FePd$ single crystal
European Physical Journal B, 2004 **41** 207-212

Mendes, E.; Hakiki, A.; Herz, J.; Boué, F.; Bastide, J.

Structure of trifunctional end-link polymer gels studied by SANS
Macromolecules, 2004, **37** 2643-2649

Menelle, A.

La réflectivité des neutrons
Journal de Physique IV, 2003, **103** 291-303

Menelle, A.; Jestin, J.; Cousin, F.

Liquid interfaces investigated by neutron reflectivity
Neutron News, 2003, **14** n°3 26-30

Menelle, A.

Upgrade of the time-of-flight reflectometer at LLB
Physica B, 2004, **350** E767-E769

Mercore, S.; Hardy, V.; Martin, C.; Simon, C.; Saurel, D.; Brulet, A.

Field dependence of the electronic phase separation in $Pr_{0.67}Ca_{0.33}MnO_3$ by small angle magnetic neutron scattering
Physical Review B, 2003, **68** 094422

Metoki, N.; Kaneko, K.; Araki, S.; Kohgi, M.; Iwasa, K.; Kuwahara, K.; Bernhoeft, N.; Mignot, J.M.; Gukasov, A.; Sato, H.; Aoki, Y.; Sugawara, H.

Neutron scattering study on the field-induced antiferro-quadrupolar ordering in the heavy fermion superconductor $PrOs_4Sb_{12}$
Journal of Magnetism and Magnetic Materials, 2004, **272** E91-E92

Michel, J.P.; Lacaze, E.; Alba, M.; de Boissieu, M.; Gailhanou, M.; Goldmann, M.

Optical gratings formed in thin smectic films frustrated on a single crystalline substrate
Physical Review E, 2004, **70** 011709

Mikke, K.; Jankowska-Kisielinska, J.; Hennion, B.

Inelastic neutron scattering near the magnetic Brillouin zone centre and at the zone boundary in Mn (18% Cu) alloy
Physica B, 2004, **350** E75-E78

Millot, N.; Aymes, D.; Bernard, F.; Niepce, J. C.; Traverse, A.; Bourée, F.; Chen, B.L.; Perriat, P.

Particle Size Dependency of Ternary Diagrams at the Nanometer Scale: Evidence of TiO_2 Clusters in Fe-Based Spinel
Journal of Physical Chemistry B, 2003, **107** 5740-5750

Mirebeau, I.; Goncharenko, I.N.

Spin liquid and spin ice under high pressure : a neutron study of $R_2Ti_2O_7$ ($R=Tb, Ho$)
Journal of Physics. Condensed Matter, 2004, **16** S653-S663

Mirebeau, I.; Goncharenko, I.N.

Spin ice and spin liquid under pressure up to 8.6 GPa : a powder neutron diffraction study of $R_2Ti_2O_7$ ($R=Tb, Ho$)
Physica B, 2004, **350** 250-253

Mirebeau, I.; Goncharenko, I.N.; Dhalle, G. Revcolevschi, A.

Pressure and field induced magnetic order in the spin liquid $Tb_2Ti_2O_7$ as studied by single crystal neutron diffraction
Physical Review Letters, 2004, **93** 187204

Mora S.; Daillant, J.; Mecke, K.; Luzet, D.; Braslau, A.; Alba, M.; Struth, B.

X-ray synchrotron study of liquid-vapor interfaces at short length scales : effect of long-range forces and bending energies
Physical Review Letters, 2003, **90** 216101

Morales, L.; Rodriguez-Carvajal, J.; Caneiro, A.

Structural and magnetic behavior of $LaMnO_{3+\delta}$ and $LaMn_{0.9}Cr_{0.1}O_{3+\delta}$ at the same "hole concentration"
Journal of Alloys and Compounds, 2004, **369** 97-100

Morfin, I.; Lindner, P.; Boué, F.

Shear-induced concentration fluctuations and form factor changes in polymer solution in the good-solvent regime
European Physical Journal E, 2004, **15** 41-45

Mouallem-Bahout, M.; Roisnel, T.; André, G.; Gutierrez, D.; Moure, C.; Pena O.

Nuclear and magnetic order in $Y(Ni, Mn)O_3$ manganites by neutron powder diffraction
Solid State Communications, 2004, **129** 255-260

Mounier, C.

Thermal neutron cross-section of magnesium
Annals of Nuclear Energy, 2004, **31** 911-921

Moussa F.; Hennion M.; Kober P.; Wang F.; Carvajal-Rodriguez J.; Reutler P.; Mukovskii Y. M.; Shulyatev D.

Approach to the insulator-metal transition in low doped manganites by neutron scattering
Journal of Magnetism and Magnetic Materials, 2003, **258-259** 259-264

Moussa, F.; Hennion, M.; Wang, F.; Kober, P.; Rodriguez-carvajal, J.; Reutler, P.; Pinsard, L.; Revcolevschi, A.

Spin waves and phonons in $La_{1-x}Sr_xMnO_3$ ($x=0.09, 0.125$) : Dynamical signatures of low-temperature phase transitions for $x=0.125$
Physical Review B, 2003, **67** 214430

Moussa, F.; Hennion, M.; Wang, F.; Gukasov, A.; Suryanarayanan, R.; Apostu, M.; Revcolevschi, A.

Field-induced ferromagnetic metallic state in the bilayer manganite $(La_{0.4}Pr_{0.6})_{1.2}Sr_{1.8}Mn_2O_7$, probed by neutron
Physical Review Letters, 2004, **93** 107202

Moussy, J.B.; Gota, S.; Bataille, A.; Guittet, M.J.; Gautier-Soyer, M.; Delille, F.; Dieny, B.; Ott, F.; Doan, T.D.; Warin, P.; Bayle-Guillemaud, P.; Gatel, C.; Snoeck, E.

Thickness dependence of anomalous magnetic behavior in epitaxial $Fe_3O_4(111)$ thin films: Effect of density of antiphase boundaries
Physical Review B, 2004, **70** 174448

Mukhamedshin, I.R.; Alloul, H.; Collin, G.; Blanchard, N.

$Na-23$ NMR evidence for charge order and anomalous magnetism in Na_xCoO_2
Physical Review Letters, 2004 **93** 167601

Muller, F.; Guenoun P.; Delsanti, M.; Deme, B.; Auvray, L.; Yang, J.; Mays, JW
Spherical polyelectrolyte block copolymer micelles: Structural change in presence of monovalent salt
 European Physical Journal E, 2004, **15** 465-472

Nagasawa, B.M.; Nad, F.; Monceau, P.; Fabre, J.M.
Pressure effect on the charge ordering phase transition in the quasi-one-dimensional conductor (TMTTF)₂SbF₆
 Journal de Physique IV, 2004, **114** 119-121

Nedkov, I.; Kolev, S.; Zadro, K.; Krezhov, K.; Merodiiska, T.
Crystalline anisotropy and cation distribution in nanosized quasi-spherical ferroxide particles
 Journal of Magnetism and Magnetic Materials, 2004, **272-276** E1175-E1176

Nicolai, B.; Cousson, A.; Fillaux, F.
Interplay quantum methyl rotation and crystal structure in the lithium acetate dihydrate : neutron diffraction, inelastic neutron scattering theory
 Chemical Physics, 2003, **292** 101-120

Oberdisse, J.
Small angle neutron scattering and model predictions for micelle-decorated colloidal silica beads
 Physical Chemistry Chemical Physics, 2004, **6** 1557-1561

Oberdisse, J.
Fragmented structure of adsorbed layer of non-ionic surfactant on colloidal silica
 Physica B, 2004, **350** E913-E916

Oberdisse, J. ; Boué F.
Rheology-structure relationship of a model nanocomposite materials
 Progress in Colloid and Polymers Science **126** (2004) 124-129

Oles, A.; Duraj, R.; Kolenda, M.; Penc, B.; Szytula, A.
Magnetic properties of DyCuSi and HoCuSi studied by neutron diffraction and magnetic measurements
 Journal of Alloys and Compounds, 2004, **363** 63-67

Ollivier J.; Rufflé, B.; Longeville, S.; Bourges, P.; Lechner, R.E.; Toudic, B.
Central peak near the incommensurate displacive phase transition of BCPS
 Chemical Physics , 2003, **292** 171-183

Onufrieva, F.; Pfeuty, P.
Spin dynamics of the electron-doped superconducting high-T_c cuprates
 Physical Review Letters, 2004, **92** 247003

Ott, F.; Cousin, F.; Menelle, A.
Surfaces and interfaces characterization by neutron reflectometry
 Journal of Alloys and Compounds., 2004., **383**, 29-38

Padureanu, I.; Arangel, D.; Kahn, R.; Radulescu, A.; Sumin, V.V.
Neutron scattering investigation of the hydrogen dynamics in transition metals
 Physica B, 2004, **350** E553-E555

Pailhes, S.; Sidis, Y.; Bourges, P.; Ulrich, C.; Hinkov, V.; Regnault, L.P.
Two resonant magnetic modes in overdoped high-T_c superconductor
 Physical Review Letters , 2003, **91** 237002

Pailhes, S.; Sidis, Y.; Bourges, P.; Hinkov, V.; Ivanov, A.; Ulrich, C.; Regnault, L. P.; Keimer, B.
Resonant magnetic excitations at high energy in superconducting YBa₂Cu₃O_{6.85}
 Physical Review Letters, 2004, **93** 167002

Pannetier, M.; Ott, F.; Fermon, C.; Samson, Y.
Surface diffraction on magnetic nanostructures in thin films using grazing incidence SANS
 Physica B , 2003, **335** 54-58

Pannetier, M.; Doan, T.D.; Ott, F.; Berger, S.; Persat, N.; Fermon, C.
Polarized neutron reflectometry for GMR sensors optimization
 Europhysics Letters , 2003, **64** 524-528

Papoular, R.J.; Kunz, M.
The hunt for hydrogen in the high-pressure phase of Ca(OH)₂ and Ca(OD)₂ : neutrons versus X-rays
 Materials Science Forum, 2004, **443** 341-344

Patoux, S. ; Wurm, C. ; Morcrette, M. ; Rouse, G. ; Masquelier, C.
A comparative structural and electrochemical study of monoclinic Li₃Fe₂(PO₄)₃ and Li₃V₂(PO₄)₃
 Journal of Power Sources, 2003, **119-121** 278-284

Paul-Boncœur, V.; Bouree-Vigneron, F.; Filipek, S.M.; Marchuk, I.; Jacob, I.; Percheron-Guegan, A.
Neutron diffraction study of ZrM₂D_x deuterides (M=Fe, Co)
 Journal of Alloys and Compounds , 2003, **356-357** 69-72

Paul-Boncœur, V.; Filipek, S.M.; Marchuk, I.; André, G.; Bourée, F.; Wiesinger, G.; Percheron-Guégan, A.
Structural and magnetic properties of ErFe₂D₅ studied by neutron diffraction and Mössbauer spectroscopy
 Journal of Physics : Condensed Matter , 2003, **15** 4349-4359

Paul-Boncœur, V.; André, G.; Bourée, F.; Guillot, M.; Wiesinger, G.; Percheron-Guégan, A.
Influence of H/D isotopic substitution on the first-order magnetic transition in YFe₂(D_{1-x}H_x)_{4.2} compounds (x=0, 0.64.)
 Physica B, 2004, **350** E27-E30

Pautrat, A.; Goupil, C.; Simon, Ch.; Charalambous, D.; Forgan, E.M.; Lazard, G.; Mathieu, P.; Brulet, A.
Distribution of transport current in a type-II superconductor studied by small angle neutron scattering
 Physical Review Letters , 2003, **90** 087002

Pépy, G.; Baroni, P.; Noirez, L.
Pressure induced reduction of the Landau-Peierls instabilities in a side-chain polymer liquid crystal with reentrant polymorphism
 Physical Review E, 2003, **67** 041714

Perez-Mato J. M.; Etrillard J.; Kiat J. M.; Liang B.; Lin C. T.
Competition between composite and modulated configurations in Bi₂Sr₂CaCu₂O_{8+δ} and its relation to oxygen stoichiometry
 Physical Review B, 2003, **67** 024504

Petitgrand, D.; Yamada, K.; Fujita, M.; Uefuji, T.
Superconductivity induced spin gap in Nd_{1.85}Ce_{0.1}Cu₄
 Physica C, 2004, **408-410** 778-779

Pfeiderer, C.; Reznick, D.; Pintschovius, L.; Lohneysen, H.v.; Garst, M.; Rosch, A.
Partial order in the non-Fermi-liquid phase of MnSi
 Nature, 2004, **427** 227-231

Pfeiderer, C ; Uhlarz, M.
Quantum criticality and partial order in itinerant magnets
 Physica C, 2004, **408-410** 376-379

Pichl, W.; Krystian, M.; Prem, M.; Krexner, K.
The low-temperature martensitic phase transition of pure lithium
 Recent Res. Devel. Mat. Sci. Engg. , 2003, **2** 1-27

Pichl, W.; Krystian, M.; Prem, M.; Krexner, K.
The martensite phase of high-purity lithium
 Journal de Physique IV France, 2003, **112** 1095-1098

- Pinsard-Gaudard, L.; Rodriguez-Carvajal, J.; Gukasov, A.; Monod, P.**
Magnetic properties of paramelaconite (Cu₄O₃) : a pyrochlore lattice with S=1/2
Physical Review B, 2004, **69** 104408
- Pintschovius L., Reichardt W., Wolf T., Klaeser M.**
In-plane anisotropy and temperature dependence of oxygen phonon modes in YBa₂Cu₃O_{6.6}
Physica C, 2003, **388-389** 211-212
- Pintschovius, L.; Reznik, D.; Pfeleiderer, C.; Löhneysen, H.v.**
Partial magnetic order in the itinerant-electron magnet MnSi
Pramana - Journal of Physics, 2004, **63** 117-123
- Pintschovius, L.; Reznik, D.; Reichardt, W.; Endoh, Y.; Hiraka, H.; Tranquada, J.M.; Uchiyama, H.; Masui, T.; Tajima, S.**
Oxygen phonon branches in YBa₂Cu₃O₇
Physical Review B, 2004, **69** 214506
- Pintschovius L.; Endoh Y.; Reznik D.; Hiraka H.; Tranquada J.; Reichardt W.; Bourges P.; Sidis Y.; Uchiyama H.; Masui T.; Tajima, S.**
Neutron scattering study of charge fluctuations and spin fluctuations in optimally doped YBa₂Cu₃O_{6.95}
Physica C, 2004 **412-414** 70-75 Part 1
- Piroux, F.; Espuche, E.; Mercier, R.; Pinéri, M.**
Water vapour transport mechanism in naphthalenic sulfonated polyimides
Journal of Membrane Science, 2003, **223** 127-139
- Prem, M.; Krexner, G.; Pleschitschnig, J.**
Helium damage in long-aged metal-tritium systems
Journal of Alloys and Compounds, 2003, **356-357** 683-687
- Prem, M.; Krexner, G.; Beuneu, F.; Vajda, P.**
Metallic colloids in lithium oxide after electron irradiation
Physica B, 2004, **350** E999-E1002
- Prokes, K.; Gukasov, A.; Takabatake, T.; Fujita, T.; Sechovsky, V.**
Magnetic form factor of URhGe
Acta Physica Polonica B, 2003, **34** 1473-1476
- Prokes, K.; Gukasov, A.; Sechovský, V.; Andreev, A.V.**
Magnetic properties of UNi_{2/3}Rh_{1/3}Al single crystal probed by polarized neutron diffraction
Journal of Magnetism and Magnetic Materials, 2004, **272** E67-E69
- Prokhnenko, O.; Goncharenko, I.; Arnold, Z.; Kamarad, J.**
Magnetism in Ce₂Fe₁₇ at pressures up to 70 kbar
Physica B, 2004, **350** 63-65
- Pujolle-Robic, C.; Noirez, L.**
Identification of nonmonotonic behaviors and stick-slip transition in liquid crystal polymers
Physical Review E, 2003, **68** 061706
- Quintana, I.; Arbe, A.; Colmenero, J.; Alegría, A.; Kahn, R.**
Molecular motions in a polymer membrane: a time-of-flight study on poly(ether sulfone)
Physica B, 2004, **350** E893-E895
- Ravy, S.; Requardt, H.; Le Bolloc'h, D.; Foury-Leylekyan, P.; Pouget, J.P.; Currat, R.; Monceau, P.; Krisch, M.**
Inelastic x-ray scattering study of charge density wave dynamics in the Rb_{0.3}Mo₃ blue bronze
Physical Review B, 2004, **69** 115113
- Renou, J.P.; Foucat, L.; Corsaro, C.; Ollivier, J.; Zanotti, J.-M.; Middendorf, H.D.**
Dynamics of collagen from bovine connective tissues
Physica B, 2004, **350** E631-E633
- Reutler, P.; Friedt, O.; Buchner, B.; Braden, M.; Revcolevschi, A.**
Growth of La_{1-x}Sr_{1+x}MnO₄ single crystals and characterization by scattering techniques
Journal of Crystal Growth, 2003, **249** 222-229
- Reznik, D.; Pintschovius, L.; Reichardt, W.; Endoh, Y.; Hiraka, H.; Tranquada, J. M.; Tajima, S.; Uchiyama, H.; Masui, T.**
Oxygen Phonon Branches in Detwinned YBa₂Cu₃O₇
Journal of Low Temperature Physics, 2003, **131** 417-421
- Reznik, D.; Bourges, P.; Pintschovius, L.; Endoh, Y.; Sidis, Y.; Masui, T.; Tajim, S.**
Dispersion of magnetic excitations in optimally doped superconducting YBa₂Cu₃O_{6.95}
Physical Review Letters, 2004, **93** 207003
- Rippel, M.M.; Lee, L.T.; Leite C.A.P.; Galembeck, F.**
Skim and cream natural rubber particles : colloidal properties, coalescence and film formation
Journal of Colloid and Interface Science, 2003, **268** 330-340
- Robertson, D.; Hellweg, T.; Tiersch, B.; Koetz, J.**
Polymer-induced structural changes in lecithin/sodium dodecyl sulfate-based multilamellar vesicles
Journal of Colloid and Interface Science, 2004, **270** 187-194
- Rodriguez-Carvajal, J.; Roisnel, T.**
Line broadening analysis using FullProf: Determination of microstructural properties*
Materials Science Forum, 2004, **443-444** 123-126
- Rols, S.; Cambedouzou, J.; Bantignies, J.-L.; Rachdi, F.; Sauvajol, J.-L.; Agafonov, V.; Rakhmanina, A.V.; Davydov, V.A.; Hennion, B.; Kahn, R.**
Lattice dynamics of pressure-polymerized phases of C₆₀: A neutron scattering investigation
Physical Review B, 2004, **70** 104302
- Romet-Lemonne, G.; Dailant, J.; Guenoun, P.; Yang, J.; Mays, J.W.**
Thickness and density profiles of polyelectrolyte brushes : dependence on grafting density and salt concentration
Physical Review Letters, 2004, **93** 148301
- Rotter, M.; Loewenhaupt, M.; Doerr, M.; Lindbaum, A.; Sassik, H.; Ziebeck, K.; Beuneu, B.**
Dipole interaction and magnetic anisotropy in gadolinium compounds
Physical Review B, 2003, **68** 144418
- Rotter, M.; Doerr, M.; Loewenhaupt, M.; Lindbaum, A.; Rotter, M.; Doerr, M.; Loewenhaupt, M.; Lindbaum, A.**
Diffraction experiments on GdCu₂In using hot neutrons
Physica B, 2004, **350** E63-E66
- Rufflé, B.; Longeville, S.**
Structural relaxation in supercooled (Na₂O-Li₂O)₂P₂O₅: a neutron spin-echo study
Physica B, 2004, **350** 41111-E1114
- Russo, D.; Baglioni, P.; Peroni, E.; Teixeira, J.**
Hydration water dynamics of a completely hydrophobic oligopeptide
Chemical Physics, 2003, **292** 235-245
- Sacchetti, F.; Altissimo, M.; Petrillo, C.; Di Fabrizio E.; Colleoni, S.; Ott, F.**
Fresnel zone plates for imaging and focussing of thermal and cold neutrons
Neutron News, 2003, **14** n°2 37-38
- Sacchetti, F.; Altissimo, M.; Petrillo, E.; Di Fabrizio, E.; Colleoni, S.; Ott, F.**
Fresnel zone plates as neutron optical elements for neutron imaging
Physica B, 2004, **350** E447-449
- Saez-Puche, R.; Jiménez, E.; Isasi, J.; Fernández-Díaz, M.T.; García-Muñoz, J.L.**
Structural and magnetic characterization of RCrO₄ oxides (R=Nd, Er and Tm)
Journal of Solid State Chemistry, 2003, **171** 161-169

Saito, S.; Hashimoto T.; Morfin, I.; Lindner, P.; Boué, F.; Pine, D.J.

Phase separation in a polymer solution induced by steady and large amplitude oscillatory shear flow
Macromolecules, 2003, **36** 3745-3748

Saurel, D.; Merccone, S.; Guiblin, N.; Hardy, V.; Brulet, A.; Martin, C.; Simon, Ch.

Small angle neutron-scattering study of the microphase separation in the $Pr_{0.66}Ca_{0.33}MnO_3$
Physica B, 2004, **350** 51-54

Schedler, R.; Witte, U.; Loewenhaupt, M.; Kulda, J.

Coupling between crystal field transitions and phonons in the 4f-electron system $CeCu_2$
Physica B, 2004, **335** 41-43

SchobingerPapamantellos, P.; Rodríguez-Carvajal, J.; André, G.; Ritter, C.; Buschow, K.H.J

Re-entrant magneto-elastic transition in $HoFe_4Ge_2$ a neutron diffraction study
Journal of Magnetism and Magnetic Materials, 2004, **280** 119-142

Schröder, L.; Watkin, D.J.; Cousson, A.; Cooper, R.I., Paulus, W.

Crystals enhancements: refinement of atoms continuously disordered along a line, on a ring or on the surface of a sphere
Journal of Applied Crystallography, 2004, **37** 545-550

Señas, A.; Rodríguez Fernández, J.; Gómez Sal, J.C.; Camp, J.; André, G.

Following out-of-stoichiometry phase coexistence with neutron techniques
Physica B, 2004, **350** E115-E118

Senas, A.; Rodriguez Fernandez, J.; Gomez Sal, J.C.; Campo, J.; Rodriguez-Carvajal, J.

From ferromagnetism to incommensurate magnetic structures: A neutron diffraction study of the chemical substitution effects in $TbPt_{1-x}Cu_x$
Physical Review B, 2004, **70** 184425

Semitelou, J.P.; Yakinthos, J.K.

Commensurate and incommensurate phases in Ho_5Sn_3 compound
Journal of Magnetism and Magnetic Materials, 2003, **261** 392-398

Serban, F.; Baczmanski, A.; Labbe, E.; Wierzbanowski, K.; Lodini, A.

Study of mechanical behaviour of austempered ductile iron using self-consistent model
Journal of Neutron Research, 2004, **12** 181-187

Shames, A.I.; Rozenberg, E.; Martin, C.; Maignan, A.; Raveau, B.; Andre, G. ; Gorodetsky, G.

Crystallographic structure and magnetic ordering in $CaMn_{1-x}Ru_xO_3$ ($x \leq 0.40$) manganites: Neutron diffraction, ac susceptibility, and electron magnetic resonance studies
Physical Review B, 2004, **70** 134433

Sidis, Y.; Pailhes, S.; Keimer, B.; Bourges, P.; Ulrich, C.; Renault, L.P.

Magnetic resonant excitations in high- T_c superconductors
Physica Status Solidi B, 2004, **241** 1204-1210

Sikolenko V.V.; Kozlenko, D.P.; Pomjakushina, E.V.; Pomjakushin, V.Yu.; Balagurov, A.M.; Keller, L; Glazkov, A.; Griбанov, A.V.; Goncharenko, I.N.; Savenko, B.N.

Structural study of $U(Pd_{1-x}Fe_x)_2Ge_2$ at high pressure
Journal of Physics : Condensed Matter, 2003, **15** 2825-2832

Sikolenko, V.V.; Pomjakushina, E.V.; Pomjakushin, V.Yu.; Griбанov, A.V.; Zimmermann, U.; Kurbakov, A.; Kozlenko, D.P.; Goncharenko, I.N.; Balagurov, A.M.

Modulated spin-density waves in uranium intermetallic compounds with $ThCr_2Si_2$ structure
Physica B, 2004, **350** E163-E166

Simon, Ch.; Merccone, S.; Hardy, V.; Martin, C.; Saurel, D.; Brulet, A.

Magnetic field induced percolation in $Pr_{0.67}Ca_{0.33}MnO_3$ by small angle magnetic neutron scattering
Journal of Magnetism and Magnetic Materials, 2004, **272** E1383-E1384

Simon, Ch.; Pautrat, A.; Poullain, G.; Goupil, C.; Leblond-Harnois, C.; Chaud, X.; Brulet, A.

Influence of twin boundaries on the flux-line-lattice structure in $YBa_2Cu_3O_{7-d}$: a small-angle neutron scattering
Physical Review B, 2004, **70** 024502

Sinchenko A.A.; Monceau P.

Tunneling spectroscopy of $NbSe_3$ in a high magnetic field
Physical Review B, 2003, **67** 233103

Soldevilla, J.G.; Blanco, J.A.; Fernandez, J.R.; Espeso, J.I.; Sal, J.C.G.; Fernandez-Diaz, M.T.; Rodriguez-Carvajal, J.; Paccard, D.

Complex magnetic ordering in $NdNi_{1-x}Cu_x$: Determination of the magnetic structure by neutron diffraction
Physical Review B, 2004 **70** 224411

Strassle T.; Saitta, A.M.; Klotz, S.; Braden, M.

Phonon dispersion of ice under pressure
Physical Review Letters, 2004, **93** 225901

Swenson, J.; Bergman, R.; Howells, W.S.; Longeville, S.

Response to Comment on "Quasielastic neutron scattering of two-dimensional water in a vermiculite clay" [J. Chem. Phys. 113.; 2873 (2000)] and "A neutron spin-echo study of confined water" [J. Chem. Phys. 115.; 11299 (2001)]
Journal of Chemical Physics, 2004 **121** 9195-9195

Swiatnicki, W.; Baudin, R.; Jura, J.; Mathon, M.H.; Glowacka, A.

TEM examination of the microstructure evolution in the duplex austenitic-ferritic steel
Voprosy Materialovedeniya, 2003, 96-103

Szuskiewicz W.; Dynowska E.; Ott F.; Hennion B.; Jouanne M.; Morhange J. F.; Sadowski J.

Short-Period GaMnAs/GaAs Superlattices: Optical and Magnetic Characterization.
Journal of Superconductivity, 2003, **16** 209-212.

Szuskiewicz, W.; Fronc, K.; Baran, M.; Szymczak, R.; Ott, F.; Hennion, B.; Dynowska, E.; Paszkowicz, W.; Pelka, J. B.; Zuberek, R.; Jouanne, M.; Morhange, J. F.

Interlayer Magnetic Coupling for Fe/Si Multilayers
Journal of Superconductivity, 2003, **16** 205-208

Tarasiuk, J.; Gerber, P.; Bacroix, B.

Monte Carlo modelling of recrystallization in metals
Journal de Physique IV, 2004 **120** 217-223

Teixeira, J.

Explorer la liaison hydrogène pour comprendre l'eau
La Recherche, 2004, 10

Tenailleau, C.; Suard, E.; Rodriguez-Carvajal, J.; Gibaud, A.; Lacorre, P.

Effect of doping and temperature on the crystal structure of $(V_{1-x}Mo_x)_2O_3$ above and below the metal/insulator transition
Journal of Solid State Chemistry, 2003, **174** 431-440

Tenailleau, C.; Suard, E.; Rodriguez-Carvajal, J.; Lacorre, P.

Influence of Mo-doping on the magnetic properties of V_2O_3
Journal of Magnetism and Magnetic Materials, 2004, **278** 57-67

Terech, P. ; Meerschaut, D. ; Desvergne, J.-P. ; Colomes, M. ; Bouas-Laurent, H.

2,3-di-n-decyloxy-6,7-dichloroanthracene (Cl_2DDOA), a new low-molecular-mass fluorescent organogelator: physical properties and structures
Journal of Colloid and Interface Science, 2003, **261** 441-450

- Thiebaut, S.; Demoment, J.; Limacher, B.; Paul-Boncour, V.; Decamps, B.; Percheron-Guegan, A.; Prem, M.; Krexner, G.**
Aging effects on palladium pressure-composition isotherms during tritium storage
Journal of Alloys and Compounds, 2003, **356-357** 36-40
- Tobias, G.; Beltran-Porter, D.; Lebedev, O.I.; Van Tendeloo, G.; Rodriguez-Carvajal, J.; Fuertes, A**
Anion ordering and defect structure in Ruddlesden-Popper strontium niobium oxynitrides
Inorganic Chemistry, 2004, **43** 8010-8017
- Török, Gy.; Lebedev, V.T.; Cser, L.; Orlova, D.N.; Sibilev, A.I.; Zgonnik, V.N.; Melenevskaya, E.Yu.; Vinogradova, L.V.; Sibileva, M.A.**
Dynamics of complexes of poly(N-vinylpyrrolidone)-C₆₀ in aqueous solution
Physica B, 2004, **350** E415-E418
- Toudic B., Le Lann, H. ; Guillaume, F. ; Lechner, R. E. ; Ollivier, J. ; Bourges, P.**
Coherent neutron scattering analysis of alkane dynamical disorder inside nanoporous urea intergrowth crystals
Chemical Physics, 2003, **292** 191-199
- Trabelsi, M.; Saidi, S.; Chefi, C.; Martin, C.; Lucas, S.; Ferry, D.; Suzanne, J.**
Thermodynamic and structural study of methanol thin films adsorbed on MgO(1 0 0)
Surface Science, 2004, **566-568** 789-793
- Tran, V.H.; Troc, R.; Andre, G.; Bouree, F.; Baenitz, M.**
Ferromagnetic ordering in UFe_{0.5}Ni_{0.5}Al
Physica Status Solidi B, 2004, **236** 356-359
- Tsegai, M.; Mathieu, R.; Nordblad, P.; Tellgren, R.; Bau, L.V.; Nam, D.N.H.; Phuc, N.X.; Khiem, N.V.; André, G.; Bourée, F.**
Magnesium substitution in Nd_{0.7}Sr_{0.3}MnO₃
Journal of Solid State Chemistry, 2004, **177** 966-971
- Trabelsi, M.; Saidi, S.; Chefi, C.; Picaud, S.; Hoang, P.N.M.; Coulomb, J.P.**
Structure of the neopentane monolayer adsorbed on MgO(0 0 1): experiments and calculations
Surface Science, 2004, **550** 133-139
- Troyanchuk, I.O.; Khomchenko, V.A.; Chobot, G.M.; Kurbakov, A.I.; Vasil'ev, A.N.; Eremenko, V.V.; Sirenko, V.A.; Shvedun, M.Yu.; Szymczak, H.; Szymczak, R.**
Spin-reorientational transitions in low-doped Nd_{1-x}Ca_xMnO₃ manganites : the evidence of an inhomogeneous magnetic state
Journal of Physics : Condensed Matter, 2003, **15** 8865-8880
- Tubiana, R.; Ceretti, M.; Menelle, A.; Annighöfer, B.; Marcantoni, M.**
Instrumental and technical developments on strain dedicated diffractometer at the LLB
Physica B, 2004, **350** E515-E516
- Tuinier, R.; Brulet, A.**
On the long-range attraction between proteins due to non-adsorbing polysaccharide
Biomacromolecules, 2003, **4** 28-31
- Uesu, Y.; Nakai, R.; Kiat, J.-M.; Ménoret, C.; Itoh, M.; Kyomen, T.**
Polar order in quantum paraelectric SrTi¹⁶O₃ and SrTi¹⁶O₃ at low temperature
Journal of the Physical Society of Japan, 2004, **73** 1139-1142
- Valkova, L.; Menelle, A.; Borovkov, N.; Erokhin, V.; Pisani, M.; Ciuchi, F.; Carsughi, F.; Spinozzi, F.; Pergolini, M.; Padke, R.; Bernstorff, S.; Rustichelli, F.**
Small angle X-ray scattering and neutron reflectivity studies of Langmuir-Blodgett films of copper tetra-tert-butyl-azaporphyrines
Journal of Allphied Crystallography , 2003, **36** 758-762
- van den Boogaard, M.; Bonnet G.; van't Hof, P.; Wang, Y.; Brochon, C.; van Hutten, P.; Lapp, A.; Hadziioannou, G.**
Synthesis of insulated single-chain semiconducting polymers based on polythiophene.; polyfluorene.; and beta-cyclodextrin
Chemistry of Materials, 2004 **16** 4383-4385
- van den Brandt, B.; Glattli, H.; Griesshammer, H.; Hautle, P.; Kohlbrecher, J.; Konter, J.A.; Zimmer, O.**
The spin-dependent and scattering length - a proposed high-accuracy measurement
Nuclear Instruments and Methods in Physics Research A, 2004, **526** 91-95
- van den Brandt, B.; Glattli, H.; Grillo, I.; Hautle, P.; Jouve, H.; Kohlbrecher, J.; Konter, J.A.; Leymarie, E.; Mango, S.; May, R.; Michels, A.; Stuhmann, H.B.; Zimmer, O.**
An experimental approach to the dynamics of nuclear polarisation
Nuclear Instruments and Methods in Physics Research A, 2004, **526** 81-90
- van der Maarel, J.R.C.; Zakharova, S.S.; Jesse, W.; Backendorf, C.; Egelhaaf, S.U.; Lapp, A.**
Supercoiled DNA ; plectonemic structure and liquid crystal formation
Journal of Physics : Condensed Matter , 2003, **15** S181-S189
- Vangeyte, P.; Leyh, B.; Auvray, L.; Grandjean, J.; Misselyn-Bauduin, A.-M.; Jerome, R.**
Mixed self-assembly of poly(ethylene oxide)-b-poly(epsilon-caprolactone) copolymers and sodium dodecyl sulfate in aqueous solution
Langmuir, 2004, **20** 9019-9028
- Venuti, V.; Crupi, V.; Majolino, D.; Migliardo, P.; Bellissent-Funel, M.C.**
Neutron diffraction study of the structure of water confined in a sol-gel silica glass
Physica B, 2004, **350** E599-E601
- Vertruyen, B.; Flahaut, D.; Hébert, S.; Maignan, A.; Martin, C.; Hervieu, M.; Raveau, B.**
Magnetic and electronic ground states of B-site-substituted LaMnO₃: from antiferromagnetism to ferromagnetism
Journal of Magnetism and Magnetic Materials, 2004, **280** 75-83
- Viallet-Guillen, V.; Collin, G.; Papoular, R.; Marucco, J.F.; Colson, D.**
Non stoichiometry and charge transfer in high Tc superconducting materials. HgBa₂CuO_{4+d}(Hg-1201) and HgBa₂Ca₂Cu₃O_{8+d}(Hg-1223)
Advances in Science and Technology , 2003, **38** 39-46
- Veira, L.G.; Ribeiro, J.L.; Chaves, M.R.; Almeida, A.; Hernandez, O.; Quilichini, M.; Kloppepieler, A.**
Anisotropic effects of bromine substitution in betaine calcium chloride hydrate
Ferroelectrics, 2004, **302** 397-399
- Vilminot, S.; Richard-Plouet, M.; Andre, G.; Swierczynski, D.; Bouree-Vigneron, F.; Kurmoo, M.**
Hydrothermal synthesis in the system Ni(OH)₂-NiSO₄ : Nuclear and magnetic structures and magnetic properties of Ni₃(OH)₂(SO₄)₂(H₂O)₂
Inorganic Chemistry , 2003, **42** 6859-6867
- Vilminot, S.; Richard-Plouet, M.; Andre, G.; Swierczynski, D.; Guillot, M.; Bouree-Vigneron, F.; Drillon, M.**
Magnetic structure and properties of Cu₃(OH)₄SO₄ made of triple chains of spins s=1/2
Journal of Solid State Chemistry, 2003, **170** 255-264
- Viret, M.; Ott, F.; Renard, J.P.; Glattli, H.; Pinsard-Gaudart, L.; Revcolevschi, A.**
Magnetic filaments in resistive manganites
Physical Review Letters, 2004, **93** 217402
- Volet, G. ; Amiel, C. ; Auvray, L.**
Interfacial properties of a diblock amphiphilic copolymer : poly(isobutylvinyl ether-b-2-methyl-2-oxazoline)
Macromolecules, 2003, **36** 3327-3336

Wang, F.; Wang, G.-J.; Hu, F.-X.; Kurbakov, A.; Shen, B.-G.; Cheng, Z.-H.

Strong interplay between structure and magnetism in the giant magnetocaloric intermetallic compound $\text{LaFe}_{11.4}\text{Si}_{1.6}$: a neutron diffraction study

Journal of Physics : Condensed Matter, 2003, **15** 5269-5278

Wang, F.; Gukasov, A.; Moussa, F.; Hennion, M.; Apostu, A.; Suryanarayanan, R.; Revcolevschi, A.

Field-induced ferromagnetic metallic state of bilayer manganite $(\text{La}_{0.4}\text{Pr}_{0.6})_{1.2}\text{Sr}_{1.8}\text{Mn}_2\text{O}_7$: a polarized neutron diffraction study

Physical Review Letters, 2003, **91** 047204

Wang, F.W.; Zhang, P.L.; Shen, B.G.; Yan, Q.D.

Crystallographic and magnetic structures of $\text{Pr}_6\text{Fe}_{13}\text{Ge}$ studied by powder neutron diffraction

Chinese Physics, 2004, **13** 918-923

Waerenborgh, J.C.; Avdeev, M.; Patrakeev, M.V.; Kharton, V.V.; Frade, J.R.

Redox behaviour of $\text{Sr}_4\text{Fe}_6\text{O}_{13+\delta}$ by Mössbauer spectroscopy and neutron diffraction

Materials Letters, 2003, **57** 3245-3250

Wolcyrz, M.; Horyn, R.; Bouree, F.; Bukowska, E..

Structural defects in LaMnO_3 phase studied by neutron diffraction

Journal of Alloys and Compounds, 2003, **353** 170-174

Wolfram, H.; Otto, H.H.; Cwik, M.; Braden, M.; André, G.; Bourée, F.; Baenitz, M.; Steglich, F.

Neutron diffraction study of the nuclear and magnetic structure of the quasi-one-dimensional compound CuSiO_3 around $T_N=8\text{K}$

Physical Review B, 2004, **69** 144115

Yaicle, C.; Martin, C.; Jirak, Z.; Fauth, F.; André, G.; Suard, E.; Maignan, A.; Hardy, V.; Retoux, R.; Hervieu, M.

Neutron scattering evidence for magnetic-field-driven abrupt magnetic and structural transitions in a phase-separated manganite

Physical Review B, 2003, **68** 224412

Yamegodo, A.; Carrado, A.; Marechal, A.M.; Pommier, S.; Prioul, C.; Lodini, A.

Residual stress redistribution due to cyclic loading in a railway

Journal of Neutron Research, 2004, **12** 63-68

Zanotti, J.M.; Smith, L.J.; Price, D.L.; Saboungi, M.L.

Influence of confinement on polymer-electrolyte relaxation dynamics

Materials Research Society Symposium Proceedings, 2004, **790**

187-196

Zotov, N.; Kirfel, A.; Beuneu, B.; Delaplane, R.; Hohlwein, D.; Reinauer, F.; Glaum, R.

Effects of transition metal oxide doping on the structure of sodium metaphosphate glasses

Physica B, 2004, **350** E1071-E1073

MAI 2005
IMPRILITH S.A. - 77310 PRINGY - FRANCE
TÉL. 01 64 09 91 01

Scientific Report 2003-2004



Laboratoire Léon Brillouin

CEA-SACLAY, 91191 GIF-SUR-YVETTE CEDEX

<http://www-llb.saclay.cea.fr>